Durham E-Theses

Electrical characteristics of amorphous silicon schottky barriers

Archibald, I. W.

How to cite:

Archibald, I. W. (1984) *Electrical characteristics of amorphous silicon schottky barriers*, Durham theses, Durham University. Available at Durham E-Theses Online: http://etheses.dur.ac.uk/7495/

Use policy

The full-text may be used and/or reproduced, and given to third parties in any format or medium, without prior permission or charge, for personal research or study, educational, or not-for-profit purposes provided that:

- a full bibliographic reference is made to the original source
- a link is made to the metadata record in Durham E-Theses
- the full-text is not changed in any way

The full-text must not be sold in any format or medium without the formal permission of the copyright holders.

Please consult the full Durham E-Theses policy for further details.

Academic Support Office, Durham University, University Office, Old Elvet, Durham DH1 3HP
e-mail: e-theses.admin@dur.ac.uk Tel: +44 0191 334 6107
http://etheses.dur.ac.uk

ELECTRICAL CHARACTERISTICS OF AMORPHOUS SILICON

SCHOTTKY BARRIERS

by

I. W. ARCHIBALD, B.Sc.

The copyright of this thesis rests with the author.
No quotation from it should be published without
his prior written consent and information derived
from it should be acknowledged.

A Thesis submitted for the

Degree of Doctor of Philosophy

at the University of Durham

December 1984

11. FEB. 1985

ABSTRACT

The behaviour of the admittance of an a-Si Schottky barrier as a function of bias, small signal measuring frequency and temperature is not well understood. In this thesis model calculations are described which are both well defined and comprehensive in their description of the Schottky barrier admittance. These calculations allow a better understanding of experimental admittance plots.

Various methods are developed for finding, from Schottky barrier admittance measurements, the density of states in the a-Si mobility gap. The methods are essentially developments of the model admittance calculations, and it should be stressed that the reliability of the deduced density of states depends on the correctness of the initial model premises. In particular it is assumed that the gap state capture cross-sections are all equal and independent of energy.

Experimental admittance measurements are presented for an n-type doped a-Si Schottky barrier. The measurements are quite consistent with the developed theory and an estimate of the density of states in the upper half of the mobility gap is calculated. The average value is $\sim 10^{17}$ $cm^{-3}eV^{-1}$ and there is a minimum situated approximately at 0.3 eV below the conduction band mobility edge. This result is in approximate agreement with the density of states deduced by the DLTS technique. It is also deduced from current-voltage measurements that, of the existing theories, Diffusion Theory probably best describes the leakage current in a-Si Schottky barriers. This deduction is arrived at using some novel analysis.

ACKNOWLEDGEMENTS

I would like to acknowledge the help of :

Professor G.G.Roberts, F.R.S. for allowing me the use of the facilities at the Department of Applied Physics and Electronics, University of Durham.

Dr. R.A.Abram for his supervision of the research, his advice and contributions, and for his positive criticisms of the thesis manuscript.

Drs. M.C.Petty, J.Bee, J.P.Lloyd and Mr.N.J.Thomas for their advice and help with the experimental techniques and measurements.

Professor W.E.Spear, Dr.P.G. LeComber (Dundee University),Dr.J.I.B.Wilson (Heriot-Watt University) and the Xerox Corporation for the provision of amorphous silicon samples.

Mrs.S.Mellanby for her capable and proficient typing of this thesis, and Mr.N.Thompson for the speedy preparation of the diagrams.

My parents for their enthusiasm and encouragement, and my father in particular for his advice on the correct usage of the English language.

The S.E.R.C. for financial support.

Finally I would like to thank all of my friends at Durham who helped make my time there so enjoyable.

CONTENTS

Page Nos

ABSTRACT (i)

ACKNOWLEDGEMENTS (ii)

CHAPTER 1: INTRODUCTION 1

CHAPTER 2: AMORPHOUS SEMICONDUCTORS - SOME BASIC CONCEPTS 4

2.1 Introduction 4

2.2 Definition, Preparation and Examples 4

2.3 Structure and Defects 6

2.4 The Nature of the Electron States 10

2.4.1 The density of states 10

2.4.2 Localised and extended states 11

2.4.3 Fermi level pinning 12

2.5 Electron Transport 13

2.5.1 Hopping conduction 13

2.5.2 Extended state conduction 15

CHAPTER 3: HYDROGENATED AMORPHOUS SILICON 17

3.1 Introduction 17

3.2 Preparation 18

3.3 Defect States in the Mobility Gap 19

3.4 Electrical Conduction 22

3.4.1 Mobility and d.c. conduction 22

3.4.2 The effects of doping 23

3.5 Other Properties and Applications 24

Page Nos

CHAPTER 4: BASIC PHYSICS OF THE a-Si SCHOTTKY BARRIER 26

4.1 Introduction 26

4.2 Theory of the Formation of a Schottky Barrier 26

4.2.1 General aspects 26

4.2.2 Barrier potential profile 30

4.2.3 Barrier height analysis: Bardeen model 33

4.3 Current-Voltage Characteristics 35

4.3.1 The mechanism for assymmetric conduction 35

4.3.2 Thermionic emission theory and Diffusion theory 36

4.3.3 Current voltage characteristics for a thin insulator MIS device 42

4.3.4 Real reverse bias current-voltage characteristics 45

4.3.5 Far-forward bias current-voltage characteristics 46

4.4 Experimental Evaluation of Schottky Barrier Parameters 48

4.4.1 Evaluation of the barrier height 48

4.4.2 Evaluation of the build-in potential 50

CHAPTER 5: A THEORY OF THE ADMITTANCE OF AN a-Si SCHOTTKY BARRIER 53

5.1 Introduction 53

5.2 Schottky Barrier Model: Energy Band Diagram 54

5.3 Treatment of Gap States 57

5.3.1 Gap state kinetics 57

5.3.2 Gap state model for a-Si 61

5.3.3 Results for a reverse-biased Schottky barrier 62

5.3.4 Results for a transient response 66

5.3.5 Results for a small sinusoidal disturbance 69

5.4 The Admittance Calculation 72

5.4.1 Admittance formulae 72

5.4.2 Calculations at a constant bias 75

5.4.3 A differential equation for the small potential 79

Page Nos

5.4.4 Simplified equations for the small potential 80

5.4.5 Solution of simplified equations 82

5.4.6 Admittance solution 85

5.5 Discussion and Illustrative Examples 87

5.5.1 Physical picture of the theory 88

5.5.2 Numerical results for some example densities of states 90

5.6 Resumé 93

CHAPTER 6: COMMENTS AND EXTENSIONS TO THE ADMITTANCE THEORY 95

6.1 Introduction 95

6.2 Admittance Calculation for a Constant Gap State Density 96

6.3 Examination of the Approximations in the Admittance Calculation 99

6.4 Admittance Calculation Including Majority Carrier Charge 105

6.5 Examination of the Majority Carrier Response 112

6.5.1 Equations governing the majority carrier response 112

6.5.2 Majority carrier response with no gap states 114

6.5.3 Majority carrier response with gap states 117

6.5.4 Frequency-dependence : transport versus capture and emission 122

6.6 Effects of Diode Leakage Current 125

6.7 Effects of Minority Carrier Processes 130

6.7.1 Admittance in reverse bias 130

6.7.2 Generation current 134

6.8 Methods for Finding N(E) from Admittance 137

6.9 Resumé 146

CHAPTER 7: EXPERIMENTAL MEASUREMENTS MADE ON a-Si SCHOTTKY BARRIERS 147

7.1 Introduction 147

7.2 Amorphous Silicon Material Details 147

7.3 Device Fabrication 148

Page Nos

7.4 Device Characterisation : apparatus,methods 150

7.4.1 Sample chambers 150

7.4.2 Current measurements 152

7.4.3 Admittance measurements 153

7.5 Device Characterisation : Results 154

7.6 Analysis of Results 157

7.6.1 Analysis of d.c. measurements 161

7.6.2 Analysis of room temperature admittance plots 161

7.6.3 Analysis of variable temperature admittance plots 163

7.6.4 Anomalous admittance-frequency plots at an elevated temperature 166

7.7 Summary of Important Results 167

CHAPTER 8: DISCUSSION AND CONCLUSIONS 169

APPENDICES 173

REFERENCES 182

CHAPTER 1

INTRODUCTION

Hydrogenated amorphous silicon (a-Si), a non-crystalline alloy of hydrogen and silicon, is a relatively new semiconductor device material which promises to have many commercial applications, for example, as a solar cell material or as a photoreceptor in the photocopying process. There are however many physical aspects of this material which are not yet completely understood and indeed there may be properties which for various applications could be better optimised.

A particular feature of a-Si is the high density of localised states evident in the semiconductor band-gap. It was the initial incorporation of hydrogen into the a-Si which drastically reduced the density of these states and allowed useful semiconductor devices to be fabricated. Nevertheless there still remain, relative to most crystalline semiconductors, a large density of localised states in the band-gap, and these states can have a large influence on the characteristics of a-Si devices.

The a-Si device studied here is the a-Si Schottky barrier. A "Schottky barrier" is popularly taken to mean any rectifying metal-semiconductor contact. It is a useful device with many applications (e.g. as in a metal-semiconductor field-effect transistor (MESFET)) and for our purposes its use is as an investigative probe of the localised band-gap states in a-Si. At this point it should perhaps be stressed that as much of this thesis is concerned with the physics of the Schottky barrier as with the physics of a-Si. Indeed the theory and analysis developed in Chapters 5 and 6 could be applied to any Schottky barrier where there is a large and continuous distribution of localised states in the semiconductor band-gap. It is, of course, a-Si Schottky barriers which were fabricated

and characterised (Chapter 7) and it has been the problem of analysing the electrical characteristics of a-Si Schottky barriers which first motivated this research. Nevertheless much of the work does have a wider relevance.

The electrical characteristics which are of chief interest here, concern the somewhat anomalous behaviour of the admittance (i.e. capacitance and conductance) of an a-Si Schottky barrier as a function of bias, small signal measuring frequency and temperature. In the literature there is some confusion as to how the various microscopic electronic processes affect the admittance behaviour. In fact a comprehensive and general description of the electron transport and capture and emission at gap states is required. Also the current analyses of experimental admittance plots lack rigorous justification and they do not extract the maximum amount of material information from the experimental data. Arguments are developed here which help clear up the general confusion about the microscopic electronic processes, and model calculations are developed which lead to a better understanding of admittance plots. The calculations also allow admittance to be used as a spectroscopic probe of the energy distribution of the band-gap density of states. It is of course particularly satisfying that real experimental admittance measurements were also made. They exemplify and give credibility to the developed theory, but importantly they also allow the extraction of useful information about the electronic properties of a-Si.

A brief outline is now given of the layout and development of the work described in this thesis. First, Chapter 2 was essentially written in response to the question ".....but what actually is an AMORPHOUS semiconductor ?" The meaning of amorphous in this context is quite subtle. It is a structural concept and as such a considerable amount of effort is expended to describe the structure of an amorphous semiconductor. Chapter 3 introduces various relevant aspects of a-Si.

In particular two proposed gap state density energy distributions are described and some of the problems relating to their experimental determination are outlined. The Schottky barrier is introduced in Chapter 4. Although this chapter is essentially a review, it is hoped that some aspects have been described from a novel viewpoint and there are in fact some new results which may better describe the current-voltage characteristics of an a-Si Schottky barrier.

The original work contained in this thesis is set out in Chapters 5, 6 and 7. Chapters 5 and 6 are discursive in nature where initial model premises are stated and results are derived which are consistent with these initial premises. The working in these chapters is undoubtedly involved and lengthy, but the mathematics and physical concepts are not intrinsically difficult. The results of the experimental Schottky barrier measurements are presented in Chapter 7 and here the analysis described in Chapters 5 and 6 is used to interpret the measurements and to deduce the localised density of states in the upper half of the band-gap. Finally, in Chapter 8, conclusions reached and unresolved problems/suggestions for future research are presented and discussed.

CHAPTER 2

AMORPHOUS SEMICONDUCTORS - SOME BASIC CONCEPTS

2.1 INTRODUCTION

Amorphous silicon (a-Si) is an amorphous semiconductor and many of the novel physical aspects of this material can be discussed within the more general context of the properties of amorphous semiconductors. Such an approach is taken here because then the basic concepts can be introduced without involving the lengthy discussion of particular material details. The specific physical properties of a-Si (in its hydrogenated form) are summarised in Chapter 3.

Much of the information contained in this chapter, and Chapter 3, is only intended as background material which will allow a better appreciation of the work described in later chapters. Therefore the aspects that are discussed have been chosen because they are relevant, and many quite important but irrelevant aspects are not discussed. Topics not discussed include, for example, the common sign reversal of the Hall co-efficient, small polaron conduction and the anomalous dispersion often seen in "time of flight" experiments. For a comprehensive review of the current understanding of amorphous semiconductors the reader is referred to the texts "Electronic processes in Non-Crystalline Materials", by N.F.Mott and E.A.Davis[1] (1979) and "Amorphous Semiconductors", edited by M.H.Brodsky[2] (1979).

2.2 DEFINITION, PREPARATION AND EXAMPLES

An amorphous solid is "non-crystalline", and by this statement it is meant that there exists no long range spatial periodicity of atomic positions. Nevertheless, due to the nature of the strong localised binding forces between atoms, there is a short range order (reasonably well defined band length, bond angle and nearest neighbour coordination number) and so importantly the positions of the atoms are not completely random.

It is often reasonable to treat the amorphous solid as a configurationally frozen liquid. Indeed a glass, which is a type of amorphous solid, is defined by the American Society for Testing Materials as "an inorganic product of fusion which has cooled to a rigid condition without crystallising". Such a process involves no discontinuity in the first order thermodynamic variables (e.g. volume, entropy), but there are second order discontinuities (e.g. specific heats, coefficient of thermal expansion) and therefore the glass formation is sometimes regarded as a second order thermodynamic transition[3]. It should be noted that the description glass or vitreous solid is normally only used to describe non-crystalline materials which are formed from the melt.

The formation of an amorphous solid requires the prevention of the nucleation and growth processes responsible for crystallisation, and for a glass, for example, this is achieved by cooling the material from a molten to a solid condition sufficiently quickly. Estimated quench rates of up to $10^6 - 10^7$ K s^{-1} have been achieved using the melt-spinning technique[4] and such rates allow the formation of a wide range of amorphous solids. There are however some materials which are beyond the current glass forming techniques. They include elemental metals, alkali halides, Si, Ge and the III-V compounds. Other common preparation techniques[3] include thermal evaporation[5], sputtering[6], glow-discharge decomposition[7] and particle bombardment[8], and these techniques extend the range of amorphous solids to include Si, Ge and the III-V compounds.

Many of the most studied amorphous semiconductors can be placed into one of two categories. They are the chalcogenide glasses which contain one or more of the chalcogenide elements S, Se or Te, and the tetrahedrally bonded amorphous semiconductors which include Si, Ge and the III-V compounds. There are of course other amorphous semiconductors such as amorphous arsenic which do not fit into either category, but for the purpose of illustrating

basic physical properties, these materials need not be explicitly considered. The two categories cited are essentially based on the interatomic bonding arrangement and their related coordination number. The chalcogenides are all 2-3 fold coordinated whereas the tetrahedrally bonded semiconductors are 4-fold coordinated. This categorisation may seem somewhat arbitrary but in fact the materials within each category turn out to have many physical properties in common.

2.3 STRUCTURE AND DEFECTS

For a non-crystalline material it is not possible to define a lattice, basis or a unit cell. These concepts allow a systematic determination of the positions of atoms in a material, and without them the determination of the interatomic spatial relationships becomes very difficult. Another problem is the definition of a defect. A defect is made evident by comparison with a perfect system, and because a perfect amorphous structure is not unambiguously defined, so it is difficult to define a defect.

The most important parameters used to describe the underlying structure of an amorphous material are :

(i) nearest neighbour coordination number,

(ii) bond lengths and their root mean square (r.m.s.)variation,

(iii) bond angle distribution,

(iv) torsion (dihedral) angle distribution,

(v) network topology - shortest path ring statistics etc.

Points (i), (ii) and (iii) refer to short range structure, and because the binding forces between atoms in an amorphous material are very similar to the binding forces between atoms in the crystal, these quantities are meaningful and can be reasonably well defined. They can be determined from standard experimental techniques such as x-ray and neutron diffraction[9], EXAFS[10] (extended x-ray absorption fine structure) and infra-red and Raman spectroscopy[11]. It turns out that the first nearest neighbour coordination number is normally the same as for the crystal and the bond

length has only a small r.m.s. variation about the crystalline value (e.g. $\pm$ 5%). It is more difficult to deduce the bond angle distribution but, for example, for amorphous germanium the spread about the crystalline value is $\pm$ 10° r.m.s.[12].

There will also be structural correlations over several atomic distances, but unfortunately this information is difficult to deduce from experiments. The problem is that the data is normally derived from a macroscopic, isotropic sample with no unit cell, and so any long range structural detail is averaged out. Therefore it has been found necessary to build theoretical models of the structure which as a pre-requisite fit the existing experimental data, but also however are capable of explaining other physical properties[13] (e.g. heat of crystallisation, effects of annealing). These models may be band-built "ball and stick" models or they may be generated on a computer. They include random network models[14-17] molecular models[18], microcrystallite models[19] and layer models[20]. In order to categorise and describe these models the concept of a topological network is often introduced. A typical two dimensional network is illustrated in Fig.2.1(a). It replaces the crystalline lattice and the structure is completed by adding suitable "decoration" (c.f.basis). Fig 2.1(b) shows two different structures which both exhibit the same topological network, but have different decoration and therefore different structures. The most useful parameters employed to describe topological networks are shortest path ring statistics. They are obtained by taking every pair of vertices and finding the smallest sized ring that contains them both. A particular structure will then have a characteristic ratio of, for example, 5 membered to 6 membered rings.

One of the most successful models used to describe the structure of amorphous semiconductors is the Continuous Random Network (CRN), first used by Zachariasen[14] (1932) to describe oxide glasses, but extended by Polk[15] (1971) for group IV amorphous semiconductors. Polk started with

a core of 5 and 6 membered rings and atoms were added so that there were no unconnected bonds in the interior. Bond length variations were kept to less than 1% and he allowed a bond angle variation of $\pm$ 20° about the crystalline value of 109°. The total number of atoms in the model was 440 and it appeared capable of infinite extension. Subsequently other similar models have been proposed where, for example, strain is minimised(16), or a different topology is used(17). All attempts seem to give a reasonably good fit to the experimental diffraction data.

The Continuous Random Network can be used in a non-rigorous way to define a defect : the CRN is taken to be the perfect system and then any deviation from this structure is classified as a defect. Such a methodology allows a systematic explanation of many of the optical, electrical and magnetic properties exhibited by amorphous semiconductors. It should be stressed however that the CRN may never exist in practice, because defects, as defined above, may be an intrinsic feature of the amorphous structure. Phillips(21) (1980) contends that for the higher coordinated semiconductors, defects are necessarily required to relieve an inherent build-up of structural strain.

The simplest point defect is the independent dangling bond. It is an unsatisfied bond which is paramagnetic when neutral (singly occupied) and diamagnetic when charged (unoccupied or doubly occupied). There is a commonly used notation for such a defect which is based on the atomic site associated with it. For example, a singly occupied dangling bond in a chalcogenide is notated C_1^o - C for chalcogenide, zero indicates the neutral charge state of the site and the one indicates the coordination number. Similarly we have T_3^o for an independent dangling bond in a tetrahedrally bonded amorphous semiconductor. These dangling bonds may form various complexes with other defects and non-bonding lone pair sites. For example, the low coordinated chalcogenides have a flexible open structure which form long chains and the chain ends (or dangling bonds) reconfigure to give valence

alternation pairs[22] (VAPS). It is proposed that one dangling bond gives up its lone electron to another dangling bond and then bonds with a lone pair. The result is a three coordinated and a singly coordinated site and we write

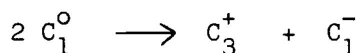

$$2\,C_1^o \longrightarrow C_3^+ + C_1^-$$

Such a "reaction" will only occur if the Coulombic repulsion of the second electron at the C_1^- site is less than the strain relaxation arising from the variation in coordination. Note that for this case a doubly occupied defect is energetically more favourable than a singly occupied defect. The defect is said to have a negative correlation energy and its physical properties are quite different to the more familiar defects which have a positive correlation energy (where the doubly occupied defect energy level is higher in energy than the singly occupied defect energy level).

The defects in tetrahedrally bonded materials are less well understood. The four-fold coordinated structure is very rigid, over coordinated sites are not allowed, and there are no non-bonding lone pairs. There is still some controversy over which defect configurations are energetically most favourable. Elliot[23] (1978) suggests that by a suitable rehybridisation it is energetically possible for an electron to transfer from one dangling bond to another thus

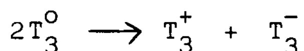

$$2T_3^o \longrightarrow T_3^+ + T_3^-$$

where the T_3^- sites takes a p-type bonding configuration. Adler[24] (1980) argues that defects such as the T_2^o and the charge pair $T_2^+ + T_3^-$ are energetically possible, and also the independent dangling bond T_3^o is itself a stable configuration. Another type of defect is the weak bond where there is no ionic-type charge transfer but the bond is stretched in order to achieve its correct coordination. Robertson[25] (1982) reviews all of these defects and it is clear that there is still some uncertainty

as to what are the principal defects in tetrahedrally banded amorphous semiconductors.

2.4 THE NATURE OF THE ELECTRON STATES

The behaviour of electrons in an amorphous semiconductor can, in some instances, be quite different to their behaviour in the crystalline counterpart. Many crystalline results become invalid and in this section, and also in the following section, various new results are described.

2.4.1 The Density of States

Despite the lack of long range order it is found, from photo-emission experiments, for example, that the energy distribution of electron states in the amorphous semiconductor is very similar to the energy distribution in the crystalline counterpart. In particular, although many of the sharp crystalline features are lost, the bandgap or at least a significant dip in the density of states between the conduction and valence bands survives. This result may be somewhat unexpected, but theoretical calculations (see chapter 2. of ref.2) show that it is the short range structural order which determines the gross features of the density of states. It should be noted of course that there are differences in detail about the band gap, and these differences do affect the electrical and optical properties of the material. These features are now examined.

First the atomic disorder gives rise to random fluctuations in the potential, which leads to a smearing out of the band edge and the formation of a band tail with a typical width of 0.1-0.2 eV. This effect is quite analogous to the band-tailing which occurs in heavily doped crystalline semiconductors. The exact shapes of the band tails are not easy to accurately determine from experiments and normally the procedure is to fit the density of states, N(E), to a power law

$$N(E) \propto E^n$$

where n is found empirically, or to an exponential

$$N(E) \propto \exp(\beta E)$$

where again β is an empirical quantity. Information about these band tails is found from optical absorption experiments (see chapter 4 of ref.2), and also more recently from the analysis of the anomalous dispersion evident in "time of flight" experiments[26].

Another important feature is the presence of defect states at energies in the band-gap. For the tetrahedrally bonded semiconductors it is found that there exists a quasi-continuous distribution of defect states of energies throughout the band-gap and the density of these states can be as high as 10^{20} cm^{-3}. The chief defect in the chalcogenides is thought to be the valence alternation pair, and at thermal equilibrium this pair is doubly occupied/unoccupied and the Fermi level lies just above the doubly occupied defect energy level. The exact energy distribution of the defect states, especially in the tetrahedrally bonded amorphous semiconductors, is not known to any certainty and an important aim of the work described in this thesis is to investigate the energy distribution of defect states found in hydrogenated amorphous silicon.

2.4.2 Localised and Extended States

Defect states are by their nature localised, but it turns out that there also exists an intrinsic localisation of electron wavefunctions arising from the disorder of the atomic positions. Anderson[27] (1958) first showed, given sufficient disorder, that all of the electron wavefunctions can be localised. The physical result of this is that at T = 0, and for an infinitely large sample, the electrical conductivity goes to zero. Mott[28] (1966) later showed that even if the disorder was insufficient to give universal localisation there would still be localisation near the band edges. He further argued that if at a given energy some states were localised, than at that energy all of the states must be localised. This prompted Cohen, Fritzsche and Ovshinsky[29] (1969) to introduce the concept of a mobility edge/mobility gap for amorphous semiconductors. It is now accepted that there exists energies E_c and E_v in the conduction and valence

band tails respectively where the electron wavefunctions change from being localised to being extended. Electrons occupying states between energies E_c and E_v can only move from state to state by thermally assisted hopping processes. Electrons occupying states at energies outside this range have extended state wavefunctions and are free to travel throughout the semiconductor. At room temperatures the mobility of electrons occupying localised states is normally orders of magnitude smaller than the mobility of electrons occupying extended states, and hence E_c and E_v are called mobility edges and the mobility gap is the range of energies $E_v < E < E_c$.

Localised states in amorphous semiconductors can be likened to the localised states of defects in crystalline semiconductors. Their properties are quite similar. The properties of the extended states are however somewhat different. There is no spatial periodicity of the atomic positions in an amorphous semiconductor and so it follows that Bloch's theorem and the concepts of crystal momentum and k-space, as applied to extended state wavefunctions, are invalid. Electrons which occupy extended states are in fact strongly scattered by the atomic disorder and they lose memory of their phase within a few atomic spacings. Therefore, although the wavefunction amplitude is always finite, there is virtually no phase correlation between atomic sites. Two important consequences follow.

(i) There are no k-selection rules for optical transitions,

(ii) electron transport cannot be described using the Boltzmann transport formalism.

Point (ii) will be discussed further in sub-section 2.5.2.

2.4.3 Fermi Level Pinning

It is a general feature of amorphous semiconductors, with only very few exceptions, that the position of the Fermi level is almost independent of temperature and impurity concentration. For the tetrahedrally bonded amorphous semiconductors this Fermi level pinning is most

σ_f, has been made by Mott[30] (1969). He shows that

$$\sigma_f = \sigma_{fo}(T) \exp(-A/T^{1/4})$$

where $\sigma_{fo}(T)$ is only slightly temperature dependent, and A is a constant. This conduction process is called "variable range hopping" - the electron hop distance varies, because although the transition probability exponentially reduces with distance, the energy difference between adjacent sites may be quite large and in such cases a transition to a distant state of similar energy may be more favourable. The characteristic of this type of conduction is a $\ln\sigma \propto T^{1/4}$ dependence.

Hopping may also occur between localised states near the mobility edge. The density of localised states in the band tails is always much larger than the density of defect states at the Fermi level and so over a certain temperature range, determined by Fermi-Dirac statistics and the density of states, it might be expected that this conduction path would be favoured. The actual hopping mechanism is normally very similar to that observed for hopping at the Fermi level but now the dominant temperature dependent term in the conductivity is due to the initial thermal excitation of electrons into the band tail. It is found that band-tail hopping conductivity, denoted σ_b, follows the relation

$$\sigma_b \simeq \sigma_{bo}(T) \exp\left[(E_F - E_A)/kT\right] .$$

E_A is the energy where the exponentially reducing electron occupancy and the fast increasing density of band-tail states give rise to a maximum in the electron density. $\sigma_{bo}(T)$ contains the $\exp(-A/T^{1/4})$ dependence but relative to the $\exp\left[(E_F-E_A)/kT\right]$ term it has only a weak temperature dependence.

often attributed to the large density of defect states situated at the Fermi level. Any movement of the Fermi level would require the filling (emptying) with electrons of a very large density of defect states. Donor (acceptor) densities, for example, are insufficient to effect any appreciable Fermi level shift. Another reason for the almost negligible effect of impurities is that the amorphous network may be able to re-arrange itself in such a way that the valency requirements of the impurity can be satisfied. For example, if boron in amorphous germanium is 3-fold rather than 4-fold coordinated, then no acceptor level is introduced. Any amorphous network which rearranges itself thus is said to follow the so-called "8-N rule" (N is the impurity valency). The chalcogenides are thought to obey this rule.

2.5 ELECTRON TRANSPORT

Electrons move through the amorphous semiconductor either by phonon assisted hopping form localised state to localised state or by extended state conduction above the mobility edge. The processes involved are now briefly described. It should be noted that only the dark d.c. conductivity properties are considered. Other important aspects, such as transport in a magnetic field, a.c. conductivity and thermopower are not considered. Hole transport can be treated in an entirely analogous fashion.

2.5.1 Hopping Conduction

At low temperatures in the tetrahedrally banded amorphous semi-conductors it is hopping conduction which is the dominant transport mechanism. There are several types of hopping conduction. First if localised states exist at the Fermi level then carriers can move between states close to the Fermi level via a phonon assisted tunnelling process. This transport is analogous to impurity conduction observed in heavily doped and highly compensated crystalline semiconductors. An estimate for the temperature dependence of the Fermi level hopping conductivity,denoted

2.5.2 Extended State Conduction

Electrons occupying extended states above the mobility edge are thought to dominate the electrical conduction in the chalcogenides. Extended state conduction is also prevalent at room temperatures in hydrogenated amorphous silicon and germanium. Now although there are broad similarities between extended state conduction in amorphous and crystalline materials, there are some important differences and these are outlined below.

First the bulk conductivity σ_{ex} shows an activated temperature dependence

$$\sigma_{ex} = \sigma_{exo}(T) \exp\left[(E_F - E_c)/kT\right]$$

where $\sigma_{exo}(T) = |e|\mu_{ex}N_c$ (μ_{ex} is the extended state mobility and N_c is the conduction band effective density of states). It is often assumed that E_c and E_F are independent of temperature. Such an assumption is not strictly correct but it is normally a good approximation. It follows that there is no range of temperatures where amorphous semiconductors are "extrinsic". Unlike many crystalline semiconductors (where $E_F = E_F(T)$) the conductivity is never independent of temperature.

The atomic disorder evident in an amorphous semiconductor leads to a mean free path at the mobility edge of about one atomic spacing. It follows from the Uncertainty principle ($\Delta p \Delta x > h$, $\Delta E = \Delta p^2/2m$) that the electron energy is poorly defined ($\Delta E > 0.1$ eV) and hence the Boltzmann transport equation cannot be used. Instead a "random phase approximation" is often used and this allows a value of the extended state mobility μ_{ex} to be calculated. The resulting expression[31] is dependent on the coordination number and the density of states at the mobility edge, but a typical value for μ_{ex} is 10 $cm^2V^{-1}s^{-1}$, and this value is in good agreement with experiment.

Localised band tail states can affect the transport of excess electrons in the conduction band. Electrons occupying extended states can fall into localised states and when this happens these electrons are effectively removed from the conduction process. Thus, if the density of free electrons is n_f and the density of trapped electrons is n_t, then the measured drift mobility μ_d, say from a time of flight experiment, will be

$$\mu_d = \mu_{ex} n_f/(n_f + n_t)$$

The drift mobility is said to be trap-limited and typically it can be 1-2 orders of magnitude smaller than the extended state mobility. It should be noted that this is the mobility of electrons which are injected, or generated in the material. For measurements at thermal equilibrium the extended state mobility μ_{ex} should be used.

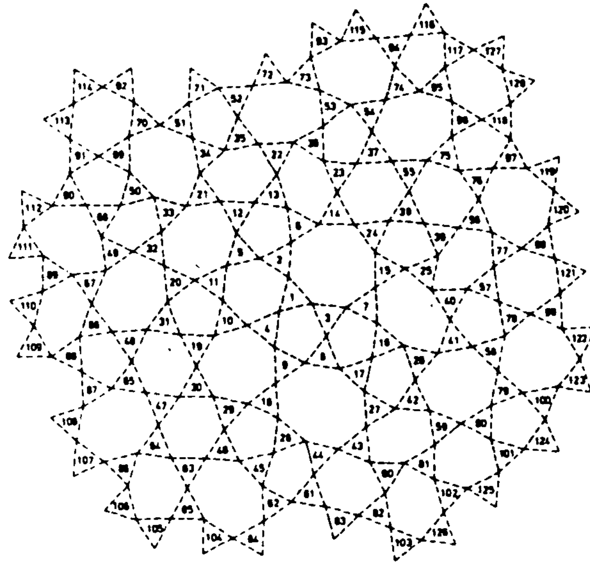

(a) Schematic representation of a 2-D topological network.

The topological units are represented by the dashed triangles.

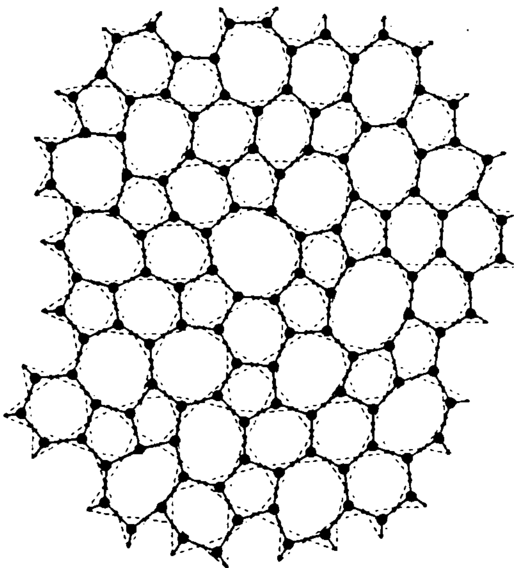

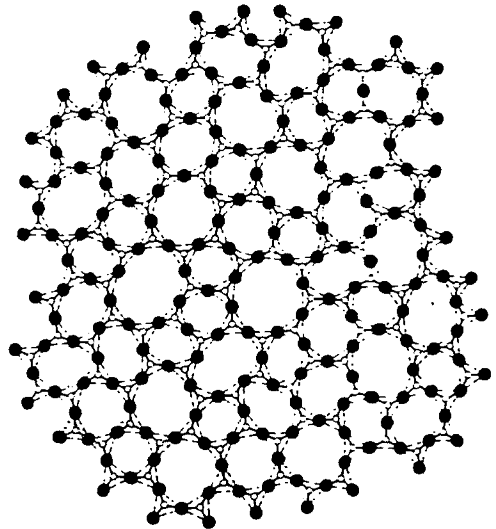

(b) Identical topological networks, but different atomic decoration.

FIGURE 2.1

CHAPTER 3

HYDROGENATED AMORPHOUS SILICON

3.1 INTRODUCTION

Hydrogenated amorphous silicon was first produced at the STL Laboratories (Sterling, Chittick et al[1,2]) in 1965 by the glow-discharge decomposition of silane (SiH_4). The properties of these amorphous silicon films were very dependent on the glow-discharge growth parameters, but it was nevertheless recognised that the films were always much more resistive than thermally evaporated amorphous silicon, and also it was found that the density of defects was much lower. Surprisingly it was not realised, until the mid-seventies, that the underlying reason for these features was the incorporation of hydrogen into the material. In fact glow-discharge amorphous silicon is a silicon-hydrogen alloy, and as such it is intrinsically different to thermally evaporated amorphous silicon.

There are two important properties of hydrogenated amorphous silicon, referred to henceforth as amorphous silicon or a-Si, which have led to its widespread application as a semiconductor device material. At room temperatures electron transport is dominated by extended state conduction and the value of the associated electron mobility is relatively high ($\mu \sim 1\ cm^2V^{-1}s^{-1}$). Also the Fermi level can be moved through most of the mobility gap either by the application of an electric field, as in a field-effect transistor (FET), or by substitutional doping. Therefore unlike nearly all other amorphous semiconductors, the response to doping of a-Si is, broadly speaking, very much like a crystalline semiconductor. Indeed for the purposes of this thesis, a-Si may simply be thought of as a low mobility crystalline semiconductor which has a particularly high density of defect states in the band-gap.

3.2 PREPARATION

There are a growing number of processes used to produce (hydrogenated) a-Si. They include chemical vapour deposition (CVD) of silanes[3], reactive evaporation[4], ion beam deposition[5], radio frequency (r.f.) sputtering[6] and the glow-discharge decomposition of silane[7]. The most commonly used process is the glow-discharge decomposition of silane, and it is this process which is briefly described here.

Fig.3.1 shows a schematic block diagram of a typical a-Si glow-discharge process. Silane(SiH_4) is made to flow through a quartz sample chamber (Q) and capacitively coupled r.f. electrodes (E) break down the silane into a plasma of electrons and positively charged radicals such as SiH, SiH_2 and SiH_3. The plasma is in direct contact with the sample substrate (at S) and if the sample is maintained at the appropriate temperature ($\sim$ 250°C), then a high quality film of a-Si may form on the surface. The deposition rate is typically 100 Å/min. Doping is achieved by adding phosphine (PH_3) or diborane (B_2H_6) and the incorporation of phosphorous or boron is found to be approximately the same as the number density ratio of the respective gas molecules.

The electronic properties of the deposited film critically depend on a large number of variables, e.g. substrate temperature, plasma density, r.f. power, the floating potentials on various internal surfaces and the system geometry. There are no accepted ideal deposition conditions and the material as grown cannot be exactly specified. For example, the amount of hydrogen incorporated into the film can vary from 5 to 60 percent of the total number of atoms[8]. Usually a system is simply set up to grow a-Si with "optimised" electronic properties. It should be stressed that a-Si produced from different systems will not in general have exactly identical properties.

The other a-Si growth techniques are not as well developed as the glow-discharge process and the resulting a-Si films tend to have a higher

defect density. Nevertheless these techniques are being improved and, for example, r.f. sputtering is becoming a viable alternative. Sputtering has the advantage that there is much greater control over the amount of hydrogen incorporation in the film.

3.3 DEFECT STATES IN THE MOBILITY GAP

It is generally accepted that most of the electrical and optical properties of a-Si depend critically on the energy distribution of the localised states, N(E), within the mobility gap. As a result an extensive amount of research has been carried out in order to find N(E). Also sought is the origin and nature of these localised states, and again much work has been carried out to achieve this end.

Currently the most important and comprehensive techniques used to find N(E) are the Field-effect (FE) technique[9-17] and Deep level transient spectroscopy (DLTS)[18-23]. Other techniques include the examination of space-charge limited currents (SCLC)[24-27] and the examination of the admittance of an a-Si Schottky barrier/ MIS structure (see Chapters 5 and 6). The various experiments show that there is a quasi-continuous distribution of states throughout the mobility gap with average densities varying from 10^{15}-10^{18} cm^{-3}. This variation can be partly explained by the different a-Si growth processes used, but there are differences in the deduced densities of states which cannot be accounted for in this way. Fig.3.2 shows typical N(E) as deduced by the Field-effect technique and by DLTS. The FE N(E) is considerably larger than the DLTS N(E), and at E_c-E $\simeq$ 0.4 eV, the FE shows a peak in N(E) whereas the DLTS N(E) shows a trough. Other measurements, especially the SCLC measurements, tend to be more in agreement with the FE N(E), but there do appear to be some results which are in more agreement with the DLTS N(E) (see Ref.22).

It is useful, for future reference, to briefly outline the Field-effect and DLTS techniques.

Field-effect technique - an insulated gate a-Si field effect transistor is fabricated, and the source-drain current I_{SD} is measured as a function of gate voltage V_G, thus giving the transconductance (I_{SD}/V_G). The space-charge, and hence the band-bending, in the a-Si is dominated by charge arising from the defect states which have been displaced relative to the Fermi level. Hence the transconductance, which is a function of the band bending, is a function of the density of defect states. This functional dependence can be used to find N(E) from a plot of I_{SD} versus V_G.

A serious uncertainty arises with the FE technique because of the undetermined interface state density at the a-Si/insulator interface. It can be expected that the density of states in the mobility gap is considerably larger at the interface than in the bulk a-Si (lattice mismatch, insulator defects, etc) and these extra interface states can have a major influence on the behaviour of the FET. For example, they normally act to reduce $I_{SD}(V_G)$ and will thus lead to an overestimate of N(E). Also they lead to an uncertainty in the interface potential and hence the energy scale for N(E).

DLTS - Deep level transient spectroscopy is one of a family of techniques which involve the thermal relaxation of a semiconductor from a non-equilibrium state occupation. The technique is based on a Schottky barrier or p^+n (n^+p) type device. For an example take the case of an n-type Schottky barrier. A large reverse bias ($\gtrsim$ 2 volts) is applied and the defect states are allowed to empty of electrons until equilibrium is reached. The states are then filled by applying a short forward bias pulse or by shining light on the sample, and the subsequent relaxation back to the dark, reverse-biased equilibrium is monitored by measuring the change in capacitance with time. In DLTS as the states empty and the capacitance reduces, the reduction in capacitance over a fixed time interval is measured as a function of temperature. From this measurement it is possible to deduce the density, energy position and capture cross-section of a defect level.

DLTS has been successfully employed in the characterisation of single defect levels in the band-gap of crystalline semiconductors. However, several new problems are encountered when the technique is applied to defects in a-Si. First, the standard DLTS analysis[28] requires that the change in capacitance is much smaller than the total measured capacitance. For a-Si this is not the case. Second, in order to set the energy scale it is necessary to be able to resolve an identifiable defect energy level. This is very difficult with a-Si because the defect-density energy distribution is quite smooth and relatively featureless. Finally it must be assumed that the time limiting factor to the relaxation process is the emission of electrons from defect states to extended states. It has been proposed that for a-Si it could be the transport of electrons in the extended states which limits the response (see Chapters 5 and 6).

It is perhaps clear that there is sufficient experimental uncertainty involved with both the Field-effect and DLTS techniques that neither deduced N(E) can be unequivocally discarded or taken to be correct. It has been recognised that other independent measurements of N(E) are required. Also, it is necessary to achieve a better understanding of the quantity that is being measured. It is not clear, for example, that the FE and DLTS techniques measure the same N(E). This point is discussed in Chapter 8.

Another aspect to be considered is the nature and origins of the defect states found in a-Si. Electron spin resonance (ESR)[29], optically detected magnetic resonance (ODMR)[30], luminescence[31] and photo-conductivity[32,33] experiments have been carried out on a-Si (the references quoted are examples of this work), but the results from these measurements prove to be somewhat inconclusive. It is considered outwith the scope of this thesis to detail the various arguments and interpretations which have been used in attempts to identify particular defects. Such a discussion would be unduly speculative. However, there are some points worthy of note.

Infra-red and Raman spectroscopy experiments[8] show that hydrogen, in the form of SiH, SiH_2 and $(SiH_2)_n$ bonds, exist in the (hydrogenated)a-Si

films, and it is proposed that much of this hydrogen has bonded to what would be defects in the mobility gap of the otherwise hydrogen-free a-Si (e.g. thermally evaporated a-Si). The hydrogen also appears to help relax the structure and there is no evidence of the voids and larger inhomogeneities which are evident in unhydrogenated a-Si. The result is that the density of gap states in hydrogenated a-Si can be $\sim$ 3 orders of magnitude smaller than the density of gap states found in unhydrogenated a-Si. Given this reduction in the defect density it might also be expected that the nature of the remaining defects is altered. There is however no firm evidence for this and indeed the general discussion in Chapter 2, section 2.3 about defects in tetrahedrally bonded amorphous semiconductors still does apply. The gap states are thought to be due to point defects of the dangling bond type and it should be noticed, with the possible exception of the case of heavy doping(34), that there is no evidence of states with a negative correlation energy. The addition of dopants does introduce some new defect states, although there is no identifiable associated donor or acceptor level. The effects of doping are discussed in the next section.

3.4 ELECTRICAL CONDUCTION

3.4.1 Mobility and D.C.Conductivity

Fig.3.3 shows plots of the drift mobility and bulk d.c. conductivity for undoped a-Si as a function of temperature. The measurements were made by LeComber and Spear(35) (1970) and the plots are interpreted as follows. First undoped a-Si turns out to be slightly n-type and therefore the plots show the electron transport behaviour. At temperatures above about 250K extended state conduction prevails with an activation energy of E_C-E_F = 0.62eV. Below this temperature hopping in the conduction band tail dominates and finally at temperatures below about 170K hopping between states close to the Fermi level dominates.

The drift mobility, which is the mobility for excess injected electrons, also shows an activated energy type dependence and this is indicative of a

trap limiting process. At room temperatures the electron drift mobility is $\sim$ 0.1 $cm^2V^{-1}s^{-1}$ and the dominant trapping centres are situated at $\sim$ 0.2 eV below the conduction band mobility edge. The results at lower temperatures are more difficult to interpret and in fact Moore[36] (1977) does not observe the pronounced kink in the mobility curve at T $\approx$ 250K. Therefore it is not sensible to attempt an interpretation. Moore also measured the hole drift mobility and found an activated energy temperature dependence of $\sim$ 0.35 eV and at room temperature the value of the mobility was $\sim 6 \times 10^{-4}$ $cm^2V^{-1}s^{-1}$. More recent drift mobility measurements have been made, and most of the results are in agreement with the above, although it is regarded that the electron drift mobility is perhaps closer to a value $\sim$ 1 $cm^2V^{-1}s^{-1}$ [37].

3.4.2 The Effects of Doping

Fig.3.4 shows the effects of doping on the d.c. bulk conductivity of a-Si. The measurements were made by Spear and LeComber[38] (1976) and the doping was achieved by the addition of phosphine (n-type) or diborane (p-type) gas to the silane in the plasma glow-discharge. Note that the conductivity can be changed by ten orders of magnitude and that the Fermi level can be moved to within $\sim$ 0.2 eV of both the valence and conduction band mobility edges.

The dopant species are phosphorous and boron and it is estimated that the efficiency of the doping process is about one third[38], i.e. only one third of the total number of dopant atoms actually act as donors/ acceptors - the a-Si structure appears to be able to adjust so as to fulfil the valence requirements of the other dopant atoms. Also it is not possible to dope the a-Si until it becomes degenerate. This has been attributed to the very high density of localised states in the band tails which must be filled with electrons/holes before the Fermi level is able to move into the extended state regions. Recently Robertson[34] (1984) argued that the dopant atoms may allow there to be overcoordinated sites, resulting in

valence alternation (c.f. chalcogenides) and hence there might be states with negative correlation energy which could "pin" the Fermi level. This is as yet only a tentative suggestion. Finally it should be noted that no discrete level has been detected which could be associated with the introduction of the dopant atoms, although it is generally accepted that doping does alter the density of states in the mobility gap.

3.5 OTHER PROPERTIES AND APPLICATIONS

There are many physical aspects and properties of a-Si which have not been discussed. For example, the optical absorption in the visible is approximately an order of magnitude larger for a-Si than for crystalline silicon - a property arising from the breakdown of the optical transition k-selection rules. Amorphous silicon is very photoconductive, and also it is sometimes found that strong visible illumination can reduce the value of the dark conductivity by several orders of magnitude[39]. No mention has been made of the anomalous sign of the Hall coefficient[40] or the anomalous dispersion sometimes observed in time of flight drift mobility measurements[36]. Also, the various proposed recombination and trapping mechanisms in a-Si[41,42] have not been discussed. There may be, for example, tunnelling transitions between localised tail states and states deeper in the mobility gap[42]. The above list is not exhaustive however it does give some indication of the various topics and properties which have been omitted.

The commercial applications of a-Si are based on the properties of high optical absorption in the visible, good photoconductivity and the ability to grow the material in large areas and relatively cheaply. It should be noted that most of the applications are still at the developmental stage although for the case of solar cells, commercial devices are already being manufactured.

The applications include:-

(i) Solar cells - although less efficient than crystalline silicon cells they have advantages of material saving (less than 1 μm thickness of a-Si is required), energy savings in their production (low temperature growth process),

a small number of process steps, and the a-Si can be deposited onto plastic substrates. An efficiency of 10.5% for a 1 cm^2 p-i-n cell has been reported[43] and it is thought that efficiencies of up to 18% might be achieved using tandem cells.

(ii) Electrophotography[44] - the combination of high dark resistivity and high photoconductivity make a-Si a good candidate as the photoreceptor material in the photocopying process. The advantages it has over existing materials is that it is mechanically hard and it is non-toxic.

(iii) Thin film transistor (TFT) arrays[45] - the ability to grow cheap large areas of a-Si is being used to develop a matrix FET addressing system for liquid crystal flat panel displays.

(iv) Non-volatile memory cells - high speed switching has been reported[46] in p-n-i structures deposited onto a conducting substrate. These devices could be used as programmable, non-volatile memories and from early results they would seem superior to the current technology (MNOS and FAMOS) in terms of switching speeds ($<$ 100 ns) operating voltages (1-8 volts) and stability.

(v) High density information storage - the amorphous to polycrystalline transition in thin silicon layers is accompanied by a large change in the optical transmission in the visible. It has been suggested[47] that by selective laser annealing a high density optical data storage system could be manufactured.

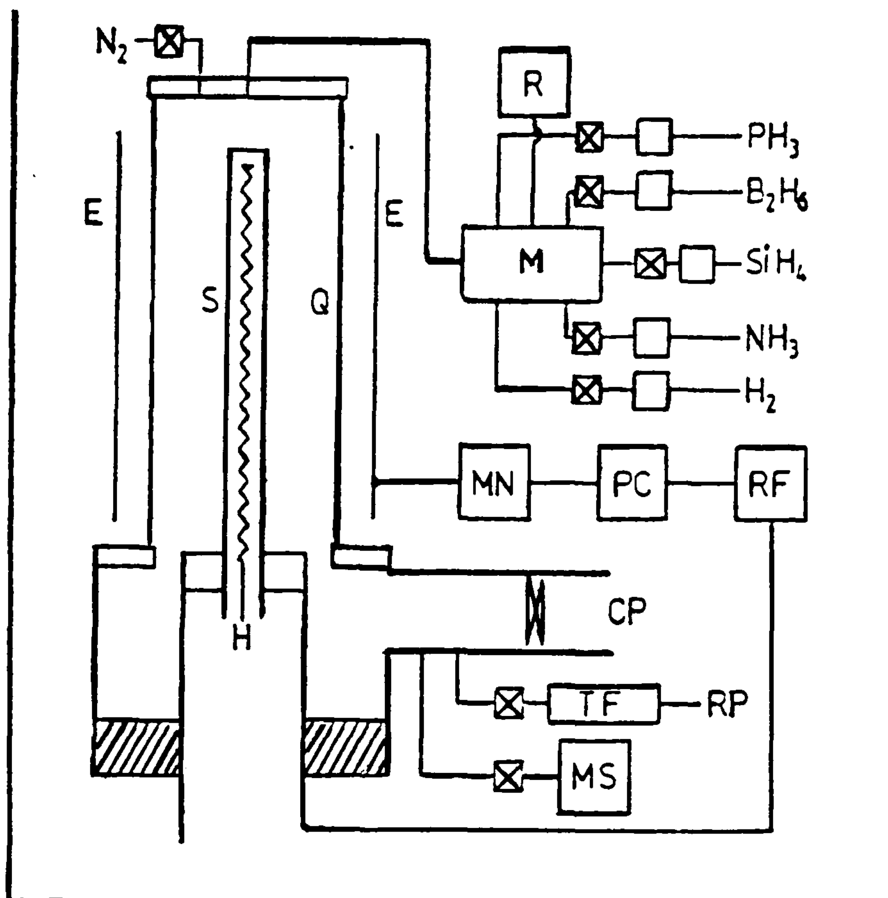

FIGURE 3.1: Vertical glow-discharge deposition system. S, sample holder ; H, electrically insulated heater ; Q, quartz sample enclosure ; E, external r.f. electrodes ; M, mixing chamber ; R, reservoir for pre-mixing of gases ; MN, matching network ; PC, power controller ; RF, r.f. generator ; CP, cryo-pump ; TF, tubular furnace ; RP, rotary pump ; MS, mass spectrometer. (Diagram courtesy of Professor W.E.Spear, Dundee University).

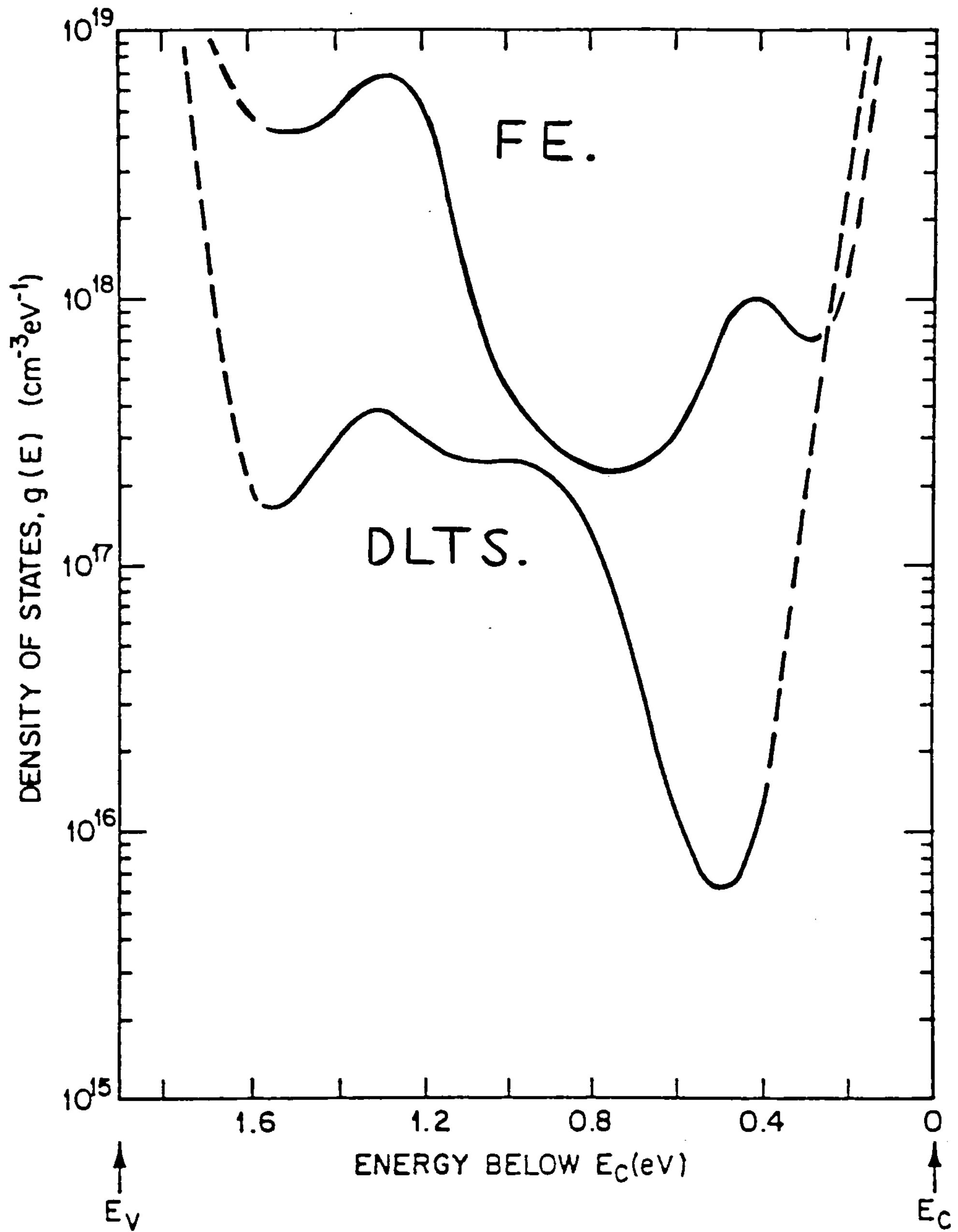

FIGURE 3.2: Typical densities of states in the mobility gap of a-Si as deduced from the Field-effect (FE.) technique and Deep level transient spectroscopy (DLTS.).

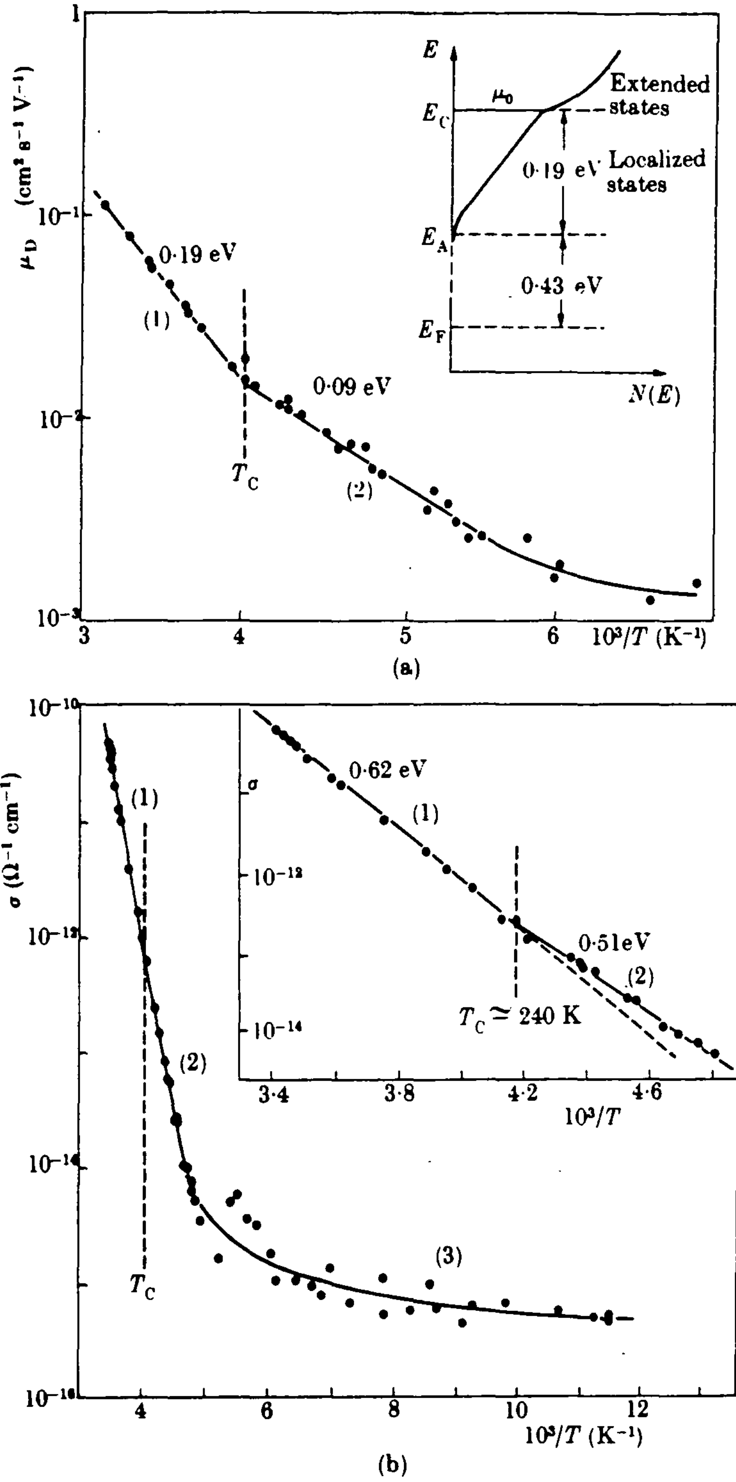

FIGURE 3.3: Measurements of the electron drift mobility (a) and bulk d.c. conductivity (b) of undoped a-Si as a function of temperature (ref.35).

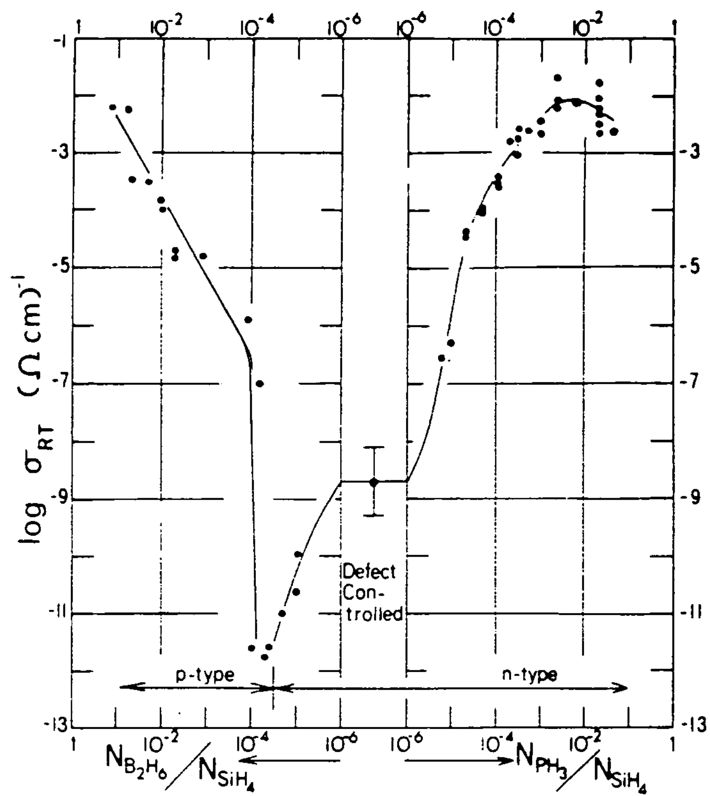

(a)

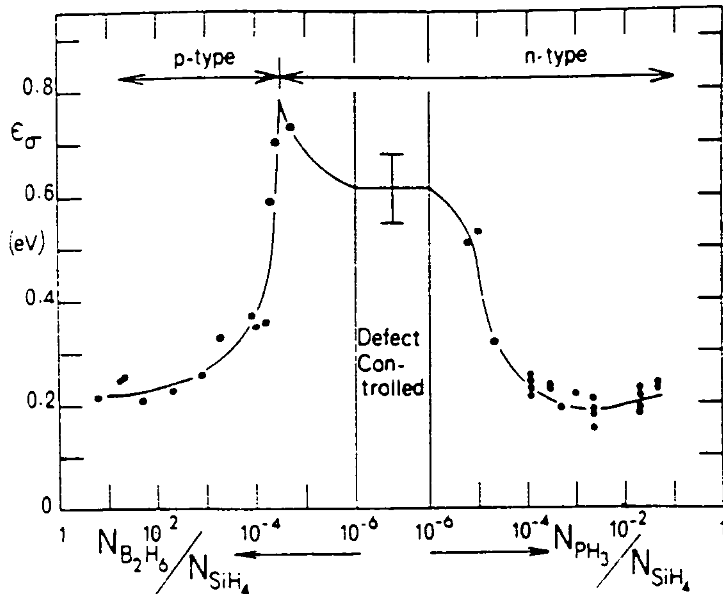

(b)

FIGURE 3.4: Measurements of the room temperature conductivity on n- and p-type a-Si as a function of gaseous composition from which the films were deposited (a), and the conductivity activation energy as measured from the same samples (b) (ref.37).

CHAPTER 4

BASIC PHYSICS OF THE a-Si SCHOTTKY BARRIERS

4.1 INTRODUCTION

The asymmetric nature of electrical conduction through metal-semiconductor contacts was first discovered more than 100 years ago. Extensive research work has been carried out since then and yet it should be noted that many aspects of the metal-semiconductor (Schottky) barrier are still not fully understood. For example there is only a qualitative understanding of the various mechanisms involved in the barrier formation[1]. Electron transport in the large and rapidly varying built-in electric field has yet to be properly described[2], and new work is being carried out to investigate the effects arising from the injection of hot carriers from the semiconductor to the metal[3].

This chapter summarises the more basic physics of the Schottky barrier device. Where possible emphasis is placed on a-Si Schottky barriers and much of the information will be directly relevant to the calculations and experiments described in Chapters 5, 6 and 7. For a more general and comprehensive review of this area of device physics the reader is referred to "Metal-Semiconductor Contacts", by E.H.Rhoderick[4] (1978) and a more recent review article[5] (1982) by the same author. Two less recent but useful texts are "Electronic Semiconductors" by E.Spenke[6] (trans.1958) and "Metal-Semiconductor Rectifiers", by H.K.Henisch[7] (1957).

Note that throughout this Chapter only Schottky barriers formed on n-type semiconductors will be considered.

4.2 THEORY OF THE FORMATION OF A SCHOTTKY BARRIER

4.2.1 General Aspects

When a metal is brought into contact with a semiconductor there will be electronic interactions close to the metal-semiconductor interface. The

electron bonding configuration will rearrange at the semiconductor surface, and if there is intimate contact between the metal and semiconductor, metal-semiconductor bonds will form. Also, the electrons in both materials will attempt to come into thermal equilibrium with each other. Electrons will diffuse from one material to the other and this effect will give rise to a macroscopic built-in electric field.

The energy of the electrons in a material is characterised by the (electro)chemical potential, and in semiconductor device physics this energy is referred to as the Fermi level, denoted E_F. It follows from thermodynamic arguments that for the metal and semiconductor electrons to be in thermal equilibrium with each other then their respective Fermi levels, denoted E_F^m and E_F^s , must be coincident. If the metal and semiconductor are brought into contact and $E_F^m \neq E_F^s$, then in order to achieve thermal equilibrium there will exist a flow of (mobile) electrons from one material to the other until the Fermi levels become coincident. Indeed just as the temperatures of the two materials determine the flow of heat, the Fermi level values determine the flow of particles. For electrons, which are charged particles, the Fermi level alignment is achieved via a macroscopic electric field which arises from the movement of charge - there will exist a built-in potential, denoted V_{BI}, such that an electron travelling between the metal and the semiconductor loses/gains an energy $E_F^m - E_F^s$. In order to relate the thermodynamic concept of a Fermi level to the physical properties of a solid, some well known results from solid state physics must now be used, and a particularly relevant text for reference is "Modern Theory of Solids", by F.Seitz[8] (1940).

According to the Sommerfeld free electron theory of metals, the most energetic metal electrons (kinetic energy typically 4-6 eV), which are also the mobile electrons, are at an energy coincident with the metal Fermi level. The metal work function, denoted Φ_m, is defined as the minimum energy required

to remove an electron from the metal to a point at rest outside in a vacuum. Hence it follows that

$$\phi_m = E_{vac} - E_F^{\ m} \tag{4.1}$$

where E_{vac} denotes the zero energy vacuum level. The work function can be measured using the photoelectric effect (typical value 4-5 eV) and in this way the position of the metal Fermi level relative to the zero energy vacuum level can be found. The energy scheme for these levels is shown in Fig.4.1(a).

The semiconductor electrons behave in a very different way to the electrons in a metal. Unlike the metal Fermi level, the value of $E_F^{\ s}$ can be strongly temperature dependent and can vary considerably with different impurity concentrations (doping etc). Also most often there are no electron states at energies which are coincident with the Fermi level. Electrons must be excited from the valence band or from impurity centres to the conduction band before they become mobile and in fact it is argued that a more physical intrinsic semiconductor energy level is the energy of the conduction band edge, denoted E_c. It proves useful to define an energy χ_s, called the semiconductor electron affinity, which is related to E_c thus,

$$\chi_s = E_{vac} - E_c \tag{4.2}$$

and this relation will be used to fix the semiconductor energy levels relative to the zero energy vacuum level. The semiconductor energy scheme is shown in Fig.4.1(a).

For the example chosen in Fig.4.1(a), the semiconductor has been chosen to be n-type, $\phi_m > \chi_s$ and $E_F^{\ s} > E_F^{\ m}$. It is shown in Fig.4.1(b) that this example will result in the formation of an n-type Schottky barrier.

Consider the situation when the metal and semiconductor are brought into contact. The semiconductor electron density has a larger total energy and so, on average, mobile semiconductor electrons which travel into the metal lose energy and thus cannot return. This results in there being net negative charge in the metal and net positive charge in the semiconductor which in turn gives rise to an electric field and the required built-in potential V_{BI}. Note that the potential is shown to be dropped across the semiconductor, and this point will be explained in the next sub-section. Thermal equilibrium is achieved when the electric field finally becomes sufficiently large to inhibit any further net electron flow to the metal and when this occurs the Fermi levels are coincident.

The most general definition of the Schottky barrier height, denoted ϕ_b, is as follows. It is the minimum energy required for an electron at the metal Fermi level (a mobile metal electron) to be able to become a mobile electron in the semiconductor bulk. If quantum-mechanical tunnelling is not allowed then from Fig.4.1(b), it is clear that

$$\phi_b = \phi_m - \chi_s \tag{4.3}$$

and this (classical) result was first derived by Mott[9] (1938). It is found from experiment however that this relation has only limited validity.

An aspect which has not yet been considered is the nature of the atomic bonding arrangement actually at the metal-semiconductor interface. The affected region typically extends over several atomic spacings (i.e. 10-20 Å) and unfortunately a quantitative description of this region is quite difficult. The electron environment near the surface of the semiconductor is very different to the environment in the bulk, and, for example, there may exist a continuous distribution of states localised at the surface which have energies in the "forbidden" band-gap. Also the surface is often very reactive and a native oxide or other adsorbed impurities may be present

at the surface. Even if the semiconductor is in intimate contact with the metal, the metal-semiconductor interface is still difficult to describe. The semiconductor valence band (bonding) states may be perturbed, and it is thought that metal electron wavefunctions which have energies corresponding to the semiconductor band-gap will actually penetrate some distance into the semiconductor[1].

It should be noted that the above effects are not well understood. It is found from experiments however, that the barrier height ϕ_b does not closely follow the Mott relation, eqn.(4.3), and the usual explanation is that the deviation is due to this thin 10-20 Å interfacial region. It is proposed that the interface states/metal-semiconductor bonding arrangement gives rise to a large electric dipole with an associated electric field approaching the dielectric breakdown strength of the semiconductor. If the dipole separation is 10 Å and the electric field is 10^7 Vcm^{-1}, then 1 volt, which is a relatively large potential, is dropped across the interfacial region. This potential drop may significantly contribute to the Fermi level alignment and it follows that less conduction band electrons are required to diffuse into the semiconductor. More importantly however, it is proposed that electrons can quantum-mechanically tunnel through the thin interfacial region and it follows that less energy is required for an electron to travel from the metal to the semiconductor bulk. The effective barrier height has therefore been reduced. A more quantitative description of this effect is given in sub-section 4.2.3.

4.2.2. Barrier Potential Profile

In this sub-section the potential drop associated with the thin interfacial region is ignored, and as a first example we consider a Schottky barrier where the semiconductor is crystalline and n-type with a donor density N_D.

The Fermi level alignment requires that there is a built-in potential, denoted V_{BI}, between the metal and the bulk semiconductor, and it is argued

as follows that V_{BI} is almost entirely dropped across the semiconductor. There must be overall charge neutrality and this means that the positive charge in the semiconductor is matched by an equal amount of negative charge in the metal. However the spatial extent of the charge in the barrier depends on the size of the charge density as compared to the intrinsic density of mobile charge. In the metal the mobile electron density is much larger than the extra electron density which flows in from the semiconductor. Simple arguments then show that the extra electrons will be accommodated within a few Thomas-Fermi screening lengths ($\sim$ 0.5 Å) of the interface. The density of mobile electrons in the semiconductor is very much smaller and in fact the flow of electrons into the metal totally depletes the mobile electron density in the semiconductor. This state of depletion can extend some distance into the semiconductor, typically $\sim$ 0.2 μm, which is the order of a few Debye lengths. Now although the spatial extent of the positive charge in the semiconductor is much larger than the spatial extent of the negative charge in the metal, electrostatic arguments show that the electric fields in both the metal and semiconductor are similar. Therefore the potential is almost totally dropped across the semiconductor.

The semiconductor conduction band electrons normally obey Maxwell-Boltzmann statistics and therefore it is reasonable to assume that there are virtually no conduction band electrons in the region where the built-in potential is finite. The charge density is then attributed to the ionised donors and it will be positive and equal to $|e|N_D$. It follows from Poisson's equation that the (average) energy of the conduction band edge E_c as a function of x is

$$E_c(x) = E_c(\infty) + |e|V_{BI}\left(1 - \frac{x}{W}\right)^2 , \quad W = \left(\frac{2\varepsilon_s\varepsilon_o}{|e|N_D}V_{BI}\right)^{1/2}, \quad x < W \qquad (4.4)$$

where the metal-semiconductor interface is at x = o, ε_s is the semiconductor

dielectric constant and W is the width of the region depleted of conduction band electrons. Eqn.(4.4) describes the barrier potential profile. Note also that the electric field, denoted $\mathcal{E}$, is given by

$$\mathcal{E}(x) = \frac{1}{|e|} \frac{d}{dx} E_c(x) = -\frac{2V_{BI}}{W} \left(1 - \frac{x}{W} \right) , x < W \qquad (4.5)$$

and $|\mathcal{E}|$ is a maximum at x = o.

It should be stressed that an individual electron travelling through the depletion region experiences quite a different electric field to the average value given by eqn.(4.5)[10]. Consider an example. If $N_D = 10^{16}$ cm^{-3}, ε_s = 11 and V_{BI} = 0.5 volts, then the depletion width is $\sim$ 0.25 μm and the average donor separation is $\sim$ 500 Å. Therefore in any chosen x direction a travelling electron will encounter an average of 5 positive charges, each charge |e| , before it reaches the metal. An energy band diagram showing a typical $E_c(x)$ as experienced by an individual electron is drawn in Fig.4.2. Note also that the electric field associated with the electron itself will give rise to an image charge in the metal and this will further perturb the barrier profile. This effect is called the Schottky effect (see Ref.4,pp.37) and it can normally be ignored because the perturbation is very small.

Similar arguments to the above apply for an n-type a-Si Schottky barrier, but in this case the main semiconductor charge contribution is attributed to deep gap states rather than ionised donors. It will be shown in Chapter 6, section 6.2 that the barrier potential profile is better described by the expression,

$$E_c(x) = E_c(\infty) + |e| V_{BI} \exp(-x/L_o) , \qquad (4.6)$$

where L_o has dimensions of length and its value is a function of the average gap state density. The extent of the depletion region can be estimated by

defining $x = W$ as the point where $E_c(W) - E_c(\infty) = kT$. Then from eqn.(4.6),

$$W = L_o \ln(|e|V_{BI}/kT) \tag{4.7}$$

and for $V_{BI} = 0.5$ volts, $W \simeq 3L_o$.

4.2.3 Barrier Height Analysis : Bardeen Model

Bardeen[11] (1947) proposed a model of the metal-semiconductor interface which can provide an analytical description of the Schottky barrier height and its dependence on the properties of the interfacial region. It is most used for the description of crystalline Si Schottky barriers. Other models such as the Unified defect model[12] may be better for Schottky barriers formed on III-V semiconductors, for example, but given the similarities between amorphous and crystalline silicon the Bardeen model is thought to be more relevant here. Many people have contributed to this barrier height analysis, and only a brief summary of the work is described below. A more thorough description is to be found in "Metal-Semiconductor Contacts", by E.H.Rhoderick[4] (1978), pp.28.

It is proposed that there exists a tunnellable layer of insulating material, thickness δ, between the metal and the semiconductor. For a-Si this insulator may be some complex silicon : oxygen : hydrogen compound and it may have very different properties to say bulk a-SiO_2. Nevertheless it is convenient to envisage it as a large band gap material with a dielectric constant $\varepsilon_i \simeq 4$ (i.e. same as a-SiO_2). At the semiconductor side of the interface and at band gap energies, there is thought to exist a continuous distribution of localised states. For a-Si these states will considerably augment the density of bulk gap states already present. The wavefunctions of these states probably extend over about 10 Å but as an approximation they are taken to be points located exactly at the interface. A further approximation is that the density of surface states per unit energy, denoted $N_{ss}(E)$,

is a constant, i.e. $N_{ss}(E) = N_{ss}$. Finally the insulating layer is assumed to be very thin, i.e. $\delta < 20$ Å. Metal electrons can then easily communicate with the interface states and therefore the electron occupancy of the interface states is controlled by the metal Fermi level E_F^m.

A neutral level is introduced for the interface state density, denoted ϕ_o. It is defined so that if $E_F^m = \phi_o$, then there is no net charge associated with the interface states. If however $E_F^m \neq \phi_o$ then the interface charge density, denoted Q_{ss}, is approximately $-|e|N_{ss}(E_F^m - \phi_o)$, (the interface states are assumed to be monovalent). It would not in general be expected that the interface state neutral level was coincident with the metal Fermi level, and it is proposed that the resultant electric dipole moment $Q_{ss}\delta$ is sufficiently large to affect the barrier potential.

Fig.4.3(a) shows the Schottky barrier energy band diagram at flat-band conditions, i.e. a sufficiently large forward bias has been applied so that no electric field exists in the semiconductor and then E_c = constant. A potential V_I^o is dropped across the insulator and if electrons can quantum-mechanically tunnel through the insulator then the flat-band barrier height, denoted ϕ_b^o, is

$$\phi_b^o = (\phi_m - \chi_s) - |e|V_I^o. \tag{4.8}$$

The charge at the interface, denoted Q_{ss}^o, is

$$Q_{ss}^o = |e|N_{ss}(\phi_o - (E_c - \phi_b^o)). \tag{4.9}$$

Gauss' law then gives V_I^o and with some rearrangement the flat-band barrier height becomes

$$\phi_b^o = \gamma(\phi_m - \chi_s) + (1 - \gamma)(E_c - \phi_o) \tag{4.10}$$

where $\gamma = \epsilon_i/(\epsilon_i + |e|\delta N_{ss})$. Note that if δ or N_{ss} goes to zero then the barrier height will follow the Mott relation, eqn.(4.3). Indeed if $\delta = 20$ Å, a significant deviation from eqn.(4.3) only occurs when N_{ss} approaches 10^{13} cm^{-2} eV^{-1}.

Normally there is an electric field in the semiconductor and this field will contribute to the electric field in the insulator. Fig.4.3(b) shows the energy band diagram for a Schottky barrier where only a small forward bias is applied. The voltage drop across the insulator is now larger and the barrier height, denoted ϕ_b, can be calculated to be

$$\phi_b = \phi_b^o - \alpha\mathcal{E}_{max}, \tag{4.11}$$

where $\alpha = \delta\epsilon_s/(\epsilon_i + |e|\delta N_{ss})$ and $\mathcal{E}_{max}$ is the (maximum) electric field at the semiconductor surface. Note that ϕ_b is in fact bias dependent. However if N_{ss} is large the electric field due to the interfacial dipole will be much larger than the electric field due to the charge in the semiconductor, and then $\phi_b \approx \phi_b^o$.

4.3 CURRENT-VOLTAGE CHARACTERISTICS

4.3.1 The Mechanism for Asymmetric Conduction

When a bias V is applied to a Schottky barrier, the charge densities in the metal and semiconductor are both affected. Importantly however the potential is almost totally dropped across the semiconductor and the asymmetric conduction follows as a direct result of this.

First it is important to define forward and reverse bias. When a potential (bias) is applied in such a way that the Schottky barrier becomes very conducting then it is said that a forward bias has been applied and this quantity is defined positive. When the bias polarity is reversed, the Schottky barrier will become very resistive and then it is said that a reverse bias has been applied and this quantity is defined negative. It will be shown that for an n-type Schottky barrier, forward bias corresponds to the case

when a negative potential is applied to the n-type semiconductor. In a similar way for a p-type Schottky barrier, forward bias corresponds to the case when a positive potential is applied to the p-type semiconductor. The case of an n-type Schottky barrier is considered here.

Consider first the electron current from the semiconductor to the metal, denoted $J_{s \rightarrow m}$. When a negative potential is applied to the n-type semiconductor (forward bias), the total energy of the bulk semiconductor electron density is increased relative to the total energy of the metal electron density. This leads to a continuous loss (flow) of electrons from the semiconductor to the metal. When a positive potential is applied to the semiconductor (reverse bias), the total energy of the bulk semiconductor electron density is reduced relative to the metal electrons. The electron flow from the semiconductor to the metal then decreases towards zero. The barrier to electron flow from the metal to the semiconductor is virtually unaffected by any applied bias and to a first approximation this current, denoted $J_{m \rightarrow s}$, is almost a constant. Hence when a forward bias is applied, a large net current flows from the semiconductor to the metal, but in reverse bias the net current from the metal to the semiconductor is very small. The current-voltage characteristics are therefore highly asymmetric.

In order that an electron may contribute to the semiconductor to metal current it must first traverse the depletion region and then it must successfully be emitted into the metal. Thermionic emission theory (TET) describes the situation when emission into the metal limits the current, and Diffusion theory (DT) describes the situation when transport through the depletion region limits the current. These two theories are now outlined.

4.3.2 Thermionic Emission Theory and Diffusion Theory

The theories of electrical conduction in Schottky barriers have been developed by several people and their work is well documented in "Metal-Semiconductor Contacts", by E.H.Rhoderick(4) (1978), pp.77. In this section Thermionic emission theory is only briefly reviewed, but some extra comments

will be made regarding Diffusion theory.

Thermionic Emission Theory (TET)

Consider the hypothetical situation where electrons are not able to communicate between the semiconductor and the metal. If a forward bias V is applied, the electric field in the semiconductor reduces and electrons diffuse into the depletion region but none is emitted into the metal. The electron density in the semiconductor will therefore adjust until the drift and diffusion currents cancel and then a new thermal equilibrium will have been attained. The new conduction band electron density, denoted n, is best described using an electron quasi-Fermi level, denoted E_{Fn}, and E_{Fn} is defined by the equation

$$n(x) = N_c \exp\left[(E_{Fn}(x) - E_c(x))/kT\right], \tag{4.12}$$

where N_c is the conduction band effective density of states. For this case, thermodynamic equilibrium is maintained and we write $E_{Fn} = E_F^{\,s}$. Note however that $E_F^{\,s}$ has increased by $|e|\,V$ relative to the metal. Fig.4.4 shows the adjusted energy band diagram.

In reality electrons can travel between the semiconductor and the metal. An expression for the semiconductor to metal current $J_{s\rightarrow m}$ can be found if it is assumed that each semiconductor electron which impinges on the metal-semiconductor interface is emitted into the metal and does not return. The conduction band electrons can be treated as a classical Maxwellian gas and so from the kinetic theory of gases(13)

$$J_{s\rightarrow m} = \frac{|e|n(o)v_{th}}{4} = \frac{|e|N_c v_{th}}{4}\, e^{-(\phi_b - |e|V)/kT}, \tag{4.13}$$

where v_{th} is the thermal velocity of the electrons ($v_{th} \sim (2kT/m)^{1/2}$). The

second equality follows from eqn.(4.12) and by setting $E_{Fn} = E_F^s$ (see Fig.4.4). If the metal to semiconductor current is assumed to be constant for all biases and equal to $-J_{s \rightarrow m}(V = o)$ then the total Schottky barrier current at bias V is

$$J(V) = \frac{|e|N_c v_{th}}{4} e^{-\phi_b/kT} (e^{|e|V/kT} - 1) , \qquad (4.14)$$

and this is often written as

$$J(V) = A^* T^2 e^{-\phi_b/kT} (e^{|e|V/kT} - 1) \qquad (4.15)$$

where A^* is a constant independent of V, T.

Eqn.(4.15) will correctly describe the Schottky barrier current-voltage characteristics if

(1) the current is sufficiently small so that thermal equilibrium in the semiconductor is maintained, i.e. $E_{Fn} = E_F^s$,

(2) all semiconductor electrons impinging on the metal cross into metal and do not return,

(3) the metal to semiconductor current is independent of bias,

(4) the semiconductor electron density is non-degenerate.

Conditions (1) and (3) will be discussed later. The correctness of condition (2) is perhaps not clear. It should be noted that each individual electron which is emitted into the metal is "hot" relative to the metal electrons. It therefore quickly loses energy by impact ionisation and other processes, and therefore cannot return to the semiconductor. As a guide the mean free path for this impact ionisation is ~ 400 Å [14].

Diffusion Theory

Consider the situation where the bulk semiconductor is not able to replenish the electron density emitted into the metal in forward bias. The current is

then limited by electron transport through the depletion region and the semiconductor electron density is significantly displaced from thermal equilibrium.

The electric field strength in the depletion region is typically $10^5 - 10^6$ V cm^{-1} and the electron concentration may vary by 10 orders of magnitude in $\sim$ 0.2 μm. It is not straightforward to describe electron transport in such an extreme environment. Classical arguments(6,15), where the conduction band electron density is treated as a Maxwellian gas, allow the electron current density to be written thus

$$J = |e|\mu n \mathcal{E} + |e| D \frac{dn}{dx} \quad ; \quad D = \frac{kT}{e}\mu \quad , \qquad (4.16)$$

where μ is the low-field electron mobility and D is the electron diffusion coefficient. These arguments require that after each collision the electron completely loses memory of its previous state, and also that the electron concentration must be approximately constant over one mean free path length, denoted ℓ. Hence eqn.(4.16) is only valid if,

$$\left.\begin{array}{ll} \text{(a)} & \ell |e| \mathcal{E} \ll kT \\ \text{(b)} & \ell \dfrac{dn}{dx} \ll n \end{array}\right\} \qquad (4.17)$$

For a typical Schottky barrier condition (a) will be fulfilled if $\mu \ll 20$ cm^{2}V^{-1} s^{-1} ($\mu \simeq |e|\ell / mv_{th}$). If however conduction is limited by electron transport through the depletion region then condition (b) will most likely break down close to the metal-semiconductor interface. It will be shown in Chapter 6, section 6.6 that according to Diffusion theory the conduction band electron quasi-Fermi level will have a very steep gradient near the interface and this will further increase dn/dx. An example is schematically shown in Fig.4.4. It follows therefore that for most cases

it is probably incorrect to use eqn.(4.16) and that more fundamental statistical arguments are required. Nevertheless a-Si has a very low extended state mobility ($\mu \approx 10\,cm^2\,V^{-1}\,s^{-1}$) and so, at least for small biases, it may be correct to use eqn.(4.16) here.

The maximum possible current which the bulk semiconductor can support is when the electron quasi-Fermi level at the interface $E_{Fn}(o)$ is coincident with the metal Fermi level. This is the limit used in Diffusion theory and from eqn.(4.16) it can be shown that the resulting current-voltage characteristics is approximately given by the equation

$$J(V) \approx |e|\mu N_c|\mathcal{E}(0,V)|e^{-\phi_b/kT}(e^{|e|V/kT}-1), \tag{4.18}$$

where $\mathcal{E}(0,V)$ is the electric field at the interface (x = o) and the bias is V. This result is derived for the a-Si case in Chapter 6, sub-section 6.6.

For an a-Si Schottky barrier it can be shown that $\mathcal{E}(0,V) \approx -(V_{BI}-V)/L_o$, where L_o is a constant. It follows that J(V) is dominated by the exponential term in eqn.(4.18) and thus it is reasonable to write,

$$J(V) = K_D e^{-\phi_b/kT}(e^{|e|V/kT}-1), \quad K_D = |e|\mu N_c(V_{BI}-V)/L_o, \tag{4.19}$$

where K_D is almost a constant. Note the similarity between this result for Diffusion theory and eqn.(4.15) which gives J(V) according to Thermionic emission theory.

<u>Thermionic Emission Theory Versus Diffusion Theory</u>

According to both theories, the current-voltage characteristics are of the form

$$J(V) = J_o(\exp(|e|V/kT)-1) \tag{4.20}$$

where J_o is approximately a constant. The actual values of J_o however, as calculated by the two theories, will differ in magnitude and also their

temperature dependencies are slightly different. Experimentally it is unlikely that the slight difference in temperature dependence can be used to deduce which theory best describes the conduction process. We concentrate here on the exact value of J_o.

Most generally in forward bias $E_F^m < E_{Fn}(o) < E_F^s$, where $E_{Fn}(o)$ is the position of the conduction band electron quasi-Fermi level at the metal-semiconductor interface. It can be shown (see section 6.6) that following the arguments used in the Diffusion theory, the current density can be written in terms of $E_{Fn}(o)$,

$$J(V) = |e|\mu N_c \, |\mathcal{E}(0,V)| e^{-\phi_b/kT} \; e^{|e|V/kT} \, (1 - e^{E_{Fn}(o)/kT}), \qquad (4.21)$$

where $E_{Fn}(o)$ is measured from the bulk semiconductor Fermi level. Experimentally at forward biases $V >> kT/|e|$ the current-voltage relation can often be written as

$$J(V) = J_o e^{|e|V/kT} \quad , V >> kT/|e| \quad , \qquad (4.22)$$

where J_o is simply taken as an experimental parameter. Substituting eqn.(4.22) into eqn.(4.21) and using the expression for $\mathcal{E}(0,V)$ then gives

$$E_{Fn}(o) = kT \; \ln(1 - B(V)J_o), \qquad (4.23)$$

where $B(V) = \dfrac{L_o e^{\phi_b/kT}}{|e|\mu N_c} \quad \dfrac{1}{V_{BI} - V}$, and J_o is found from experiment.

Fig.4.5 shows a plot of $E_F^s - E_{Fn}(o)$ versus BJ_o for a forward bias such that $V_{BI} - V = 0.2$ volts. If the value of BJ_o exceeds 0.1 then the drop in the conduction band electron quasi-Fermi level quickly becomes significant,

and also note that B is largest for low mobility materials. This equation will be used in Chapter 7 to estimate $E_{Fn}(o)$ from experimental current-voltage plots.

From experiments it is thought that Thermionic emission theory is applicable for high mobility semiconductors. Even for low mobility semiconductors it has not been conclusively shown that Diffusion theory gives a better description[16]. Recently it has been proposed that Diffusion theory is correct for a-Si Schottky barriers[17-19] and this proposition is investigated further in Chapter 7. As a word of caution it should be remembered that Diffusion theory is based on a current density equation which may not be applicable in the electron environment of the semiconductor depletion region.

4.3.3. Current-Voltage Characteristics for a Thin Insulator MIS Device

A thin insulator MIS device is a Schottky barrier-like device where the insulator is sufficiently thin so that electrons can quantum-mechanically tunnel between the metal and the semiconductor. Indeed according to the Bardeen model even an "ideal" Schottky barrier is more properly described as a thin insulator MIS device and the considerations in this section form a natural extension to that model.

In sub-section 4.2.3 it was shown that the presence of a thin insulating layer sandwiched between the metal and semiconductor can affect the Schottky barrier height ϕ_b. In particular it was shown that the barrier height becomes dependent on the electric field in the depletion region and hence $\phi_b = \phi_b(V)$. If the insulator thickness δ is greater than 10-15 Å then a significant proportion of any applied bias may be dropped across the insulator and this is a common cause of "non-ideal" Schottky barrier current-voltage statistics. For a thin insulator MIS device the current-voltage

characteristics often obey the relation

$$J = J_o \exp(|e|V/\eta kT)\,(1 - \exp(-|e|V/kT))$$

$$\approx J_o \exp(|e|V/\eta kT), \quad V >> kT/|e| \qquad (4.24)$$

where J_o and η are approximately constant. J_o is called the saturated current density and η is called the ideality factor. If J_o and η are known it is possible to deduce some information about the interfacial region.

It can no longer be generally assumed that the states at the semiconductor-insulator interface are in equilibrium with the metal. Card and Rhoderick[20-21] (1971) introduce two separate interface state densities :

N_{ss}^{s} = density of interface states in equilibrium with the semiconductor

N_{ss}^{m} = density of interface states in equilibrium with the metal.

If Diffusion theory applies, or $\delta \rightarrow o$ then $N_{ss}^{s} = 0$. Otherwise it may be expected that both densities are finite and the exact values will depend on the insulator thickness. Card and Rhoderick assume that the densities are constant over the relevant energy range and they can then calculate the ideality factor. For an a-Si Schottky barrier the electric field in the semiconductor is rather different to that found in a crystalline Si Schottky barrier (see sub-section 4.2.2), but the analysis is easily adjusted to give,

$$\eta = 1 + \left\{ \left[\frac{\varepsilon_s \varepsilon_o / L_o + |e| N_{ss}^{s}}{1 + (\delta/\varepsilon_i \varepsilon_o)|e| N_{ss}^{m}} \right] \frac{\delta}{\varepsilon_i \varepsilon_o} \right\} \qquad (4.25)$$

where ε_s and ε_i are the dielectric constants of the a-Si and the insulator

respectively. L_o effectively replaces the depletion width W, it has units of length and is defined in Chapter 6, section 6.2.

There are several important points arising from eqn.(4.25). First note that η is always greater than unity. Also, the interface states in equilibrium with the metal may be thought of as an extension of the metal and they act to pin the barrier height and thus reduce η. The interface states in equilibrium with the semiconductor act in the very opposite manner and they result in an increase in η. Card and Rhoderick[21] (1971) show that for a crystalline Si: oxide : metal system $N_{ss}^{m} >> N_{ss}^{s}$ if $\delta < 25$ Å, and $N_{ss}^{s} >> N_{ss}^{m}$ if $\delta >> 25$ Å. McGill et al[22] (1979) examine a similar system for a-Si and they argue that even for $\delta < 25$ Å there may still be a large proportion of the interface states in equilibrium with the semiconductor. If the a-Si is etched in HF before the metal is evaporated on top, the insulator thickness should be less than 25 Å but even then it may not be possible to make the simplification $N_{ss}^{s} = 0$.

Another effect of the insulating layer is to reduce the number of electrons emitted to and from the metal. The extended state wavefunctions can penetrate into the insulator but their amplitudes will exponentially reduce with distance. The penetration also depends on the height of the energy step, denoted χ, which is required before an electron can travel freely from the semiconductor via the insulator conduction band to the metal. Card and Rhoderick[20] develop analysis using a very simple model which shows that the effect of the insulating layer is to reduce the emission constant A^* by $\exp(-\chi^{1/2}\delta)$. It is difficult to make an accurate estimate for χ but experiments have shown that if $\delta \sim 20$ Å then the emission constant may be reduced by 1-2 orders of magnitude.

When insulator thicknesses are greater than ~ 50 Å the current values are very small and the device behaves more like a thick insulator MIS structure. It will then be more certain that the electron quasi-Fermi

level is flat and coincides with the bulk Fermi level. Also the states at the semiconductor-insulator interface will be in equilibrium with the semiconductor and this can affect the current mechanisms. If a forward bias is applied the interface states will fill with electrons but there will be a continuous leakage of these electrons through the insulator to the metal, and this gives rise to a new current. The inverse process occurs when a reverse bias is applied. Electrons will tunnel from the metal into empty interface states and from there they will be thermally excited into the semiconductor conduction band. If a large forward or reverse bias is applied, the metal Fermi level can be made to be coincident with the valence or conduction band of the semiconductor. At such biases this tunnelling current increases by orders of magnitude. Indeed the scanning of the metal Fermi level through a range of semiconductor energy levels has been used as a spectroscopic tool to investigate interface state densities[23]. Balberg et al, in a series of papers[24-27] have studied these effects in thin insulator a-Si MIS structures.

4.3.4 Real Reverse Bias Current-Voltage Characteristics

Experimentally it is found that the reverse bias current is often considerably larger than the values predicted by eqns.(4.15), (4.19) or (4.24). The Schottky barrier is said to have "soft" reverse bias characteristics and there are three common reasons :

1. Thermionic field emission
2. Edge effects
3. Generation current

Thermionic field emission refers to the process where electrons tunnel through part of the semiconductor depletion region. It has been discussed how electrons can tunnel through a thin insulating layer and it may be expected that they could tunnel through a similar thickness of semiconductor. The effect on the barrier height is normally very small because

the electric field in the depletion region is much smaller than the electric field in the insulator. The effect can become prevalent however at large reverse biases/heavy doping when the electric field strength in the depletion region is large. Padovani and Stratton[28] (1966) have developed analysis to describe this effect.

Edge effects are the most common reason for soft reverse bias characteristics. Yu and Snow[29] (1968) have shown that the electric field near the edge of the metal contact may be significantly larger than in the rest of the diode (the electric field lines are more crowded due to the abrupt edge of the contact and also the adjacent semiconductor-air interface may introduce larger charge densities). The result is that in reverse bias when the electric field is very large, appreciable tunnelling/barrier-height lowering occurs at the contact edge and this leads to an increase in reverse bias current. The effect can be eliminated by introducing a guard-ring around the diode (normally a reverse-biased p-n junction).

If the various tunnelling effects are negligible then generation current may dominate the reverse bias current. Electrons travel from the metal to the semiconductor valence band, they are thermally excited to the conduction band and are then swept to the back contact by the built-in electric field. The limiting process is the thermal excitation rate and thus generation current is more important in low-lifetime semiconductors such as GaAs. An estimate of the generation current in a reverse biased a-Si Schottky barrier is made in Chapter 6, sub-section 6.7.2.

4.3.5 Far-Forward Bias Current-Voltage Characteristics

When the forward bias approaches the value of the built-in potential V_{BI}, the Schottky barrier is said to be in far-forward bias. At such biases the current is no longer limited by the barrier region, but instead the

current can be

1. limited by the electron supply from the back contact,
2. limited by the bulk resistance of the sample,
3. space-charge limited due to an injecting back contact.

If the semiconductor bulk Fermi level lies close to the conduction band edge (i.e. $E_c - E_F < 0.1$ eV), then near flat-band conditions the emission current $n(o)v_{th}/4$ becomes very large. At such biases the back contact may not be able to supply sufficient carriers and so the current is limited. This effect is very common in crystalline Si and GaAs Schottky barriers.

In materials where the Fermi level lies deeper in the band-gap the electron emission current near flat-band may not be very large. The back contact may be able to supply the required current and then the resistance of the semiconductor bulk will limit the current. The far-forward bias current will approximately follow the relation

$$I = I_o \left\{ \exp \left[|e|(V - I R_s)/kT \right] - 1 \right\} \quad , V < V_{BI} \qquad (4.26)$$

and at very large biases

$$I \simeq (V - V_{BI})/R_s \quad , V >> V_{BI} \qquad (4.27)$$

where R_s is the bulk series resistance. Eqn.(4.27) is often used to find the bulk resistance and the built-in potential[30]. It should be noted however that there may also be a potential drop associated with the back contact.

If the semiconductor is very resistive then at high current values the back contact may inject charge and then the current becomes space-charge limited. The I-V relation for such cases should follow a power law $I \propto V^m$

where $m > 1$. The exact value of m depends on the trapping levels in the semiconductor and on the magnitude of the injection[31].

The far-forward bias characteristics of a-Si Schottky barriers normally fall into categories 2 and 3. This is because even at high doping levels $E_c - E_F > 0.2$ eV. Space-charge limited currents are more likely in undoped a-Si and several workers[32,33] have observed power law relationships for such barriers. It is more common however to observe a bulk resistance limited regime and from variable temperature far-forward bias I-V measurements it is then possible to deduce the position of the bulk semiconductor Fermi level.

4.4 EXPERIMENTAL EVALUATION OF SCHOTTKY BARRIER PARAMETERS

4.4.1 Evaluation of the Barrier Height

The barrier height of a Schottky diode depends on the exact fabrication details. It is not possible, for example, to predict with any accuracy the barrier height of a particular metal-semiconductor combination. Therefore it is important to measure the barrier height for each device studied. There are two standard techniques :

(a) Barrier height from current-voltage measurements

The forward bias current for a near-ideal Schottky diode follows the relation

$$J(V) = J_o \exp(|e|V/\eta kT), \qquad V \gg kT/|e| \tag{4.28}$$

where

$$J_o = \begin{cases} A^* T^2 \exp(-\ \phi_b(o)/kT), & \text{Thermionic emission theory} \\ K_D \exp(-\ \phi_b(o)/kT), & \text{Diffusion theory} \end{cases} \tag{4.29}$$

Note that if $\eta > 1.1$ then A^* may incorporate a significant tunnelling term $\exp(-\chi^{1/2}\delta)$ and also K_D has a linear bias dependence which can normally be

ignored. A plot of ℓnJ versus V gives a straight line, and

$$\eta = \frac{|e|}{kT} \cdot \frac{1}{(\text{slope})} , \qquad \text{slope} = \frac{d}{dV} (\ell n\, J). \tag{4.30}$$

Extrapolating to V = 0 gives J_o. If $A^*(K_D)$ are known substitution into eqn.(4.29) gives the zero bias, room temperature barrier height $\phi_b(o)$.

A more reliable method of finding the barrier height is to make J-V plots at various temperatures. A plot of $\ell nJ_o(T)/T^2$ (or ℓnJ_o) versus 1/T should give a straight line with gradient $\phi_b(o)/k$. Strictly speaking the calculated barrier height is for zero temperature but the variation of ϕ_b with temperature is expected to be small. Note that this method directly measures the barrier activation energy. The device area and A^* (K_D) need not be known, but note that $A^*(K_D)$ can be found from the intercept at 1/T = 0.

(b) Barrier height from internal photoemission

The photoelectric determination of the Schottky barrier height involves shining monochromatic light of varying wavelength onto the metal contact. The metal electrons have a small but finite photoelectric cross-section and some electrons are excited by the incident photons to surmount the barrier. They enter the semiconductor and are swept to the back contact by the built-in electric field and this gives rise to a measurable photocurrent. If the incident light only excites metal electrons, and a constant number of the electrons which are excited into the semiconductor successfully reach the back contact, then following the theory of Fowler[34] (1931), the photoresponse current R obeys the following relation

$$R \approx C(h\upsilon - \phi_b)^2 , \qquad h\upsilon - \phi_b >> kT, \tag{4.31}$$

where υ is the frequency of the incident light and C is a constant.

Experimentally the requirements are that

(i) the metal thickness does not exceed the hot electron attenuation length (typically between 200-700 Å [14]),

(ii) the photocurrent is only a small perturbation from thermal equilibrium,

(iii) only sub-band gap light is used. Otherwise electron-hole pairs will be created in the semiconductor and this will dominate the photocurrent.

A plot of $(\text{photocurrent})^{1/2}$ versus $h\nu$ should be a straight line and extrapolating to zero response gives the barrier height. This technique has proved very successful but there are instances where it fails. Non-linearities have been observed in thin MIS devices[35] where it is thought that a significant amount of electrons occupying interface states are excited by the sub-band gap light. It is noticeable that very few photo-emission experiments have been reported for a-Si Schottky barriers[36]. One explanation could be that the relatively high densities of gap states lead to unwanted photoexcited carriers and thus results have been unusable. Certainly Mishima, Hirose and Osaka[19] (1981) find that their photocurrent does not follow eqn.(4.31). Their explanation of an energy-dependent mobility is not entirely satisfactory. In Chapter 7 evidence will be presented which agrees with the view that gap states may often dominate the photocurrent.

4.4.2 Evaluation of the Built-in Potential

The Schottky barrier height ϕ_b is related to the zero bias built-in potential, denoted V_{BI}, thus

$$\phi_b = (E_c - E_F) + |e|\, V_{BI} \qquad (4.32)$$

where E_c and E_F are the bulk semiconductor conduction band edge and Fermi level respectively. Therefore if the bulk Fermi level position is known then it is possible to deduce V_{BI} from the measurements of barrier height.

There are also however several independent methods for finding the built-in potential.

For an n-type crystalline semiconductor with donor density N_D, the Schottky barrier capacitance often fits the equation

$$C = \left(\frac{|e|\varepsilon_s\varepsilon_o N_D}{2}\right)^{\frac{1}{2}} \left(V_{BI} - V - \frac{kT}{|e|}\right)^{-\frac{1}{2}} \tag{4.33}$$

where V is positive for forward biases. Then a plot of $1/C^2$ versus V should be a straight line and extrapolating this line to $1/C^2 = 0$ gives $V_{BI}-kT/|e|$. Serious errors can arise however if there is an appreciable thickness of insulator between the metal and semiconductor, or if deep traps affect the space-charge in the depletion region. An insulator will act as a dielectric capacitor in series with the depletion region, and any interface states which are in equilibrium with the semiconductor will contribute to the depletion region charge response. Cowley[37] (1966) and Fonash[38] (1983) have developed analyses for thin insulator MIS devices and they show that it is often still possible to deduce V_{BI} from a plot of $1/C^2$ versus V. However if the semiconductor has a large density of deep traps the analysis of capacitance data becomes quite complicated and then an estimate using the barrier capacitance is often not possible. This is the case for a-Si Schottky barriers.

If the far-forward bias characteristics of the Schottky barrier are limited by the bulk resistance, then eqn.(4.27) may be used to estimate the zero bias built-in potential. The I-V plot will be a straight line and extrapolating this line to I = 0 gives V_{BI}. However this method may seriously overestimate V_{BI} if there is a significant potential drop across the back contact.

For a-Si Schottky barriers it is perhaps best simply to measure ϕ_b and E_c-E_F and use eqn.(4.32) to find V_{BI}. A property of a-Si is that its

bulk conductivity shows an activated temperature dependence - irrespective of doping it behaves like an intrinsic semiconductor and over a range of temperatures $E_c - E_F \simeq$ constant. Therefore if the Schottky barrier is bulk resistance limited in far-forward bias then variable temperature I-V plots will give $E_c - E_F$. The built-in potential then follows from a measurement of ϕ_b.

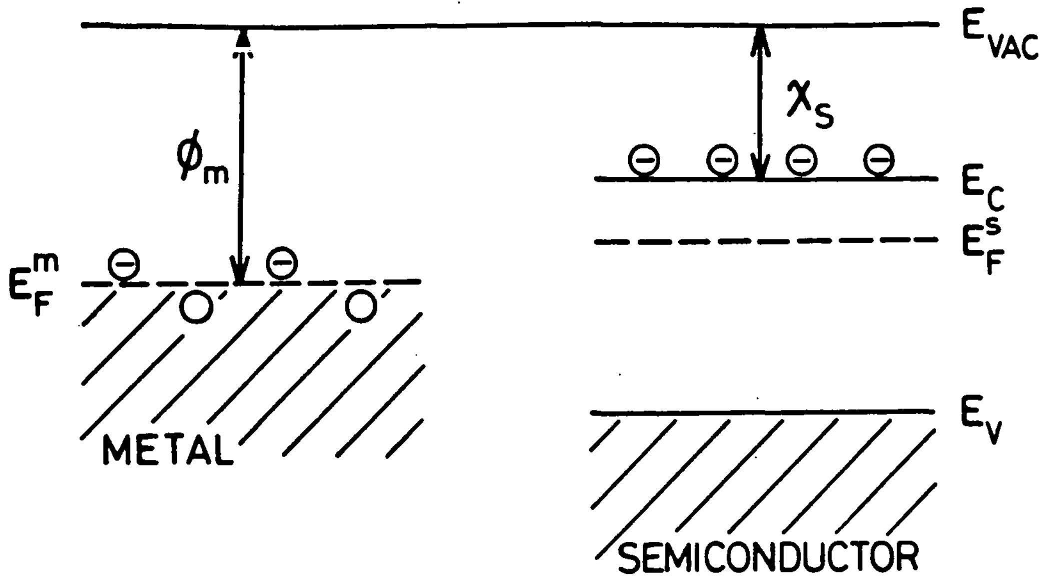

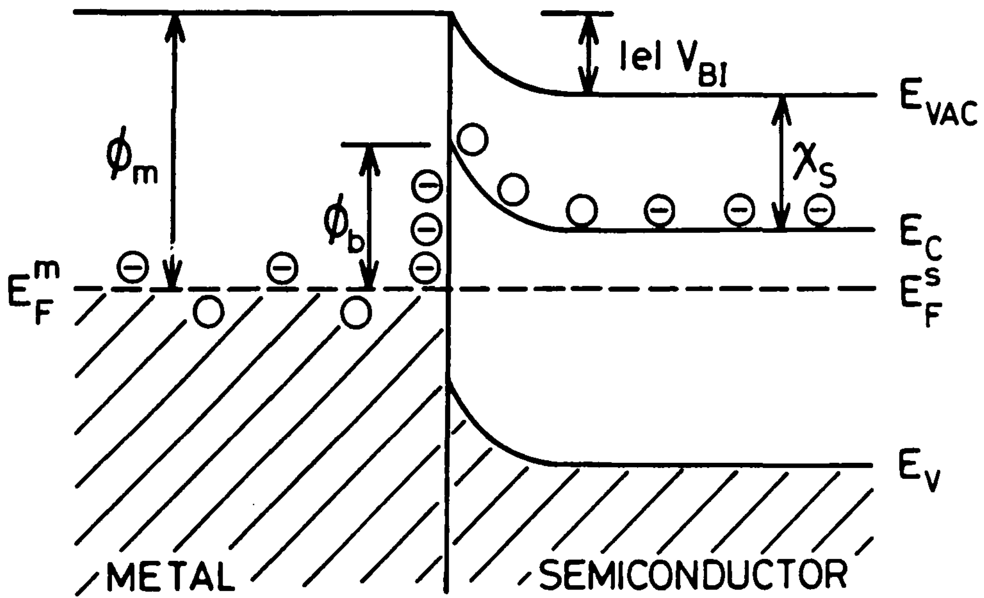

FIGURE 4.1: Energy band diagrams of a metal and semiconductor (a) at a distance apart, (b) in intimate contact.

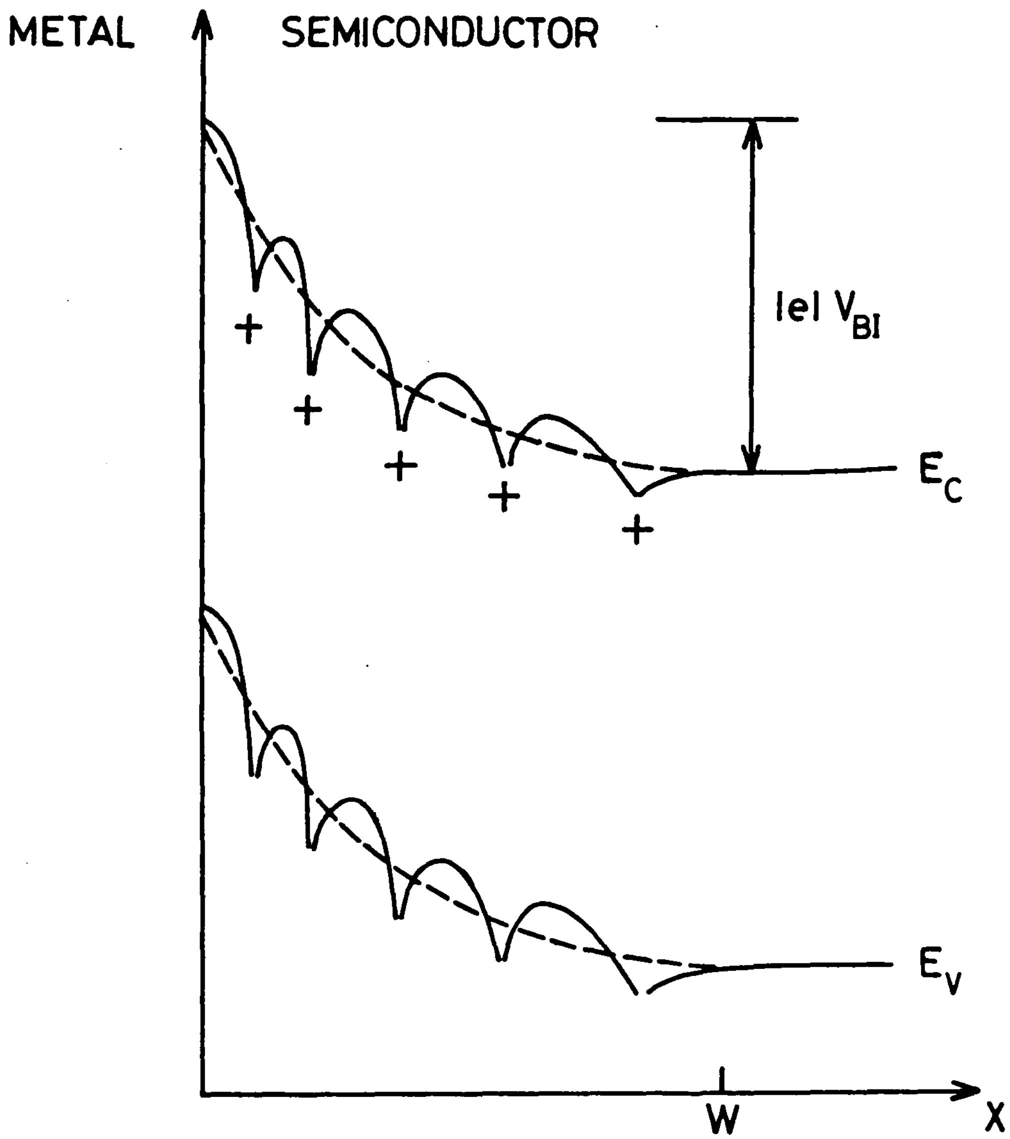

FIGURE 4.2: Schematic diagram of the energy bands in the depletion region of a Schottky barrier as experienced by a free electron.

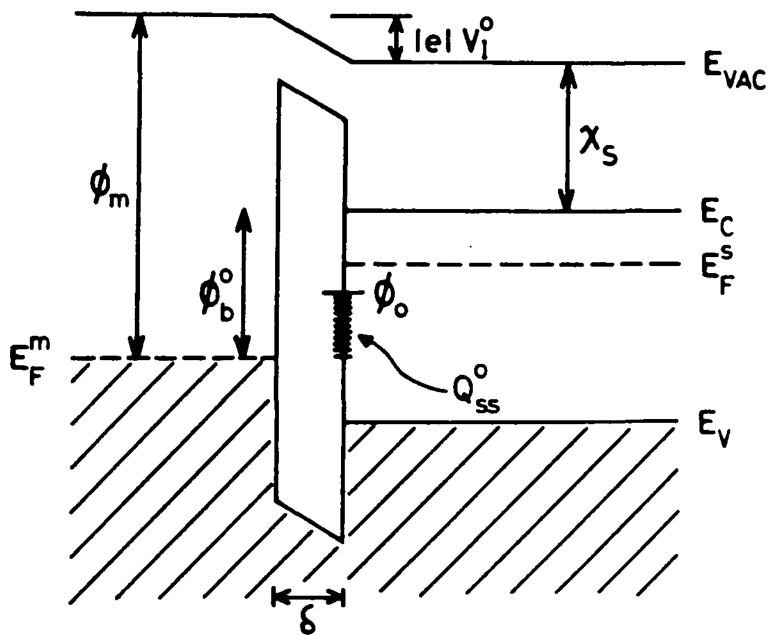

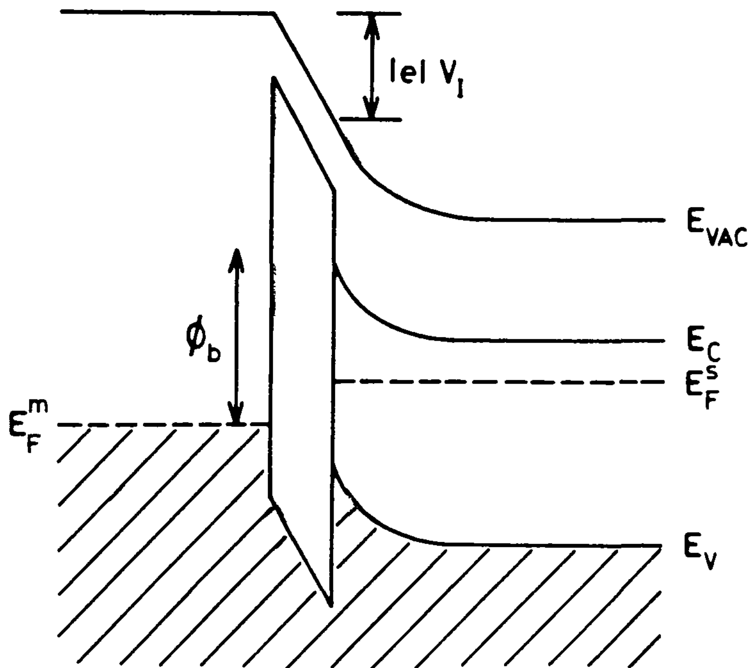

FIGURE 4.3: Bardeen model of the Schottky barrier energy band diagram (a) at flat band conditions and (b) when only a small forward bias is applied. The insulator thickness δ has been greatly exaggerated.

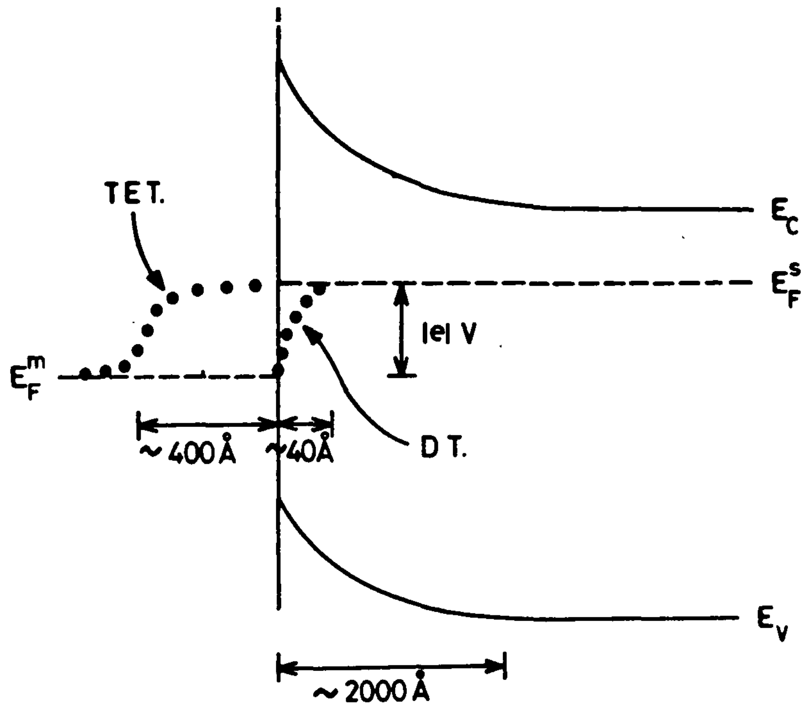

FIGURE 4.4: Energy band diagram for a Schottky barrier in forward bias. The dotted lines indicate the position of the conduction band electron quasi-Fermi level as according to Diffusion theory (DT.) and Thermionic emission theory (TET.).

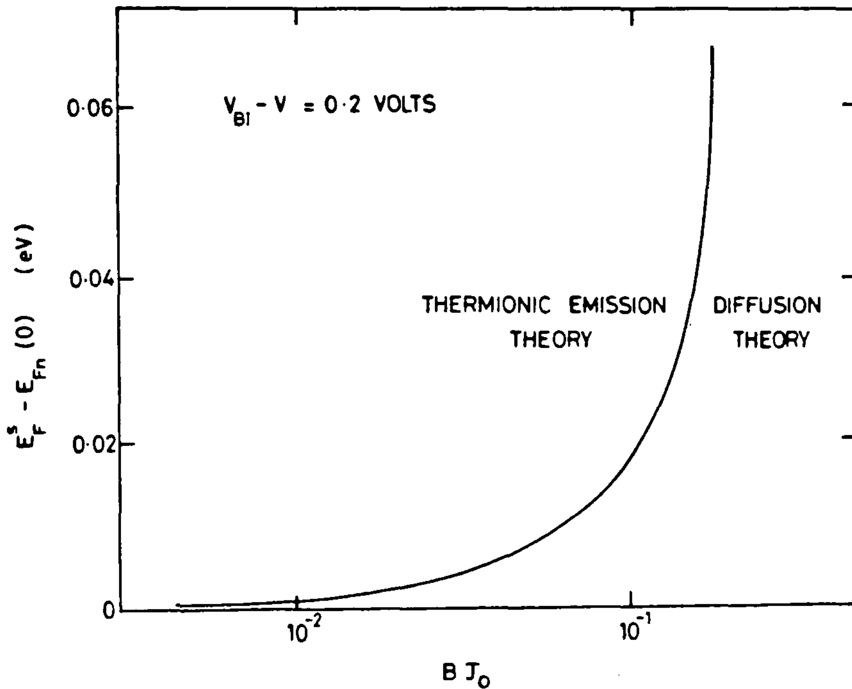

FIGURE 4.5: A plot of the drop in the conduction band electron quasi-Fermi level as a function of J_O . See eqn.(4.23).

CHAPTER 5

A THEORY OF THE ADMITTANCE OF AN AMORPHOUS SILICON SCHOTTKY BARRIER

5.1 INTRODUCTION

The admittance of a Schottky barrier is usually measured by applying a small sinusoidal potential at a given frequency, and the barrier admittance is given by the ratio of the resultant current to the applied potential. Most often admittance is separated into its real and imaginary parts. Conductance (G) is the real part and the imaginary part is obtained from the capacitance (C). C and G can be functions of bias (V), temperature (T) and signal angular frequency (ω), and by varying V, T, ω information can be deduced about the Schottky barrier and the material properties of the semiconductor.

A useful application of Schottky barrier admittance measurements has been in the investigation of deep level defects in semiconductors. Roberts and Crowell[1] (1970) developed theory to show how discrete deep levels may be detected using C-V measurements. Maserjian[2] (1969) made a study of the admittance problem for the case of a continuous distribution of deep levels, and Losee[3] (1975) developed a numerical routine for the "admittance spectroscopy" of deep defect levels. More recently thermally stimulated relaxation experiments[4] have been developed where admittance is used to monitor the relaxation. These experiments (e.g. Deep Level Transient Spectroscopy (DLTS)) have now become almost standard in the electrical characterisation of semiconductors.

Recently, various admittance measurements have been made on amorphous silicon (a-Si) Schottky barriers [5-18]. The results however have proved difficult to interpret. Amorphous silicon has an extremely large density of states deep in the mobility gap and these states significantly affect the

charge response in the barrier. Also, most of the measurements have been made on undoped a-Si Schottky barriers. At room temperature undoped a-Si has a low bulk conductivity and the related bulk dielectric relaxation time is typically $\sim$ 0.1 sec. Most admittance measurements use signal frequencies which are greater than 10 Hz and so many measurements simply examine the "high-frequency" dielectric behaviour of the a-Si.

This chapter looks at the low frequency admittance when deep states in the mobility gap have a large influence on the barrier charge response. A theoretical model is set up, equations are derived to describe the charge response, and then these equations are solved for the admittance. It should be noted that many assumptions and approximations will be made. These will be examined in Chapter 6. Chapter 6 will also develop the calculations to allow a more quantitative analysis of experimental admittance results.

The reader is referred to three papers which are particularly relevant to the theory of this chapter. They are the papers by Viktorovitch and Moddel[6] (1980), Abram and Doherty[19] (1982) and Cohen and Lang[20] (1982). Also, the analysis is similar to that found in MIS (Metal-Insulator-Semiconductor) theory - the proposed energy distribution of bulk deep states in a-Si is quite similar to the two dimensional distribution of interface states in MIS devices - and a good text on MIS physics is "MOS Physics and Technology" by Nicollian and Brews[21] (1982). Finally, much of the analysis and discussion in the later sections of this chapter is also found in a paper by Archibald and Abram[22] (1983).

5.2 SCHOTTKY BARRIER MODEL : ENERGY BAND DIAGRAM

The aim of this section is to set up an energy band diagram and coordinate system for the Schottky barrier and to define various important functions which will be used later to help solve for the admittance.

The energy band diagram shown in Fig 5.1 is for an n-type Schottky barrier under a d.c. reverse bias V_R. The barrier profile is described by the function $|e|\ \psi(x)$ where x is the distance from the metal-semiconductor

interface. This function reaches a value $|e|\psi_s$ at the interface, ψ_s being the sum of the built-in potential and the reverse bias V_R. It should be noted that the potential $\psi(x)$ and the electrostatic potential have opposite sign. When a positive voltage is applied to the Schottky barrier, ψ_s is reduced and the Schottky barrier is said to be forward-biased.

The other function described in the energy band diagram is the conduction band electron quasi-Fermi level (q.f.l.), denoted E_{Fn}. This function is used to describe the density of electrons occupying states above the conduction band mobility edge. If Maxwell-Boltzmann statistics are applicable, and under steady-state conditions, the conduction band electron density , denoted n_o, can be found from E_{Fn} thus

$$n_o(x) = N_c \exp\left\{ \left[E_{Fn} - (E_c + |e|\psi(x)) \right] /kT \right\} , \qquad (5.1)$$

where N_c is the conduction band effective density of states, and E_c is the energy of the conduction band mobility edge in the neutral bulk. The subscript 'o' is used to indicate equilibrium conditions. Under such equilibrium conditions it is often assumed that the electrons in the depletion region are in thermal equilibrium with electrons in the neutral bulk. If this is the case, then the electron q.f.l. is a constant and coincides with the bulk Fermi level E_F. This assumption has been made in Fig 5.1. Of course when a bias is applied, current flows through the device, and then the system is not strictly in thermodynamic equilibrium. At finite biases therefore $E_{Fn} = E_F$ is only an approximation.

The barrier admittance is usually measured by applying a small sinusoidal potential, at angular frequency ω , superimposed on the d.c. bias. The applied small signal has the effect of setting up a time-varying

potential $\phi(x,t)$ throughout the barrier. Then the total barrier potential, denoted Ψ, is

$$\Psi(x,t) = \psi(x) + \phi(x,t) \quad . \tag{5.2}$$

$\phi(x,t)$ depends on the applied a.c. potential, the response of the conduction band electrons and on the emptying and filling of states in the mobility gap. This function will be evaluated later.

The small signal may also introduce a time-varying component to the electron q.f.l. E_{Fn}. At low signal frequencies the conduction band electrons might be expected to maintain thermal equilibrium with the bulk and then $E_{Fn} = E_F$. However at sufficiently high frequencies thermal equilibrium will not be maintained and E_{Fn} will vary with position and time. The time-varying part of E_{Fn} is separated out thus

$$E_{Fn}(x,t) = E_F + \delta E_{Fn}(x,t) \ , \tag{5.3}$$

and it follows from eqns. (5.1) and (5.2) that the total time-varying conduction band electron density is

$$n(x,t) = n_o(x)\exp\left\{ \left[\delta E_{Fn}(x,t) - |e|\phi(x,t) \right] /kT \right\} \quad . \tag{5.4}$$

If the signal is small so that $\phi \ll kT/|e|$, then the time-varying part of n, denoted δn, can be approximately written as

$$\delta n(x,t) \simeq \frac{n_o(x)}{kT} \left(\delta E_{Fn}(x,t) - |e|\phi(x,t) \right) \ , \quad \phi \ll kT/|e| \ . \tag{5.5}$$

Note that as the signal frequency tends to infinity, then the electron response δn must tend to zero. Therefore at large signal frequencies it

follows from eqn. (5.5) that $\delta E_{Fn} \approx |e|\phi$. Normally signal frequencies are chosen so that $\delta E_{Fn} << |e|\ \phi$.

5.3 TREATMENT OF GAP STATES

As stated in the introduction to this chapter, deep states in the mobility gap, referred to here as gap states, significantly affect the charge response of an a-Si Schottky barrier. It is necessary therefore to evaluate this gap state charge contribution.

5.3.1 Gap State Kinetics

The gap state electron occupancy will normally be determined by capture and emission processes between gap states and extended states in the conduction and valence bands (localised state to localised state transitions are thought to be much less probable). A simple approach is taken here, similar to that by Shockley and Read(23) (1952), and a good text on the subject is "Semiconductor Statistics" by J.S. Blakemore(24) (1962).

Consider a single level of monovalent gap states (or traps), of density N_T situated in the mobility gap at energy E_T. The density of those gap states which are occupied by electrons, denoted n_T, is given by

$$n_T = N_T \ f_T \ , \qquad (5.6)$$

where the occupation function f_T is the probability that a gap state at energy E_T is occupied. At thermal equilibrium the density of occupied traps is a constant and detailed balance(24) applies to each individual capture and associated emission process. In particular it follows that the

rate of electrons captured by traps = rate of electrons emitted from traps,

rate of holes captured by traps = rate of holes emitted from traps.

Algebraically, this may be written as

$$\left.\begin{aligned} c_n n_o N_T(1-f_{TO}) &= e_n N_T f_{TO} \\ c_p p_o N_T f_{TO} &= e_p N_T(1-f_{TO}) \end{aligned}\right\} , \qquad (5.7)$$

where,

c_n = probability per unit time that a conduction band electron is captured by an empty trap,

e_n = probability per unit time that a trapped electron is emitted to the conduction band

and c_p, e_p are similarly defined for holes and the valence band. n_o and p_o are the electron and hole densities at thermal equilibrium and f_{TO} is the occupation function at thermal equilibrium.

At thermal equilibrium the gap state occupancy function is given by the Fermi-Dirac function.

$$\text{i.e.}\quad f_{TO} = \frac{1}{\exp\left[(E_T-E_F)/kT\right]+1} , \qquad (5.8)$$

where E_F is the semiconductor Fermi level and degeneracy terms have been ignored. The free carrier densities may also be written in terms of E_F. Assuming the semiconductor is non-degenerate,

$$n_o = N_C \exp\left[(E_F-E_C)/kT\right], \; p_o = N_V \exp\left[(E_V-E_F)/kT\right] \qquad (5.9)$$

where N_C and N_V are the effective density of states in the conduction and valence bands respectively.

Several important results which relate the capture and emission

coefficients follow from eqns. (5.7), (5.8) and (5.9). They are

$$\left.\begin{aligned} e_n &= c_n n_o(1-f_{TO})/f_{TO} = c_n N_c \exp\left[(E_T - E_C)/kT\right] \\ e_p &= c_p p_o f_{TO} / (1-f_{TO}) = c_p N_V \exp\left[(E_V - E_T)/kT\right] \end{aligned}\right\} , \quad (5.10)$$

and

$$\left.\begin{aligned} c_n n_o + e_n &= c_n n_o / f_{TO} \\ c_p p_o + e_p &= c_p p_o /(1-f_{TO}) \end{aligned}\right\} . \quad (5.11)$$

Hence under thermal equilibrium conditions the emission coefficients e_n, e_p may be got from their respective capture coefficients c_n, c_p. The capture coefficients are often taken to be the more intrinsic property of the defect level. Their value depends on the transition processes (e.g. multiphonon, auger, radiative) and may be functions of, for example, the energy position of the state, the charge of the state, temperature and free carrier concentration. Capture coefficients are difficult quantities to calculate and normally they are simply found from experiments.

Now consider the system when an external stimulus (e.g. light or bias) disturbs the free carrier densities from their thermal equilibrium values. Then

$$\left.\begin{aligned} n &= n_o + \Delta n, \quad p = p_o + \Delta p \\ n_T &= n_{TO} + \Delta n_T \text{ and } f_T = f_{TO} + \Delta f_T \end{aligned}\right\} . \quad (5.12)$$

By assigning appropriate signs to each capture and emission process in eqn. (5.7), the contributions can be summed to give the time rate of change

of the gap state electron occupancy.

$$\frac{dn_T}{dt} = c_n n N_T(1-f_T) - e_n N_T f_T - c_p p N_T f_T + e_p N_T(1-f_T) \qquad (5.13)$$

The capture and emission coefficients are assumed to be unchanged from their thermal equilibrium values. This assumption is often used and it follows that the capture and emission coefficients are still related by eqn. (5.10).

Eqn. (5.13) is used to find the disturbed occupation function f_T. Consider first the case when the stimulus does not vary with time. Then $dn_T/dt = 0$, and rearranging eqn.(5.13) gives

$$f_T = \frac{c_n n + e_p}{c_n n + e_n + c_p p + e_p} \qquad (5.14)$$

If the stimulus does vary with time, then the time-varying part of f_T is $\Delta f_T(t)$, and this is found by substituting the time-varying values for n and p of eqn. (5.12)into eqn. (5.13). The thermal equilibrium terms cancel giving

$$\frac{d}{dt}(\Delta f_T(t)) = \left(c_n(1-f_{TO})\Delta n(t) - c_p f_{TO}\Delta p(t)\right)$$
$$- \left(c_n n_o + e_n + c_p p_o + e_p + c_n \Delta n(t) + c_p \Delta p(t)\right) \Delta f_T(t) \qquad (5.15)$$

This is a differential equation of the form

$$\frac{dy}{dt} = A(t) - B(t)y$$

and for certain distrurbances $\Delta n(t)$, $\Delta p(t)$ the equation may be solved for $\Delta f_T(t)$.

Results (5.14) and (5.15) form the basis of the calculations performed in the following sub-sections. However, a-Si has a distribution of deep states and in order to use these single trap level results a suitable gap state model is required. The calculations are therefore interrupted to introduce such a model.

5.3.2 Gap State Model for a-Si

Amorphous silicon has an extremely large density of localised states ($\sim 10^{17}$ cm^{-3} eV^{-1}) distributed throughout the mobility gap and these states can be separated into two categories. There are band-tail states which lie close to the mobility edge, and there are deep states, referred to as gap states, which lie deep in the mobility gap. The band-tail states affect the transport of majority carriers, but otherwise they need not be explicitly considered. A gap state is arbitrarily defined to be any localised state existing at an energy greater than 0.2 eV from either mobility edge. It is these gap states which most affect the barrier charge.

The origins and exact nature of the gap states in a-Si are not well understood and so it is only sensible to propose a very simple gap state model which keeps the analysis simple and clear. The following points describe the proposed model.

(1) The various deep levels form a continuous distribution of localised states in the mobility gap and this distribution is described by a density of states function $N(E)$; the number of states per unit volume lying between energies E and E + dE is $N(E)dE$.

(2) $N(E)$ does not vary appreciably over energies of the order of kT.

(3) The gap state electron and hole capture coefficients are assumed to be equal and independent of energy, i.e. $c_n = c_p$ = constant, for all gap states at all energies.

(4) Large electric fields (e.g. 10^5 V cm^{-1}) do not affect the kinetics of capture and emission. Also, even at such high electric fields, electrons cannot tunnel directly from one gap state to another.

Probably the most contentious assumption is that the capture coefficients are a constant for all gap states. What is actually important is that gap states close in energy have similar capture coefficients. The statistics of the system give rise to emission rates which are exponentially dependent on energy, and this exponential will dominate the gap state occupancy if the capture coefficients are more slowly varying. This situation is more probable than having a constant capture coefficient, but ultimately experimental proof is required. Assumption (4) is included so that the previous results derived from the arguments of detailed balance and thermodynamic equilibrium are valid in the depletion region of the Schottky barrier. Lang et al[8] have recently questioned the correctness of this assumption.

Finally it proves convenient to fix the energy scale of N(E) from the energy of the conduction band mobility edge. Hence a gap state at energy E in the neutral bulk becomes a gap state at energy $E + |e|\psi(x)$ in the Schottky barrier depletion region. The electron quasi-Fermi level E_{Fn} may be assumed to be equal to the bulk Fermi level E_F throughout the barrier, and so in the depletion region a gap state at the quasi-Fermi level corresponds to a gap state energy $E_F - |e|\psi(x)$.

5.3.3. Results for a Reverse-Biased Schottky Barrier

This sub-section calculates the electron occupancy of gap states when a constant reverse bias is applied to an a-Si Schottky barrier. A good account of the problem for discrete deep levels is to be found in Chapter 4 of "Metal-Semiconductor Contacts" by E.H.Rhoderick[25] (1978).

A reverse bias will reduce the free carrier densities relative to their thermal equilibrium values, and so it is useful to introduce quasi-Fermi levels (q.f.l's). They are defined in the usual way.

$$n = N_c \exp\left[(E_{Fn}-\tilde{E}_c)/kT\right], \quad p = N_v \exp\left[(\tilde{E}_v-E_{Fp})/kT\right], \qquad (5.16)$$

where E_{Fn} = conduction band electron q.f.l.,

E_{Fp} = valence band hole q.f.l.,

and $\tilde{E}_c$ and $\tilde{E}_v$ are taken to be the <u>absolute</u> energy values for the conduction band and valence band mobility edges respectively, (i.e. $\tilde{E}_c$ and $\tilde{E}_v$ implicitly include the term $|e|\psi(x)$).

An n-type reverse-biased Schottky barrier is considered. It is assumed that the quasi-Fermi levels are constants and that E_{Fn} coincides with the bulk semiconductor Fermi level, and E_{Fp} coincides with the metal Fermi level. A useful expression for the occupation function f_T follows by substituting eqns. (5.10) and (5.16) into eqn. (5.14) and setting $c_n = c_p$ and $N_c = N_v$. Then,

$$f_T = \frac{e^{(E_{Fn}-\tilde{E}_c)/kT} + e^{(\tilde{E}_v-E_T)/kT}}{e^{(E_{Fn}-\tilde{E}_c)/kT} + e^{(E_T-\tilde{E}_c)/kT} + e^{(\tilde{E}_v-E_{Fp})/kT} + e^{(\tilde{E}_v-E_T)/kT}} . \quad (5.17)$$

Note that each exponential term is associated with a particular capture or emission process, and if the term is small then the process is unimportant. This equation is now used to find the gap state electron occupancy in the Schottky barrier.

An energy band diagram is shown in Fig 5.2 and here the barrier is divided into four regions according to which are the dominant capture and emission processes (the arrows indicate electron transitions). Examples are chosen from each of the four regions and approximations are made which simplify eqn. (5.17) in each case. The dashed line in the figure describes an important result which follows from the consideration of the examples. This line is drawn so that almost all of the gap states above the line are empty, whereas gap states below the line are full. The line may be thought

to represent a gap state quasi-Fermi level, but as the examples will demonstrate the occupancy energy-dependence is not always that of a Fermi-Dirac function. Also, an aid to the calculation is the mid-gap energy level E_i, $E_i = (\tilde{E}_c + \tilde{E}_v)/2$.

Example 1: $E_{Fn} > E_i$ (region I, Fig 5.2)

Throughout this region the term $\exp\left[(\tilde{E}_v - E_{Fp})/kT\right]$ is very small, i.e. hole capture from the valence band is negligible. With this fact in mind now consider gap states at energies (a) $E_T > E_i$, (b) $E_T = E_i$ and (c) $E_T << E_i$.

(a) $E_T > E_i$, then $\exp\left[(\tilde{E}_v - E_T)/kT\right] << \exp\left[(E_T - \tilde{E}_c)/kT\right]$, $\exp\left[(E_{Fn} - \tilde{E}_c)/kT\right]$

and so from eqn.(5.17)

$$f_T \simeq \frac{1}{\exp\left[(E_T - E_{Fn})/kT\right] + 1} . \tag{5.18}$$

(b) $E_T = E_i$, then $\exp\left[(E_T - \tilde{E}_c)/kT\right] = \exp\left[(\tilde{E}_v - E_T)/kT\right]$ and so from eqn. (5.17)

$$f_T \simeq \frac{1 + \exp\left[(E_T - E_{Fn})/kT\right]}{2\exp\left[(E_T - E_{Fn})/kT\right] + 1} . \tag{5.19}$$

(c) $E_T << E_i$, then $\exp\left[(E_T - \tilde{E}_c)/kT\right] << \exp\left[(\tilde{E}_v - E_T)/kT\right]$, $\exp\left[(E_{Fn} - \tilde{E}_c)/kT\right]$

and so from eqn. (5.17), $f_T \simeq 1$.

Eqn.(5.18) is the most important result. In the upper half of the band gap the gap state occupancy is described by a Fermi-Dirac function

with E_F replaced by E_{Fn}. This implies that states in the upper half of the mobility gap are in thermal equilibrium with the conduction band electrons and that the processes of electron capture and emission balance in detail. Near mid-gap and below, hole emission to the valence band becomes important and here f_T moves slightly closer to unity than the value predicted from eqn. (5.18). However, this deviation is small and so it is reasonable to ignore all hole processes (capture and emission) throughout region I.

Example 2: $E_{Fn} = E_i$, $E_{Fp} > E_i$ (region II, Fig.5.2).

The calculation is restricted to finding the gap state energy where $f_T = 1/2$. This energy is denoted $E_T(1/2)$. First, hole capture can again be neglected, i.e. $\exp\left[(\tilde{E}_v - E_{Fp})/kT\right] \simeq 0$. Then substituting $E_{Fn} = E_i$ and $E_T(1/2) = E_i + \Delta E_i$ into eqn. (5.17) gives the result $\sinh(\Delta E_i/kT) = 1/2$, i.e. $\Delta E_i \simeq kT/2$. Hence the effect of hole emission from gap states near mid-gap to the valence band is to slightly shift the half occupancy point towards the conduction band, i.e. eqn. (5.18) would underestimate the electron occupancy in this region.

Example 3: $E_{Fn} < E_i$, $E_{Fp} > E_i$ (region III, Fig 5.2)

Throughout this region the conduction and valence bands are both strongly depleted of free carriers, and therefore over a certain range of gap state energies near E_i (depending on the exact values of E_{Fn} and E_{Fp}) electron capture as well as hole capture can be neglected. Then from eqn. (5.17) the occupancy function becomes

$$f_T \simeq \frac{1}{\exp\left[2(E_T - E_i)/kT\right] + 1} \quad , \; E_T \sim E_i \; . \qquad (5.20)$$

Hole emission competes against electron emission, the rates are approximately equal at $E_T = E_i$, and hence $f_T = 1/2$ at $E_T = E_i$. Note also that detailed

balance has broken down and in fact this region is the dominant source of reverse bias generation current (see sub-section 6.7.2).

Example 4: $E_{Fn}, E_{Fp} < E_i$ (region IV, Fig 5.2)

The barrier height of some Schottky barriers is larger than half band-gap. For such barriers minority carrier processes will dominate close to the metal-semiconductor interface. Eqn. (5.17) shows that the hole q.f.l. controls the gap state occupancy in a similar way to the electron q.f.l. in regions I and II.

Most a-Si Schottky barriers have barrier heights between 0.7 and 0.9 eV. The mobility gap is $\sim$ 1.8 eV and therefore region IV can only be small in spatial extent. Further due to the exponential nature of the electron statistics, region II is also very small, and thus to a good approximation we need only consider regions I and III. In this chapter only region I is considered, and the Fermi-Dirac function of eqn.(5.18) is used to describe the gap state occupancy throughout. Chapter 6, sub-section 6.7.1 takes proper account of region III and this extends the calculation to include the case when a large reverse bias is applied.

5.3.4 Results for a Transient Response

The results of this sub-section are not directly required for the subsequent admittance calculation, but they are important for relaxation experiments such as Deep Level Transient Spectroscopy (DLTS) and they also contribute to a better general understanding of the admittance problem. Given the parenthetic nature of this sub-section only one level of mano-valent gap states is considered.

Consider a stimulus which begins at time t = 0, and from then on gives rise to a constant disturbance Δn, Δp of the free carrier densities. This may be the case, for example, when a constant reverse bias is applied to a Schottky barrier or when the barrier is exposed to constant band-gap illumination.

Eqn. (5.15) is used to find the time-varying part of the electron occupancy, denoted $\Delta n_T(t)$, for a monovalent gap state level, density N_T situated at energy E_T. Eqn. (5.15) becomes

$$\frac{d}{dt}\left(\Delta f_T(t)\right) = A - B\Delta f_T(t) \quad , \qquad (5.21)$$

where $A = c_n(1-f_{To})\Delta n - c_p f_{To}\Delta p$,

$$B = c_n n_o + e_n + c_p p_o + e_p + c_n\Delta n + c_p\Delta p$$

Note that A and B are independent of time and the initial condition is $\Delta f_T(0) = 0$. Multiplying the solution for $\Delta f_T(t)$ by N_T gives

$$\Delta n_T(t) = \Delta n_T(\infty)\ (1 - e^{-t/\tau}) \quad , \qquad (5.22)$$

where $$\Delta n_T(\infty) = \frac{c_n(1-f_{To})\Delta n - c_p f_{To}\,\Delta p}{c_n n_o + e_n + c_p p_o + e_p + c_n\Delta n + c_p\Delta p} \cdot N_T$$

and

$$\tau^{-1} \doteqdot c_n n_o + e_n + c_p p_o + e_p + c_n\Delta n + c_p\Delta p \quad .$$

$\Delta n_T(\infty)$ is the change in gap state occupancy after sufficient time has passed for the gap states to come into equilibrium with the disturbed free carrier densities. τ is often called the relaxation time or gap state lifetime and it indicates the time necessary for the gap states to reach their new equilibrium value.

As an illustrative example a simplified case is chosen where $n_o \gg p_o$, and $\Delta n \gg \Delta p$. These conditions often hold when a constant bias is applied to an n-type Schottky barrier. Then hole processes can most

often be completely ignored and $\Delta n_T(\infty)$ and τ become

$$\Delta n_T(\infty) = \frac{c_n(1-f_{To})\Delta n}{c_n n_o + e_n + c_n\Delta n} \cdot N_T, \quad \tau^{-1} = c_n n_o + e_n + c_n\Delta n. \qquad (5.23)$$

Now three different bias conditions are considered in turn.

1. Large forward bias applied to a Schottky barrier :

A gap state level is chosen such that $c_n\Delta n >> c_n n_o + e_n$, and from eqn. (5.23), $\Delta n_T(\infty) = N_T(1-f_{To})$ and $\tau^{-1} = c_n\Delta n$. This means that all empty states are filled and the filling time is inversely proportional to the size of the disturbance. Note also that given $c_n\Delta n >> c_n n_o + e_n$, then the filling time is otherwise independent of the energy level of the state.

2. Very small forward (or reverse) bias applied to a Schottky barrier :

If $|c_n\Delta n| << c_n n_o + e_n$ then from eqn. (5.23) and eqn.(5.11), $\Delta n_T(\infty) = N_T(1-f_{To})f_{To}\Delta n/n_o$ and $\tau^{-1} = c_n n_o/f_{To}$. The number of empty states which are filled is now proportional to the size of the disturbance, but more importantly the filling time is independent of Δn. Note also that through the function f_{To} the filling time is exponentially dependent on the energy position of the state.

3. Large reverse bias applied to a Schottky barrier :

It is assumed that $\Delta n = -n_o$ ($-n_o$ is the maximum value for Δn in reverse bias). From eqn. (5.23) $\Delta n_T(\infty) = N_T f_{To}$ and $\tau^{-1} = e_n$. This means that all filled states become empty and the emptying time is given by the inverse of the gap state emission coefficient.

It is important to note that although in each case the relaxation follows an exponential decay, the actual relaxation times are very different. Note, for example, that a gap state can be filled much quicker than it can be emptied. This is because a very large number of free carriers can be introduced to the conduction band but the maximum defficiency of carriers

is $-n_o$; the capture rate can be greatly enhanced but the maximum reduction is of course to zero. For the small disturbance case this asymmetry is no longer important and so emptying and filling times tend to the same value.

5.3.5 Results for a Small Sinusoidal Disturbance

An admittance measurement involves applying a small sinusoidal potential to the Schottky barrier and, under steady-state conditions, this will give rise to a sinusoidal variation of the free carrier densities. In this sub-section the exact relationship between the small potential and the free carrier disturbances is not explicitly considered. The relationship, for example, may be complex and frequency-dependent. Also only majority carrier processes are considered. Minority carrier processes, and in particular hole emission, are important in reverse bias, but these effects are adequately dealt with separately in Chapter 6, sub-section 6.7.1.

Eqn.(5.15) is used to find the time-varying part of the occupancy function f_T for a single gap state level of energy E_T. Ignoring hole processes and assuming that $c_n \Delta n << c_n n_o + e_n$, this equation becomes

$$\frac{d}{dt} \delta f_T(t) = c_n(1-f_{To})\delta n(t) - (c_n n_o + e_n)\delta f_T(t), \tag{5.24}$$

where δ replaces Δ to emphasize that eqn.(5.24) is correct for small disturbances only. If $\delta f_T(t) = \delta f_T(\omega)e^{i\omega t}$ then the differentiation can be performed and eqn. (5.24) rearranges to give

$$\delta f_T(\omega) = \frac{c_n(1-f_{To})/(c_n n_o + e_n)}{1 + i\omega/(c_n n_o + e_n)} \cdot \delta n(\omega). \tag{5.25}$$

Using the result $c_n n_o + e_n = c_n n_o / f_{To}$, eqn. (5.25) becomes

$$\delta f_T(\omega) = \frac{f_{To}(1-f_{To})}{1 + i\omega f_{To}/c_n n_o} \cdot \frac{\delta n(\omega)}{n_o}. \tag{5.26}$$

These results have been written in the frequency domain.

Eqn. (5.26) describes the time-varying change in electron occupancy for a single gap state level. Amorphous silicon has a continuous distribution of these levels described by the density of states function $N(E_T)$. The total time-varying response for all of the gap states, denoted $\delta n_T(\omega)$, follows by integrating the product $\delta f_T N(E_T)$ through the complete gap state energy range. It is sufficient here to choose $\tilde{E}_c$ and $\tilde{E}_v$ to be the integration limits (the tilde signifies that $|e|\psi(x)$ is included in the terms), and then

$$\delta n_T(\omega) = \int_{\tilde{E}_v}^{\tilde{E}_c} \frac{f_{To}(1 - f_{To})}{1 + i\omega f_{To}/c_n n_o} \cdot \frac{\delta n(\omega)}{n_o} N(E_T) dE_T \,. \qquad (5.27)$$

The function f_{To} is the gap state occupancy function for thermal equilibrium conditions and it is given by the Fermi-Dirac function, eqn.(5.8). From eqn. (5.8) it is easily shown that $df_{To}/dE_T = -f_{To}(1-f_{To})/kT$, and this allows the integral variable in eqn. (5.27) to be changed to f_{To} with limits $f_{To}(\tilde{E}_c) \sim 0$ and $f_{To}(\tilde{E}_v) \sim 1$. Also the integrand is strongly peaked at the Fermi level with peak width $\sim kT$. Therefore if $N(E_T)$ varies little over energies of the order of kT, then $N(E_T)$ may be replaced by the constant $N(E_F)$ and the solution of the integral follows.

$$\delta n_T(\omega) \simeq kT\, N(E_F) \frac{\delta n(\omega)}{n_o} \int_0^1 \frac{df_{To}}{1 + i\omega f_{To}/c_n n_o} \,,$$

$$= kT\, N(E_F) \frac{\ln(1 + i\omega\tau)}{i\omega\tau} \cdot \frac{\delta n(\omega)}{n_o} \,, \qquad (5.28)$$

and $\tau = 1/c_n n_o$. Note that this result was first derived by Lehovec [26]

(1966) to describe the response of a continuous distribution of states at the interface of an MOS (Metal-Oxide-Semiconductor) structure.

The function τ now takes a simple form. Substituting $n_o = N_c \exp[(E_F - \tilde{E}_c)/kT]$ allows $\tau = 1/c_n n_o$ to be written thus,

$$\tau = \frac{1}{c_n N_c} \exp\left[(\tilde{E}_c - E_F)/kT\right] , \tag{5.29}$$

and comparison with eqn. (5.10) shows that τ is equal to the inverse of the emission coefficient for gap states situated at the Fermi level. It is argued that as the largest change in electron occupancy occurs at the Fermi level, it is those states at the Fermi level which dominate the response and hence dominate the value of τ. We can derive a more approximate expression for the gap state response which highlights the physical origins of τ and also contains a simpler frequency-dependence.

At zero temperatures df_{To}/dE_T, and hence the function $-f_{To}(1-f_{To})/kT$, becomes a delta function centred at $E_T = E_F$. Then at T = 0 the integral in eqn. (5.27) is easily solved to give

$$\delta n_T(\omega) = \frac{kT\, N(E_F)}{1 + i\omega\tau} \cdot \frac{\delta n(\omega)}{n_o} , \quad T = 0 , \tag{5.30}$$

and at finite temperatures this result becomes an approximation to eqn. (5.28). Note that the frequency-dependent term $1/(1 + i\omega\tau)$ is identical to that of a debye response [27,28], and such a response is appropriate for a system relaxing exponentially with a relaxation time τ.

The frequency-dependent terms in eqns. (5.28) and (5.30) are now separated into their real and imaginary components.

$$\frac{\ln(1 + i\omega\tau)}{i\omega\tau} = \frac{\tan^{-1}\omega\tau}{\omega\tau} + i\,\frac{\ln(1 + \omega^2\tau^2)}{2\omega\tau} , \tag{5.31}$$

$$\frac{1}{(1 + i\omega\tau)} = \frac{1}{(1 + \omega^2\tau^2)} + i\,\frac{\omega\tau}{(1 + \omega^2\tau^2)} . \tag{5.32}$$

Fig 5.3 shows the functions plotted against $\ln(\omega\tau)$. The plots are broadly similar and the differences turn out to have only a minor effect. The peak in the function $\omega\tau/(1 + \omega^2\tau^2)$ occurs at $\omega\tau = 1$ and the peak in $\ln(1 + \omega^2\tau^2)/2\omega\tau$ occurs at $\omega\tau = 1.98$. Although the peaks vary in height, the areas under the peaks are actually equal (see section 6.3). For the real parts $1/(1 + \omega^2\tau^2) = 1/2$ at $\omega\tau = 1$, and $\tan^{-1}(\omega\tau)/\omega\tau = 1/2$ at $\omega\tau = 2.33$ and apart from this slight shift they are again very similar.

The analyses in Chapter 6, section 6.3 will show that eqn. (5.30) is a good approximation for the gap state response. It is also a simpler expression than eqn. (5.28) and so eqn. (5.30) will be used in preference for the subsequent admittance calculation. Cohen and Lang [20] (1982) also use this approximation.

5.4 ADMITTANCE CALCULATION

The admittance calculation described in this section involves quite complicated analysis. Therefore in order to keep the various arguments and resulting equations as simple as possible, several considerations which turn out to be of secondary importance are neglected. In particular this includes the consideration of all minority carrier effects and the effects of diode leakage current.

5.4.1 Admittance Formulae

The barrier admittance at angular frequency ω and d.c. surface potential ψ_s is usually measured by applying a small signal potential $v = v_o \exp(i\omega t)$ superimposed on the d.c. bias V. The ratio of the resultant current density ($j = j_o \exp(i\omega t)$) to the applied potential gives the differential admittance per unit area.

$$\text{i.e.,} \qquad Y(\psi_s, \omega) = j/v \; . \qquad (5.33)$$

Throughout this section all admittances, capacitances and conductances are for unit area, and henceforth explicit reference to this will be dropped.

Admittance can be separated into its real and imaginary parts thus.

$$Y = G + i\omega C \ , \tag{5.34}$$

and this equation defines capacitance and conductance. G is the conductance and it gives the in-phase component of the current, and C is the capacitance which gives the out of phase component of the current. The reason for the product ωC appearing in the expression can be explained by considering the charge response.

Let $Q(\psi_s,\omega)$ be the charge in the barrier, and let V be the voltage across the barrier. Then assuming the charge flows in the positive x direction when a positive voltage is applied,

$$j = \frac{dQ}{dt} = \frac{dQ}{dV} \cdot \frac{dV}{dt} \ , \tag{5.35}$$

and writing $dV/dt = i\,\omega v'$, eqns. (5.33) and (5.35) give

$$Y(\psi_s,\omega) = i\omega \frac{dQ}{dV}(\psi_s,\omega). \tag{5.36}$$

The capacitance is the real part of $dQ(\psi_s,\omega)/dV$ and the "zero-frequency" or static capacitance, denoted $C(\psi_s,0)$, is defined as the change in charge due to an infinitely slow incrementation of voltage.
This may be written,

$$C(\psi_s,\ 0) \equiv \left[\frac{dQ}{dV} \right]_{t \to \infty} \tag{5.37}$$

Another admittance formula is used for the calculations, and this is found by looking more closely at the barrier charge Q and relating Q to the potential via Poisson's equation. When a small signal is applied it

has the effect of setting up a time-varying potential $\phi(\psi_s,x,t)$ throughout the barrier. This potential is defined in section 5.2 and has the opposite sign to the electric potential v. Poisson's equation may be explicitly written in terms of this potential.

$$\frac{d^2}{dx^2}\left((\psi(x) + \phi(\psi_s,x,t)\right) = \frac{1}{\varepsilon\varepsilon_o} \left(\rho(x) + \rho_\phi(\psi_s,x,t) \right), \qquad (5.38)$$

where $\rho(x)$ is the charge density due to the d.c. bias and $\rho_\phi(\psi_s,x,t)$ is the charge density due to the a.c. signal. In general ϕ and ρ_ϕ will depend on the d.c. bias and this has been explicitly indicated. The d.c. problem can be solved separately and eqn. (5.38) reduces to

$$\frac{d^2}{dx^2} \phi(\psi_s,x,t) = \frac{1}{\varepsilon\varepsilon_o} \rho_\phi(\psi_s,x,t) , \qquad (5.39)$$

with the d.c.solution entering eqn.(5.39) through the charge density ρ_ϕ.

The total time-varying charge in the barrier, denoted $Q_\phi(\psi_s,x,t)$, is

$$Q_\phi(\psi_s,x,t) = \int_0^\infty \rho_\phi(\psi_s,x,t)dx = -\varepsilon\varepsilon_o \frac{d\phi}{dx} (\psi_s,x,t) \Bigg|_{x=0} . \qquad (5.40)$$

The first equality in eqn. (5.40) is simply the definition of Q_ϕ in terms of the charge density ; the second follows from eqn. (5.39).

An expression for the small signal current (and hence admittance)can be found using eqn. (5.40). First it is assumed that the metal is electrically isolated from the semiconductor (diode leakage and hole currents are ignored). It is only necessary to calculate the current at any one point in the circuit and it proves convenient to choose the plane

at the semiconductor back contact ($x = \infty$). Then, because charge flowing through the back contact cannot communicate directly with the metal, any charge flowing into the semiconductor must reside in the depletion region and thus contribute to Q_ϕ . Note also that for increasing Q_ϕ the associated current is flowing in the negative x direction and using eqn. (5.40) it follows that the small signal current density is,

$$j(\psi_s,x,t) = -\frac{dQ_\phi}{dt} = i\omega\varepsilon\varepsilon_o \frac{d\phi}{dx}(\psi_s,x,t)\Big|_{x=0} . \qquad (5.41)$$

The small signal potential may also be written in terms of ϕ , $v = -\phi(x=o)$, and so from the definition of admittance,

$$Y(\psi_s,\omega) = \frac{-i\omega\varepsilon\varepsilon_o \frac{d\phi}{dx}(\psi_s,x,\omega)\Big|_{x=o}}{\phi(\psi_s, 0,\omega)} . \qquad (5.42)$$

Note that we choose to write this expression in the frequency domain.

It is now clear how a solution for admittance may be obtained. First $\psi(x)$ is found by solving Poisson's equation for the d.c. case. Then an expression for $\rho_\phi(\psi_s,x,\omega)$ is obtained, and the a.c. part of Poisson's equation is solved to give $\phi(\psi_s,x,\omega)$. Once $\phi(\psi_s,x,\omega)$ is found substitution in eqn.(5.42) gives the admittance directly. The following sub-sections work through these steps.

5.4.2 Calculations at a Constant Bias

A Schottky barrier can only be in thermal equilibrium if the metal Fermi level and the semiconductor Fermi level are coincident. It was shown in Chapter 4 that for an n-type barrier this is achieved by electrons diffusing from the semiconductor into the metal. This results in a region of space-charge near the metal-semiconductor interface which creates the required built-in potential for the Fermi level alignment.

There are two contributions to the barrier space-charge. First the electron diffusion depletes the density of electrons occupying band-tail states and states above the mobility edge, and this gives rise to positive charge. Also the electron occupancy of deep gap states must reduce so as to maintain thermal equilibrium with the conduction band electrons, and this reduction further contributes to the positive charge. In crystalline materials it is normally the first contribution, the contribution due to majority carriers which dominates. In a-Si however, it is most often the contribution due to deep gap states which is the larger, and in fact for this calculation we ignore majority carrier charge.

An n-type Schottky barrier is considered and any charge due to the electron occupancy of band-tail states or states situated above the mobility edge is ignored. Gap states in the depletion region which are at energies between E_F and $E_F - |e|\psi(x)$ have been pulled above the Fermi level and to a first approximation these gap states all lose one electron (i.e.we assume gap states are monovalent and zero temperature statistics apply). This approximation leads to a very simple expression for the charge density.

$$\rho(x) = |e| \int_{E_F-|e|\psi(x)}^{E_F} N(E)\,dE \qquad (5.43)$$

where N(E) is the gap state density energy distribution and the energy scale is fixed to the value of the conduction band mobility edge in the neutral bulk (see sub-section 5.3.2). Also, at a finite bias the conduction band electron quasi-Fermi level E_{Fn} should replace E_F, but it is assumed throughout that $E_{Fn} = E_F$.

From eqn. (5.43), Poisson's equation becomes

$$\frac{d^2\psi}{dx^2} = \frac{|e|}{\epsilon\epsilon_0} \int_{E_F-|e|\psi(x)}^{E_F} N(E)\,dE , \qquad (5.44)$$

and $\psi(x)$ is subject to the boundary conditions

$$\psi(o) = \psi_s, \; \psi(\infty) = o, \quad \left.\frac{d\psi}{dx}\right|_{x=\infty} = 0 \; . \tag{5.45}$$

The well known identity

$$\frac{d^2\psi}{dx^2} = \frac{1}{2}\frac{d}{d\psi}\left(\frac{d\psi}{dx}\right)^2 , \tag{5.46}$$

allows the integral variable in eqn.(5.44) to be changed from x to $\psi(x)$. Integrating over ψ from $\psi(\infty) = 0$ to $\psi(x_o) = \psi_o$, and choosing the negative square root gives

$$\left.\frac{d\psi}{dx}\right|_{\psi = \psi_o} = -\left(\frac{2|e|}{\varepsilon\varepsilon_o}\int_o^{\psi_o}\int_{E_F-|e|\psi}^{E_F} N(E)dEd\psi\right)^{\frac{1}{2}} \tag{5.47}$$

A second integration gives

$$x(\psi_o) = \int_{\psi_o}^{\psi_s} \frac{d\psi'}{\left(\frac{2|e|}{\varepsilon\varepsilon_o}\int_o^{\psi'}\int_{E_F-|e|\psi}^{E_F} N(E)dEd\psi\right)^{\frac{1}{2}}} \tag{5.48}$$

Eqns. (5.47) and (5.48) may appear cumbersome because they are written in terms of ψ rather than x. This approach is often used and proves to be a straightforward method for calculating $\psi(x)$. However other numerical methods have also been used[20], and it should be stressed here that the final

admittance results are independent of the particular method employed to calculate $\psi(x)$.

The total barrier charge, denoted Q, can also be written in terms of ψ.

$$Q = \int_0^\infty \int_{E_F-|e|\psi(x)}^{E_F} N(E)dEdx = \varepsilon\varepsilon_o \int_0^\infty \frac{d^2\psi}{dx^2} dx = -\varepsilon\varepsilon_o \frac{d\psi}{dx}\bigg|_{\psi=\psi_s} , \quad (5.49)$$

and substituting eqn. (5.47) for $d\psi/dx$ gives

$$Q = \left(2|e|\varepsilon\varepsilon_o \int_0^{\psi} \int_{E_F-|e|\psi}^{E_F} N(E)dEdx \right)^{\frac{1}{2}} . \quad (5.50)$$

The static, zero-frequency capacitance $C(\psi_s, 0)$ is the voltage derivative of Q, and so

$$C(\psi_s,0) = -\frac{dQ}{dV} = \frac{dQ}{d\psi_s} = \frac{\left(\frac{|e|\varepsilon\varepsilon_o}{2}\right)^{\frac{1}{2}} \int_{E_F-|e|\psi_s}^{E_F} N(E)dE}{\left(\int_0^{\psi_s} \int_{E_F-|e|\psi}^{E_F} N(E)dEd\psi \right)^{\frac{1}{2}}} , \quad (5.51)$$

which is a result obtained by a number of workers. Note that for the first equality a minus sign is required. This is because a positive increment in V gives rise to a reduction in Q.

5.4.3 A Differential Equation for the Small Potential

When a small sinusoidal potential is applied across the Schottky barrier, there results in two distinct time-varying components to the barrier charge. The electron density in the conduction band and band-tail states will vary, and as a response to this the electron occupancy of deep gap states will vary. If band-tail state density is assumed negligible, then the total time-varying charge density, denoted ρ_ϕ , may be written as

$$\rho_\phi(\psi_s,x,\omega) = -|e| \left(\delta n(\psi_s,x,\omega) + \delta n_T(\psi_s,x,\omega)\right) , \tag{5.52}$$

where δn is the density of excess electrons above the mobility edge, and δn_T is the excess density of electrons occupying deep traps. Results (5.5) and (5.30) for n and n_T are used. They allow ρ_ϕ to be written in terms of ϕ and δE_{Fn}, and the dependencies on bias, position and frequencies are indicated explicitly.

$$\text{i.e. } \rho_\phi(\psi_s,x,\omega) = -|e|\left(\frac{n_o(\psi_s,x)}{kT} + \frac{N(E_F-|e|\psi(x)}{1+i\omega\tau(\psi_s,x)}\right)\left(\delta E_{Fn}(\psi_s,x,\omega)-|e|\phi(\psi_s,x,\omega)\right). \tag{5.53}$$

We also write

$$\tau(\psi_s,x) = \tau_o \exp\left\{ \left[(E_c - E_F)+ |e| \psi(x) \right] /kT \right\} , \tag{5.54}$$

where $\tau_o = 1/c_n N_c$ and E_c is the energy of the conduction band mobility edge in the neutral bulk. Note that E_c replaces $\tilde{E}_c$ and the term $|e|\psi(x)$ is indicated explicitly.

There are two physical effects which may lead to a frequency-dependence in ρ_ϕ. First the transport of the conduction band electrons is not infinitely fast and so they may not be able to respond to the small signal. This would result in a finite value for δE_{Fn}. Second, the gap states empty and fill

according to the processes of emission and capture and this requires time τ . If the product $\omega\tau \sim 1$ gap state capture and emission will lead to a strong frequency-dependence.

A simultaneous treatment of both of these frequency-dependent effects is very difficult and such a treatment is not attempted here. For this calculation it is assumed that the transport of conduction band electrons is sufficiently fast so that $\delta E_{Fn} \simeq 0$. This is a contentious assumption (see for example Viktorovitch and Moddel[6] (1980)) and its validity is discussed in Chapter 6, sub-section 6.5.4. It is also assumed that the main charge contribution is due to the electron occupancy of gap states and then $\delta n \simeq 0$. Using these approximations, the a.c. part of Poisson's equation, eqn. (5.39), becomes

$$\frac{d^2}{dx^2} \phi(\psi_s, x, \omega) = \frac{|e|^2}{\varepsilon\varepsilon_o} \frac{N(E_F - |e|\psi(x))}{1 + i\omega\tau(\psi_s, x)} \phi(\psi_s, x, \omega) \quad , \tag{5.55}$$

and given a solution for $\psi(x)$ this equation may be solved to find the admittance.

5.4.4. Simplified Equations for the Small Potential

Eqn. (5.55) shows that $\phi(\psi_s, x, \omega)$ will be complex, and writing $\phi = \phi_R + i\phi_I$ allows the equation to be separated into its real and imaginary parts.

$$\frac{d^2\phi_R}{dx^2} = \frac{|e|^2}{\varepsilon\varepsilon_o} \left(\frac{N(E_F - |e|\psi)}{1 + \omega^2\tau^2} \phi_R + \frac{\omega\tau}{1 + \omega^2\tau^2} N(E_F - |e|\psi) \phi_I \right), \tag{5.56}$$

$$\frac{d^2\phi_I}{dx^2} = \frac{|e|^2}{\varepsilon\varepsilon_o} \left(\frac{N(E_F - |e|\psi)}{1 + \omega^2\tau^2} \phi_I - \frac{\omega\tau}{1 + \omega^2\tau^2} N(E_F - |e|\psi) \phi_R \right). \tag{5.57}$$

The product $\omega\tau$ increases very rapidly with decreasing $x(\omega\tau \propto \exp[|e|\psi(x)/kT]$, and in Fig.5.4 the function $1/(1+\omega^2\tau^2)$ and $\omega\tau/(1+\omega^2\tau^2)$ are plotted as a function of x for a typical barrier. The parameters are noted in the figure caption. It is convenient to define a point x_c where $\omega\tau(x_c) = 1$. This point can be found using the equation

$$|e|\psi_c = kT\ \ln(1/\omega\tau_o) - (E_c - E_F)\ , \tag{5.58}$$

where $\psi_c = \psi(x_c)$, $\tau_o = 1/c_n N_c$ and E_c is the energy of the conduction band mobility edge in the neutral bulk. From Fig. 5.4 it is clear that $1/(1+\omega^2\tau^2)$ changes rapidly from ~ 1 to ~ 0 at x_c and $\omega\tau/(1+\omega^2\tau^2)$ is strongly peaked at this point, its value falling off rapidly on either side.

Consider now the region of barrier $x \gg x_c$. Here $\omega\tau \ll 1$ and only the first terms on the right-hand side of eqns.(5.56) and (5.57) are significant. Then,

$$\frac{d^2\phi_R}{dx^2} \simeq \frac{|e|^2}{\varepsilon\varepsilon_o} N(E_F - |e|\psi)\phi_R \qquad , x \gg x_c\ , \tag{5.59}$$

$$\frac{d^2\phi_I}{dx^2} \simeq \frac{|e|^2}{\varepsilon\varepsilon_o} N(E_F - |e|\psi)\phi_I \qquad , x \gg x_c\ . \tag{5.60}$$

We are free to choose the phase of ϕ at any one point in the barrier and it is convenient to make use of this and take ϕ to be real at some particular point $x \gg x_c$. From eqn.(5.60) it follows that $\phi_I(x) = 0$ for all $x \gg x_c$. Note also that by choosing the phase thus, ϕ_I will be much smaller than ϕ_R even close to x_c. Hence near x_c and for $x < x_c$,

eqns. (5.56) and (5.57) become

$$\frac{d^2\phi_R}{dx^2} \approx 0 \qquad , x < x_c \quad (5.61)$$

$$\frac{d^2\phi_I}{dx^2} \approx - \frac{|e|^2}{\varepsilon\varepsilon_o} \frac{\omega\tau}{1 + \omega^2\tau^2} N(E_F-|e|\psi)\phi_I \qquad , x < x_c \quad (5.62)$$

Eqn (5.61) follows because $1/(1 + \omega^2\tau^2) \sim 0$ and $\phi_I \sim 0$, and eqn.(5.62) follows because $\phi_I \sim 0$. Further note that because ϕ_I is small near x_c, eqn. (5.59) is still a good approximation for ϕ_R close to but greater than x_c.

The above approximations give expressions for $\phi_R(x)$ throughout the barrier without any reference to ϕ_I. The physical interpretation of this is that because the out of phase charge response is quite small, its effect on ϕ_R can be neglected. The result is that $\phi_R(x)$ can now be calculated without recourse to ϕ_I, and this greatly simplifies the problem.

5.4.5 Solution of Simplified Equations

It turns out that the admittance can be calculated without obtaining an explicit expression for $\phi_R(x)$. It will become apparent that it suffices to find

$$\left. \frac{1}{\phi_R} \frac{d\phi_R}{dx} \right|_{x = 0} ,$$

and this quantity can be obtained in a straightforward fashion. For $x > x_c$,

eqn. (5.59) must be solved. In Appendix A it is shown that

$$\frac{1}{\phi_R(x)} \frac{d\phi_R(x)}{dx} = - \frac{\dfrac{|e|}{\varepsilon\varepsilon_o} \displaystyle\int_{E_F-|e|\psi(x)}^{E_F} N(E)dE}{\left(\dfrac{2|e|}{\varepsilon\varepsilon_o} \displaystyle\int_o^{\psi(x)} \int_{E_F-|e|\psi}^{E_F} N(E)dEd\psi \right)^{\frac{1}{2}}} \quad , \; x > x_c \tag{5.63}$$

satisfies the equation and the boundary conditions at $x = \infty$. The motivation for trying this solution actually comes from the expression of the static capacitance in sub-section 5.4.2, eqn. (5.51), and accordingly the symbol $-c(\psi(x),o)/\varepsilon\varepsilon_o$ is used to represent the right-hand side of eqn.(5.63).

For $x < x_c$ eqn. (5.61) must be solved and the general solution is

$$\phi_R(x) = Ax + B \quad , \quad x < x_c \quad , \tag{5.64}$$

where A and B are constants. The constants are found by matching the logarithmic derivatives of the two potentials at x_c, and from this it is easily shown that

$$\frac{1}{\phi_R} \frac{d\phi_R}{dx} \bigg|_{x = o} = - \frac{1}{\varepsilon\varepsilon_o} \frac{C(\psi_c,o)}{1 + (x_c/\varepsilon\varepsilon_o)C(\psi_c,o)} \; . \tag{5.65}$$

where $\psi_c = \psi(x_c)$.

Next consider ϕ_I. For $x > x_c$, the choice of phase allows the approximation

$$\phi_I(x) \simeq o \quad , \qquad x > x_c \; . \tag{5.66}$$

For $x < x_c$, we assume that $\phi_R(x)$ is known and then eqn. (5.62) can be integrated directly. One integration gives

$$\frac{d\phi_I}{dx} \simeq - \frac{|e|^2}{\varepsilon\varepsilon_o} N(E_F - |e|\psi_c)\phi_R(x_c) \int_o^{\infty} \frac{\omega\tau}{1+\omega^2\tau^2} dx \qquad (5.67)$$

Here, because of the relatively peaked nature of $\omega\tau/(1 + \omega^2\tau^2)$ it has been possible to approximate $\phi_R(x)$ and $N(E_F-|e|\psi(x))$ by the constants $\phi_R(x_c)$ and $N(E_F-|e|\phi_c)$. The integral in eqn. (5.67) can be evaluated by transforming the variables, first from x to $\psi(x)$ and then from $\psi(x)$ to $\tau(x)$:

$$\int_o^{\infty} \frac{\omega\tau}{1+\omega^2\tau^2} dx \simeq \left(\left.\frac{d\psi}{dx}\right|_{x = x_c} \right)^{-1} \int_o^{\psi_s} \frac{\omega\tau}{1+\omega^2\tau^2} d\psi ,$$

$$\simeq \frac{kT}{|e|} \left(\left.\frac{d\psi}{dx}\right|_{x = x_c} \right)^{-1} \int_{\sim o}^{\sim\infty} \frac{\omega}{1+\omega^2\tau^2} d\tau ,$$

$$\frac{kT}{|e|} \left(\left.\frac{d\psi}{dx}\right|_{x = x_c} \right)^{-1} \frac{\pi}{2} . \qquad (5.68)$$

Hence,

$$\left.\frac{d\phi_I}{dx}\right|_{x=o} \simeq - \frac{|e|}{\varepsilon\varepsilon_o} N(E_F-|e|\psi_c)\ \phi_R(x_c) \left(\left.\frac{d\psi}{dx}\right|_{x=x_c} \right)^{-1} kT\,\frac{\pi}{2} . \tag{5.69}$$

Finally, $\phi_I \sim 0$ at $x = x_c$ and the significant contribution to $d\phi_I/dx$ comes from the region of space near x_c. This implies that $d\phi_I/dx$ will be a constant for most of $x < x_c$ and this constant is equal to $d\phi_I/dx\,\big|_{x=o}$.

Hence it is a good approximation to write

$$\phi_I(o) \simeq - x_c \left.\frac{d\phi_I}{dx}\right|_{x=o} . \tag{5.70}$$

5.4.6 Admittance Solution

The admittance expression, eqn. (5.42), is written in terms of the real and imaginary parts of ϕ,

$$Y(\psi_s\omega) = -i\omega\varepsilon\varepsilon_o \left. \frac{\left(\phi_R \frac{d\phi_R}{dx} + \phi_I \frac{d\phi_I}{dx}\right) + i\left(\phi_R \frac{d\phi_I}{dx} - \phi_I \frac{d\phi_R}{dx}\right)}{\phi_R^2 + \phi_I^2} \right|_{x=o} , \tag{5.71}$$

and with some rearrangement the capacitance and conductance become

$$C(\psi_s \omega) \;=\; \frac{1 + K_2}{1 + K_1} \left(- \;\frac{\varepsilon\varepsilon_o}{\phi_R} \;\frac{d\phi_R}{dx} \right) \Bigg|_{x\,=\,o} \quad , \tag{5.72}$$

$$G(\psi_s, \omega) \;=\; \frac{\omega\varepsilon\varepsilon_o}{1 + K_1} \left(\frac{1}{\phi_R} \;\frac{d\phi_I}{dx} \;-\; \frac{\phi_I}{R^2} \;\frac{d\phi_R}{dx} \right) \Bigg|_{x\,=\,o} \quad , \tag{5.73}$$

where K_1 and K_2 are small compared to unity if $\psi_c >> kT/|e|$. K_1 and K_2 are evaluated in Chapter 6, section 6.3, but it suffices here to discard them.

An expression for capacitance immediately follows from eqns. (5.65) and (5.72).

$$\boxed{C(\psi_s, \omega) \;=\; \frac{C(\psi_c, o)}{1 + (x_c/\varepsilon\varepsilon_o)C(\psi_c, o)}} \tag{5.74}$$

Conductance is found using several of the results of the previous sub-section. Substituting for $d\phi_I/dx \,\Big|_{x=o}$ and $\phi_I(o)$, (eqns. (5.69) and

(5.70)) and noting that $\phi_R(x_c) = \phi_R(o) + x_c d\phi_R/dx \Big|_{x=o}$, eqn.(5.73) gives

$$G(\psi_s,\omega) = -\omega|e|N(E_F-|e|\psi_c)\left(\frac{\phi_R(x_c)}{\phi_{R(o)}}\right)^2\left(\frac{d\psi}{dx}\Big|_{x=x_c}\right)^{-1} kT\,\frac{\pi}{2}\,. \tag{5.75}$$

It is easily shown that $\phi_R(x_c)/\phi_R(o) = C(\psi_s,\omega)/C(\psi_c,o)$, and using eqns. (5.47) and (5.51) for $d\psi/dx\Big|_{x=x_c}$ and $C(\psi_c,o)$ respectively, we obtain

$$\boxed{G(\psi_s,\omega) = \omega\frac{\pi}{2}\;\frac{C^2(\psi_s,\omega)}{C(\psi_c,o)}\;\frac{kTN(E_F-|e|\psi_c)}{\displaystyle\int_{E_F-|e|\psi_c}^{E_F} N(E)dE}} \tag{5.76}$$

Hence an approximate solution for admittance has been found. Identical expressions have been obtained by Cohen and Lang[20] (1982) but they use a rather different method based on the theory of Losee[3] (1975). An advantage of the present approach is that it deals directly with the potential and gives a clearer view of the physics.

5.5 DISCUSSION AND ILLUSTRATIVE EXAMPLES

The aim of this section is to give some insight into the physics behind the admittance calculation. Various density of states distributions are considered, and eqns.(5.74) and (5.76) are used to generate illustrative examples of admittance plots.

5.5.1 Physical Picture of the Theory

It has been stated that current is the time rate of change of charge, and it follows that an in-phase charge response corresponds to an out of phase current response, and an out of phase charge response corresponds to an in-phase current response. Therefore the out of phase charge response gives rise to conductance and the in-phase charge response gives rise to capacitance.

The barrier may be divided into three regions determined by the nature of the charge response to the small signal : they are a region of total response ($x > x_c$), a region of partial response ($x \sim x_c$) and a region of no response ($x < x_c$). The region of total response and the region of no response are purely capacitive and have associated capacitances $C(\psi_c,o)$ and $\varepsilon\varepsilon_o/x_c$ respectively. The region of partial response contributes both to the capacitance and the conductance. The capacitive part is discarded as it is normally much smaller than either of the other two capacitance contributions. The conductive part is equally small, but it must be kept in the calculation because the partial response region is the sole source of conductance. Also, note that on applying a reverse bias, the no-response region widens and the other two regions, though shifted spatially, remain unchanged. Increasing the signal frequency affects all three regions. The no response and partial response regions widen, and the total response region commensurately reduces in size. This picture of three distinct regions can now be used to give a better understanding of the capacitance and conductance plots.

The capacitance is considered first. From eqn. (5.74) it is clear that the capacitance consists of two capacitors $C(\psi_c,o)$ and $\varepsilon\varepsilon_o/x_c$ connected in series. $C(\psi_c,o)$ is the more difficult quantity to evaluate, it is associated with the total response region, and can be found using eqn. (5.51). A more concise, but entirely equivalent expression to eqn.(5.51)

is (see Roberts and Crowell[1] (1970))

$$C(\psi_c, o) = \frac{\varepsilon\varepsilon_o \rho(\psi_c)}{Q_c} \tag{5.77}$$

where $\rho(\psi_c)$ is the state charge density at x_c, and Q_c is the static charge per unit area of barrier $x > x_c$. These two quantities are independent of the surface potential ψ_s and therefore $C(\psi_c, o)$ is independent of bias. Also as the signal frequency increases, both $\rho(\psi_c)$ and Q_c will reduce and their ratio stays approximately constant. Therefore over a moderately large range of frequency and bias $C(\psi_c, o)$ is almost a constant. In contrast, the geometric capacitance $\varepsilon\varepsilon_o/x_c$ associated with the no response region does vary with frequency and bias, and most often it is this component which determines the nature of capacitance plots. For example, increasing the signal frequency or applying a reverse bias widens the no response region, and as $\varepsilon\varepsilon_o/x_c$ is inversely proportional to the width of this region, the no-response capacitance reduces and so the total capacitance $C(\psi_s, \omega)$ also reduces.

For conductance the source of in-phase current may be attributed to N_p states per unit area, situated near x_c and bounded by the peak in the function $\omega\tau/(1 + \omega^2\tau^2)$. The value of N_p is approximately given by,

$$N_p \approx N(E_F - |e|\psi_c)|e|\phi_R(x_c)\delta x \tag{5.78}$$

where $\delta x = \left(d\psi/dx \Big|_{x=x_c}\right)^{-1} kT/|e|$. It is argued that the value of conductance depends primarily on the affected density of states at x_c, the spatial extent of the partial response region and the value of ϕ_R at x_c. This information is more precisely contained in eqn. (5.75) and in fact taking proper account of the effects of ϕ_I leads to a $\phi_R(x_c)^2$ dependence.

Note that δx is inversely proportional to the gradient of the barrier profile at x_c, and so because $d\psi/dx$ decreases with increasing x, δx must widen as x_c moves closer to the neutral semiconductor bulk. Also, it was stated after eqn. (5.75) that $\phi_R(x_c)/\phi_R(o) = C(\psi_s,\omega)/C(\psi_c,o)$ and it follows from this that the value of $\phi_R(x_c)$ is smallest when x_c is near the semiconductor neutral bulk.

Now consider applying a reverse bias to the Schottky barrier. The partial response region moves further from the metal surface and its spatial extent stays approximately constant ; $\phi_R(x_c)$ decreases, δx is little changed and so the conductance decreases. With increasing signal frequency, δx increases and $\phi_R(x_c)$ decreases, and they change in such a way that the product $\phi_R(x_c)^2\delta x$ remains approximately constant. Hence from eqns. (5.75) and (5.78), $G(\psi_s,\omega) \underset{\sim}{\propto} \omega$.

It is clear that the value of capacitance and conductance also depend on the density distribution of gap states N(E). This dependence is discussed more fully in Chapter 6, but some comment is appropriate here. First, the capacitance samples gap states over a large range of energy and space. Therefore this measurement is good for finding a reliable average value of N(E). It is however insensitive to detailed structure. The conductance is a sample of a much more localised region - it probes states at x_c and energy $E = E_F-|e|\psi_c$, and therefore this measurement is much more sensitive to the structure in N(E). However, it is also important to note that $\phi_R(x_c)$ and δx depend on the whole barrier region and so it follows that a knowledge of the whole range of N(E) is required to predict $G(\psi_s,\omega)$ accurately.

5.5.2 Numerical Results for Some Example Densities of States

The admittance results of section 5.4 are of the form,

$$Y = f(N(E),\ \tau\ ,\ \psi_s,\ \omega)$$

where f is some quite complicated function. In this sub-section, frequency and bias plots are generated for three different density of states distributions. These plots give a better appreciation of this function f.

The three model density of states are (see Fig.5.5): (a) a constant N(E) with a small peak, (b) N(E) similar to that suggested by Spear, Le Comber and Snell[9] (1978), and (c) N(E) similar to that suggested by Lang, Cohen and Harbison[8] (1982). The other required parameters are $E_c - E_F = 0.35$ eV (n-type), $\tau_o = 10^{-14}$ s, $\epsilon = 11$ and $T = 300$ K. These values and values for ω and ψ_s were substituted into expressions (5.74) and (5.76) and the necessary integrations were performed on a desk-top computer. The frequency plots were calculated for a surface potential $\psi_s = 0.7$V as this value corresponds approximately to zero bias conditions (i.e. we assume that $V_R = \psi_s - 0.7$V). Also the voltage derivative of a typical d.c. J-V plot was calculated and plotted in the G-V graphs to demonstrate the effect of the diode leakage current. In forward bias this current will dominate and in fact it will become so large that experimentally the gap state admittance cannot be measured. Dashed lines are used when it is considered that the measurements are not able to be made experimentally.

Example (a) was chosen to illustrate the effect of structure in N(E). First look at the C-V and G-V plots (Figs 5.6 (i) and (ii)). In the experimentally accessible regions the capacitance and conductance both decrease with reverse bias. This is due to the widening of the no response region thus decreasing the values of $\epsilon\epsilon_o/x_c$ and $\phi_R(x_c)$. At very low frequencies where there is total gap state response ($\psi_c > \psi_s$) the C-V plot is affected by the peak in N(E) but for the chosen parameters this requires considerable forward bias. Also the C-V peak is an order of magnitude smaller than the peak in N(E).

Now look at the frequency plots (Fig 5.6 (iii)). The capacitance decreases quite uniformly with increasing frequency although there is a

slight perturbation due to the peak in N(E). This general decrease with increasing frequency occurs because fewer and fewer gap states are able to respond. It does not however reflect any trend in N(E). The conductance is divided by ω before being plotted against frequency (G/ω and C have the same units ($Fm^{-2} \equiv \Omega^{-1} m^{-2} s$) and so a better comparison can be made). Note that on average G/ω is an order of magnitude smaller than C, but importantly the peak in G/ω is over twice the size of the constant background. This is approximately the same ratio as the peak in N(E). Physically the partial response region is scanned through a range of energies (shown in Fig.5.5) and at each frequency the value of conductance is proportional to the value of N(E) at energy $E = E_F - |e|\psi_c$. Indeed comparing the relevant range of N(E) with the $G/\omega - \omega$ plot shows that G/ω closely follows N(E) throughout.

Examples (b) and (c) indicate the results which might be expected from experiments (see Figs 5.7 and 5.8). The plots confirm all that has been said before, but there are several extra points worthy of note. Firstly compare the 0 Hz C-V curves (Figs 5.7(i) and 5.8(i)) with their respective density of states curves in Fig 5.5. The capacitance at surface potential ψ_s appears to quite closely follow N(E) at energy $E_F - |e|\psi_s$. This occurs because there is total charge response in the barrier and for such cases $C(\psi_s, o)$ is proportional to $\rho(\psi_s)$. it is important however not to be misled by this. The C-V plot is a linear plot whereas N(E) is plotted logarithmically. Therefore we deduce that a very large change in N(E) actually results in quite a small change in capacitance. Also for the chosen value of τ_o frequencies less than 10^{-6} Hz are required to experimentally achieve this total response of gap states. In the more realistic experimental region (solid lines) the C-V plots and G-V plots are once again featureless and not particularly informative.

The frequency plots (Figs 5.7(iii) and 5.8 (iii)) are probably the most useful from an experimental point of view. Compare their general shape with the range of gap states probed (see Fig 5.5). Clearly the $G/\omega-\omega$ plots do reflect the density of states and they simply confirm the lack of structure over the relevant range of N(E). An important anomaly however is evident, and this is seen by comparing the values of G/ω for examples (a) and (b) (Figs 5.6 (iii) and 5.7 (iii)). Note that the magnitudes of G/ω are almost identical whereas the densities of states (and the capacitances) differ by a factor of two (example (c) also shows up this anomaly). The conclusion therefore is that although $G/\omega-\omega$ plots appear to accurately reflect trends in N(E) they are not entirely reliable for calculating the exact value of N(E).

5.6 RESUMÉ

A chief aim of this chapter was to set up a Schottky barrier model which could be used to describe the charge response in an a-Si Schottky barrier. This was done, and then mathematical approximations were made which gave an analytical solution for admittance (eqns. (5.74) and (5.76)). The theoretical capacitance and conductance expressions were used to generate theoretical admittance plots for a model density of states and an assumed gap state lifetime τ. These plots are of considerable help in the interpretation of experimental admittance results.

Finally, many assumptions and approximations are made throughout the course of this work and it is useful to list here for reference the most important of them.

1. At all times the free majority carriers remain in thermal equilibrium with each other, i.e. $E_{Fn}(x,t) = E_F$.
2. N(E) varies little over energies of the order of kT, and at the Fermi level there is an abrupt change in state occupancy between unity and zero - zero temperature statistics are used.

3. The gap state capture coefficients are independent of energy and moreover the electron coefficient equals the hole coefficient.

4. A sizeable fraction of gap states respond to the applied small potential. This is quantified by the inequality $|e|\psi_c >> kT$.

5. The charge contribution of majority carriers is ignored.

6. The effects of diode leakage current are ignored.

7. Minority carrier processes are ignored.

Most of these points are discussed at some length in Chapter 6.

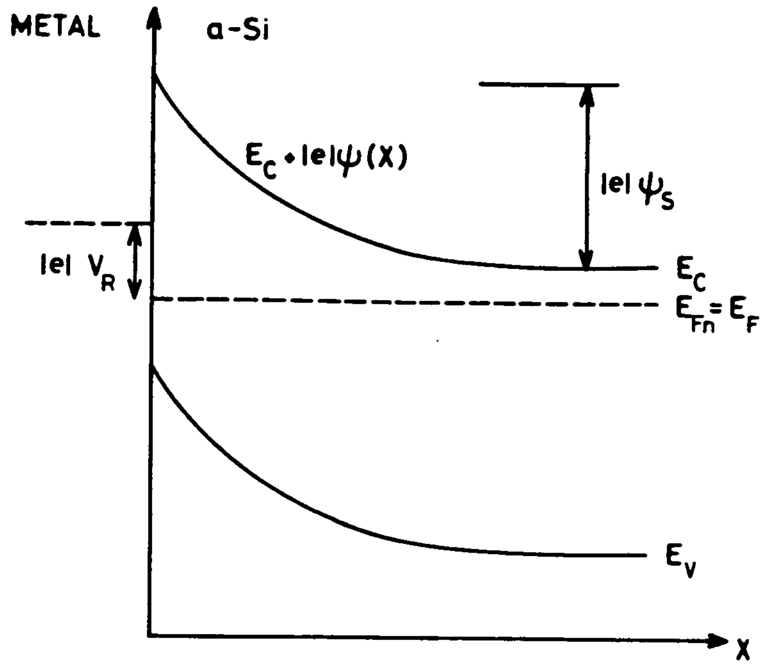

FIGURE 5.1: The electron energy band diagram for an n-type doped a-Si Schottky barrier under a d.c. reverse bias V_R.

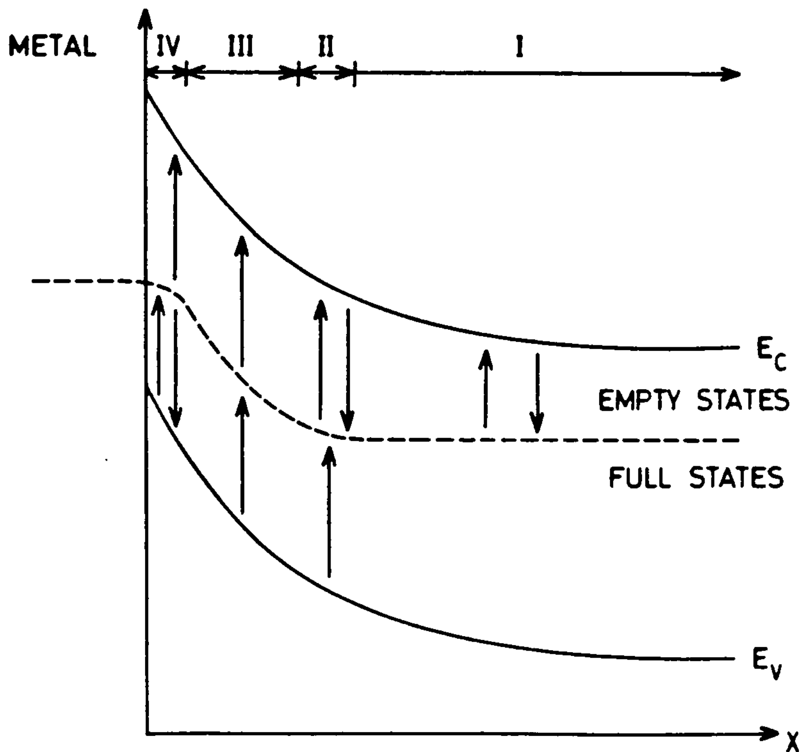

FIGURE 5.2: Electron energy band diagram showing important electron transitions. The arrows indicate the electron direction (reverse direction for holes). Regions I-IV are referred to in the text.

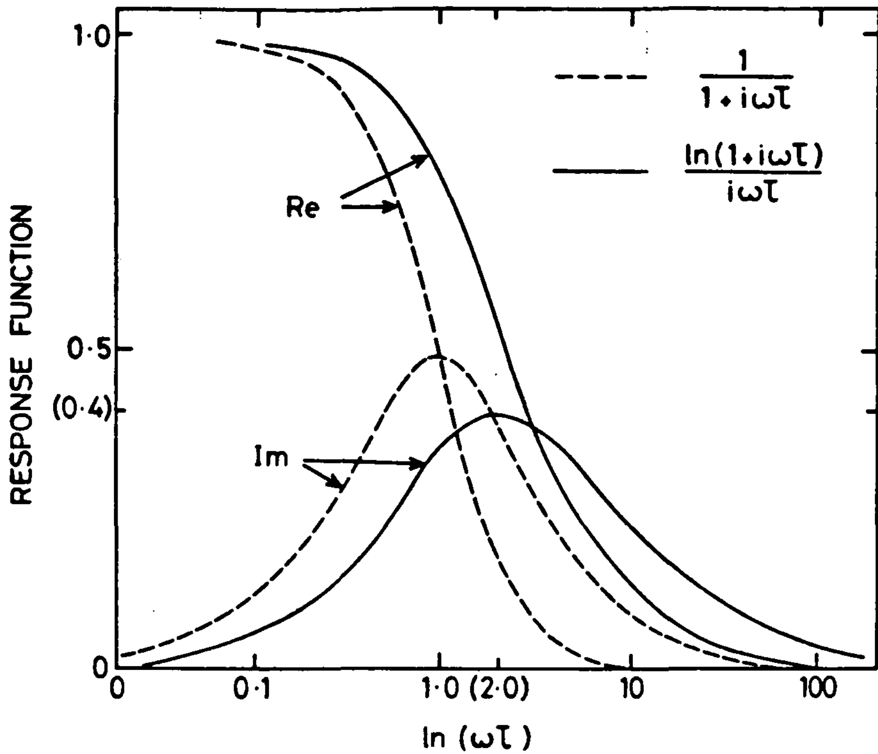

FIGURE 5.3: Gap state response functions (from eqns.(5.31) and (5.32)).

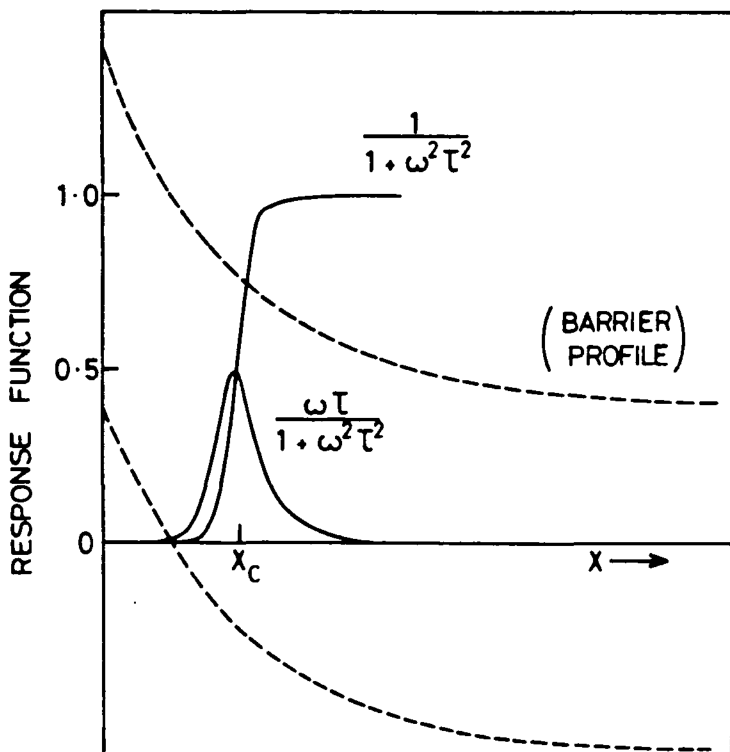

FIGURE 5.4: Gap state response as a function of x. Parameters are, constant $N(E) = 10^{17}$ cm^{-3} eV^{-1}, $E_C - E_F = 0.35$ eV, $\tau_o = 10^{-4}$ s, T = 300K, $\omega = 10^5$ rad.s^{-1}, $\psi_s = 0.5$ V.

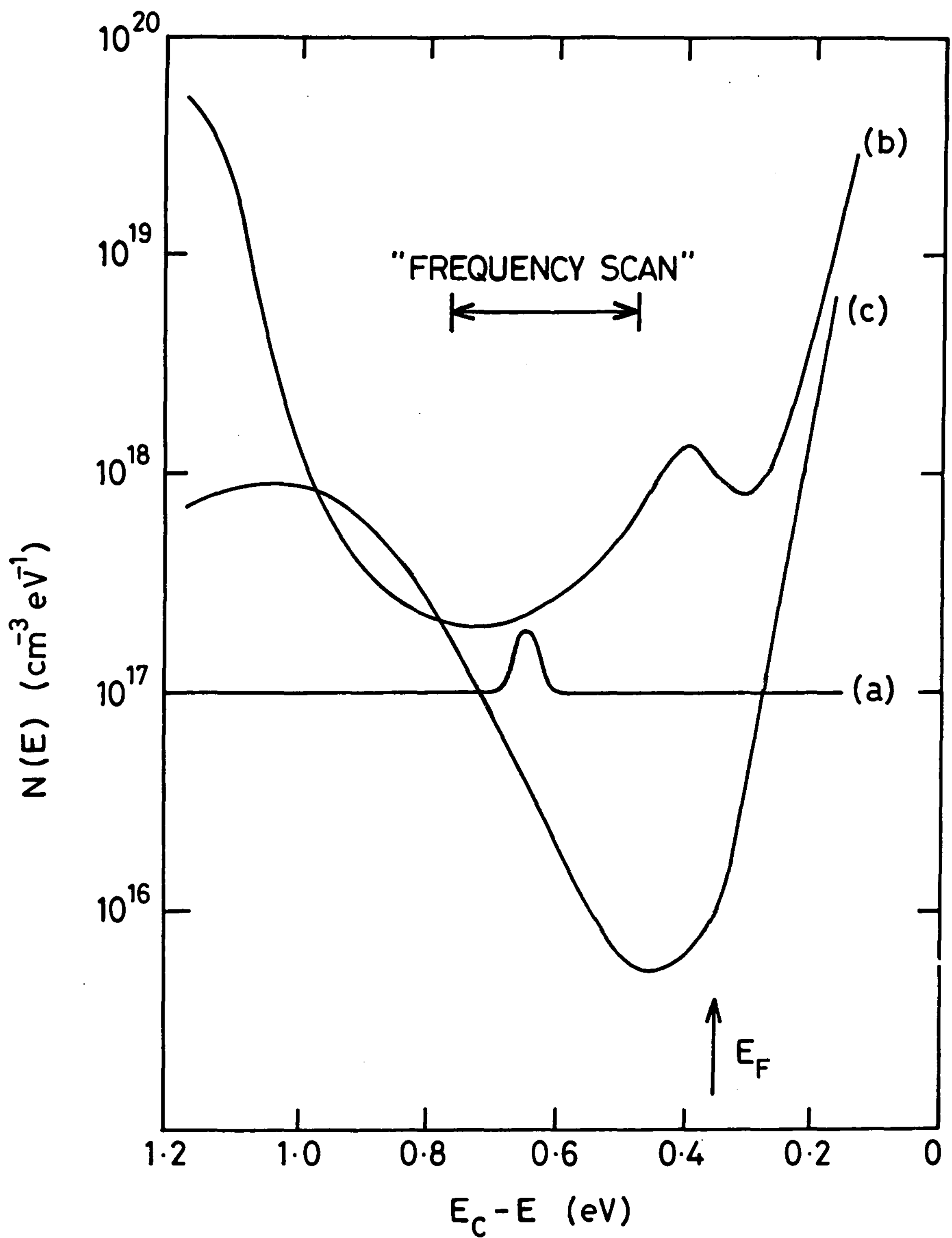

FIGURE 5.5: The density of states used in the calculations. Curve (a) is a constant N(E) with a small peak, curve (b) is an N(E) similar to that suggested by Spear et al[9], and curve (c) is an N(E) similar to that suggested by Lang et al[8]. E_C-E is the energy below the conduction band mobility edge and the 'frequency scan' is the range of energies $E_F-|e|\psi_c$ for the frequency range 10-10^5 Hz. $E_C-E_F = 0.35$ eV, $\tau_o = 10^{-14}$ s, T = 300K and $\epsilon = 11$.

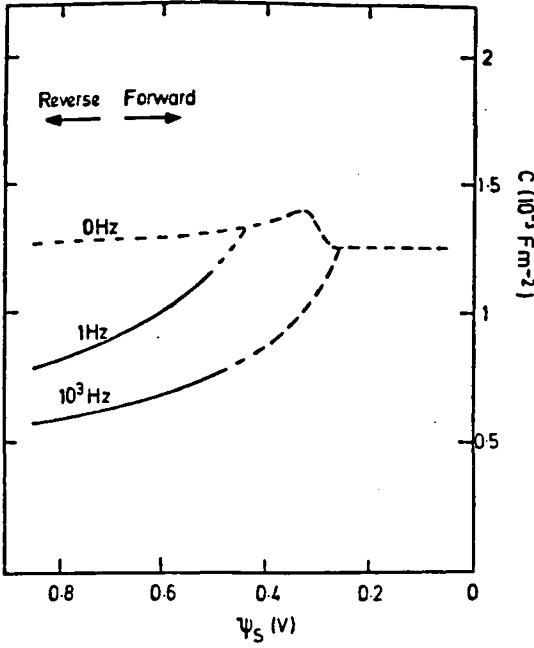

(i) C–V plot

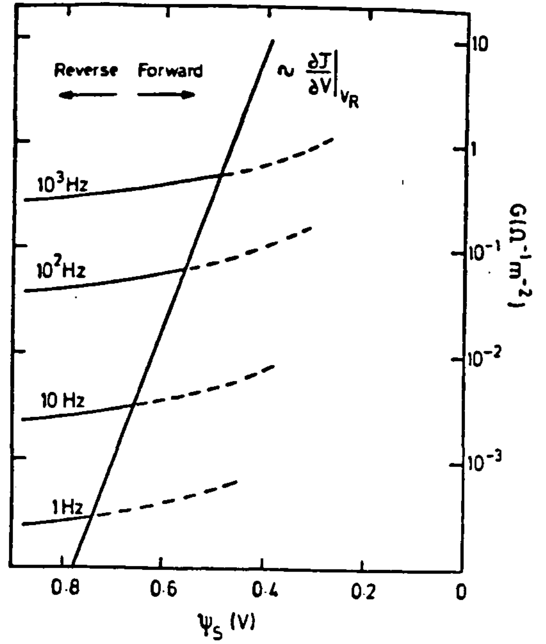

(ii) G–V plot

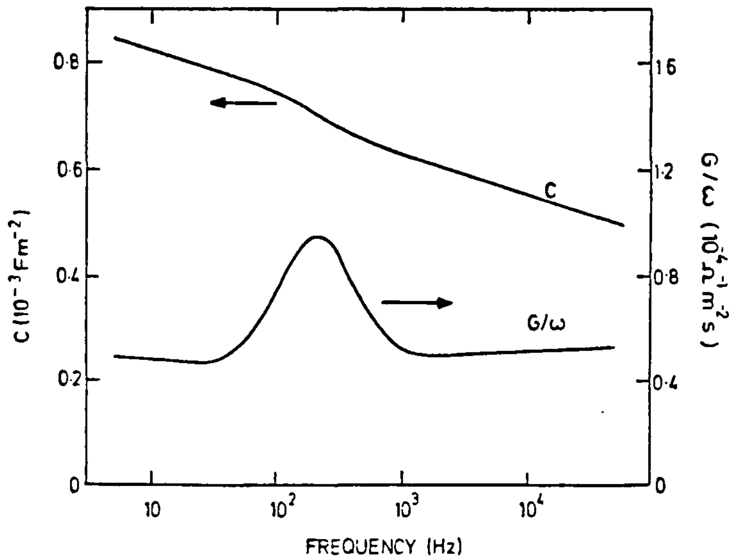

(iii) G/ω, $C-\omega$ plots

FIGURE 5.6: Admittance plots for a constant N(E) with a peak (example (a), Fig.5.5). ψ_S = 0.7V for the G/ω, $C-\omega$ plots and dashed lines are used in the voltage plots when the measurement is not experimentally possible.

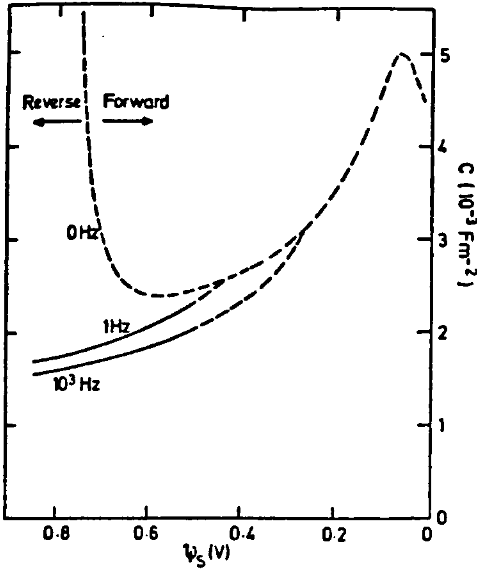

(i) C-V plot

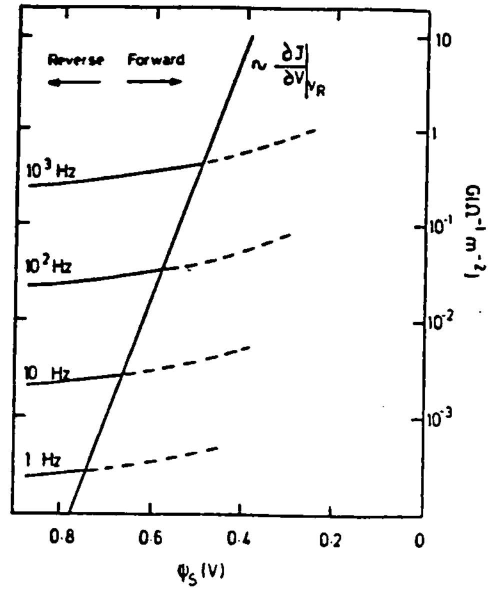

(ii) G-V plot

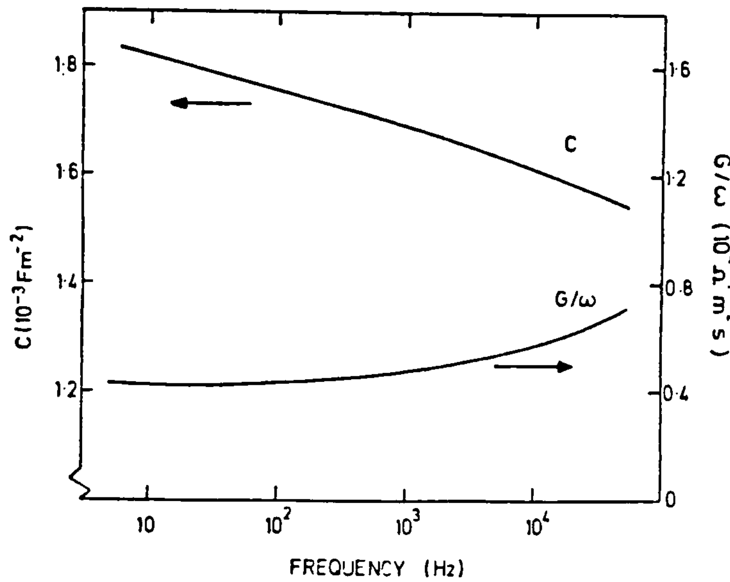

(iii) G/ω, C-ω plots

FIGURE 5.7: Admittance plots for an N(E) similar to that suggested by Spear et al[9] (example (b), Fig 5.5), ψ_s = 0.7V for the G/ω, C-ω plots and dashed lines are used in the voltage plots when the measurement is not experimentally possible.

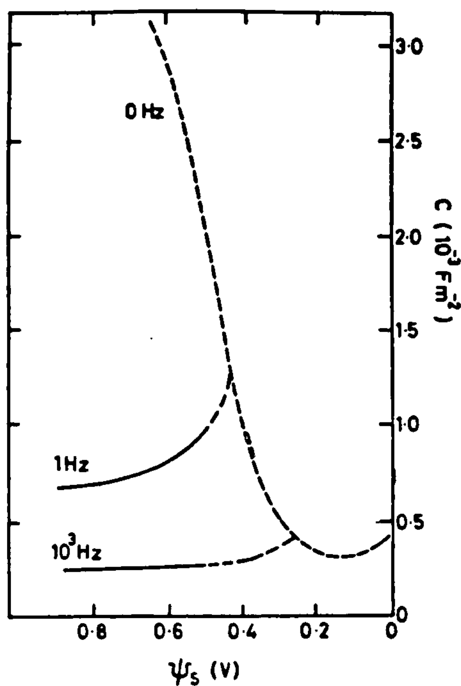

(i) C-V plot

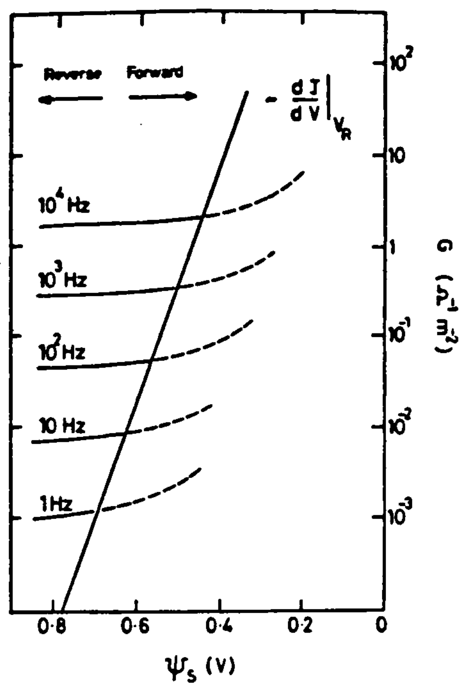

(ii) G-V plot

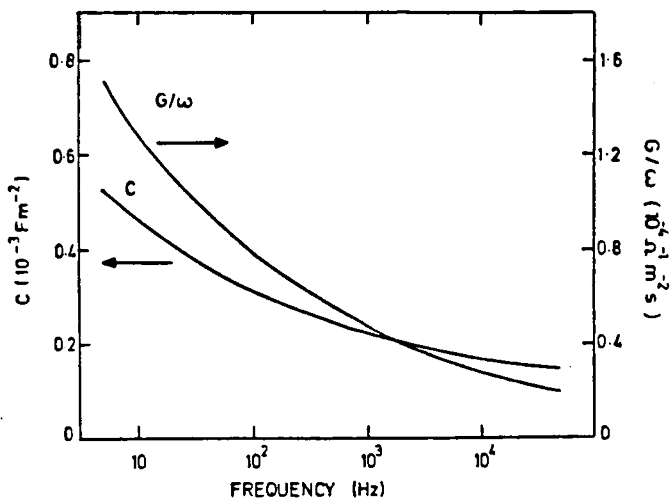

(iii) G/ω, C-ω plots

FIGURE 5.8: Admittance plots for an N(E) similar to that suggested by Lang et al[8] (example (c),Fig 5.5). ψ_s = 0.7V for the G/ω, C-ω plots and dashed lines are used in the

CHAPTER 6

COMMENTS, AND EXTENSIONS TO THE ADMITTANCE THEORY

6.1 INTRODUCTION

The admittance calculation described in Chapter 5 involved quite lengthy arguments, and for conciseness and clarity many of the assumptions and approximations were made without proper justification. These assumptions and approximations are listed at the end of Chapter 5 and now in this chapter each listed point is examined in detail.

First the various admittance results are made simpler by assuming a density of gap states which is independent of energy. The validity of many of the arguments used in this chapter is independent of the exact nature of N(E). Then the various mathematical approximations (e.g. the use of zero temperature statistics) are examined. The approximations are all shown to be accurate to within a few percent. The effects of the majority carriers are examined. It is demonstrated how the majority carrier charge can be included in the admittance calculation and later we include the diode leakage current associated with majority carriers. Section 6.5 looks at the response of the majority carriers to the small time-varying potential. It is argued in an analytical but non-rigorous fashion that the majority carrier transport is unlikely to limit the charge response in the barrier. This section is somewhat speculative in nature but it very successfully demonstrates the underlying physics behind the majority carrier response problem. Finally the effects of minority carrier processes are examined and the admittance calculation is successfully adjusted to include these effects.

Section 6.8 addresses the problem of how the theory developed in Chapters 5 and 6 can be used to interpret experimental admittance results. A very simple iterative numerical routine is described which regenerates

N(E) from the theoretically generated C, G $-\omega$ plots. If the admittance theory is correct then this method can be used to find the a-Si gap state density from experimental C,G$-\omega$ plots. This section shows that the calculations are internally consistent.

Note that throughout this chapter, the Schottky barrier is taken to be n-type, and the notation and various functions follow those defined in Chapter 5.

6.2 ADMITTANCE CALCULATION FOR A CONSTANT GAP STATE DENSITY

The admittance calculation is greatly simplified if the density of gap states is assumed to be a constant independent of energy. Many of the results derived here will be referred to later.

The gap state density is chosen to be

$$N(E) = N, \quad E_F - |e|\psi_s < E < E_F , \tag{6.1}$$

where N is a constant. Using zero temperature statistics, Poisson's equation becomes

$$\frac{d^2\psi}{dx^2} = \frac{|e|}{\varepsilon\varepsilon_o} \int_{E_F-|e|\psi(x)}^{E_F} N \, dE = \frac{|e|^2}{\varepsilon\varepsilon_o} N\psi(x) , \tag{6.2}$$

and the solution

$$\psi(x) = \psi_s \exp(-x/L_o) \quad , \quad L_o = \left(\frac{\varepsilon\varepsilon_o}{|e|^2 N}\right)^{\frac{1}{2}} , \tag{6.3}$$

satisfies eqn.(6.2) and the boundary conditions $\psi(o) = \psi_s$, $\psi(\infty) = o$ and $d\psi/dx\big|_{x=o} = o$. Note that L_o has the dimensions of length. From Gauss's Law, the total charge in the barrier is

$$Q = -\varepsilon\varepsilon_o \left.\frac{d\psi}{dx}\right|_{x=o} = \varepsilon\varepsilon_o \frac{\psi_s}{L_o} , \tag{6.4}$$

and the static, zero-frequency capacitance follows.

$$C(\psi_s,o) \equiv \left[\frac{dQ}{d\psi_s}\right]_{t\to\infty} = \frac{\varepsilon\varepsilon_o}{L_o} = (\varepsilon\varepsilon_o|e|^2N)^{1/2} . \tag{6.5}$$

At finite signal frequencies the differential equation for the small potential (eqn. (5.55), sub-section 5.4.3) must be introduced. For a constant gap state density this equation becomes

$$\frac{d^2}{dx^2}\,\phi(\psi_s,x,\omega) = \frac{1}{1+i\omega\tau(\psi_s,x)}\cdot\frac{1}{L_o^2}\,\phi(\psi_s,x,\omega), \tag{6.6}$$

where $\tau(\psi_s,x) = \tau_o\exp\left\{\left[(E_c - E_F) + |e|\psi_s\exp(-x/L_o)\right]/kT\right\}$.

Unfortunately, even with this simplification, the differential equation cannot be solved analytically without making the same approximations as before. Separating ϕ into its real and imaginary parts, the approximations of sub-section 5.4.4. give

$$\frac{d^2\phi_R}{dx^2} \simeq \begin{cases} o & , \; x < x_c \\ \dfrac{\phi_R}{L_o^2} & , \; x > x_c \end{cases} , \tag{6.7}$$

$$\frac{d^2\phi_I}{dx^2} \simeq \begin{cases} -\dfrac{\omega\tau}{1+\omega^2\tau^2}\cdot\dfrac{\phi_R}{L_o^2} & , \; x < x_c \\ o & , \; x > x_c \end{cases} , \tag{6.8}$$

where $x = x_c$ is defined by the equality $\omega\tau(x_c) = 1$. Eqn.(6.7) can be integrated directly. Matching the logarithmic derivatives of ϕ_R at $x = x_c$,

and setting $\phi_R(o) = 1$ gives

$$\phi_R(x) \simeq \begin{cases} 1 - \dfrac{x}{x_c + L_o} & , \quad x < x_c \\[2ex] \dfrac{L_o}{x_c + L_o} \exp\left[(x_c - x)/L_o \right] & , \quad x > x_c \end{cases} \qquad (6.9)$$

The phase of ϕ is chosen so that at points $x >> x_c$ $\phi_I = o$, and so from eqn. (6.8), it follows that $\phi_I(x) = o$ for all $x > x_c$. For $x < x_c$ the integration variable can be changed from x to $\psi(x)$ and then from $\psi(x)$ to $\tau(x)$. Following the arguments of sub-section 5.4.5 this then gives

$$\phi_I(x) \simeq \begin{cases} -\dfrac{\pi}{2} \dfrac{kT}{|e|\psi_s} \dfrac{\exp(x_c/L_o)}{(x_c + L_o)} (x_c - x), & x < x_c \\[2ex] o & , \quad x > x_c \end{cases} \qquad (6.10)$$

A typical example of $\phi_R(x)$ and $\phi_I(x)$ is plotted in Fig.6.1 (see section 6.3). Importantly, except for large x_c(i.e. $|e|\psi(x_c) \sim kT/|e|$), $\phi_R >> \phi_I$.

Expressions for capacitance and conductance can be obtained directly from eqns. (6.9) and (6.10). Direct substitution into eqns. (5.72) and (5.73) of sub-section 5.4.6 gives

$$C(\psi_s,\omega) = \frac{\epsilon\epsilon_o}{x_c + L_o} = \frac{(\epsilon\epsilon_o|e|^2 N)^{\frac{1}{2}}}{1 + \ln(\psi_s/\psi_c)} , \qquad (6.11)$$

and,

$$G(\psi_s,\omega) = \omega \frac{\pi}{2} \varepsilon\varepsilon_o \frac{kT}{|e|\psi_s} \frac{L_o}{(x_c + L_o)^2} \exp(x_c/L_o)$$

$$= \omega \frac{\pi}{2} \frac{kT}{|e|\psi_c} \frac{(\varepsilon\varepsilon_o|e|^2N)^{1/2}}{(1 + \ln(\psi_s/\psi_c))^2} \qquad (6.12)$$

where $|e|\psi_c = kT \ln(1/\omega\tau_o) - (E_c - E_F)$. The capacitance expression is identical to that derived by Viktorovitch and Moddel[1] (1980). The conductance is a new expression. Note that from this expression it is easily shown that over a large frequency range the conductance is approximately proportional to frequency.

6.3 EXAMINATION OF THE APPROXIMATIONS IN THE ADMITTANCE CALCULATION

Several mathematical approximations were made in the course of the admittance calculations. They were the use of zero temperature statistics, the simplifications to the differential equation for Φ, and the discarding of the small terms K_1 and K_2 (see sub-section 5.4.6). These approximations are now examined in turn.

Zero Temperature Statistics

There are two separate instances where zero temperature statistics is used. In sub-section 5.4.2 the d.c. charge density due to deep gap states was approximated thus

$$\rho(x) \simeq |e| \int_{E_F - |e|\psi(x)}^{E_F} N(E)\,dE \quad . \qquad (6.13)$$

A first estimation of the error in $\rho(x)$ can be found using an expansion of

the Fermi-Dirac integral where $(kT)^4$ and higher power terms have been discarded.

$$\rho(x) \approx |e| \int_{E_F=|e|\psi(x)}^{E_F} N(E)dE + |e| \frac{\pi^2}{6} (kT)^2 \left(\left.\frac{dN}{dE}\right|_{E=E_F} - \left.\frac{dN}{dE}\right|_{E=E_F-|e|\psi(x)} \right) \tag{6.14}$$

For a derivation of eqn.(6.14) use for example Mott and Jones[2] (1936), pp.175. This equation shows that if the density of states function N(E) changes by less than a factor of two over any energy range kT then the approximation is reasonable. It is thought that this condition should hold except perhaps near the mobility edges. Moreover, finite temperature calculations have been made for $\rho(x)$ in Field Effect experiments[3,4]. It is shown that removing the approximation does affect the calculation, but the change is quite small. Therefore eqn.(6.13) is thought to be a sufficiently good estimate of $\rho(x)$.

The second instance where zero temperature statistics is used is in the estimation of the gap state response characterised by the function $1/(1 + i\omega\tau)$ (see sub-section 5.3.5). A more accurate response function is $\ln(1 + i\omega\tau)/i\omega\tau$ and this function was examined in sub-section 5.3.5. There are three points worth noting.

In sub-section 5.4.5, the calculation to find ϕ_I required the integration of $\omega\tau/(1 + \omega^2\tau^2)$ from $x = \infty$ to $x = o$. Using the more accurate

response function, the equivalent integration is

$$\int_{\infty}^{0} \frac{\ln(1 + \omega^2\tau^2)}{2\omega\tau}\, dx \simeq \left[\left.\frac{d\psi}{dx}\right|_{x=x_c} \right]^{-1} \int_{0}^{\psi_s} \frac{\ln(1 + \omega^2\tau^2)}{2\omega\tau}\, d\psi$$

$$\simeq \frac{kT}{|e|} \left[\left.\frac{d\psi}{dx}\right|_{x=x_c} \right]^{-1} \int_{\sim 0}^{\sim\infty} \frac{\ln(1 + \omega^2\tau^2)}{2\omega\tau^2}\, d\tau$$

$$\frac{kT}{|e|} \left[\left.\frac{d\psi}{dx}\right|_{x=x_c} \right]^{-1} \cdot \frac{\pi}{2} \qquad (6.15)$$

which is the same answer as before. i.e. the area under both peaked functions is identical and therefore the approximation for $d\phi_I/dx|_{x=o}$ remains unaffected.

The main effect of finite temperature is to shift the response function towards the metal-semiconductor interface. The real part of the function, $\tan^{-1} \omega\tau/\omega\tau = \frac{1}{2}$ at $\omega\tau = 1.98$, and the maximum value of the imaginary part, $\ln(1 + \omega^2\tau^2)/2\omega\tau$ is at $\omega\tau = 2.33$. Therefore x_c would be better defined by the equality $\omega\tau(x_c) = 2$. It follows that if the zero temperature response function is used to estimate for $\tau_o\left(= 1/c_n N_c\right)$ then the estimate will be too small by a factor of two.

Finally, the function $1/(1 + i\omega\tau)$ markedly underestimates the residual gap state response at high signal frequencies. It has been demonstrated that the main charge response arises from the change in electron occupancy of gap states at the Fermi level. However there is some charge

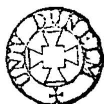

response associated with gap states of energies above and below the Fermi level. At high frequencies, the electron occupancy of states above the Fermi level may still respond to the small signal and the function $\ln(1 + i\omega\tau)/i\omega\tau$ much better describes this response. It turns out that at such high frequencies the admittance is further complicated by the partial response of majority carriers (see sub-section 6.5.4) and so it is not important to accurately model the gap state response in this high frequency regime.

Simplifications of the Differential Equation for the Small Potential

In order to obtain analytic expression for capacitance and conductance several approximations were made to the differential equation for the small potential ϕ. It should be observed that the differential equation (given by eqn.(5.55), sub-section 5.4.3) can be solved directly using standard numerical techniques. A complete numerical solution however would require an involved and lengthy procedure and a much simpler, non-rigorous numerical procedure can be used to show that the approximate analytical solutions are sufficiently accurate.

The constant gap state density $N(E) = N$ case was chosen and eqns.(6.9) and (6.10) were used as a first estimate for the small potential $\phi = \phi_R + i\phi_I$. These results for $\phi(x)$, and the d.c. solution for $\psi(x)$ were substituted into the complete differential equation for the small potential, eqn.(6.6). The differential equation was then integrated twice to give a second estimate for $\phi(x)$. The parameters used were $N = 10^{17}$ cm^{-3} eV^{-1}, $E_c - E_F = 0.35$ eV, $\tau_o = 10^{-14}$ s, $\psi_s = 0.5$ volts, $f = 10$ kHz, $T = 300$ K and $\epsilon = 11$, and a plot of the two estimates for ϕ is drawn in Fig 6.1. The estimates are almost identical and so, at least for the chosen example, the simplifications appear to be justified. The calculation was repeated at various signal frequencies, and for each case estimates for capacitance and conductance were found. Table 6.1 summarises the results. Note that the estimates are consistent to within a few percent, although large deviations do occur at frequencies where $\psi_c \lesssim 3kT/|e|$.

Frequency (Hz)	Cut-Off Potential (V) $\omega\tau(\psi_c) = 1$	Capacitance (10^{-4} Fm^{-2})		$\frac{(C_1-C_2)}{C_2}^*$ x 100	$\frac{\text{Conductance}}{\omega}$ (10^{-4} $\Omega^{-1}m^{-2}s$)		$\frac{(G_1-G_2)}{G_2}^*$ x 100
		1st estimate	2nd estimate		1st estimate	2nd estimate	
0.5	0.454	11.1	11.5	-3.5%	0.90	0.82	+ 9.2%
1	0.436	10.7	11.1	-3.5%	0.88	0.85	+ 3.4%
10	0.377	9.5	9.8	-3.6%	0.80	0.81	- 1.9%
10^2	0.317	8.4	8.7	-3.6%	0.73	0.75	- 1.8%
10^3	0.257	7.3	7.6	-3.8%	0.69	0.70	- 0.8%
10^4	0.198	6.3	6.6	-4.0%	0.67	0.665	+ 1.0%
10^5	0.138	5.3	5.6	-4.6%	0.685	0.65	+ 4.8%
10^6	0.079	4.3	4.5	-5.7%	0.77	0.68	+12.6%
10^7	0.019	2.9	2.0	+29%	1.42	5.5	-290%

* Negative sign implies that 1st estimate is smaller than 2nd estimate

TABLE 1: Estimated Admittance Values : $N = 10^{17}$ cm^{-3} eV^{-1}, $E_c-E_F = 0.35$ eV, $\tau_o = 10^{-14}$ s, $\psi_s = 0.5V$, T = 300 K, $\varepsilon = 11$. For method of estimation see text.

Evaluation of the Small Discarded Terms K_1, K_2

In sub-section 5.4.6 capacitance and conductance were written thus

$$C(\psi_s,\omega) = \frac{1+K_2}{1+K_1}\left(-\frac{\varepsilon\varepsilon_o}{\phi_R}\frac{d\phi_R}{dx}\right)\Bigg|_{x=o}, \tag{6.16}$$

and

$$G(\psi_s,\omega) = \frac{\omega\varepsilon\varepsilon_o}{1+K_1}\left(\frac{1}{\phi_R}\frac{d\phi_I}{dx} - \frac{\phi_I}{\phi_R^2}\frac{d\phi_I}{dx}\right)\Bigg|_{x=o}, \tag{6.17}$$

and K_1 and K_2 were taken to be small terms. From eqn. (5.71) sub-section 5.4.6,

$$K_1 = \left(\frac{\phi_I}{\phi_R}\right)^2\Bigg|_{x=o} \tag{6.18}$$

and

$$K_2 = \left(\frac{\phi_I \frac{d\phi_I}{dx}}{\phi_R \frac{d\phi_R}{dx}}\right)\Bigg|_{x=o}. \tag{6.19}$$

Using the same arguments as those used to calculate C and G, these terms

can be written thus

$$K_1 = \left\{ \frac{\pi}{2} \; kT \; \frac{N(E_F - |e|\psi_c)}{\int_{E_F - |e|\psi_c}^{E_F} N(E)\,dE} \left(1 - \frac{C(\psi_s, \omega)}{C(\psi_c, o)} \right) \right\}^2 \qquad (6.20).$$

and

$$K_2 = \left\{ \frac{\pi}{2} \; kT \; \frac{N(E_F - |e|\psi_c)}{\int_{E_F - |e|\psi_c}^{E_F} N(E)\,dE} \right\}^2 \left(1 - \frac{C(\psi_s, \omega)}{C(\psi_c, o)} \right), \qquad (6.21)$$

and for a constant density of states $N(E) = N$, these results simplify to

$$K_1 = \left(\frac{\pi}{2} \; \frac{kT}{|e|\psi_c} \; \frac{\ln(\psi_s/\psi_c)}{(1 + \ln(\psi_s/\psi_c))} \right)^2 \qquad (6.22)$$

and

$$K_2 = \left(\frac{\pi}{2} \; \frac{kT}{|e|\psi_c} \right)^2 \cdot \frac{\ln(\psi_s/\psi_c)}{(1 + \ln(\psi_s/\psi_c))} \; . \qquad (6.23)$$

Fig 6.2 shows a plot of the functions $(1 + K_2)/(1 + K_1)$ and $1/(1 + K_1)$ versus cut-off potential ψ_c for the $N(E) = N$ case. This plot confirms that if $\psi_c > 3kT/|e|$ then K_1 and K_2 are sufficiently small to be neglected.

6.4 ADMITTANCE CALCULATION INCLUDING MAJORITY CARRIER CHARGE

In the treatment of gap state kinetics (sub-section 5.3.1), interactions were assumed to occur only between gap states and states described by an extended wavefunction. It was therefore sensible to define a majority carrier/conduction band electron as an electron which occupies a state above the conduction band mobility edge. Subsequently, the total charge in the barrier was calculated using zero temperature statistics. This method adequately accounts for charged states between gap state energies $E_F - |e|\psi_s < E < E_F$, but it ignores any charge residing in band-tail states or states above the mobility edge. In order to account for this charge it is best to define majority carrier charge as any charge residing in states which are at energies significantly above the semiconductor Fermi level E_F. The symbol n^* will be used to denote the associated electron density. The density of electrons occupying states above the conduction band mobility edge will continue to be called the conduction band electron density and be denoted by n.

A reasonable estimate of the density of states at the mobility edge is $N(E_c) \simeq 5 \times 10^{21}$ cm^{-3} eV^{-1}. Then, using Maxwell-Boltzmann statistics and assuming that $N(E) \simeq N(E_c)$ for $E > E_c$, the conduction band effective density of states is approximately $kTN(E_c)$. Measurements of electron drift mobility show that the mobility is trap controlled. It is strongly temperature dependent but at room temperature the value is estimated to be approximately ten times smaller than the calculated extended state mobility. This suggests that electrons only spend about one tenth of their time in extended states, and the rest of the time they occupy shallow traps in the band-tail. It follows that a good estimate of the total majority carrier density at room temperature is given by

$$n^* = N^*_c \exp\left[(E_F - E_c)/kT\right], \qquad (6.24)$$

where $N^*_c \simeq 10\ kTN(E_c) \simeq 1.3 \times 10^{20}\ cm^{-3}$.

Eqn.(6.24) gives the approximate density of electrons occupying states above E_F in the neutral semiconductor bulk, and this density is denoted n_B. The steady state majority carrier density in the depletion region can now be written as

$$n^*_o(x) = n_B \exp(-|e|\psi(x)/kT) \tag{6.25}$$

and from eqn.(5.5) the time-varying part of the majority carrier density can be written as

$$\delta n^*(x,t) = \frac{n_B}{kT} \exp(-|e|\psi(x)/kT)\ (\ \delta E_{Fn}(x,t) - |e|\psi(x,t)\ ). \tag{6.26}$$

This equality requires that the band-tail states always maintain equilibrium with the conduction band.

Consider first the case when the majority carrier charge is the dominant charge density in the barrier. This is normally the case for crystalline Schottky barriers. The depletion approximation is used. This approximation states that between $x = o$ and $x = W$ the d.c. charge density is $|e|n_B$ and at $x = W$ the charge density abruptly falls to zero. W is called the depletion width. Using this approximation Poisson's equation becomes

$$\frac{d^2\psi}{dx^2} = \frac{\rho_{maj}(x)}{\varepsilon\varepsilon_o} \simeq \begin{cases} \dfrac{|e|n_B}{\varepsilon\varepsilon_o} & , x < W \\ o & , x > W \end{cases} \tag{6.27}$$

and the boundary conditions are $\psi(o) = \psi_s$, $\psi(W) = o$ and $d\psi/dx \Big|_{x=W} = o$.

Eqn (6.27) is easily solved, and for $x < W$

$$\psi(x) = \frac{|e|n_B}{\varepsilon\varepsilon_o}(W-x)^2 = \psi_s\left(1 - \frac{x}{W}\right)^2, \tag{6.28}$$

where $W = (2\varepsilon\varepsilon_o\psi_s/|e|n_B)^{\frac{1}{2}}$. The total charge in the barrier is

$$Q = |e|n_B W = (2\varepsilon\varepsilon_o|e|n_B\psi_s)^{\frac{1}{2}} \quad (6.29)$$

and the static, zero-frequency capacitance follows.

$$C(\psi_s,o) = \frac{dQ}{d\psi_s} = \left(\frac{|e|n_B\varepsilon\varepsilon_o}{2\psi_s}\right)^{\frac{1}{2}} = \frac{\varepsilon\varepsilon_o}{W} \quad (6.30)$$

Note that at this level of approximation the Schottky barrier behaves as a simple parallel plate capacitor with plate separation W and capacitance $\varepsilon\varepsilon_o/W$. A small change in bias widens or narrows the depletion region and essentially the only change in charge density is at the depletion edge. It follows that the x-dependence of the small signal is

$$\phi(x) = \frac{\phi_s}{W}(W-x) \quad , \quad x < W \quad (6.31)$$

where $\phi(o) = \phi_s$.

Unlike the barrier dominated by gap state charge, this capacitance is frequency-independent over a large range of signal frequencies (see sub-section 6.5.2). Therefore eqns. (6.30) and (6.31) are correct at finite measuring frequencies and the only conductance term is that due to diode leakage.

Consider now the more general case where majority carrier charge and gap state charge are both important. Using eqn.(6.25) and eqn.(5.43) of sub-section 5.4.2, Poisson's equation becomes

$$\frac{d^2\psi}{dx^2} = \frac{1}{2}\frac{d}{d\psi}\left(\frac{d\psi}{dx}\right)^2 = \frac{|e|}{\varepsilon\varepsilon_o}\left(n_B(1 - e^{-|e|\psi/kT}) + \int_{E_F-|e|\psi}^{E_F} N(E)dE\right). \quad (6.32)$$

The inserted identity allows eqn.(6.32) to be integrated through ψ and hence,

$$\left.\frac{d\psi}{dx}\right|_{\psi=\psi_o} = -\left\{\frac{2|e|}{\varepsilon\varepsilon_o}\left[\left(\psi_o - \frac{kT}{|e|} + \frac{kT}{|e|} e^{-|e|\psi_o/kT}\right) n_B + \int_o^{\psi_o}\int_{E_F-|e|\psi}^{E_F} N(E)\,dE\,d\psi\right]\right\}. \quad (6.33)$$

If $\psi_o \gg kT/|e|$ then the terms in kT may be discarded and one more integration gives

$$x(\psi_o) = \left(\frac{\varepsilon\varepsilon_o}{2|e|}\right)^{1/2} \int_{\psi_o}^{\psi_s} \frac{d\psi'}{\left(n_B\psi' + \int_o^{\psi'}\int_{E_F-|e|\psi}^{E_F} N(E)\,dE\,d\psi\right)^{1/2}} . \quad (6.34)$$

The barrier charge and hence the static, zero-frequency capacitance follows from eqn.(6.33),

$$C(\psi_s,o) = \left(\frac{|e|\varepsilon\varepsilon_o}{2}\right)^{1/2} \frac{n_B + \int_{E_F-|e|\psi_s}^{E_F} N(E)\,dE}{\left(n_B\,\psi_s + \int_o^{\psi_s}\int_{E_F-|e|\psi}^{E_F} N(E)\,dE\,d\psi\right)^{1/2}} , \quad (6.35)$$

and for a constant gap state density N(E) = N this result simplifies to

$$C(\psi_s, o) = \frac{2C_{maj}^2 + C_{gap}^2}{(4C_{maj}^2 + C_{gap}^2)^{1/2}} \tag{6.36}$$

where C_{maj} is the capacitance if only majority carriers are considered (eqn. (6.30)) and C_{gap} is the capacitance if only gap states are considered (eqn. (6.5)).

At finite frequencies the differential equation for the small potential must be introduced. It is assumed that the majority carrier response is complete (i.e. $\delta E_{Fn} = o$). Then following eqn. (5.53) and using eqn.(6.26).

$$\frac{d^2}{dx^2}\phi(\psi_s, x, \omega) = \frac{|e|^2}{\varepsilon\varepsilon_o}\left(\frac{N(E_F - |e|\psi(x))}{1 + i\omega\tau(\psi_s, x)} + \frac{n_B}{kT} e^{-|e|\psi(x)/kT}\right)\phi(\psi_s, x, \omega). \tag{6.37}$$

Explicit reference to the functional dependencies on bias, position and frequency is dropped, and writing $\phi = \phi_R + i\phi_I$ allows eqn. (6.37) to be separated into its real and imaginary parts.

$$\frac{d^2\phi_R}{dx^2} = \frac{|e|^2}{\varepsilon\varepsilon_o}\left(\frac{N(E_F - |e|\psi)}{1 + \omega^2\tau^2}\phi_R + \frac{\omega\tau}{1 + \omega^2\tau^2} N(E_F - |e|\psi)\phi_I + \frac{n_B}{kT} e^{-|e|\psi/kT}\phi_R\right), \tag{6.38}$$

$$\frac{d^2\phi_I}{dx^2} = \frac{|e|^2}{\varepsilon\varepsilon_o}\left(\frac{N(E_F - |e|\psi)}{1 + \omega^2\tau^2}\phi_I - \frac{\omega\tau}{1 + \omega^2\tau^2} N(E_F - |e|\psi)\phi_R + \frac{n_B}{kT} e^{-|e|\psi/kT}\phi_I\right). \tag{6.39}$$

Following sub-section 5.4.4. these equations can be approximated to

$$\left.\begin{aligned} \frac{d^2\phi_R}{dx^2} &\simeq \frac{|e|^2}{\varepsilon\varepsilon_o}\left(N(E_F-|e|\psi) + \frac{n_B}{kT}\, e^{-|e|\psi/kT}\right)\phi_R \qquad (6.40) \\ \frac{d^2\phi_I}{dx^2} &\simeq \frac{|e|^2}{\varepsilon\varepsilon_o}\left(N(E_F-|e|\psi) + \frac{n_B}{kT}\, e^{-|e|\psi/kT}\right)\phi_I \qquad (6.41) \end{aligned}\right\} , x > x_c$$

$$\left.\begin{aligned} \frac{d^2\phi_R}{dx^2} &\simeq 0 \qquad (6.42) \\ \frac{d^2\phi_I}{dx^2} &\simeq -\frac{|e|^2}{\varepsilon\varepsilon_o}\frac{\omega\tau}{1+\omega^2\tau^2} N(E_F-|e|\psi)\,\phi_I \qquad (6.43) \end{aligned}\right\} x < x_c \text{ and } \psi(x_c) \gg kT/|e| ,$$

where x_c is defined by $\omega\tau(x_c) = 1$. Note that eqns. (6.42) and (6.43) require that $\psi(x_c) \gg kT/e$ because only then can majority carriers be neglected.

Direct comparison with the previous simplified equations for the small potential (see sub-section 5.4.4) shows that the general solution for $x < x_c$ is identical to the case when majority carrier charge is negligible. Further if the same phase is chosen for ϕ (i.e. $\phi_I = 0$ at some point $x > x_c$) from eqn. (6.41), $\phi_I(x) = 0$ for all $x > x_c$. Eqn.(6.40) does appear however to be significantly different, but it is shown in Appendix A that the relation

$$\frac{1}{\phi_R(x)}\frac{d\phi_R(x)}{dx} = \frac{d}{d\psi}\left(-\frac{d\psi(x)}{dx}\right) = -\frac{C(\psi(x),o)}{\varepsilon\varepsilon_o} \qquad (6.44)$$

satisfies eqn.(6.40) and the required boundary conditions at $x = \infty$. In fact the complete relation only holds if the small terms in kT are not discarded after eqn. (6.33), but of course eqn.(6.35) for $C(\psi(x),o)$ is still a good approximation and this approximate value can be used in calculations.

It follows from the above considerations that capacitance and conductance can be evaluated using exactly the same expressions as before (eqns. (5.74) and (5.76)), but now x_c is found using eqn.(6.34) and $C(\psi_c,o)$ is found using eqn. (6.35). Several example calculations have been carried out and it was found that if $N(E) > 10^{17}$ cm^{-3} eV^{-1} then majority carrier charge has negligible effect on the admittance. Some effect is seen if the density of states suggested by Lang et al[5] (see Fig.5.5, sub-section 5.5.2) is used and if the Fermi level is only 0.2 eV below E_c. This corresponds to very heavy n-type doping and a large part of this density of gap states is less than 10^{17} cm^{-3} eV^{-1}.

Fig.6.3 shows frequency plots generated using the N(E) suggested by Lang et al, $E_c-E_F = 0.2$ eV, $\tau_o = 10^{-14}$ s, $\psi_s = 0.55$ volts, $\epsilon = 11$, T = 300 K and $N_c^* = 1.3 \times 10^{20}$ cm^{-3}. Also shown are the plots calculated without majority carrier charge (dashed lines) and the majority carrier capacitance without gap states (dashed line with circles). The majority carrier charge leads to an increase in the capacitance and conductance and the fractional increase for both is $\sim$ 35%. It must be noted however that at $E_c-E_F = 0.2$ eV the Fermi level almost lies in the band tail and there may be appreciable error in the analysis. It is clear from these plots, possible errors accepted, that some caution must be taken in the analysis of heavily doped a-Si Schottky barriers. Note in particular that the Lang N(E) results in a gap state capacitance which is almost frequency independent. This frequency-independence can be equally well explained if majority carrier charge were to dominate the charge response and so some other distinguishing evidence (e.g. conductance) is required.

6.5 EXAMINATION OF THE MAJORITY CARRIER RESPONSE

In Chapter 5 the admittance calculation could only proceed if it was assumed that at all times the conduction band electrons remain in thermal equilibrium with each other. Any transport of electrons however must lead to some deviation from thermal equilibrium and we examine here the transport of the majority carriers arising from the time-varying small potential.

It will become clear that it is very difficult to derive a general analytic expression for the majority carrier response, and in this section the calculations are somewhat speculative in nature and they lack the mathematical rigour of previous sections. The intention is to illustrate the underlying physics and to make comment on the assertion that majority carrier transport limits the barrier charge response[1]. A completely self-consistent solution to the majority carrier response problem would require the use of numerical techniques.

6.5.1 Equations Governing the Majority Carrier Response

An n-type Schottky barrier has two distinct electron currents : an electron drift current due to the built-in and applied electric fields, and a particle diffusion current due to the spatially varying electron density. Only electrons occupying non-localised states are able to take part in the transport and so the appropriate current density equation is

$$J(x,t) = |e|\mu_{ex}\, n \frac{d}{dx}\, \Psi(x,t) + |e|\, D_{ex}\, \frac{d}{dx}\, n\,(x,t)\ , \qquad (6.45)$$

where n is the conduction band electron density, $\Psi = \psi + \phi$ is the total barrier potential, μ_{ex} is the extended state electron mobility and D_{ex} is the extended state electron diffusion constant. It should be noted that only the current directly associated with electron transport is considered. In particular, eqn. (6.45) does not include displacement current. A useful

result follows by substituting

$$n(x,t) = N_c \exp\left\{\left[E_{Fn}(x,t) - (E_c + |e|\Psi(x,t))\right] /kT\right\} \qquad (6.46)$$

into eqn. (6.45) and using the well known Einstein relation

$D = \mu kT/|e|$. This gives

$$J(x,t) = \mu_{ex} n\,(x,t) \frac{d}{dx} E_{Fn}(x,t). \qquad (6.47)$$

E_{Fn} is the conduction band electron quasi-Fermi level and eqn. (6.47) demonstrates that any movement of conduction band electrons must result in a finite gradient to E_{Fn}. Note that the gradient is largest for small μ, n.

It was shown in the last section that electrons occupying band-tail states can be incorporated into the admittance calculation by adjusting the value of the conduction band effective density of states N_c to N_c^*. A similar adjustment can be made here : if it is assumed that electrons occupying band-tail states always maintain equilibrium with the conduction band electrons, then the majority carrier density n^* can replace n in eqns. (6.45) and (6.47), but note that then μ_{ex} must also be replaced by the trap-limited mobility, denoted μ.

Consider now the application of a small sinusoidal potential. It gives rise to the following small disturbances.

$$\left.\begin{aligned} n^*(x,\omega) &= n_o^*(x) + \delta n^*(x,\omega) \\ n_T(x,\omega) &= n_{TO}(x) + \delta n_T(x,\omega) \\ E_{Fn}(x,\omega) &= E_F + \delta E_{Fn}(x,\omega) \\ \Psi(x,\omega) &= \psi(x) + \phi(x,\omega) \end{aligned}\right\} . \qquad (6.48)$$

The intention is to find an expression for $\delta E_{Fn}(x,\omega)$ and this is done by

introducing the current continuity equation

$$\frac{d}{dx} J(x,t) = - \frac{d}{dt} \rho(x,t) = -i\omega\rho_{\phi}(x,\omega), \tag{6.49}$$

where $\rho_{\phi} = -|e| (\delta n^{*} + \delta n_{T})$. Eqn. (6.47) is used for J and eqn.(5.53) is used for ρ_{ϕ}. These equations are substituted into eqn. (6.49) and neglecting small second order terms this gives

$$\mu n_{o}^{*} \frac{d^{2}\delta E_{Fn}}{dx^{2}} + \mu \frac{dn_{o}^{*}}{dx} \frac{d\delta E_{Fn}}{dx} = i\omega|e| \left(\frac{n_{o}^{*}}{kT} + \frac{N(E_{F}-|e|\psi)}{1+i\omega\tau} \right) (\delta E_{Fn} - |e|\phi) \tag{6.50}$$

and note that n^{*} and the trap-limited mobility μ are used. Also required is the a.c. part of Poisson's equation.

$$\frac{d^{2}\phi}{dx^{2}} = - \frac{|e|}{\epsilon\epsilon_{o}} \left(\frac{n_{o}^{*}}{kT} + \frac{N(E_{F}-|e|\psi)}{1+i\omega\tau} \right) (\delta E_{Fn} - |e|\phi), \tag{6.51}$$

and $\delta E_{Fn}(x,\omega)$, $\phi(x,\omega)$ can now be found from the simultaneous solution of eqns. (6.50) and (6.51). Appropriate boundary conditions are likely to be

$$\phi(o) = \phi_{s}, \quad \phi(\infty) = o, \quad \left.\frac{d\phi}{dx}\right|_{x=\infty} = o, \quad \delta E_{Fn}(\infty) = o. \tag{6.52}$$

An exact solution of these equations is difficult and is not attempted. Instead certain approximations can be made which lead to reasonable estimates of the majority carrier response, and for our purposes this proves sufficient.

6.5.2 Majority Carrier Response with no Gap States

Consider an n-type Schottky barrier with no deep gap states (N(E) = o), no band-tail states ($n^{*} = n$) and a uniform bulk majority carrier density, denoted n_{B}. The treatment of this case is somewhat easier than the case

where there is a large density of gap states.

According to the depletion approximation described in section 6.4, the d.c. barrier profile is

$$\psi(x) = \frac{|e|n_B}{\varepsilon\varepsilon_o}(W-x)^2 , \qquad W = \left(\frac{2\varepsilon\varepsilon_o}{|e|n_B}\psi_s\right)^{\frac{1}{2}} , \tag{6.53}$$

where W is the depletion width and ψ_s is the potential at the metal-semiconductor interface. This result can be used to find dn_o/dx : differentiating eqn. (6.25) for n_o and then differentiating $\psi(x)$ gives

$$\frac{dn_o}{dx} = -\frac{|e|n_o(x)}{kT}\frac{d\psi}{dx} = \frac{|e|n_o(x)}{kT}\frac{|e|n_B}{\varepsilon\varepsilon_o}(W-x) , \quad x< W \tag{6.54}$$

Over a certain frequency range it is possible to deduce an approximate solution of the a.c. part of Poisson's equation, eqn. (6.51), without recourse to the current continuity equation, eqn. (6.50). It was argued in section 6.4, that at sufficiently low frequencies the main effect of the small signal is to change the charge density at the boundary between the neutral bulk and the depletion region. If sufficient charge is able to flow between the back contact and the depletion edge at $x = W$, then it follows that the solution for ϕ is

$$\phi(x) = \frac{\phi_s}{W}(W-x), \quad x < W. \tag{6.55}$$

Now let the resistance of the bulk semiconductor from $x = W$ to the back contact be R, and denote the capacitance of the depletion region as $C(= \varepsilon\varepsilon_o/W)$. R and C are in series and therefore from simple a.c. theory eqn. (6.55) is correct for signal frequencies which fulfil the condition $\omega << 1/RC$. Note also that if $\omega << 1/RC$ then $\delta E_{Fn}(x > W) = o$. Substituting eqns. (6.54) and (6.55) into eqn. (6.50) and using this boundary condition now allows an estimate

to be made for the majority carrier response time in the depletion region.

For $\omega << 1/RC$ and $x < W$, eqn. (6.50) becomes

$$\frac{d^2 \delta E_{Fn}}{dx^2} \quad \frac{|e|}{kT} \quad \frac{|e| n_B}{\varepsilon \varepsilon_o} (W-x) \frac{d \delta E_{Fn}}{dx} = i \frac{\omega |e|}{\mu kT} \left(\delta E_{Fn} - \frac{|e| \phi_s}{W} (W-x) \right), \qquad (6.56)$$

and the following solution is suggested,

$$\delta E_{Fn}(x,\omega) = \frac{\omega}{\omega^2 + \omega_D^2} (\omega + i\omega_D) \frac{|e|\phi_s}{W} (W - x) , \qquad x < W, \qquad (6.57)$$

where $\omega_D = |e|\mu n_B / \varepsilon\varepsilon_o$. Note that ω_D is the inverse of the bulk dielectric relaxation time. Also this solution for $\delta E_{Fn}(x,\omega)$ fits the boundary condition $\delta E_{Fn} = 0$ at $x = W$ and as $\omega \rightarrow o$, $\delta E_{Fn} \rightarrow o$ and as $\omega \rightarrow \infty$ $\delta E_{Fn} \rightarrow |e|\phi$, which is the required behaviour. It is difficult to mathematically justify eqn. (6.57) (eqn. (6.56) is a complex linear second order differential equation - eqn. (6.57) is a particular integral, the complementary function has been set to zero and the required asymptotic behaviour of the solution has been used instead of a second boundary condition). Nevertheless it will be shown that eqn. (6.57) is in agreement with physical arguments to be discussed. It is simply accepted here that if $\omega <<$ 1/RC then eqns.(6.55) and (6.57) give ϕ and δE_{Fn} respectively. These solutions can be substituted into eqn. (5.5), which relates δn to δE_{Fn} and ϕ, thus giving

$$\delta n(x,\omega) = - \frac{n_o(x)}{kT} \frac{\omega_D}{\omega^2 + \omega_D^2} (\omega_D - i\omega) \frac{|e|\phi_s}{W} (W - x), \quad x < W \qquad (6.58)$$

and note that when $\omega = \omega_D$ the real and imaginary parts of δn become equal. Therefore a sensible estimate of the majority carrier response time in the depletion region is simply the bulk dielectric relaxation time.

Eqn.(6.58) is not a rigorous result and indeed at angular frequencies approaching ω_D carriers in the bulk cannot respond, $\delta E_{Fn}(x \geq W) \neq o$ and the solution must fail. Nevertheless it is clear that if $\omega << \omega_D$ then we may expect almost total majority carrier response. This result is assumed in many depletion region admittance calculations. See, for example, "MOS Physics and Technology" by Nicollian and Brews(6) (1982), pp.101. Note also that in a p-n junction there is a further frequency-limiting effect due to minority carrier injection. See, for example, Shockley(7) (1949).

The underlying physics of the system can be understood using the following arguments based on the case of a transient response. If a small forward bias is applied at time t = o, then at time $t = o^+$ the energy band diagram is tilted on its side as shown in Fig.6.4. At time $t = o^+$ the quasi-Fermi level has a constant gradient and so from eqn. (6.47) the instantaneous current flowing at any point x must be proportional to $n_o(x)$. Hence large currents flow through the neutral bulk where n_o is large, but moving into the depletion region the current rapidly falls off. Now for the conduction band electrons to come into equilibrium with each other, the electron density at each point x must change and this change is also proportional to $n_o(x)$. Therefore at any point x the magnitude of the current is proportional to the required change in electron density. And so it is quite reasonable, despite the large variation in electron density, for the response time to be a constant and equal to the bulk dielectric relaxation time.

6.5.3 Majority Carrier Response with Gap States

Consider an n-type Schottky barrier with a constant gap state density (i.e. N(E) = N), and assume that the charge contribution from gap states dominates the barrier charge. The calculation is made simpler if it is assumed that all electrons occupying gap states always maintain equilibrium with the conduction band electrons. Then the gap state electron occupancy will follow the conduction band electron quasi-Fermi level $E_{Fn}(x, \omega)$. Also

electrons in band-tail states and electrons above the conduction band edge will be considered together and their total density is denoted n^*.

Eqn. (6.3) gives the d.c. barrier profile as

$$\psi(x) = \psi_s \exp(-x/L_o), \qquad L_o = \left(\frac{\varepsilon\varepsilon_o}{|e|^2 N} \right)^{1/2}, \tag{6.59}$$

and so

$$\frac{dn_o^*}{dx} = - \frac{|e|n_o}{kT} \frac{d\psi}{dx} = \frac{|e|n_o^*}{k\,T} \frac{\psi(x)}{L_o} \tag{6.60}$$

The assumptions that $N >> n_o^*/kT$ and $\omega\tau << 1$ for all x, simplify eqn. (6.50) to give

$$\frac{d^2\delta E_{Fn}}{dx^2} + \frac{|e|}{kT}\frac{\psi(x)}{L_o}\frac{d\delta E_{Fn}}{dx} = i\,\frac{\omega|e|}{\mu}\frac{N}{n_B}\,e^{|e|\psi(x)/kT}\left(\delta E_{Fn} - |e|\phi\right) \tag{6.61}$$

where n_B is the density of majority carriers in the bulk and μ is the trap limited electron mobility. Eqn. (6.25) has been used for $n_o^*(x)$.

Despite the various simplifications it is still difficult to estimate the majority carrier response time. We resort to a priori arguments where the justification of many of the assumptions and approximations lies in the self-consistency of the results. In order to convince the reader that the arguments are correct, two complementary approaches are taken. An intuitive physical approach is outlined here and a more mathematical approach is described in Appendix B.

It is first assumed that a reasonable estimate for $\phi(x)$ is the total response value ($\delta E_{Fn} = 0$, for all x)

$$\phi(x) = \phi_s \exp(-x/L_o). \tag{6.62}$$

It will be shown later that the only important requirement is that ϕ is real. Given this estimated solution for the a.c. part of Poisson's equation (eqn. (6.51)), the result is substituted into eqn. (6.61) and writing $\delta E_{Fn} = \delta E_{Fn}(1) + i\delta E_{Fn}(2)$, eqn. (6.61) is separated into its real and imaginary parts.

$$\frac{d^2}{dx^2}\,\delta E_{Fn}(1) + \frac{|e|}{kT}\,\frac{\psi(x)}{L_o}\,\frac{d}{dx}\,\delta E_{Fn}(1) = -\,\frac{\omega|e|}{\mu}\,\frac{N}{n_B}\,e^{|e|\psi(x)/kT}\,\delta E_{Fn}(2) \tag{6.63}$$

$$\frac{d^2}{dx^2}\,\delta E_{Fn}(2) + \frac{|e|}{kT}\,\frac{\psi(x)}{L_o}\,\frac{d}{dx}\,\delta E_{Fn}(2) = \frac{\omega|e|}{\mu}\,\frac{N}{n_B}\,e^{|e|\psi(x)/kT}\left(\delta E_{Fn}(1) - |e|\phi_s e^{-x/L_o}\right) \tag{6.64}$$

A frequency is chosen such that for large x, $\delta E_{Fn} \simeq o$. Moving towards $x = o$ the right-hand sides of eqns. (6.63) and (6.64) increase in magnitude very rapidly. This is because of the term $\exp(|e|\psi(x)/kT)$. At some well defined point the gradients of $\delta E_{Fn}(1)$ and $\delta E_{Fn}(2)$ must suddenly become appreciable (for this argument the second order derivative terms are ignored). It follows that close to this point, $\delta E_{Fn}(1)$ and $\delta E_{Fn}(2)$ become finite. It is thought that the magnitudes of $\delta E_{Fn}(1)$ and $\delta E_{Fn}(2)$ will increase very rapidly so that the magnitude of the right-hand side of eqn. (6.64) will reduce. This will lead to a reduction in the rate of increase of $\delta E_{Fn}(2)$ and moreover we propose that $\delta E_{Fn}(2)$ reaches a maximum value and begins to quickly reduce again to zero (i.e. $\delta E_{Fn}(2)$ is a peaked function). From eqn. (6.63) the rate of increase of $\delta E_{Fn}(1)$ will then reduce and it is expected that $\delta E_{Fn}(1)$ will tend towards the maximum value $|e|\phi$. Because of the quickly varying exponential in eqns. (6.63) and (6.64) it is argued that this change from $\delta E_{Fn} \simeq o$ to $\delta E_{Fn} \simeq |e|\phi$ occurs within a few kT of barrier.

Fig 6.5 shows an estimate of $\delta E_{Fn}(1)$ and $\delta E_{Fn}(2)$ schematically plotted in an energy band diagram. The diagram shows the Schottky barrier in the forward bias part of the cycle and then ϕ is negative. We assume that there exists a point where the real and imaginary parts of the disturbance are equal and this point is denoted x_{cm}. At points $x \ll x_{cm}$ the majority carrier response is shown to be close to zero, and at points $x \gg x_{cm}$ the response is almost complete. At $x = x_{cm}$ it is reasonable to assume that $\delta E_{Fn}(1) \approx \frac{1}{2} |e|\phi(x_{cm})$ and so from eqn. (5.5) and the fact that, at $x = x_{cm}$, the real and imaginary parts of δn are equal,

$$\delta E_{Fn}(1) \approx \delta E_{Fn}(2) \approx \frac{1}{2} |e|\phi(x_{cm}) , \qquad x = x_{cm}. \tag{6.65}$$

This assumption has been made in Fig.6.5. The peak in $E_{Fn}(2)$ is also shown to be at $x = x_{cm}$, but this is not a necessary requirement for the calculation.

According to the above model it is clear that the barrier charge response is very similar to the case when capture and emission kinetics was taken to be the charge limiting process. The point $x = x_{cm}$ replaces $x = x_c$, and importantly from previous arguments when $\psi(x_{cm}) \gg kT/|e|$ then $\phi(x)$ is almost completely real (i.e. $\phi_R \gg \phi_I$). These results are perhaps not unexpected and indeed they are in agreement with the equivalent circuit model developed by Viktorovitch and Moddel[1] (1980) to describe the majority carrier response. We now concentrate on finding a relation between the signal frequency and the point $x = x_{cm}$.

Little can be said about the second order derivatives of δE_{Fn}. However, it is reasonable to assume that $d\delta E_{Fn}(1)/dx$ attains its maximum value at $x = x_{cm}$ and therefore

$$\left. \frac{d^2}{dx^2} \delta E_{Fn}(1) \right|_{x=x_{cm}} \approx 0. \tag{6.66}$$

An estimate of $d\delta E_{Fn}(1)/dx \Big|_{x=x_{cm}}$ is obtained by assuming that $\delta E_{Fn}(1)$ changes from zero to $|e|\phi(x_{cm})$ within approximately 3kT of barrier around $x=x_{cm}$. If this distance is denoted Δx then

$$\Delta x \simeq \left(\frac{d\Psi}{dx} \Big|_{x=x_{cm}} \right)^{-1} \frac{3kT}{|e|} = \frac{3kT}{|e|\Psi(x_{cm})} \cdot L_o \qquad (6.67)$$

and

$$\frac{d}{dx}\,\delta E_{Fn}\,(1) \Big|_{x=x_{cm}} \simeq -\frac{|e|\phi(x_{cm})}{\Delta x} \simeq -\frac{|e|\phi(x_{cm})\,|e|\Psi(x_{cm})}{3kT\ L_o} \qquad (6.68)$$

Substituting results (6.65), (6.66) and (6.68) into eqn. (6.63) then gives the required expression

$$\omega(x_{cm}) \simeq \omega_D \left(\frac{|e|\Psi(x_{cm})}{kT} \right)^2 \exp\left(-|e|\Psi(x_{cm})/kT \right), \qquad (6.69)$$

where $\omega_D = |e|\mu n_B/\varepsilon\varepsilon_o$. Note that the value of $\phi(x_{cm})$ appears on both sides of eqn. (6.63) and thus it cancels out. Importantly therefore eqn.(6.69) is independent of the exact value of $\phi(x)$ although the condition that ϕ is real must still hold. Finally the "majority carrier response time", denoted $\tau_{maj}(x)$ may be taken as the inverse of eqn. (6.69) and it can be written thus.

$$\tau_{maj}(x) \simeq \frac{\varepsilon\varepsilon_o}{|e|\mu N_c^*} \left(\frac{kT}{|e|\Psi(x)} \right)^2 \exp\left\{ \left[(E_c - E_F) + |e|\Psi(x) \right] /kT \right\}, \qquad (6.70)$$

where N_c^* is the effective density of states for majority carriers.

Eqn. (6.70) will be shown to be consistent with the underlying physics and of course note that the proposed solution for $\delta E_{Fn}(x,\omega)$ is consistent with the differential equations (6.63) and (6.64). Nevertheless certain of the assumptions (e.g. $\delta E_{Fn}(2)$ is a peaked function, there exists a point where the real and imaginary parts of n are equal, etc.) have not been properly justified. The reader is referred to Appendix B where a more rigorous mathematical argument is used to estimate the majority carrier response. Similar expressions to eqn.(6.70) are derived in this appendix using quite different analysis, and this agreement lends greater credibility to the various assumptions used here.

The underlying physics can be understood using a similar argument to that used for the zero gap state density case. For this previous case the majority carrier current and the required number of carriers were both proportional to $n_o(x)$ and so it was argued that the majority carrier response time was a constant independent of x. Now however the majority carrier current is still proportional to $n_o(x)$ but the required number of carriers is proportional to N, the gap state density. N is a constant, $n_o(x)$ is an exponential and hence the appearance of the exponential term in eqn. (6.70). The $(kT/|e|\psi(x))^2$ term in eqn. (6.70) can be attributed to the effects of particle diffusion - close to $x = x_{cm}$ there is a large gradient in $E_{Fn}(1)$ and this leads to an enhanced electron diffusion current. Note also that τ_{maj} is independent of N, and this is a consequence of the dependence of the electric field on the gap state density.

6.5.4 Frequency-Dependence: Transport Versus Capture and Emission

The admittance calculation described in Chapter 5 assumed that the barrier charge response was limited by the electron capture/emission lifetime of gap states, denoted here as τ_{gap}. It is clear however that a similar frequency dependent admittance could arise if the majority carrier response time, denoted τ_{maj}, limits the charge response. Experimental evidence has not conclusively shown which is the limiting mechanism.

Archibald and Abram[8] (1983) argued that whichever mechanism limited the charge response, the electron occupancy of gap states would respond to a constant majority disturbance according to the equation

$$\frac{d}{dt} n_T(t) = -\frac{n_T(t) - n_{To}(\infty)}{\tau} \qquad (6.71)$$

where $n_T(t)$ is the electron occupancy at time t, $n_{TO}(\infty)$ is the new equilibrium occupancy approached as $t \rightarrow \infty$ and τ is taken to be

$$\tau = \tau_o \exp\left\{\left[(E_c - E_F) + |e|\psi(x)\right]/kT\right\} . \qquad (6.72)$$

τ_o is then simply an adjustable parameter. Eqn.(6.71) leads to a $1/(1+i\omega\tau)$ frequency-dependence for $\rho_\phi(x,\omega)$ and intuitively this was thought to be a realistic dependence to describe either of the two proposed charge limiting processes.

For the case where capture and emission processes limit the charge response, the calculations in Chapter 5 show that eqns. (6.71) and (6.72) do adequately describe the response. If the charge response is limited by majority carrier transport, new physics must be introduced and it is not immediately obvious that eqn. (6.71) is even justified as an approximation. The broad features of the frequency-dependence however have been shown to be quite similar to a $1/(1 + i\omega\tau)$ form, and it has been possible to calculate a "lifetime" for majority carrier response, denoted τ_{maj}. We now argue that it is sensible to compare τ_{gap} with τ_{maj} and the charge response follows from whichever is the larger quantity.

Approximate values for τ_{maj} and τ_{gap} are calculated as follows. From eqn. (6.70), taking $\varepsilon = 11$, $\mu = 0.1$ cm^2 V^{-1} s^{-1}, $N_c^* = 1.3 \times 10^{20}$ cm^{-3}

(see eqn. 6.24),

$$\tau_{maj} \approx 5 \times 10^{-13} \left(\frac{kT}{|e|\psi(x)} \right)^2 \exp\left\{ \left[(E_c - E_F) + |e|\psi(x) \right] / kT \right\} \text{ secs} \tag{6.73}$$

Note thatthe product μN_c^* can be found from a measurement of the pre-exponential term in a d.c. bulk conductivity experiment. Also typical room temperature values for $(kT/|e|\ \psi(x))^2$ range from ~ 1 down to $\sim 10^{-3}$. Reliable values for the capture coefficients of defects in a-Si are not available but a reasonable value for a neutral defect at room temperature is $c_n = 10^{-8}$ cm^{-3} s^{-1} (capture cross-section $\sigma \sim 10^{-15}$ cm^2). Then if $N_c = 1.3 \times 10^{19}$ cm^{-3}

$$\tau_{gap} = \frac{1}{c_n n_o} \approx 8 \times 10^{-12} \exp\left\{ \left[(E_c - E_F) + |e|\psi(x) \right] / kT \right\} \text{ secs} \tag{6.74}$$

Experimentally the proposed best fit values for τ_o range from 10^{-12} down to 10^{-14} secs. There is significant scope for error in eqns.(6.73) and (6.74) and therefore both estimates for τ are reasonable.

It is possible to interpret the results of this section as follows. The frequency-dependence of the admittance is determined by the cut-off position $x = x_c$ and this is obtained from the condition $\omega\tau(x_c) = 1$. At high signal frequencies approaching the inverse of the bulk dielectric relaxation time, the cut-off position will be close to the neutral semi-conductor bulk, $kT/|e|\psi(x) \sim 1$, and then the charge response is likely to be influenced by both response limiting mechanisms. At lower signal frequencies the cut-off position will move into the depletion region, the $(kT/|e|\psi(x))^2$ term reduces $\tau_{maj}(x_c)$ relative to $\tau_{gap}(x_c)$, and therefore it is expected that capture and emission processes will then dominate the charge response.

For undoped a-Si Schottky barriers the high frequency regime corresponds to signal frequencies greater than about 1 Hz. Several authors, for example refs. (1,9), have developed equivalent circuits involving resistors and capacitors to describe the charge response at these frequencies. The models use an approximation, referred to by Henisch[10] (1957), p.204, as "Festschichthypothese", where the depletion region is treated as a spatially varying resistor with resistivity $1/|e|\mu n_o^*(x)$. Bardeen[12] (1949) points out that this approximation neglects particle diffusion current and it follows that the models can only have a limited validity. Nevertheless a more accurate analysis would require a complete numerical solution of eqns. (6.50) and (6.51) and this appears quite difficult. We are therefore limited to this qualitative type analysis, and so admittance measurements made at such frequencies will not be very informative. For undoped barriers it is perhaps better to measure admittance at elevated temperatures, for then at the same measuring frequencies the cut-off position is shifted towards $x = o$. See, for example, Gibb and Long[11] (1984).

6.6 EFFECTS OF DIODE LEAKAGE CURRENT

In a Schottky barrier the assumption that the metal is electrically isolated from the semiconductor is quite incorrect. Indeed the application of a bias can lead to large leakage currents flowing between one and the other and this can have a significant effect on the measured admittance.

If Thermionic emission theory describes the diode leakage current, $E_{Fn} = E_F$, and the previous admittance calculation remains unaffected except that the leakage current must be added as a conductance term in parallel. Often the leakage current density at a constant bias, denoted $J_L(V)$, follows the relation

$$J_L(V) = J_o\,(e^{|e|V/\eta kT} - 1) \qquad (6.75)$$

where J_o is a constant and η is the ideality factor. Assuming complete majority carrier response to the measuring signal, the diode leakage

conductance at bias V is simply,

$$G_L(V) = \left.\frac{dJ_L}{dV}\right|_V = \frac{|e|}{\eta kT} J_o e^{|e|V/\eta kT} \tag{6.76}$$

and G_L can be found from a d.c. J-V plot.

If Diffusion theory better describes the diode leakage current, then close to the metal-semiconductor interface $E_{Fn} \neq E_F$, and thus there must be some error in the previously calculated admittance. It is important to evaluate this effect because it is thought that Diffusion theory may better describe d.c. conduction in an a-Si Schottky barrier.

Consider an n-type a-Si Schottky barrier with bulk Fermi level E_F and barrier height ϕ_b. If a forward bias V is applied then the following relationship should hold

$$\phi_b = (E_c + |e|\psi_s) - (E_F - |e|V) \tag{6.77}$$

where E_c is the energy of the conduction band mobility edge in the neutral bulk and ψ_s is the semiconductor surface potential at bias V. It is now assumed that minority carrier current is negligible and that there is no generation or recombination of carriers within the semiconductor. Then the current is a constant at all points x and is denoted by J. From eqns.(6.46) and (6.47) it is straightforward to show that

$$J = kT\mu_{ex} N_c e^{-(E_c + |e|\psi(x)/kT} \frac{d}{dx} (e^{E_{Fn}(x)/kT}) \tag{6.78}$$

where μ_{ex} is the extended state electron mobility.

For this calculation the energy scale is set so that the bulk Fermi level $E_F = 0$ and it is assumed that $E_{Fn}(\infty) = E_F = 0$. The intention is to find $E_{Fn}(x)$ and to this end eqn.(6.78) is integrated from some point x to

$x = \infty$. This gives

$$J = \frac{kT\mu_{ex} N_c e^{-E_c/kT} (1 - e^{E_{Fn}(x)/kT})}{\int_x^{\infty} e^{|e|\psi(x)/kT} dx} \qquad (6.79)$$

It is reasonable to use the constant gap state density case for the barrier profile $\psi(x)$. The integral in eqn.(6.79) cannot be solved analytically but if $\psi(x)$ is expanded using Taylor's theorem,

$$\psi(x) = \psi_s e^{-x/L_o} = \psi_s (1 - \frac{x}{L_o} + \frac{x^2}{2L_o^2} - \ldots), \qquad (6.80)$$

and keeping only the first two terms

$$\int_x^{\infty} \exp \frac{|e|\psi_s}{kT} \exp(-x/L_o) \; dx \simeq \frac{kT}{|e|\psi_s} L_o \exp\left(\frac{|e|\psi_s}{kT} (1 - \frac{x}{L_o}) \right) \qquad (6.81)$$

Eqn. (6.81) will be a good approximation if the main contribution to the integral comes from points $x \ll L_o$. Note that the integral limit x must be chosen so that $x \ll L_o$.

A very similar approximation to the above is often made when $\psi(x)$ is parabolic :

$$\psi(x) = \psi_s (1 - \frac{x}{W})^2 \simeq \psi_s (1 - \frac{2x}{W}) , \qquad x \ll W \qquad (6.82)$$

with solution,

$$\int_{x}^{W} \exp \frac{|e|\psi_s}{kT}\left(1 - \frac{x}{W}\right)^2 dx \simeq \frac{kT}{|e|\psi_s} \frac{W}{2} \left\{ \exp\left(\frac{|e|\psi_s}{kT}\left(1 - \frac{2x}{W}\right)\right) - \exp\left(-\frac{|e|\psi_s}{kT}\right) \right\} \quad (6.83)$$

For this case it is only sensible to integrate to W. Numerical solutions of the integrals for a parabolic and exponential $\psi(x)$ were compared with their respective approximate solutions. The approximation to the exponential is slightly poorer than the approximation to the square, but if $\psi(x) >> kT/|e|$ then the error in both cases is only a few percent.

The maximum possible shift of the electron quasi-Fermi level is given by the condition $E_{Fn}(o) = E_F - |e|V$, and this is the condition required for Diffusion theory to apply. This value for $E_{Fn}(o)$ is substituted into eqn.(6.79), and eqn. (6.81) is used for the integral evaluated at x = o. Eqn.(6.77) is used to write the result in terms of the barrier height ϕ_b. Then

$$J \simeq |e|\mu_{ex} N_c \frac{\psi_s}{L_o} e^{-\phi_b/kT} \left(e^{|e|V/kT} - 1\right) \quad (6.84)$$

Rearranging eqn.(6.79) and substituting eqn.(6.84) for J gives the maximum deviation of $E_{Fn}(x)$ from E_F.

$$E_{Fn}(x) \simeq kT\ln\left\{1 - \left(1 - e^{-|e|V/kT}\right)e^{-\frac{|e|\psi_s}{kT} \cdot \frac{x}{L_o}}\right\} \quad (6.85)$$

Remember that E_F has been set to zero and that the expression is only accurate for $\psi_s >> kT/|e|$ and $x << L_o$.

Fig. 6.6 plots $E_{Fn}(x)$ for a barrier under forward bias. The example

chosen has a zero bias surface potential $\psi_{so} = 0.5$ volts, $L_o = 80$ nm ($N \simeq 10^{17}$ cm^{-3} eV^{-1}), T = 300 K, and the forward bias is V = 0.2 volts. Note that appreciable deviation from E_F only occurs in the last 4 nm or equivalently the last kT of barrier. This deviation can well be ignored.

In reverse bias (V < 0) the deviation from E_F can extend much further into the semiconductor. Moreover reverse bias currents are often much larger than the current predicted by eqn. (6.84). This may be due to electrons tunnelling from the metal (especially near the device edges) or even generation current. The result is that it is difficult to predict a value for $E_{Fn}(x)$. However it can be expected, even for barriers where Thermionic emission theory describes the forward bias characteristics, that at large reverse biases there will be considerable deviation from E_F. Despite this the effect on admittance is likely to be small. This is because in reverse bias, as demonstrated in sub-section 5.3.3, E_F does not control the electron occupancy of gap states close to the metal-semiconductor interface.

Bardeen[12] (1949) argued that even if Diffusion theory better describes d.c. conduction, it is still admissible to treat conductance due to diode leakage as a parallel admittance component. For an a-Si Schottky barrier the conclusion here is that, at least to a good approximation, this procedure is still valid. It should be noted however that irrespective of the conduction process, the complete analysis fails under large forward bias conditions. When very large currents flow through the device, the barrier potential $\psi(x)$ is determined by resistive elements, and the system is far removed from the bounds of quasi-thermal equilibrium. The barrier behaviour can be modelled using equivalent circuits (see, for example, Snell et al[13] (1979)) but it is perhaps better to avoid this bias regime if meaningful interpretation is required.

6.7 EFFECTS OF MINORITY CARRIER PROCESSES

When a reverse bias is applied to an n-type Schottky barrier, the conduction band electron quasi-Fermi level E_{Fn} will be below mid-gap energy E_i at points close to the metal-semiconductor interface. In sub-section 5.3.3 it was shown that when $E_{Fn} < E_i$ hole emission from gap states to the valence band pins the gap state occupancy at approximately mid-gap. Hole emission will also give rise to generation current. These two effects are examined here. Also, note that if the barrier height of the Schottky barrier is less than half of the band-gap then the valence band hole density is always very small. This is normally the case for a-Si Schottky barriers and so in this section the hole capture rate at gap states can be set to zero.

6.7.1 Admittance in Reverse Bias

In sub-section 5.3.3, the reverse-biased Schottky barrier was divided into four distinct regions according to which were the dominant capture and emission processes. It was shown that typically most of the charge in the barrier is contained within two of the four regions and in this section the two smaller regions are ignored. The approximation is that where $E_{Fn} > E_i$ only electron emission and electron capture are important, and where $E_{Fn} < E_i$ only electron emission and hole emission are important. The gap state occupancy function f_T is then given by eqns.(5.18) and (5.20) of sub-section 5.3.3.

$$f_T(E_T) = \begin{cases} \dfrac{1}{e^{(E_T-E_{Fn})/kT} + 1} & , E_{Fn} > E_i \\ \\ \dfrac{1}{e^{2(E_T-E_i)/kT} + 1} & , E_{Fn} < E_i \end{cases} \qquad (6.86)$$

Fig.6.7 schematically illustrates this result in an energy band diagram. A difficulty arises in defining f_T at the point where $E_{Fn} = E_i$, denoted x_g, but as zero temperature statistics are mostly used it is sufficient

to note that at $x = x_g$, $f_T(E_i) = 1/2$. This is a slight underestimate of the electron occupancy at $x = x_g$.

Poisson's equation now becomes

$$\frac{d^2\psi}{dx^2} = \begin{cases} \rho_g/\varepsilon\varepsilon_o & , x < x_g \\ \dfrac{|e|}{\varepsilon\varepsilon_o} \displaystyle\int_{E_F-|e|\psi(x)}^{E_F} N(E)dE & , x > x_g \end{cases} , \quad (6.87)$$

where ρ_g is a constant and is given by

$$\rho_g = |e| \int_{E_i}^{E_F} N(E)dE . \quad (6.88)$$

At points $x > x_g$, $\psi(x)$ is obtained using the analysis of sub-section 5.4.2. For $x < x_g$, eqn.(6.87) can be integrated directly. Integrating twice from $x = x_g$ to a point $x < x_g$ gives

$$\psi(x) = \frac{\rho_g}{2\varepsilon\varepsilon_o} (x-x_g)^2 + \left.\frac{d\psi}{dx}\right|_{x=x_g} .(x-x_g) + \psi_g , \quad x < x_g , \quad (6.89)$$

where $\psi_g = (E_F-E_i)/|e|$, $d\psi/dx \,|_{x=x_g}$ is obtained from the solution of $\psi(x)$ for $x > x_g$ and x_g follows from the boundary condition $\psi(o) = \psi_s$. Substituting

this boundary condition into eqn.(6.89) gives

$$x_g = \frac{\varepsilon\varepsilon_o}{\rho_g}\left\{ \left.\frac{d\psi}{dx}\right|_{\psi=\psi_g} + \left[\left.\frac{d\psi}{dx}\right|^2_{\psi=\psi_g} + \frac{2\rho_g}{\varepsilon\varepsilon_o}(\psi_s-\psi_g)\right]^{1/2} \right\}, \psi_s > \psi_g, \quad (6.90)$$

and the square root is taken to be positive.

The total charge in the barrier is simply the sum of the charge from the two regions.

$$Q = \left[2|e|\varepsilon\varepsilon_o \int_o^{\psi_g} \int_{E_F-|e|\psi}^{E_F} N(E)dEd\psi \right]^{1/2} + x_g\rho_g \qquad , \psi_s > \psi_g, \quad (6.91)$$

but a more useful expression for Q is found using the identity $d^2\psi/dx^2 = 1/2\ d/d\psi(d\psi/dx)^2$ and noting that $Q = -\varepsilon\varepsilon_o d\psi/dx|_{x=o}$, Poisson's equation can be rewritten thus

$$\frac{d}{d\psi}\left[\frac{d\psi}{dx}\right]^2 = \begin{cases} \dfrac{2\rho_g}{\varepsilon\varepsilon_o} & , \psi < \psi_g \\ \dfrac{2|e|}{\varepsilon\varepsilon_o}\displaystyle\int_{E_F-|e|\psi}^{E_F} N(E)dE & , \psi > \psi_g \end{cases} , \quad (6.92)$$

and integrating from $\psi = o$ to $\psi = \psi_s$ gives

$$Q = \left\{ 2|e|\varepsilon\varepsilon_o \left[\int_o^{\psi_g}\int_{E_F-|e|\psi}^{E_F} N(E)dEd\psi + \frac{\rho_g}{|e|}(\psi_s-\psi_g)\right]\right\}^{1/2}, \psi_s>\psi_g. \quad (6.93)$$

The static, zero-frequency capacitance $C(\psi_s,0) = dQ/d\psi_s$, and so from eqn.(6.93)

$$C_{rev}(\psi_s,0) = \left(\frac{\varepsilon\varepsilon_o}{2|e|}\right)^{\frac{1}{2}} \frac{\rho_g}{\left\{ \int_o^{\psi_g} \int_{E_F-|e|\psi}^{E_F} N(E)dEd\psi + \frac{\rho_g}{|e|}(\psi_s-\psi_g) \right\}^{\frac{1}{2}}} \tag{6.94}$$

where the subscript "rev" is used to indicate that eqn.(6.94) is a reverse bias expression. Note that an interesting result follows from eqn.(6.94) A plot of $C_{rev}^{-2}(\psi_s,o)$ against ψ_s should give a straight line with gradient $2/\varepsilon\varepsilon_o\,\rho_g$.

At finite signal frequencies, expressions for capacitance and conductance follow in a very straightforward fashion. It has been pointed out that at points $x < x_g$ the conduction band electron density does not affect the gap state electron occupancy. Therefore the charge density stays constant and the whole region behaves as a simple dielectric parallel plate capacitor with capacitance $\varepsilon\varepsilon_o/x_g$. This dielectric capacitance is connected in series with the rest of the barrier and therefore the total capacitance $C_{rev}(\psi_s,\omega)$ is

$$C_{rev}(\psi_s,\omega) = \left[\frac{1}{C(\psi_g,\omega)} + \frac{x_g}{\varepsilon\varepsilon_o}\right]^{-1} = \frac{C(\psi_g,\omega)}{1 + (x_g/\varepsilon\varepsilon_o)C(\psi_g,\omega)} \tag{6.95}$$

where $C(\psi_g,\omega)$ is the capacitance previously calculated for the region $x > x_g$. It is easily shown that at $\omega = o$, eqn. (6.95) reduces to the static result of eqn.(6.94). Examination of the previous calculation for conductance (see section 5.4) shows that the conductance in reverse bias is simply obtained by substituting $C_{rev}(\psi_s,\omega)$ into the already derived expression for conductance (eqn. (5.76), sub-section 5.4.6).

The above consideration now allow the barrier admittance to be calculated for any reverse bias. Note that the theoretical C, G-V plots of sub-section 5.5.2 are in error, and so these calculations are corrected and an illustrative example is given. In sub-section 5.5.2 the maximum surface potential was $\psi_s = 0.9$ volts, $E_c - E_F$ was set to be 0.35 eV and the mobility gap is approximately 1.8 eV. The plots are therefore in error for $\psi_s > 0.55$ volts. At $\psi_s = 0.9$ volts and at finite frequencies it was found that the old calculations typically tended to overestimate C and G by about 1-2%. At zero frequency conditions a more major adjustment occurs. It has been shown that the region $x < x_g$ behaves as a simple dielectric capacitance, and so the 0Hz capacitance must start to reduce when $\psi_s > \psi_g$. The reduction is entirely analogous to the finite frequency case when $\psi_s > \psi_c$. The corrected C-V plot for example (c) of sub-section 5.5.2 (i.e. N(E) similar to that proposed by Lang et al[5] (1982)) is drawn in Fig 6.8. Note that the change at finite frequencies is very small.

Finally it should be remembered that the approximations at the beginning of this sub-section do lead to some inaccuracy. Hole emission will lead to an increase in the gap state occupancy near $x = x_g$ and this will give rise to some error in the calculated value for $\psi(x)$. The maximum error for admittance will occur at very low signal frequencies. The calculated capacitance will be a slight overestimate and at zero frequency the conductance will be given by the voltage derivative of the generation current (see next sub-section). These deviations are expected however to be quite small.

6.7.2 Generation Current

The d.c. reverse bias characteristics of a Schottky barrier may be dominated by the generation of free electrons and holes within the depletion region. An estimate of this current can be found using the results of sub-sections 5.3.3 and 6.7.1. Note that the approach taken here requires

explicit knowledge of the gap state density and their capture coefficients. In this respect the calculation is quite different to the usual calculation of generation current where the recombination/generation lifetime simply takes an assumed value. See, for example, Sah, Noyce and Shockley[14] (1957).

For an n-type Schottky barrier, generation current arises when there is a net transfer of electrons from the valence band to the conduction band from whence they are swept to the back contact by the electric field. Normally, the fastest and hence dominant transfer process is via a state in the band gap - a gap state emits a hole to the valence band and subsequently emits an electron to the conduction band. The transfer rate is limited by the slower of the two processes and this means that if gap state electron and hole emission coefficients are similar, the transfer will only occur via mid-gap states. Also, at points $x > x_g$ ($E_{Fn} > E_i$), , mid-gap states are almost fully occupied with electrons, hole emission to the valence band is negligible, and so the transfer rate is greatly diminished.

The two region approximation is carried over from the last sub-section, and it follows from this approximation that only the $x < x_g$ region contributes to the generation current. The following observations are approximately correct within the region $x < x_g$:

all electrons emitted from the valence band to states above mid-gap (hole emission) are subsequently emitted to the conduction band ; all electrons emitted from gap states below mid-gap to the conduction band (electron emission) are subsequently replaced by electrons from the valence band.

It follows that if each successful transfer results in an electron reaching the back contact, the generation current, denoted J_{gen}, is

$$J_{gen} \simeq |e|x_g \left\{ \int_{E_i}^{E_c} (1-f_T(E))N(E)e_p(E)dE + \int_{E_v}^{E_i} f_T(E)N(E)e_n(E)dE \right\}$$

(6.96)

where $f_T(E)$ is given by eqn.(6.86) for the $E_{Fn} < E_i$ case, and e_n and e_p are the gap state electron and hole emission rates. From eqn.(5.10), sub-section 5.3.1

$$\left. \begin{aligned} e_n(E_T) &= c_n N_c \exp\left[(E_T-E_c)/kT \right] \\ e_p(E_T) &= c_p N_v \exp\left[(E_v-E_T)/kT \right] \end{aligned} \right\} \qquad (6.97)$$

and we choose to set $c_n N_c = c_p N_v = \tau_o^{-1}$ where τ_o is a constant. A justification for using e_n and e_p in eqn. (6.96) can be found from the large reverse bias transient response example examined in sub-section 5.3.4.

The dominant contribution to the integrals in eqn.(6.96) comes from gap state energies close to $E_T = E_i$. Therefore it is reasonable to replace N(E) by the constant $N(E_i)$. Substituting the relevant results into eqn.(6.96) then gives

$$J_{gen} \simeq \frac{\pi}{2} \frac{|e|x_g kTN(E_i)}{\tau(E_i)} \qquad (6.98)$$

where $\tau(E_i) = \tau_o \exp\left[(E_c-E_v)/2kT \right]$ (eqn.(6.98) is most easily derived by changing the integral variable in eqn.(6.96) to $y = (E-E_i)/kT$).

The bias dependence of the generation current is perhaps not obvious. However, if the gap state density is taken to be constant ($N(E) = N$), then the equation for x_g, eqn(6.90), simplifies to give

$$J_{gen} = \frac{\pi}{2} \frac{kT}{|e|} \frac{(\varepsilon\varepsilon_o |e|^2 N)^{\frac{1}{2}}}{\tau(E_i)} \left(2 \frac{\psi_s}{\psi_g} - 1\right)^{\frac{1}{2}} , \quad \psi_s > \psi_g. \qquad (6.99)$$

Therefore when $\psi_s >> \psi_g$, the generation current is approximately proportional to the square root of the surface potential ψ_s. Also given N and τ_o it is possible to estimate the actual magnitude of J_{gen}.

6.8 METHODS FOR FINDING N(E) FROM ADMITTANCE

The admittance expressions show that capacitance and conductance are functions of N(E) over the range of gap state energies $E_i < E < E_F$(E_i = mid-gap energy). It follows therefore that over this gap state energy range, experimental admittance plots can be used to find estimates for the gap state density. There are however several difficulties.

The main problem arises from the very simple gap state model used to derive the admittance expressions (see sub-section 5.3.2). There is in fact very little reliable information about the types of defects present, their relation densities, their capture coefficients, etc., upon which to base a model. This issue is discussed in Chapters 2 and 3, but it is sufficient here to note that serious errors may arise from the analysis if, for example,

1. there are large variations in N(E) over energies of the order of kT,

2. gap states have capture coefficients which vary by orders of magnitude over the range of energies considered,

3. capture coefficients show an activated energy, exp (E/kT) temperature dependence,

4. capture and emission is significantly electric field dependent,

5. majority carrier transport limits the barrier charge response.

Certainly the above possibilities cannot be totally discounted.

Another more minor consideration is that all but the very simplest calculations to obtain N(E) from admittance require some computation. Best-fit methods may require very involved and complicated computer programs (c.f. Field Effect Experiments[15]). Finally the experimental admittance measurements and the more general electrical characterisation of the a-Si Schottky barrier is generally not trivial. Difficulties such as a poor ohmic back contact, large bulk resistance, non-ideal d.c. J-V plot, etc. significantly complicate any analysis.

Four separate methods for finding N(E) are now outlined. Some illustrative calculations will be made and they will use the example density of states described in sub-section 5.5.2. These densities of states are plotted in Fig.5.5. Remember that example (a) is a *constant* N(E) with a peak, example (b) is an N(E) similar to that suggested by Spear, Le Comber and Snell[16] (1978), and example (c) is an N(E) similar to that suggested by Lang, Cohen and Harbison[5] (1982).

Method 1 : Static C-V plot

At elevated temperatures and sufficiently low signal frequencies it may be possible to measure what is essentially the zero-frequency capacitance $C(\psi_s,o)$. The required results then come from sub-section 5.4.2.

$$C(\psi_s,o) = \frac{dQ}{d\psi_s} = -\varepsilon\varepsilon_o \frac{d}{d\psi_s}\left(\left.\frac{d\psi}{dx}\right|_{x=o}\right) , \qquad (6.100)$$

and

$$\left.\frac{d\psi}{dx}\right|_{x=o} = -\left(\frac{2|e|}{\varepsilon\varepsilon_o}\int_o^{\psi_s}\int_{E_F-|e|\psi}^{E_F} N(E)dEd\psi\right)^{1/2} . \qquad (6101)$$

From eqn.(6.101) it is clear that

$$N(E_F - |e|\psi_s) = \frac{\varepsilon\varepsilon_o}{2|e|} \frac{d^2}{d\psi_s^2}\left(\frac{d\psi}{dx}\bigg|_{x=o}^{2} \right),$$

$$= \frac{\varepsilon\varepsilon_o}{|e|}\left\{ \left[\frac{d}{d\psi_s}\left(\frac{d\psi}{dx}\bigg|_{x=o} \right) \right]^2 + \frac{d}{d\psi_s}\left(\frac{d}{d\psi_s} \frac{d\psi}{dx}\bigg|_{x=o} \right) \frac{d\psi}{dx}\bigg|_{x=0} \right\}, \quad (6.102)$$

and it follows from eqns.(6.100) and (6.102) that

$$N(E_F - |e|\psi_s) = \frac{1}{|e|\varepsilon\varepsilon_o}\left\{ C^2(\psi_s,o) + \frac{d}{d\psi_s}\left[C(\psi_s,o) \right] . \int_o^{\psi_s} C(\psi,\ o)\ d\psi \right\} . \quad (6.103)$$

Hirose et al, in a series of papers(17-20), have employed this method to calculate N(E) from C-V measurements on thick insulator MIS structures. The problem with the technique is that the gap state capacitance is required at flat-band (ψ_s=o) and diode leakage current precludes the taking of such a measurement. The problem is removed if an MIS structure is used. Also Abram and Doherty(21) (1982) have demonstrated that relatively simple numerical methods can be used to evaluate eqn.(6.103) without the introduction of any serious numerical error.

Method 2 : Finite frequency C-V plots

Eqn.(5.74), sub-section 5.4.6, gives the frequency-dependent capacitance $C(\psi_s,\omega)$ as

$$C(\psi_s,\omega) = \frac{C(\psi_c,o)}{1 + (x_c/\varepsilon\varepsilon_o)C(\psi_c,o)}, \quad (6.104)$$

and eqn.(5.48), sub-section 5.4.2 gives x_c as

$$x_c(\psi_s,\omega) = \int_{\psi_c}^{\psi_s} \frac{d\psi'}{\left(\frac{2|e|}{\varepsilon\varepsilon_o}\int_o^{\psi'}\int_{E_F-|e|\psi}^{E_F} N(E)DEd\psi\right)^{\frac{1}{2}}}, \tag{6.105}$$

where $\psi_c = \psi(x_c)$. The potential ψ_c is independent of ψ_s and so it follows that

$$\frac{d}{d\psi_s} C^{-1}(\psi_s,\omega) = \frac{1}{\varepsilon\varepsilon_o}\frac{d}{d\psi_s} x_c(\psi_s,\omega) = \left(2|e|\varepsilon\varepsilon_o\int_o^{\psi_s}\int_{E_F-|e|\psi}^{E_F} N(E)dEd\psi\right)^{-\frac{1}{2}} \tag{6.106}$$

Hence

$$N(E_F-|e|\psi_s) = \frac{1}{2|e|\varepsilon\varepsilon_o}\frac{d^2}{d\psi_s^2}\left[\left(\frac{d}{d\psi_s} C^{-1}(\psi_s,\omega)\right)^{-2}\right]. \tag{6.107}$$

Abram and Doherty[21] (1982) derived this result but as the authors pointed out, the required numerical multiple differentiation is well known to be difficult. Even in model calculations they were not able to generate sensible results using simple numerical techniques and thus it is argued that this method for finding N(E) is unlikely to be useful for real experimental data.

Method 3 : G-ω plot (+ capacitance)

First note that the constant gap state density (N(E) = N) admittance expressions, eqns. (6.11) and (6.12), can be rearranged to given an explicit expression for N, and in the case of a varying density of gap states these

expressions can be used to estimate the average value of N(E). Eqns.(6.11) and (6.12) give

$$N = \frac{1}{\varepsilon\varepsilon_o |e|^2} \left\{ (1 + \ln(\psi_s/\psi_c)) \, C(\psi_s,\omega) \right\}^2 , \qquad (6.108)$$

and

$$N = \frac{1}{\varepsilon\varepsilon_o |e|^2} \left\{ \frac{2}{\pi} \frac{|e|\psi_c}{kT} (1 + \ln(\psi_s/\psi_c))^2 \frac{G(\psi_s,\omega)}{\omega} \right\}^2 , \qquad (6.109)$$

where

$$|e|\psi_c = kT \ln(1/\omega\tau_o) - (E_c - E_F) \qquad (6.110)$$

In sub-section 5.5.1 it was pointed out that the value of conductance is proportional to the density of gap states affected by the "partial response region" at x_c, i.e. $G(\psi_s,\omega) \tilde{\propto} N(E_F-|e|\psi_c)$. Also over a large frequency range $G(\psi_s,\omega) \tilde{\propto} \omega$. It is argued that as a plot of G/ω versus ω scans the partial response region through a range of gap state energies $E = E_F-|e|\psi_c(\omega)$, then at any angular frequency ω

$$N(E_F-|e|\psi_c(\omega)) \simeq K \frac{G(\psi_s,\omega)}{\omega} , \qquad (6.111)$$

where K is approximately a constant independent of frequency.

The estimation procedure follows. Values for E_F, ψ_s, τ_o and T are assumed known. Conductance (and capacitance) are measured over as large a range of signal frequencies as possible (but without exceeding the condition $\psi_c < 3kT/|e|$). A mid-range frequency value is chosen, denoted ω_K, and from eqn.(6.110) the gap state energy E_K corresponding to the condition $\omega_K\tau(E_K) = 1$ is found ($E_K = E_F-|e|\psi_c(\omega)$). Substituting the

values for $C(\omega_K)$ and $G(\omega_K)$ into eqns. (6.108) and (6.109) respectively gives a reasonable estimate for $N(E_K)$. Further substitution into eqn.(6.111) gives an estimate for the constant K. Now each value of $G(\omega)$ is multiplied by K/ω giving a density of states value, and eqn.(6.110) is used to fix the results on the gap state energy scale.

The validity of this procedure is demonstrated by considering an example calculation. Eqn.(5.76), sub-section 5.4.6 was used to generate theoretical G-ω plots over a frequency range 4Hz $< f < 6 \times 10^4$ Hz. The parameters used were $E_c-E_F= 0.35$ eV, $\psi_s = 0.5$ volts, $\tau_o = 10^{-14}$ sec, T = 300 K. Two densities of states were used, that proposed by Spear et al and that proposed by Lang et al (see sub-section 5.5.2). A value of K for each different version of the density of states was found by choosing a particular value $N(E_K)$ and dividing it by the relevant $G(\omega_K)/\omega_K$ value. The densities of states could then be regenerated by multiplying each value of $G(\omega)/\omega$ by K. Fig.6.9 shows a plot of the results of this calculation. Note that the example densities of states are quite different, but in both cases the fit is reasonable.

This method for finding N(E) is very straightforward and will be used later to find N(E) from experimental G-ω plots. The main problems with the method are associated with experimental difficulties. There may be a large diode leakage conductance, and it is difficult to find an accurate value of τ_o. These problems are discussed more fully in Chapter 7.

Method 4 : C,G- ω, V plots

A procedure is now described which uses iterative techniques to find a solution for N(E). If the choices of the barrier parameters ψ_s and τ_o are correct then this method should give good agreement between the experimental admittance plots (i.e. C,G-ω, V) and plots generated using the theoretical admittance expressions. The procedure itself only requires data from C,G-ω measurements.

Eqn. (5.76), sub-section 5.4.6 is rearranged thus

$$N(E_F-|e|\psi_c) = \frac{2}{\pi kT}\int_{E_F-|e|\psi_c}^{E_F} N(E)dE \; \frac{G(\omega_s,\omega)/\omega}{C(\psi_s,\omega)\left(1-\frac{x_c}{\varepsilon\varepsilon_o}C(\psi_s,\omega)\right)}, \quad (6.112)$$

where x_c and ψ_c are given by eqns.(6.105) and (6.110) respectively. Values for E_F, ψ_s, τ_o and T are assumed known and capacitance and conductance are measured over as large a range of signal frequencies as possible (but without exceeding the condition $\psi_c \leq 3kT/|e|$). From drawn plots of C,G-ω , it is possible by interpolation to find the measured values of C and G which correspond to equal intervals of $\psi_c(\omega)$ (see eqn.(6.110)). The maximum and minimum values of ψ_c are denoted ψ_c(max) and ψ_c(min) respectively. At every value of ψ_c, the corresponding measured values of C and G are substituted into eqn.(6.112) and if a trial estimate for N(E), say N(E) = N,is substituted in to eqn.(6.112) then the integrations can be performed to give a second estimate for N(E). This estimate gives values of N(E) at equal gap state energies and over the energy range $E_F-|e|\psi_c(\max) < E < E_F-|e|\psi_c(\min)$. Outside this energy range it is only sensible to set

$$\left.\begin{aligned} N(E) &= N(E_F-|e|\psi_c(\max)) \quad , \quad E_i < E < E_F-|e|\psi_c(\max) \\ N(E) &= N(E_F-|e|\psi_c(\min)) \quad , \quad E_F-|e|\psi_c(\min) < E < E_F \end{aligned}\right\} \quad (6.113)$$

and these density of states points will be referred to as "endpoints". The second estimate for N(E) can now be substituted back into eqn.(6.112) and the procedure repeated to find a third estimate, and thus the iteration proceeds. Typically after 6-7 iterations the estimate has converged and if the correct barrier parameters were used it will be shown that the result usually generates

adequate fits to all of the admittance plots (i.e. C,G- ω, V). Several examples calculations are now considered.

Eqns.(5.74) and (5.76) were used to generate theoretical C,G-ω,V plots. All three example densities of states were used from sub-section 5.5.2, and thus three sets of plots were generated. The other required parameters were taken to be E_C-E_F= 0.35 eV, $\tau_o = 10^{-14}$ s,ϵ = 11 and T = 300K. For the frequency plots ψ_s = 0.5 volts and the chosen frequency range was 4 Hz < f < 6 x 10^4 Hz. These plots now play the role of experimental measurements.

Estimates for N(E) were iteratively calculated from the theoretical C,G-ω plots and here the correct barrier parameters were used. Fig.6.10 plots the estimates for the N(E) suggested by Spear et al and for the N(E) suggested by Lang et al. The estimate for the Lang N(E) is a very close fit, but the estimate for the Spear N(E) is comparatively rather poor. This rather poor fit is due to the erroneous endpoint values of N(E) close to E_F. The barrier profile $\psi(x)$, and hence x_c, is very sensitive to the density of states values near E_F and because the endpoint is significantly in error, the whole estimate for N(E) has converged to a slightly shifted value. A more accurate estimate would require some other knowledge of N(E) near $E = E_F$.

Estimates for N(E) were iteratively calculated using the theoretical C,G- ω plots but incorrect values for ψ_s and τ_o were used in the iterations. This calculation is instructive because in practice the barrier parameters cannot always be measured with great accuracy. Fig.6.11 shows some typical results. The effect of error in ψ_s is shown using the Lang N(E) and ψ_s = 0.45, 0.55 volts. The regenerated N(E) are still reasonable fits. The effect of error in τ_o is shown using the peaked N(E) and $\tau_o = 10^{-13}$, 5 x 10^{-15} s. The general shape of the peak is almost unaffected although there is a shift in energy. This energy shift can be predicted almost exactly by substituting the values for τ_o into eqn.(6.110).

Experimentally the best check of the correctness of the estimated density of states is to use the theoretical admittance expressions, eqns.(5.74) and (5.76), to generate theoretical admittance plots and to compare these plots with experiment. As an example the above calculations can be continued one step further where we attempt to regenerate the original admittance data. By going through this complete cycle it can be deduced how sensitive the method is to errors in the choice of barrier parameters. It turns out that the conductance plots are relatively insensitive to any inconsistencies. This is because the estimation of N(E) directly uses a rearranged form of the theoretical conductance expression. Capacitance however is calculated from an independent expression and it turns out that a C-V plot proves to be the best check of the estimate for N(E).

As an example the Lang N(E) was chosen and theoretical admittance plots were calculated using, in particular, $\tau_o = 10^{-14}$ s. Iterative estimates for N(E) were then calculated using the theoretical C,G-ω plots and $\tau_o = 10^{-14}$, 10^{-15} s. These estimates for N(E) are shown in Figs.6.10 and 6.11 respectively. Each estimate N(E) along with its assumed τ_o value was used to calculate a new C-V plot. Fig.6.12 shows the original C-V plot (solid line), the regenerated C-V plot assuming $\tau_o = 10^{-14}$ s (dashed line) and the regenerated C-V plot assuming $\tau_o = 10^{-15}$ s (dashed line with circles). Note that neither regenerated plot is an exact fit to the original but this is because of the arbitrarily estimated values at the endpoints of N(E). More importantly the $\tau_o = 10^{-14}$ s curve is a much better fit than the $\tau_o = 10^{-15}$ s curve. It could be deduced from these plots alone that the more correct value for τ_o was 10^{-14} s.

In summary, this method uses iterative computational techniques to find N(E) from C,G-ω plots. The solution can be checked for consistency by subsequently generating a C-V plot and comparing the answer with experiment.

If the correct barrier parameters are chosen a good estimate for N(E) can be found after ∿ 6 iterations. It should be noted however that the correctness of this method when real experimental data is used will depend on the model assumptions on which the admittance theory is based. Note that this calculation helps demonstrate that the developed admittance theory is internally consistent.

6.9 RESUMÉ

The admittance calculation described in Chapter 5 has been extended. It has been shown how charge associated with band tail states and states above the mobility edge can be included. This charge contribution was calculated to be very small except perhaps for heavily doped a-Si. Also, it has been shown how the effects of hole emission can be incorporated into the calculation. Hole emission is important in reverse bias.

The physical and mathematical approximations involved in the admittance calculation were examined and justified. The majority carrier response time was calculated and it was shown that at sufficiently low frequencies/high temperatures, the transport of majority carriers is unlikely to limit the barrier charge response. Diode leakage current was examined and it was shown that its effect on the barrier charge can only be small.

Finally various methods were described for finding N(E) from admittance measurements. Two of these methods are completely new and they have proved very successful in dealing with model densities of states. These methods show that the admittance calculation is correct within the limits of the barrier model, and they should allow a more systematic analysis of experimental admittance results.

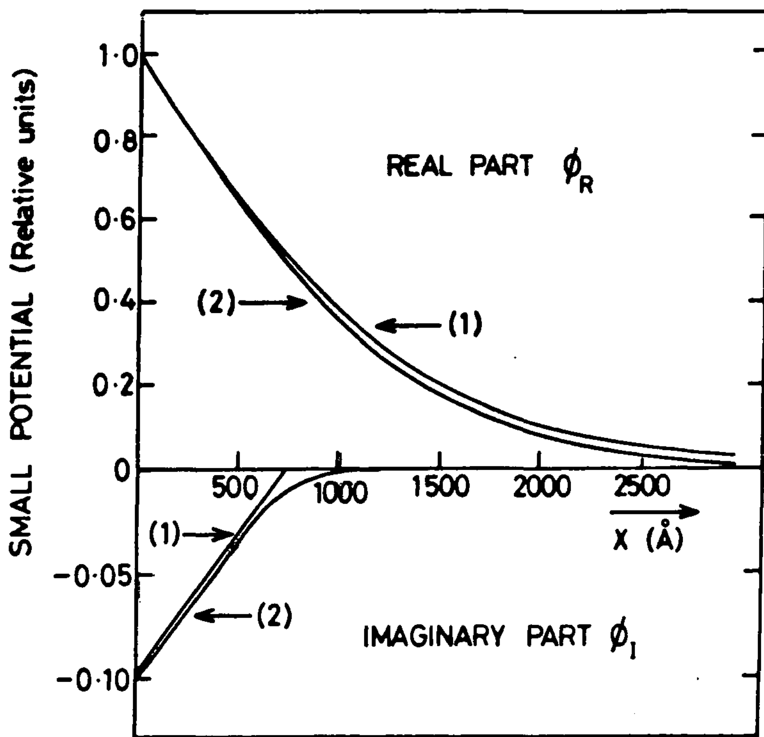

FIGURE 6.1: Two estimates for $\phi_R(x)$ and $\phi_I(x)$; $N = 10^{17}$ cm^{-3} eV^{-1}, $E_c - E_F$ = 0.35 eV, $\tau_o = 10^{-14}$ s, ψ_s = 0.5 volts, T = 300K ε = 11. Analytical estimate (1), numerical estimate (2).

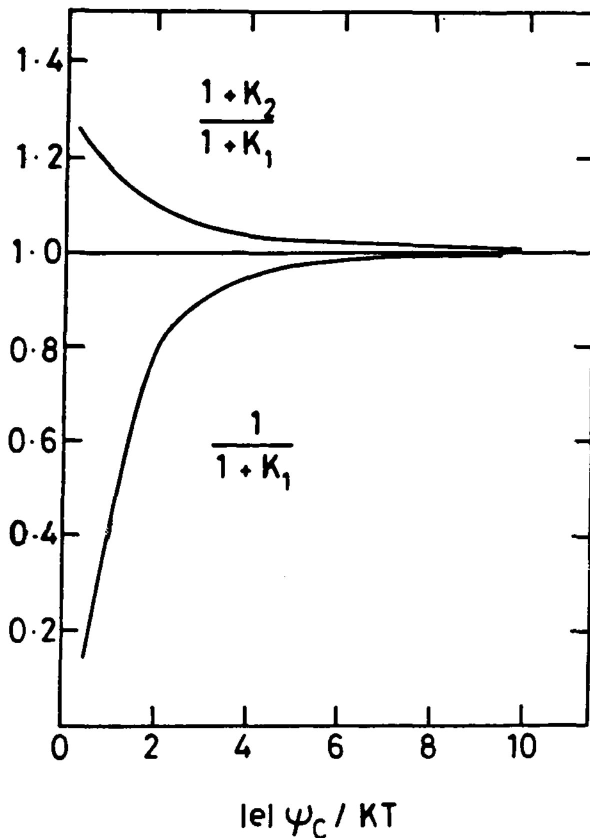

FIGURE 6.2: Plot of discarded terms in the admittance calculation as a function of ψ_c . N(E) = N case is chosen.

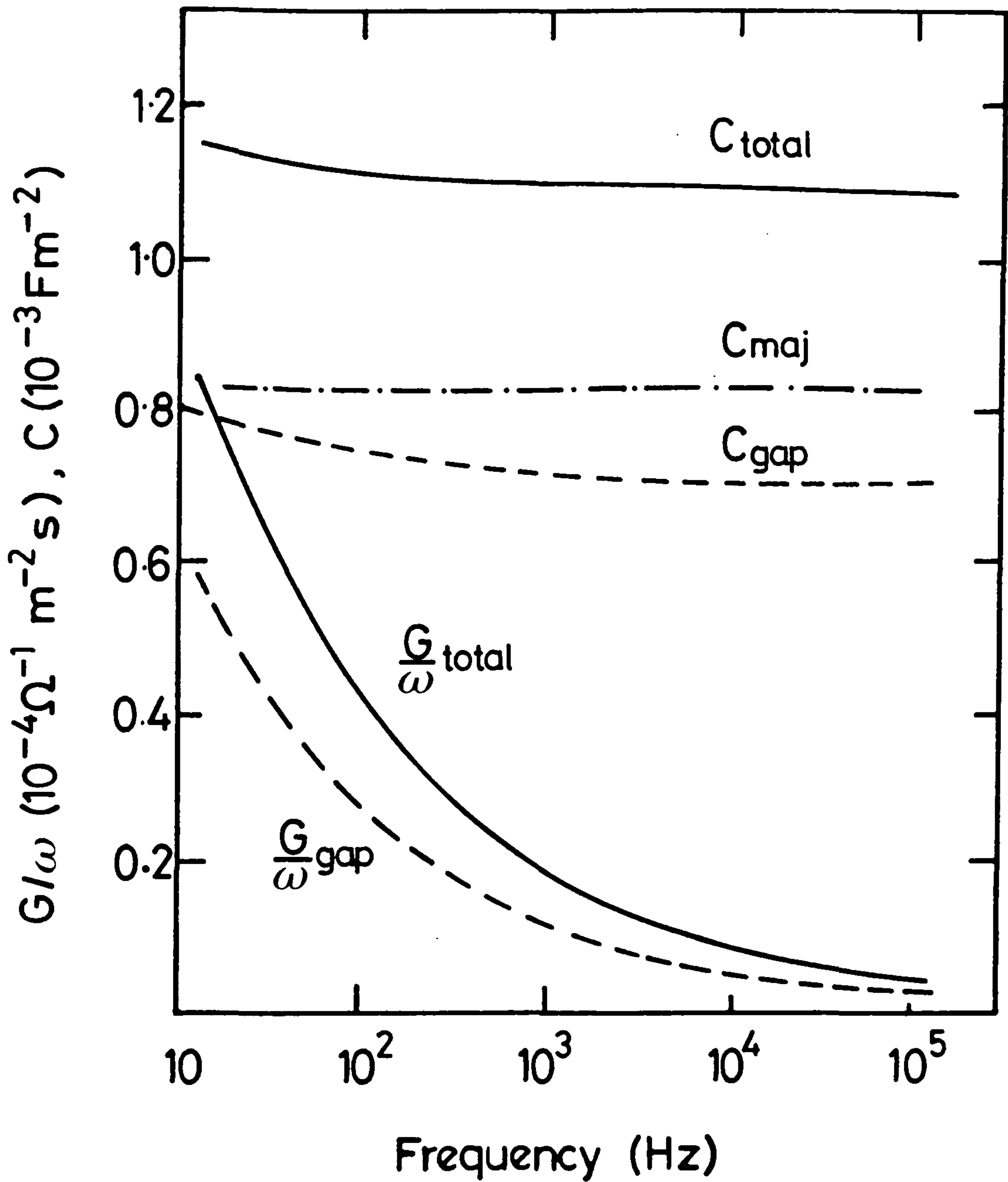

FIGURE 6.3: Admittance-frequency plots for the example discussed in section 6.4: $E_c-E_F = 0.2$ eV, $\tau_o = 10^{-14}$ s, $\psi_s = 0.55$ volts, $\epsilon = 11$, $T = 300K$, $N_c^* = 1.3 \times 10^{20}$ cm^{-3} and N(E) according to Lang et al[5].

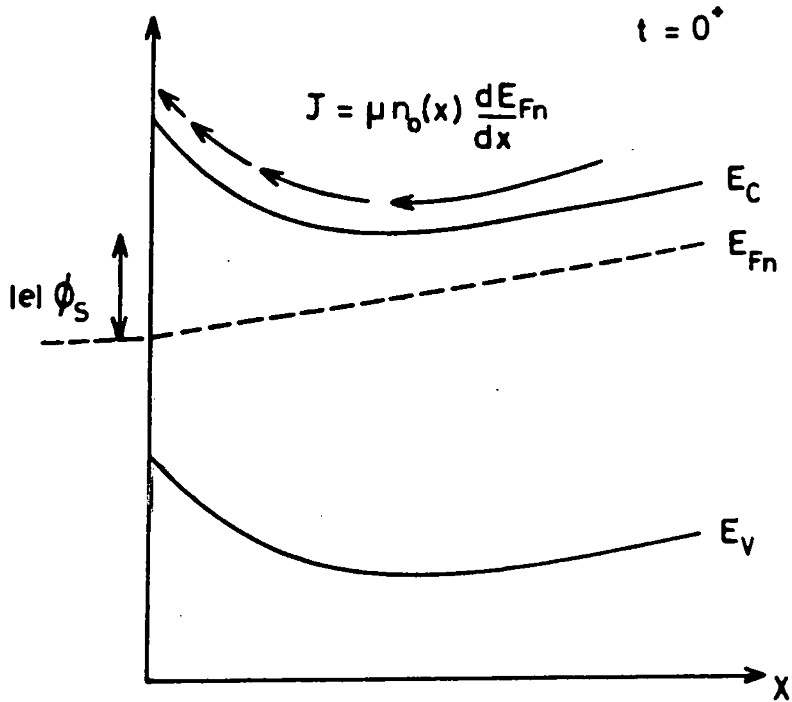

FIGURE 6.4: Small forward bias at time t = o resulting in a small surface potential $|e|\phi_s$ (exaggerated in diagram).

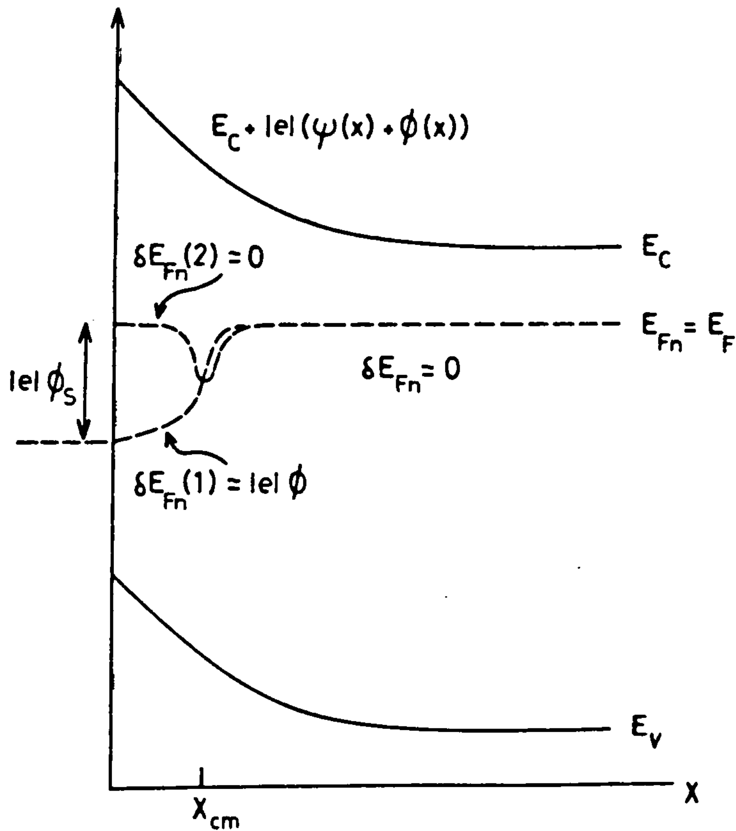

FIGURE 6.5: Exaggerated diagram showing the perturbed amplitudes of the conduction band electron quasi-Fermi level. $\delta E_{Fn} = \delta E_{Fn}(1) + i\delta E_{Fn}(2)$. The Schottky barrier is chosen to be in the forward bias part of the cycle and so $|e|\phi<o$. Also $\delta E_{Fn}(1) = \delta E_{Fn}(2)$ at $x \approx x_{cm}$.

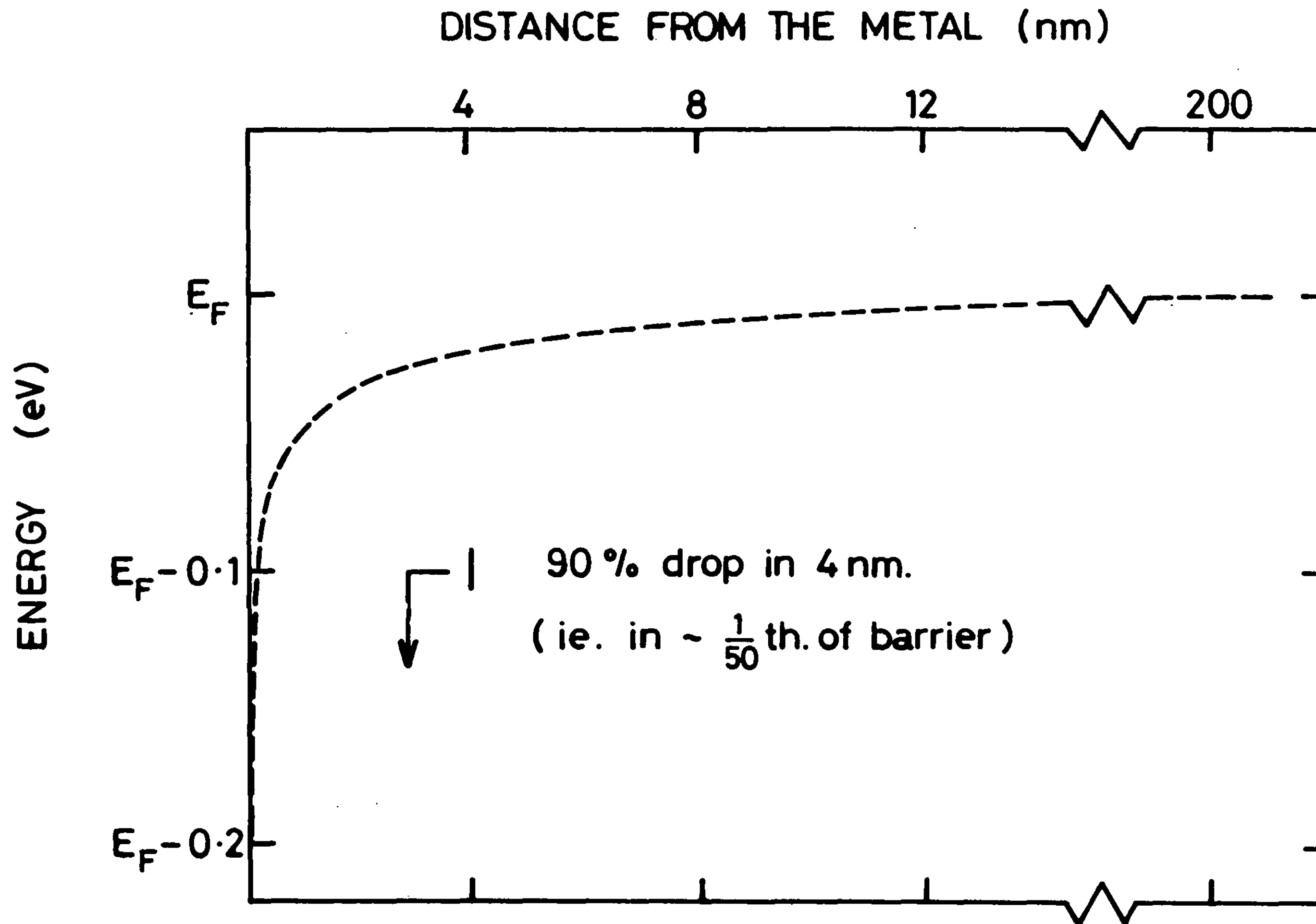

FIGURE 6.6: Plot of $E_{Fn}(x)$ near to the metal-semiconductor interface as according to Diffusion theory, V = 0.2 volts, ψ_s = 0.3 volts, L_o = 80 nm, T = 300K.

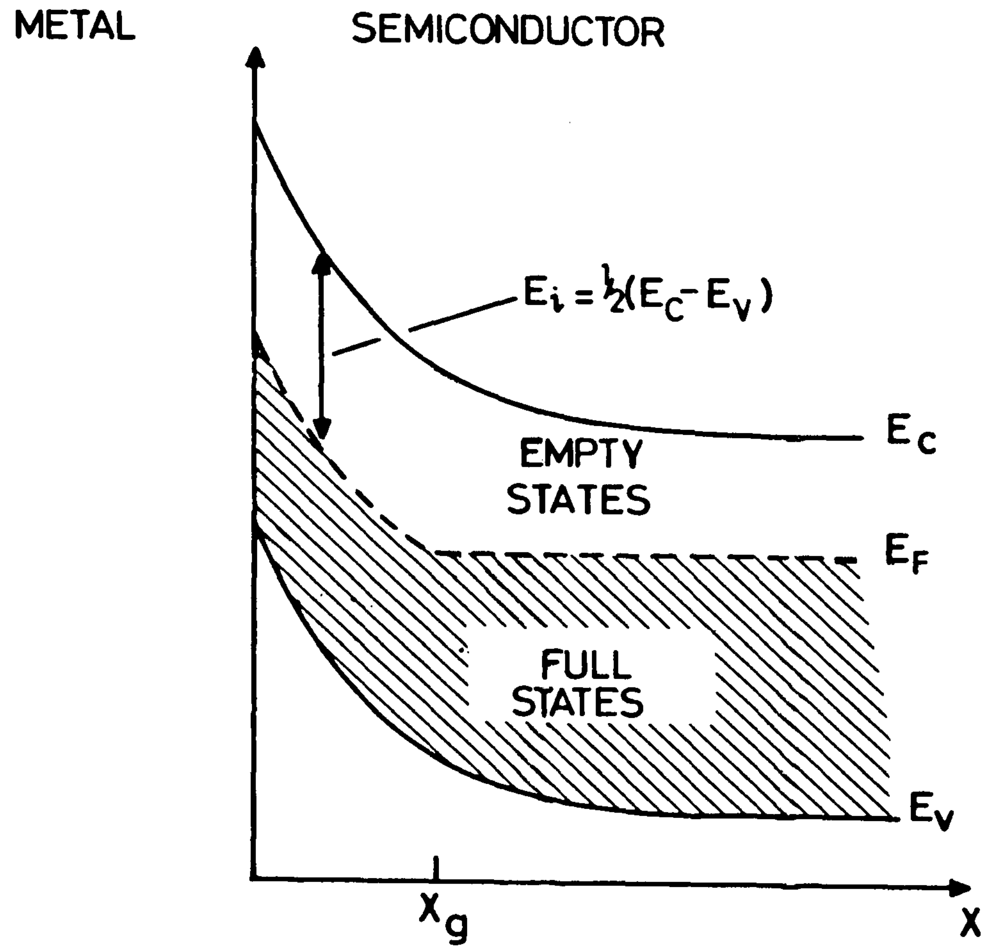

FIGURE 6.7: Schottky barrier energy band diagram in reverse bias.

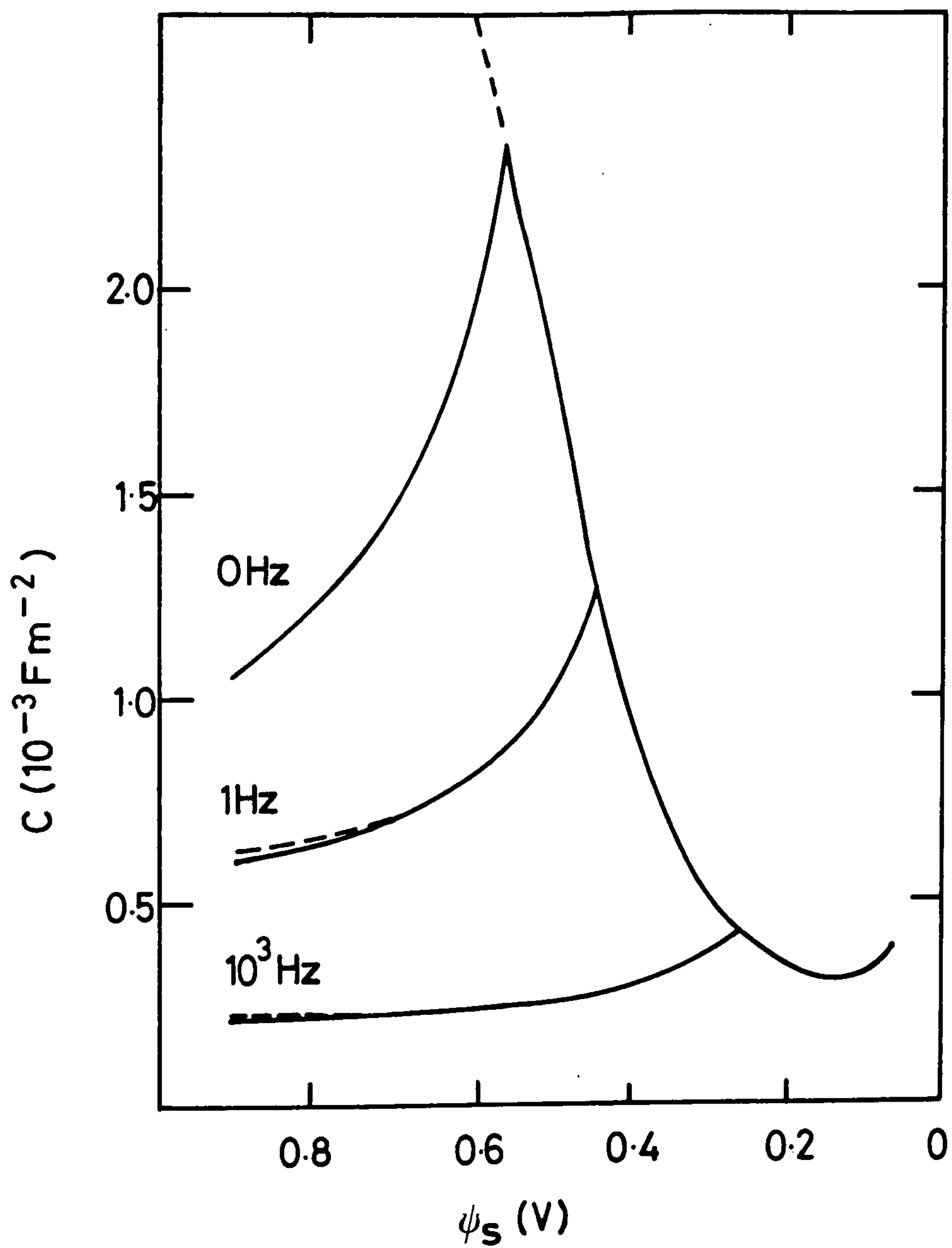

FIGURE 6.8: Corrected C-V plot for Lang N(E), $E_c-E_F = 0.35$ eV, $E_c-E_i = 0.9$ eV, $\tau_o = 10^{-14}$s, T = 300K, $\varepsilon = 11$. Dashed lines correspond to the calculation in sub-section 5.5.2.

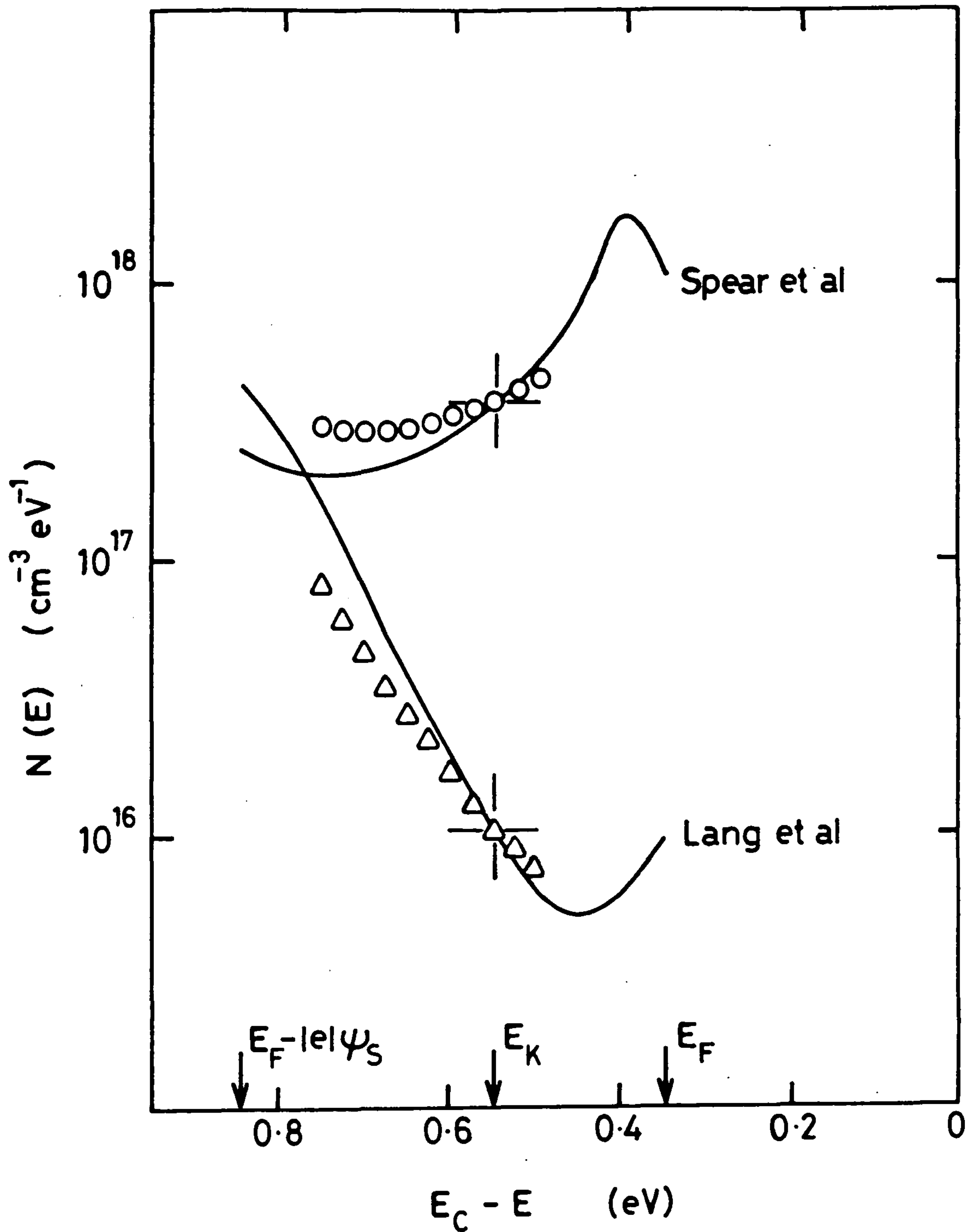

FIGURE 6.9: N(E) estimates using the G-ω plot (method 3). The cross indicates the point used to calculate the multiplying constant K.

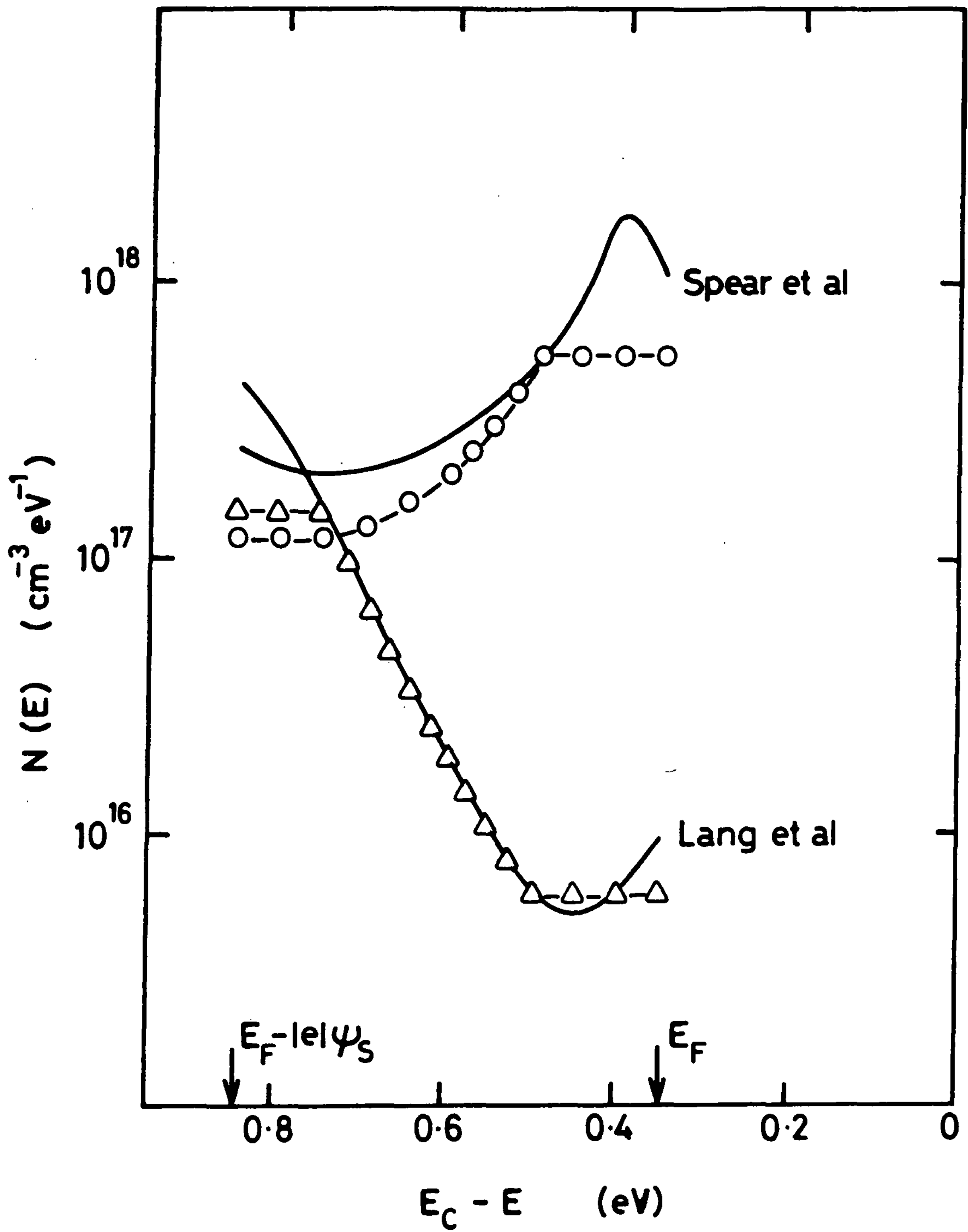

FIGURE 6.10: N(E) estimates from C,G-ω plots (method 4).

The correct barrier parameters have been used.

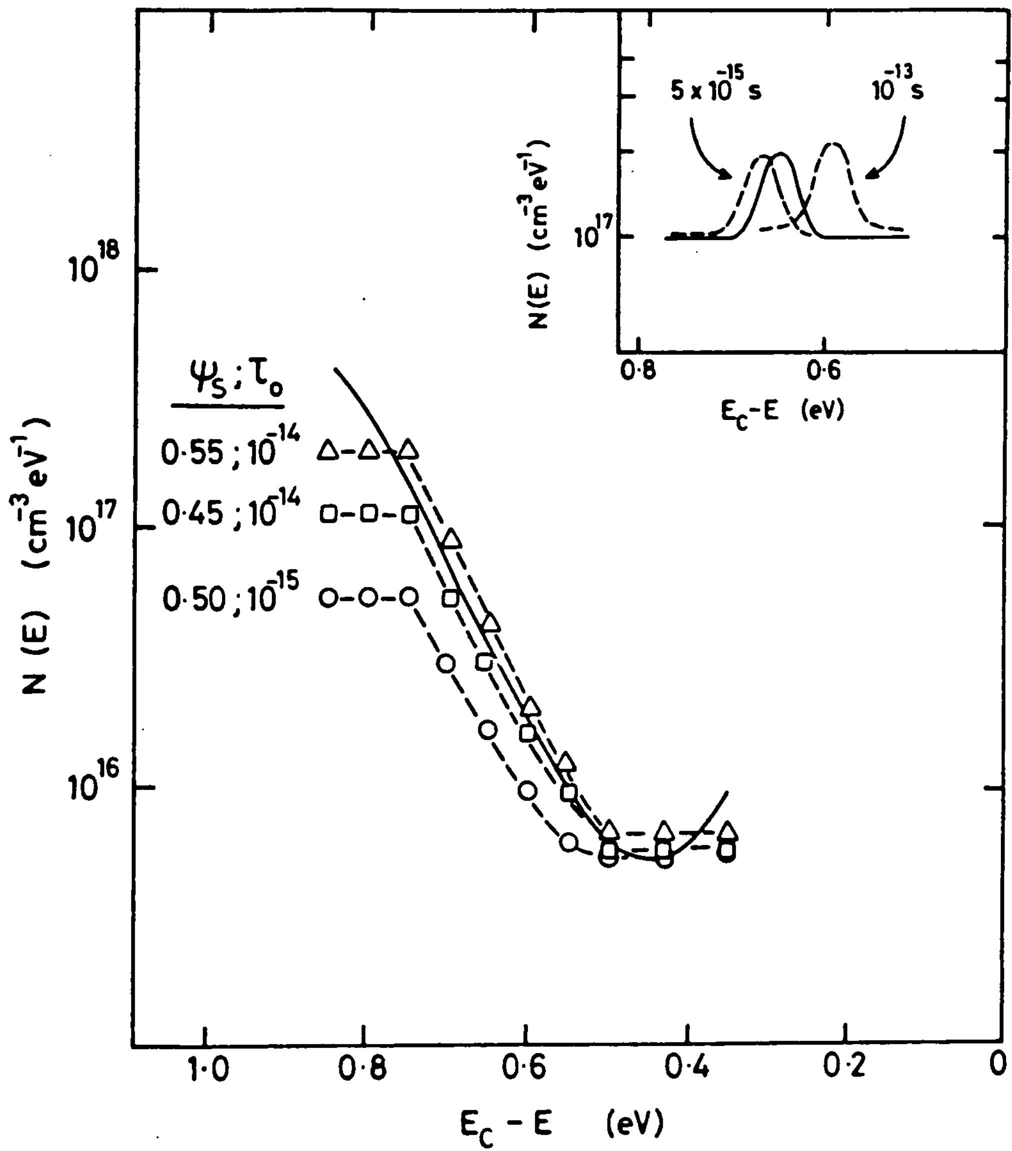

FIGURE 6.11: N(E) estimates from C,G-ω plots (method 4). Incorrect barrier parameters have been used. The correct parameters are ψ_s = 0.5 volts, $\tau_o = 10^{-14}$ s.

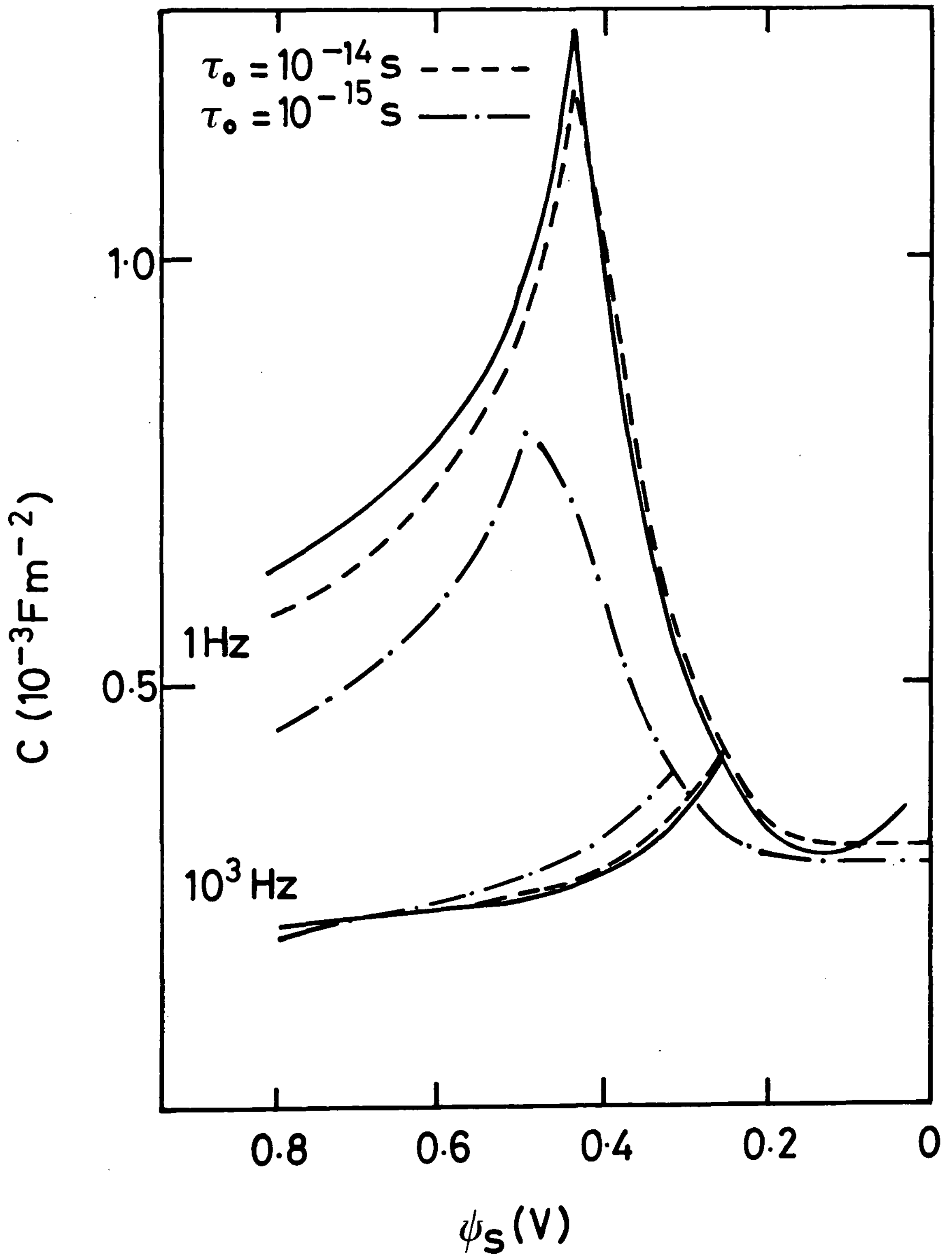

FIGURE 6.12: C-V plot from the Lang N(E) and $\tau_o = 10^{-14}$ s (solid line). The other curves are C-V plots calculated from the regenerated Lang N(E) (method 4).

CHAPTER 7

EXPERIMENTAL MEASUREMENTS MADE ON a-Si SCHOTTKY BARRIERS

7.1 INTRODUCTION

In this chapter it is described how amorphous silicon (a-Si) Schottky barriers were fabricated and the methods used to characterise the devices are briefly outlined. Current-voltage measurements were made at various temperatures, admittance was measured as a function of bias, measuring frequency and temperature, and internal photoemission experiments were performed. An important aim of the experimental work was to discover how well the theory in Chapters 5 and 6 describes experimental admittance results. In fact the agreement between experiment and theory is shown to be very good and therefore it has been possible to deduce a considerable amount of information about the electronic density of states in the mobility gap of a-Si. The analysis of the experimental results is described in section 7.6.

7.2 AMORPHOUS SILICON MATERIAL DETAILS

The a-Si samples used in this study, with one exception, were all prepared by the glow-discharge technique at the University of Dundee The samples consisted of a stainless steel substrate on which was deposited an n^+-type doped layer followed by an n-type doped layer. The substrate temperature at deposition was maintained at about 250° C and from the growth conditions the total thickness of the a-Si film was estimated to be about 0.6 μm.

The current-voltage characteristics of an *undoped* a-Si Schottky barrier are also reported in the results. The undoped sample was obtained from the Xerox Corporation, Palo Alto, California, and once again it was grown using the glow-discharge technique. As received, the sample consisted of a glass substrate, coated with ITO, on which was deposited an n^+-type doped layer followed by an undoped layer of a-Si. The deposition temperature was about 230°C and the thickness of the a-Si film was estimated to be about 1 μm.

The Xerox and the Dundee samples were designed so that they should have a good ohmic back contact and that sandwich structure Schottky barrier/ MIS devices could be easily fabricated. There were however some technical difficulties. The a-Si film would often flake off from the substrate and this was thought to be due to the poor adhesive properties of the n^+-type doped layer[1]. Also, because the a-Si film is very thin, any inhomogeneities in the substrate could lead to uneven growth and so give rise to pin-holes in the film[2]. On several samples only a small fraction of the fabricated Schottky barriers were rectifying (e.g. $\sim$ 1/5th) and this was attributed to pin-holes acting as electrical shorts between the top and bottom contacts.

7.3 DEVICE FABRICATION

The Schottky barriers were made using the following fabrication procedure.

1. The sample, as received, was first refluxed for 2-3 hours in isopropyl alcohol (IPA).
2. It was then etched for 2 mins in buffered HF (40% HF, 40% NH_4F in 1 : 5 volume ratio) followed by a thorough rinse in very pure water ("Milli-Q" reagent grade[3]).
3. The freshly etched sample was immediately inserted into an Edwards 306 vacuum coating system and the system was pumped down to 10^{-6} torr.
4. 100-200 Å of palladium (Pd)/gold (Au) was evaporated onto the top surface of the sample, and this was done by resistive heating from a tungsten filament/ molybdenum boat. The electrode pattern (a matrix of 0.5 mm diameter circular dots) was defined by a mask in contact with the top surface and the thickness of deposited metal was estimated using a quartz crystal thickness monitor.
5. The finished sample with evaporated top contacts was mounted on a glass microscope slide and silver paste was used to make electrical contact to the back electrode.
6. Samples were always kept in the dark but no other precautions were taken (e.g. storing in dry nitrogen).

The reflux and etch procedures were intended to provide a clean, oxide-free top surface on which to evaporate the metal. Buffered HF strips the oxide but it should only be a very slow etch of the a-Si (etch rates on crystalline Si have been measured at $\sim$ 17 Å/min[4]). On occasions however the etch would destroy the sample. Large areas of the a-Si would flake off from the substrate and this was thought to be due to the etchant penetrating to the n^+ back contact and degrading the film adhesion. It was also found that the samples could only be used once. A repeat of the etch procedure greatly increased the density of pin-holes in the film.

In order to make near-ideal Schottky barriers it is important that the etched a-Si is placed under high vacuum as quickly as possible, thus minimising fresh oxide growth. The Edwards vacuum system is specified to pump down to 10^{-4} torr in 2½ mins, and it took approximately 3 mins to dry the sample and fix it to the contact mask in the vacuum chamber. It has also been found in this laboratory that the most ideal Schottky barriers are made when the evaporation is performed as soon as a high vacuum is achieved (i.e. 10^{-6}-10^{-7} torr). Although the vacuum system was fitted with a liquid nitrogen cold trap and an alumina sorb, it is thought that some silicone oil vapour from the diffusion pump could enter the vacuum chamber and that over a prolonged time this vapour may degrade the semiconductor surface. Therefore evaporations were always carried out within 2-3 hours of the sample entering the vacuum system.

Only Au and Pd were used as top contact materials. Au was used because of the ease of evaporation. The Au evaporation rate could be closely controlled and thus it was straightforward to make say 150 Å semi-transparent contacts suitable for measurements under illumination. Unfortunately Au devices were found to be unstable. After a short time, perhaps only a few days, the rectifying properties of these devices disappeared. Other workers[5] have encountered similar problems and it is thought that the effect is due to the Au atoms diffusing into the a-Si. Pd is a much more difficult metal

to evaporate. A tungsten filament was used as the resistive heating element, and hot spots on the filament made close control of the evaporation rate difficult. The hot spots gave rise to short bursts of evaporation with deposition rates of up to 5-10 Å/sec. Nevertheless good stable Schottky barriers could be made in this way - the devices showed no ageing effects over a period of 3 months. One Pd device did however lose its rectifying properties after being kept at a temperature of 370 K for a few hours. Again this was probably due to diffusion of the metal into the relatively open structure of the a-Si.

Finally light induced changes in the material properties of a-Si have been reported[6]. Such effects are not uncommon in semiconductors[7] and the only sensible course of action was to store the samples in the dark and device illumination was kept to a minimum.

7.4 DEVICE CHARACTERISATION : APPARATUS AND METHODS

The standard method for testing each Schottky barrier was a measurement of current versus voltage (I-V). This measurement proved to be the most effective for checking the film for unwanted electrical shorts (e.g.pinholes), testing the ohmicity of the back contact and examining the properties of the interface between the metal and semiconductor. A measurement of I-V at various temperatures allowed a good estimate to be made of the Schottky barrier height. Internal photoemission measurements were made. Monochromatic light was directed onto the top metal contact and a plot of (current response/photon)$^{1/2}$ versus photon energy (the so called Fowler plot) was drawn in an attempt to estimate the Schottky barrier height. Finally admittance measurements were made as a function of bias, measuring frequency and temperature. The experimental set-up used to make these measurements was quite complex and therefore a separate sub-section is devoted to this.

7.4.1 Sample Chambers

Ambient external electrical noise often proved to be the dominant noise contribution for both the d.c. and a.c. measurements. It was important

therefore that the sample and contacts were electrically shielded from as much of this noise as possible. In this department[5] a custom built sample chamber has been designed to provide adequate shielding. Also variable temperature measurements were made in a commercial exchange gas cryostat. Both of these pieces of apparatus are now described.

Custom built sample chamber

The basic design of the sample chamber is shown in Fig.7.1. The outer shielding was made of brass and the outside connexions were gas tight enabling the chamber to be evacuated, filled with dry nitrogen etc. Containers of silica gel (desiccant) were mounted in the base of the sample chamber so as to reduce the ambient levels of moisture. Moisture can be detrimental to the electrical insulation, and unwanted E.M.F's may be generated from chemical reactions associated with water. Samples were mounted on a temperature controlled copper table. A Peltier heater could be used to vary the sample temperature from $-20^{o}C$ to $+ 40^{o}$, however this facility was not used. Electrical contact to the Schottky barrier was made via a gold ball (diameter $\sim$ 0.2 mm) attached to a micromanipulator arm. This enabled a large number of contacts to be tested quickly and easily. The electrical wiring was connected to the outside via an aluminium connection box and coaxial cables were used to connect this box to the necessary instrumentation.

Exchange gas cryostat

An Oxford Instruments DN704 liquid nitrogen exchange gas cryostat was used for the variable temperature measurements. The design of this instrument is quite standard, however there are a few points worthy of note.

The cryostat sample chamber can accommodate samples with dimensions of up to 6 cm x 2.5 cm. Such relatively large dimensions were very convenient but because the active volume of the chamber is large a temperature change could take up to 45 mins to stabilise. Also, because of the possibility of thermal gradients, there was some uncertainty as to the actual temperature

of the sample. The errors involved were of the order of 1-2 K. One major problem arose from the method of wiring used to connect the sample to the outside environment. The wiring consisted of many thin varnished wires bunched together and wrapped around the sample rod. The total length of each wire was about 30 cm. This arrangement gave rise to a sizeable capacitance contribution in parallel with the sample - the capacitance of a sample without a connexion to the top contact, but otherwise connected in the sample chamber, was measured to be 10-15 pF (cf.intrinsic sample capacitance of about 200 pF). It was not possible to allow for this stray capacitance in the admittance calibration procedure and so this value of capacitance was simply subtracted from all measured capacitance data.

Finally the cryostat temperature could be varied from 77K to 400K. The maximum temperature was limited by the melting point of the cryostat indium seals. In practice the maximum temperature was further reduced because at high temperatures the Schottky barrier silver paste contacts tended to detach. The maximum temperature used in these experiments was 370K.

7.4.2 Current Measurements (I-V and internal photoemission experiments)

Currents from 10^{-13} to 10^{-2} amps were measured using Keithley model 410A and 414A picoammeters. For the I-V experiments a Time Electronics type 2003S d.c. voltage calibrator was used as the constant voltage source. It can supply up to 25 mA of current and has a voltage range, in steps of 10^{-8} volts, from 10^{-8} volts to 10^{-2} volts. For the internal photoemission experiments a bunch of optical fibres coupled to a Bausch and Lomb high intensity grating monochromator was used to direct the light onto the Schottky barrier top contact. The long wavelength transmission cut-off of the optical fibre was $\sim$ 1.4 μm (photon energy $\sim$ 0.85 eV) and the complete optical system was calibrated for photon flux versus wavelength by replacing the sample with an Oriel 3810 thermopile, the output of which was measured using a Keithley 181 nanovoltmeter. The thermopile has a response proportional to the

incident light intensity and therefore dividing the output voltage by the photon energy gave a relative value of the incident photon flux. An average light intensity was estimated to be approximately 3 watts/m^2.

7.4.3 Admittance Measurements

A block diagram of the experimental admittance set-up is shown in Fig.7.2. The system was based on a Brookdeal Ortholoc model 9502 two phase lock-in amplifier which was used here as a phase sensitive voltmeter. The required sinusoidal potential was supplied using a Farnell FG3 function generator and the signal output was $\sim$ 3 volts r.m.s. Two outputs were taken from the function generator, one as a reference signal for the Ortholoc and one to the sample via the mixing circuit.

The mixing circuit diagram is shown in Fig 7.3(a). This circuit is a modification of a circuit designed by N.Evans[8]. It isolates the a.c. and d.c.supplies, reduces the a.c. amplitude to $\sim$ 15 mV r.m.s. and helps filter out unwanted a.c. from the d.c. supply (especially mains 50 Hz). The d.c. + a.c. output of this circuit was connected to the sample. The sample impedance was always greater than 1 kΩ and the maximum current was 10^{-6} A. Under such conditions the effective output impedance of the mixing circuit was always negligible.

A specially designed sensing circuit was used to detect the small signal current which flows through the sample as a result of the small signal potential. The circuit is a modification of one designed by Boudry[9] (1978), and the circuit diagram is shown in Fig.7.3(b). The main circuit component is the virtual earth amplifier (AD34) with capacitive feedback C_F. This component converts the small signal input current i_s to an output voltage $v_o = i_s/j\omega C_F$ where ω is the angular frequency of the small signal. There is also an active feedback loop which is designed to filter out any low frequency noise and d.c. current up to a maximum value of $\sim$ 1μA. In forward bias the current flowing through the Schottky barrier could be as large as 1 mA and at these current levels the sensing circuit would cease to operate.

The bias range was therefore restricted to biases typically less than + 0.3 V.

The output from the sensing circuit was directly connected to the phase sensitive voltmeter. The Brookdeal Ortholoc can detect voltages as small as 1 μV and over a frequency range of 5Hz to 100 kHz it can accurately detect phase shifts of less than 10^{-2} rads[10]. The output is displayed on two channels which give the ratio of the in-phase to out of phase components of the input signal measured relative to the reference signal. Normally a Farnell multimeter (DM131) was connected to the Ortholoc outputs and this gave a 3 significant figure digital read-out.

The admittance system was calibrated using low-leakage polystyrene capacitors. The calibration circuit, mixing circuit and sensing circuit were all housed in a metal box for shielding - the limiting factor for low frequency measurements was external electrical noise. The accuracy of the system was limited by the Brookdeal Ortholoc and the smaller of the two output readings became unreliable if it was smaller by more than $\sim 10^{-2}$. A small systematic error was also present because the system was calibrated to a capacitor which was external to the sample chamber. For experiments performed in the exchange gas cryostat this could lead to errors of up to 15 pF in the measured sample capacitance.

7.5 DEVICE CHARACTERISATION : RESULTS

First the current-voltage characteristics of an undoped a-Si/Pd Schottky barrier is reported (see Fig.7.4(a)). The ideality factor increases with forward bias and at V = + 0.2 volts the value is 2. The far-forward bias regime is accurately described by the power Law $J \propto V^m$ where m = 3.9. This power law is indicative of the current being space-charge limited due to an injecting back contact. The current densities are in general lower than those found in the n-type barriers to be described next (see Fig.7.4(b)), and it is thought that the back contact may in fact be limiting the current throughout. This would at least explain the large ideality factor. Because

of this non-ideality no other measurements were made on this diode.

The rest of the results in this section are for measurements made on one n-type doped a-Si/Pd Schottky barrier. This diode is chosen because it showed the most ideal current-voltage characteristics. Many other contacts on the same sample showed almost identical characteristics. Fig.7.4(b) shows a room temperature lnJ versus V plot for the diode. The ideality factor is a constant at ~ 1.3 and in far-forward bias ($V > 0.6$ volts) the I-V relation is linear giving a value of the room temperature bulk resistance of about 85Ω. The current increases with increasing reverse bias but there is no simple I-V relation. The rectification ratio at $V = \pm 1$ volt is $\sim 10^6$.

In order to evaluate the various Schottky barrier parameters, current-voltage measurements were taken at temperatures between 280K and 360K. The results are summarised below :

Temperature (K)	J_o (Acm^{-2})	Ideality η	Bulk Resistance (Ω)
280	1.3×10^{-8}	1.33	159
290	3.85×10^{-8}	1.32	108
300	1.03×10^{-7}	1.33	82.2
320	6.85×10^{-7}	1.30	46.5
340	3.1×10^{-6}	1.28	29.1
360	1.35×10^{-5}	1.30	-

Thermionic emission theory
$$\phi_b(th) = 0.70 \pm 0.03 \text{ eV}$$
$$A^* = 7 \pm 4 \text{ Acm}^{-2} \text{ K}^{-2}$$

Diffusion theory
$$\phi_b(diff) = 0.75 \pm 0.03 \text{ eV}$$
$$K_D = 6 \pm 4 \times 10^5 \text{ Acm}^{-2}$$

$$R = R_o \exp\left[(E_c - E_F)/kT\right] \Rightarrow E_c - E_F = 0.30 \pm 0.005 \text{ eV}$$

The ideality factor was found to be approximately independent of temperature which implies that at least in forward bias there is no appreciable thermionic field emission. The size of the factor is typical of values quoted for a-Si Schottky barriers although Thompson et al[11] (1981) have fabricated palladium silicide (Pd_2Si) a-Si Schottky barriers with $\eta = 1.05$. The diode resistance in far-forward bias closely followed an activated temperature dependence with activation energy 0.30 eV. This energy corresponds to the energy difference between the conduction band mobility edge and the bulk Fermi level at zero temperature. The quoted barrier heights and constants A^*, K_D were found using the $J_o(T)$ dependence and eqn. (4.29). The barrier heights are for zero bias and for zero temperature. As expected the temperature dependence of J_o was equally well described by Thermionic emission theory and Diffusion theory.

An internal photoemission experiment was performed and Fig.7.5 shows the resulting Fowler plot. The plot is not the expected straight line and instead there is considerable structure. The experimental equipment has been successfully used in this department[12] to estimate the barrier heights of many different Schottky barriers, and therefore the observed structure is thought unlikely to be spurious. The measured current densities were larger than usual for this internal photoemission experiment and it is suggested that this is because there is a large extra current contribution arising from the photoexcitation of gap state electrons. No similar Fowler plot data has been reported for a-Si, however Crandall[13] (1980) has found similar structure in the measured sub-band gap absorption of a-Si Schottky barrier solar cell devices. He argues that the structure is due to interference effects (sample thickness $\sim$ photon wavelength) but it may also be due to the intrinsic sub-band gap optical absorption properties of the a-Si.

Capacitance and conductance were measured as a function of bias, measuring frequency and temperature. Fig.7.6 shows the room temperature plots for C, G versus V and C, G/ω versus frequency and the dashed line in Fig.7.6(c) corresponds to the conductance after diode leakage conductance has been subtracted. These plots form the basis of the a-Si gap state density analysis described in the next section. Fig.7.7 shows plots of C, G/ω versus T over the temperature range 80K to 370K. These plots are for zero bias and the dashed lines in the conductance plots correspond to the contribution due to diode leakage. Finally Fig.7.8 shows plots of C,G/ω versus frequency at various biases and at an elevated temperature of 360K. These measurements were made in an attempt to find the point where the value of the capacitance saturates. This capacitance would correspond to the case where all of the a-Si gap states were responding to the small signal.

7.6 ANALYSIS OF RESULTS

The experimental results for the n-type doped a-Si/Pd Schottky barrier are now analysed using the theory described in Chapters 4,5 and 6.

7.6.1 Analysis of d.c. Measurements

First an estimate for the Schottky barrier interface state density is made,then a value for the pre-exponential of the a-Si bulk conductivity is found, and then some comments are made about whether Thermionic emission theory or Diffusion theory better describes the electrical conduction mechanism. Finally the reverse bias current-voltage characteristics are discussed.

Evaluation of the interface state density

An estimate of the interface state density is found using eqn.(4.25) for the ideality factor ,

$$n = 1 + \left\{ \frac{\varepsilon_s \varepsilon_o / L_o + |e| N_{ss}^{s}}{1 + (|e| \delta N_{ss}^{m} / \varepsilon_i \varepsilon_o)} \frac{\delta}{\varepsilon_i \varepsilon_o} \right\} , \tag{7.1}$$

and the symbols are defined in sub-section 4.3.3. This expression assumes that the insulating layer between the metal and semiconductor is the only reason for the non-ideal current-voltage characteristics and that Thermionic emission theory applies. Now given the preparation conditions of the a-Si top surface it is estimated that $\delta \approx 20$ Å and a reasonable value for the dielectric constant of the insulator is $\varepsilon_i \approx 4$. It will be shown later that an average value for the gap state density is $\sim 2 \times 10^{17}$ cm^{-3} eV^{-1} which gives $L_o \approx 550$ Å for $\varepsilon_s \approx 11$. Then if $n = 1.3$ it can be deduced that

$$N_{ss}^{s} \geq 2 \times 10^{12} \; cm^{-2} \; eV^{-1} ,$$

with equality if $N_{ss}^{m} = 0$. Remember that states in equilibrium with the metal (N_{ss}^{m}) reduce n and states in equilibrium with the semiconductor (N_{ss}^{s}) increase n. McGill et al[14] (1979) report similar values for undoped a-Si/nickel Schottky barriers. It should also be noted that if $\delta \approx 20$ Å then it is probably not correct to set $N_{ss}^{m} \approx 0$. Therefore the actual interface state density may be considerably larger than the lower limit value quoted here.

Evaluation of the conductivity pre-exponential (σ_o)

The bulk conductivity for n-type doped a-Si can be written thus

$$\sigma = \sigma_o \exp\left[(E_F - E_c)/kT\right] \tag{7.2}$$

where $\sigma_o = |e|\mu_{ex}N_c$; μ_{ex} is the electron *extended* state mobility and N_c is the conduction band effective density of states. This expression ignores any temperature dependence of E_c, E_F (see sub-section 2.5.2). From a measurement of the low temperature/high frequency interelectrode capacitance ($= \varepsilon_s\varepsilon_o/\ell$, ℓ = sample thickness) it is calculated that $\ell \approx 0.26$ μm. This result is obtained from the C-T plots (Fig.7.7(a)). The bulk resistance at T = 300K was about 85 Ω and it follows that the room temperature bulk resistivity of the a-Si is about 6.5 k Ω cm. This value is consistent with

other values quoted for $E_c - E_F \approx 0.3$ [15]. From the measured activation energy it then follows that

$$\mu_{ex} N_c \approx 1 \times 10^{20} \ (\text{cmVs})^{-1}$$

and note that this product is simply $\sigma_o / |e|$. The main error in this estimate is probably due to the uncertainty of the area of the contact - up to $\sim 20\%$. If the density of states at the mobility edge $N(E_c) \approx 5 \times 10^{20}$ cm^{-3} eV^{-1} and taking $N_c \approx kTN(E_c)$, then $\mu_{ex} \approx 7$ cm^2 V^{-1} s^{-1}. This value is also consistent with other estimates for mobility.

Thermionic emission theory versus Diffusion theory

It has been shown in Chapter 4, sub-section 4.3.2 that the deviation of the conduction band electron quasi-Fermi level E_{Fn} from the bulk Fermi level E_F can be found from the equation

$$E_{Fn}(o) - E_F = kT\ell n\ (1 - B(V)J_o), \tag{7.3}$$

where $B(V) = \dfrac{L_o \exp(\ \ \phi_b/kT)}{|e|\mu_{ex} N_c} \ \dfrac{1}{V_{BI} - V}$, $V >> kT/\ e$.

$E_{Fn}(o)$ is the energy of the conduction band electron quasi-Fermi level at the interface, J_o is the experimental value for the saturated current density and the expression for B is only correct for forward bias and near-ideal barriers. There is some uncertainty as to the value of the Schottky barrier height ϕ_b. The only successful method for evaluating ϕ_b here has involved using the results for Thermionic emission theory/Diffusion theory. From Thermionic emission theory ϕ_b = 0.70 eV and from Diffusion theory ϕ_b = 0.75 eV. However whichever value of ϕ_b is taken, and taking L_o = 550 Å, $\mu_{ex} N_c = 1 \times 10^{20}$ $(\text{cmVs})^{-1}$, V_{BI} = 0.5 volts and V = + 0.2 volts, then $BJ_o \gtrsim 0.1$, and within experimental error $kT < E_{Fn}(o) - E_F < 0.2$. Therefore there is at least an

appreciable drop in the electron quasi-Fermi level.

It is also useful to compare the experimental values for the constants K_D and A^* with the expected theoretical values. Substituting appropriate values into the theoretical expression for K_D(eqn.4.19) gives

$$K_D = |e|\mu_{ex}N_cV_{BI}/L_o \simeq 1.5 \times 10^6 \text{ Acm}^{-2},$$

and following the calculations for crystalline Si it would be expected that

$$A^* \simeq 100 \text{ Acm}^{-2} \text{ K}^{-2}.$$

The experimental estimates for K_D and A^* follow from the $J_o(T)$ dependence and are

$$K_D = 6 \times 10^5 \text{ Acm}^{-2}$$

$$A^* = 7 \text{ Acm}^{-2} \text{ k}^{-2}$$

Experiment and theory are in good agreement for K_D, but there is apparently poor agreement for the values of A^*. It should be noted however the $\exp(-\chi^{1/2}\delta)$ term associated with the thin insulating layer has not been allowed for. For $\eta \simeq 1.3$ it is quite reasonable to expect an order of magnitude reduction in A^*. Therefore there is in fact reasonable agreement in both cases.

The most sensible conclusion is that there is some drop in the conduction band electron quasi-Fermi level, but the drop is less than the Diffusion theory limit $E_F-|e|V$. It is argued however that Diffusion theory will best describe the current-voltage characteristics of an ideal a-Si Schottky barrier where any insulating layer is very thin. Then the electron

emission rate from the a-Si into the metal will be larger than for the non-ideal diode and this should result in further depletion of the conduction band electron density at the interface.

Reverse bias current

In reverse bias the current-voltage relation showed no power law and simply increased gradually. The current was too large by orders of magnitude to be a generation current (see eqn.(6.99)) and the most likely cause of the increase with bias was thought to be edge effects. Also there were large time delays (e.g. 30 mins) before the current measurements at each reverse bias achieved a constant value, and this was attributed to the slow emptying of gap states. Therefore it should be noted that in reverse bias it would not be correct to use the voltage derivative of the d.c. J-V plot as an estimate for the diode leakage conductance. In forward bias these time delays were not evident.

7.6.2 Analysis of Room Temperature Admittance Plots

The room temperature admittance plots will be used to find a consistent gap state density energy distribution N(E). First however the G-V plots are examined and it is argued that even at high measuring frequencies there is complete majority (free carrier) response.

Fig.7.6(b) shows plots of ℓnG versus V at various measuring frequencies. For these plots the main point of interest is that in forward bias the conductance becomes frequency-independent and $\ell nG \propto V$. It is found that at these biases the plots are in good agreement with the expression for the voltage derivative of the d.c. J-V plot,

$$\text{i.e. } G(V) \simeq \frac{|e|}{\eta kT} \exp\left(|e|V/\eta kT\right), \qquad \eta = 1.3.$$

This result is not unexpected but it requires that the majority carriers are able to respond to the small signal. Otherwise the conductance would be frequency-dependent and its value would be less than the value predicted from the above relation.

Methods 3 and 4 of section 6.8 will now be used to find an estimate for N(E) which is consistent with the admittance theory developed in Chapters 5 and 6. The most difficult experimental problem is to find the contribution to conductance from the partial response of gap states. At zero bias the diode leakage conductance dominates up to measuring frequencies of about 1 kHz (gap state conductance $\tilde{\propto}$ frequency). Therefore a very careful evaluation of this conductance is required. The values that were used were found from the voltage derivative of the d.c. J-V plot and these values were subtracted from the measured values of conductance. The resulting gap state conductance is plotted as a dashed line in Fig.7.6(c). Another problem is the evaluation of the gap state lifetime parameter τ_o. As a trial and error first guess $\tau_o = 10^{-13}$ s was used.

The evaluation of N(E) now follows. The Schottky barrier parameters were taken to be $\phi_b = 0.75$ eV, $E_c - E_F = 0.30$ eV (therefore $\psi_s = 0.45$ volts) and $\tau_o = 10^{-13}$ s. The measured values of C and G/ω at f = 800 Hz were substituted into eqns. (6.108) and (6.109) to give average values for the gap state density, denoted N.

From G/ω : $N = 2.0 \times 10^{17}$ cm^{-3} eV^{-1}

From C : $N = 1.0 \times 10^{17}$ cm^{-3} eV^{-1}

The average of the two values was taken and method 3 was used to generate N(E). The result is shown in Fig.7.9 (circles). Also shown in the figure are the gap state densities suggested by Spear et al[16] (1978) and Lang et al[17] (1982). Method 4 was used to calculate N(E) by iterative means. Constant endpoints were used first and it was found that the convergence took many iterations ($\sim$ 12) and the result was a curve with a discontinuous kink at the endpoint nearest the Fermi level. This curve is also plotted in Fig.7.9(dashed lines). In order to remove the kink in the curve it was necessary to change the constant endpoint N(E) to an

N(E) which increases towards E_F. The solid line in the middle of Fig.7.9 shows the best "smooth" curve estimate. This estimate was achieved using a much less number of iterations ($\sim$ 6) than for the constant endpoint case.

There was no real justification for using the value $\tau_o = 10^{-13}$s in the calculations and other values were tried. Fig.7.10 shows the best smooth curve estimates for $\tau_o = 5 \times 10^{-13}$, 10^{-12} s. For each case in order to obtain a smooth curve it was required that N(E) increased towards E_F. Note that the curves are all very similar. Finally, the self-consistency of these results was checked by substituting the calculated values for N(E) with appropriate barrier parameters into the theoretically derived admittance expressions, eqns. (5.74) and (5.76). The resulting C-V plots are shown in Fig.7.11. The N(E) estimate using $\tau_o = 10^{-12}$ s gives the best fit. A more systematic iterative fitting procedure might allow an even closer fit than this, but it is argued, given the approximations involved in the theory, that this fit is sufficiently good.

Compare now the estimated density distribution of gap states with that suggested by Spear et al[16] (1978) and that suggested by Lang et al[17] (1982). These N(E) are also plotted in Fig.7.10, and it is clear that the N(E) derived from the admittance data best fits the Lang N(E). It must be noted however that the estimate is for a relatively small range of gap state energies. For this energy range an average value for N(E) is about 2×10^{17} cm^{-3} eV^{-1}, and if $\varepsilon_s = 11$ then $L_o = (\varepsilon_s \varepsilon_o / |e|^2 N)^{1/2} \approx 550$ Å. Such a value will be shown to be consistent with independent measurements described in the next sub-section.

7.6.3 Analysis of Variable Temperature Admittance Plots

Fig 7.7 shows plots of C and G/ω versus T at zero bias and measuring frequencies of 100 Hz and 10 kHz. Some useful results follow from an examination of the low temperature step in the capacitance plot. This step occurs at a temperature when the bulk majority carrier density (and hence the bulk conductivity) becomes sufficiently large that the bulk carriers

respond to the measuring signal and charge is presented to the depletion edge. The capacitance at the low temperature side of the step is the interelectrode capacitance

$$C = \varepsilon_s \varepsilon_o / \ell \; , \quad \ell = \text{sample thickness},$$

and at the high temperature side the capacitance is approximately

$$C \simeq \varepsilon_s \varepsilon_o / W, \quad W = \text{depletion width}.$$

From the measurement of the interelectrode capacitance and taking $\varepsilon_s = 11$, then $\ell \simeq 0.26$ μm. The capacitance increases by about 30% at the capacitance step and so it follows that the depletion width $W \simeq 0.18$ μm. Another estimate of the depletion width follows from eqn.(4.7),

$$W \simeq L_o \, \ell n(|e|V_{BI}/kT) \simeq 0.16 \text{ μm},$$

where $L_o \simeq 550$ Å and $V_{BI} = 0.5$ volts are used. Clearly the various results are quite consistent. The peak in the conductance plot is also associated with the onset of majority carrier response. It follows from a.c. theory and contains no extra information about the majority carrier response.

Beyond the onset of majority carrier response the capacitance continues to increase with increasing temperature and this is due to the response of gap states. More and more gap states are able to respond with increasing temperature. The conductance also increases with temperature and this is due to an increase in the partial response of gap states - it is argued in Chapter 5, section 5.5 that the width of the partial response region is proportional to kT. Also note that at about T = 300K the 100 Hz conductance curve begins to rapidly increase. This is due to the exponential temperature dependence of the diode leakage current. At $T \gtrsim 300$K the dominant contribution for the conductance measured at 100 Hz is the diode

leakage conductance and this contribution was estimated from d.c. J-V plots and is plotted in dashed lines.

The C,G-T plots have not been used to estimate N(E). There is however a simple relationship f which maps C(T) onto C(ω),

$$\text{i.e. } C(\omega) = f\left[C(T)\right].$$

This relationship is derived using the admittance theory in Chapter 5 and it can be used to further show the consistency between experiment and theory.

The theoretical capacitance expression, eqn.(5.74), is based on a two region total response/no response approximation and the value of the capacitance at any ω, T is uniquely defined by the position x_c where the gap state response goes to zero. This position is defined by the equality $\omega\tau(x_c T) = 1$ and it follows that

$$\omega = \frac{1}{\tau_o} \exp\left\{-\left[(E_c + |e|\psi(x_c)) - E_F\right]/kT\right\} \tag{7.4}$$

where eqn.(5.54) has been used for τ. This relation can be used to find equivalent values for ω and T. If $\omega_1\tau(x_c,T_1) = \omega_2\tau(x_c,T_2) = 1$, then

$$\omega_2 = \left(\frac{T_2}{T_1}\right)^2 \tau_o^{(T_1-T_2)/T_2} \omega_1^{T_1/T_2} , \tag{7.5}$$

or equivalently

$$\ln\omega_2 = \frac{T_1}{T_2}\ln\omega_1 + \left(\frac{T_1}{T_2} - 1\right)\ln\tau_o + 2\ln\left(\frac{T_2}{T_1}\right). \tag{7.6}$$

where it has been assumed that τ_o has a weak $1/T^2$ dependence ($\tau_o = 1/c_n N_c$, $c_n \propto T^{1/2}$, $N_c \propto T^{3/2}$). Hence a change in angular frequency ω_1 to ω_2 should result in approximately the same change in capacitance as a change in

temperature T_1 to T_2 if ω_1, ω_2, T_1 and T_2 are related by the above equations.

Eqns. (7.5), (7.6) were used to map the C-T plots onto the room temperature C-ω plot and the result is shown in Fig.7.12. Two values for τ_o were used, $\tau_o = 10^{-12}$ s and $\tau_o = 10^{-13}$s and both values give a good fit. Given the various approximations involved, an exact fit would not be expected and so the result is encouraging. Nevertheless the fitting procedure is clearly quite insensitive to the barrier parameters and certainly the fit does not offer conclusive proof of the correctness of the admittance theory.

7.6.4 Anomalous Admittance-Frequency Plots at an Elevated Temperature

In an attempt to find the saturated capacitance value (i.e. the capacitance when all of the gap states are able to respond), the admittance was measured as a function of frequency at temperature T = 360K. The result is shown in Fig.7.8. At zero bias and at measuring frequencies less than 30Hz the conductance becomes too large for the phase sensitive detection system to measure the capacitance. However the capacitance does appear to become constant at this frequency and taking $\tau = 2\pi/30$ and $\phi_b = 0.75$ eV then $\tau_o \simeq 2 \times 10^{-13}$s.

A reverse bias was applied to the Schottky barrier so as to reduce the diode leakage conductance and this allowed the barrier capacitance to be measured down to the low frequency limit of the apparatus of ~ 4 Hz. At these low frequencies the measured capacitance decreased in value and the conductance increased in a similar way as before. The capacitance behaviour was somewhat unexpected.

A reduction in the measured capacitance at low frequencies/high temperature has been observed before by Gibb and Long(18) (1984) and Viktorovitch(19) (1981). Gibb and Long propose that the decrease is due to a hole current between the metal and semiconductor which is thought to short-circuit the capacitance. There does not however appear to be any physical justification for this suggestion. Viktorovitch suggests that if Diffusion theory were to correctly describe the electrical conduction

mechanism then gap states near the metal-semiconductor interface would be in equilibrium with the metal and this would lead to a reduction in the capacitance. This conclusion also does not appear to have any justification. It is the author's own view that the most likely reason for the reduction in the measured capacitance is that there is some common unforeseen experimental artefact which gives rise to an erroneously small measurement of capacitance. As yet however no satisfactory reason has been found.

7.7 SUMMARY OF IMPORTANT RESULTS

The results of the measurements made on the n-type doped a-Si/Pd Schottky barriers are summarised below.

1. The best estimates of the Schottky barrier device parameters were,

$\eta = 1.3 \pm 0.1$	:	ideality factor
$\phi_b = 0.75 \pm 0.03$ eV	:	zero bias barrier height
$V_{BI} = 0.45 \pm 0.05$ V	:	zero bias built-in potential
$R_s = 85 \pm 5\ \Omega$	:	room temperature bulk resistance
$\ell = 0.26 \pm 0.05\ \mu m$	:	a-Si sample thickness

2. The following a-Si material parameters were deduced.

$E_c - E_F = 0.30 \pm 0.005$ eV

$\mu_{ex} N_c = 10^{20}\ (\text{cmVs})^{-1}$ ∿ 50% possible error

$\tau_o = 1/c_n N_c = 10^{-12} - 10^{-13}$ s

A gap state density distribution N(E) was found which fitted the admittance theory to the experimental plots. Over the energy range 0.4 eV < E_c-E < 0.7 eV the average value of N(E) was about 2 x 10^{17} cm^{-3} eV^{-1} and the distribution followed that suggested by Lang et al[17] (1982), (see Fig.7.10).

3. From the measured ideality factor it was estimated that there must be at

least 2 x 10^{12} cm^{-2} eV^{-1} states at the interface which are in equilibrium with the semiconductor. The analysis assumes that $\delta \simeq 20$ Å, $\epsilon_i = 4$ and that Thermionic emission theory applies.

4. In forward bias it was estimated that there must be an appreciable (greater than kT for V = 0.2 volts) deviation of the conduction band electron quasi-Fermi level from the bulk Fermi level.

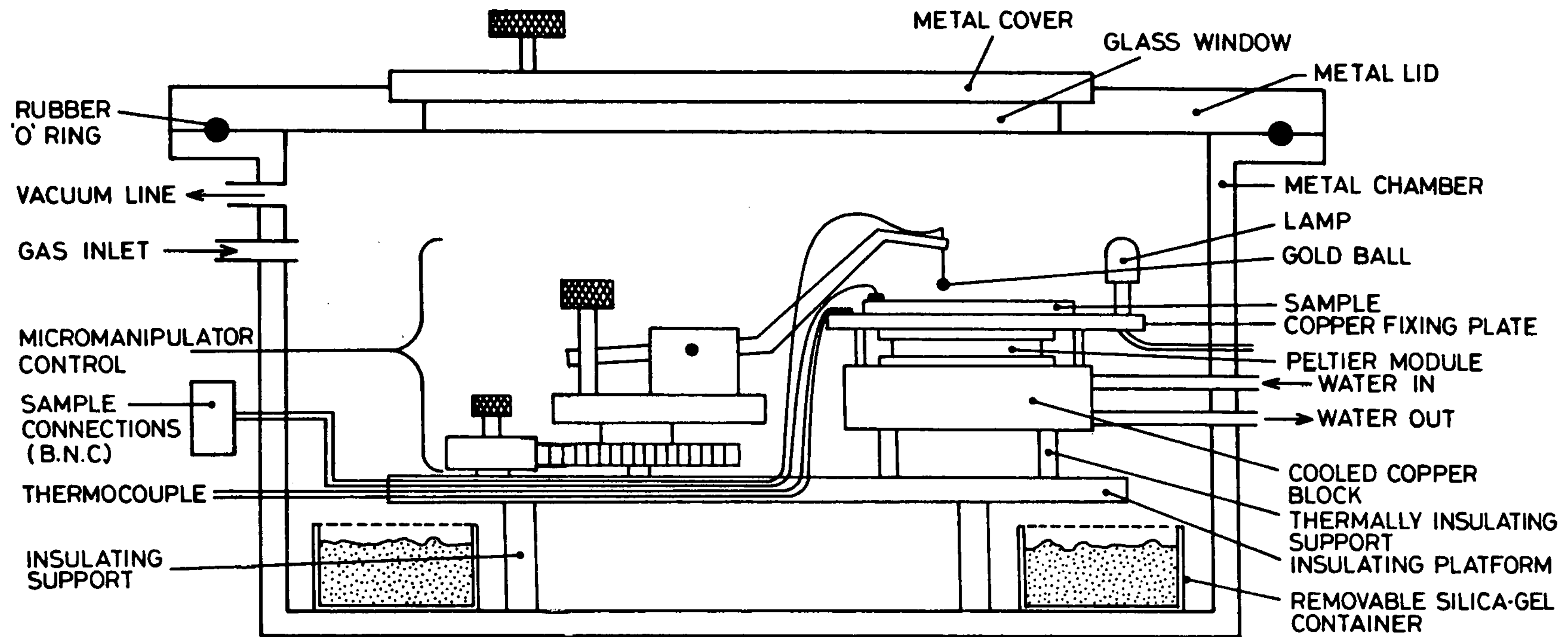

FIGURE 7.1: Diagram of the sample chamber used for the room temperature measurements.

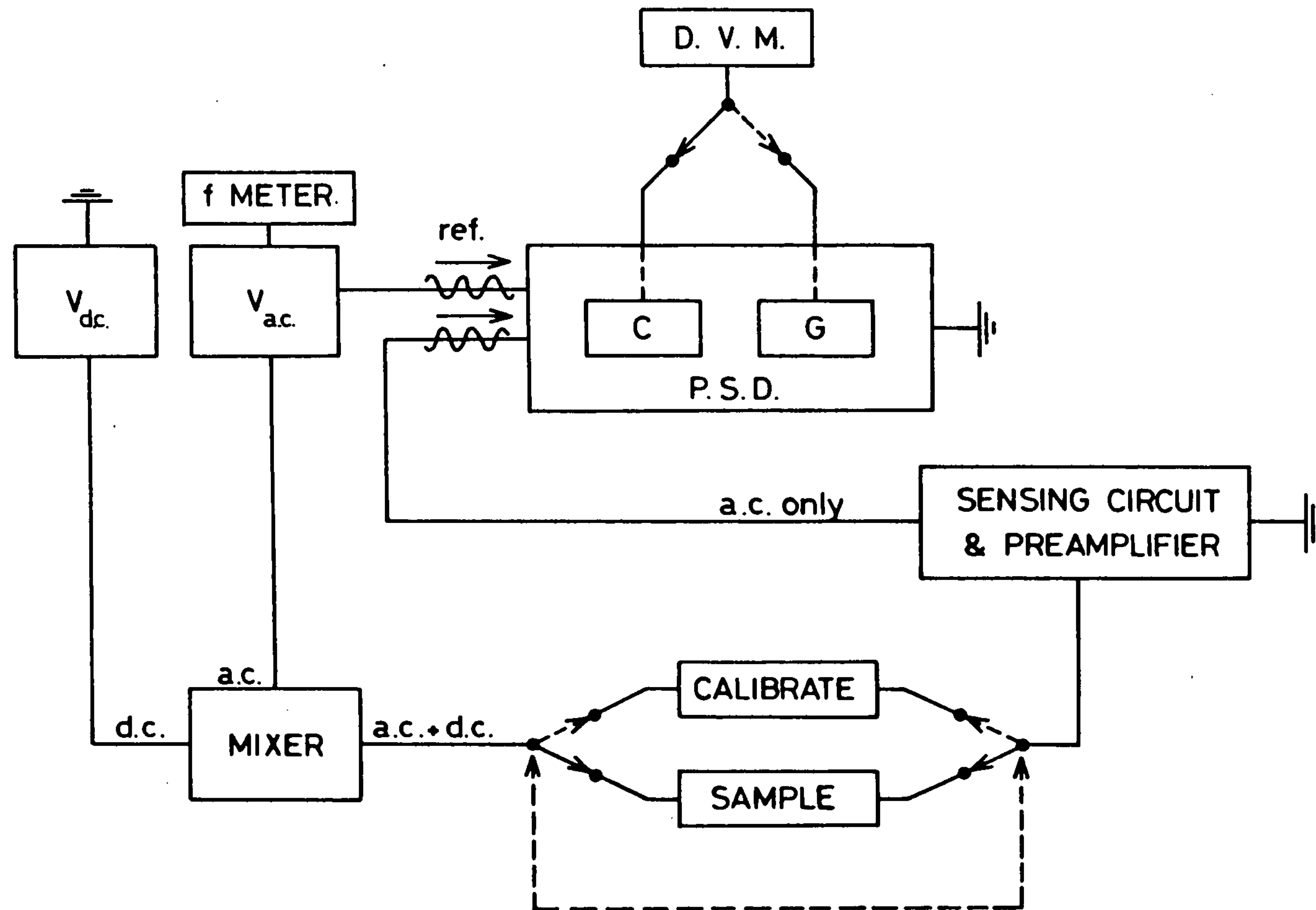

FIGURE 7.2: Block diagram of the experimental set-up used to measure the admittance of the Schottky barrier.

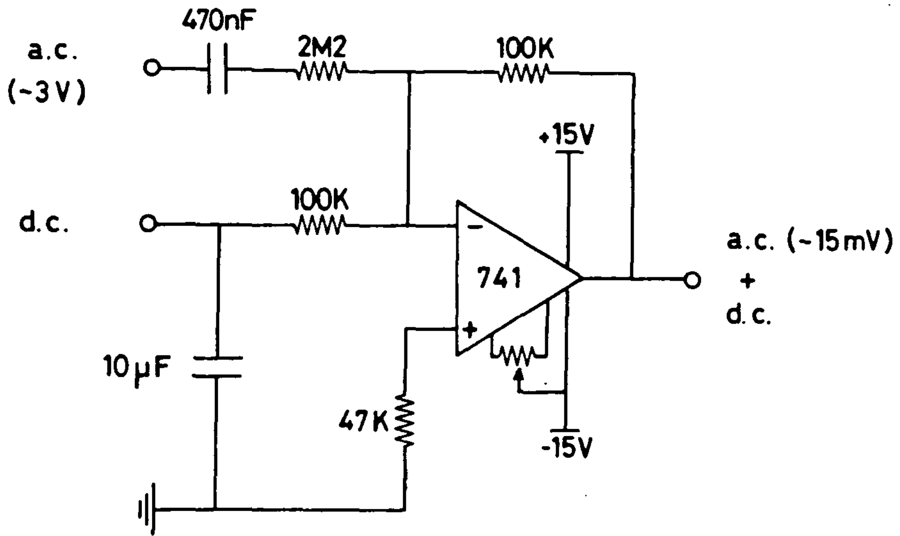

FIGURE 7.3(a): The admittance set-up : a.c. and d.c. mixing circuit.

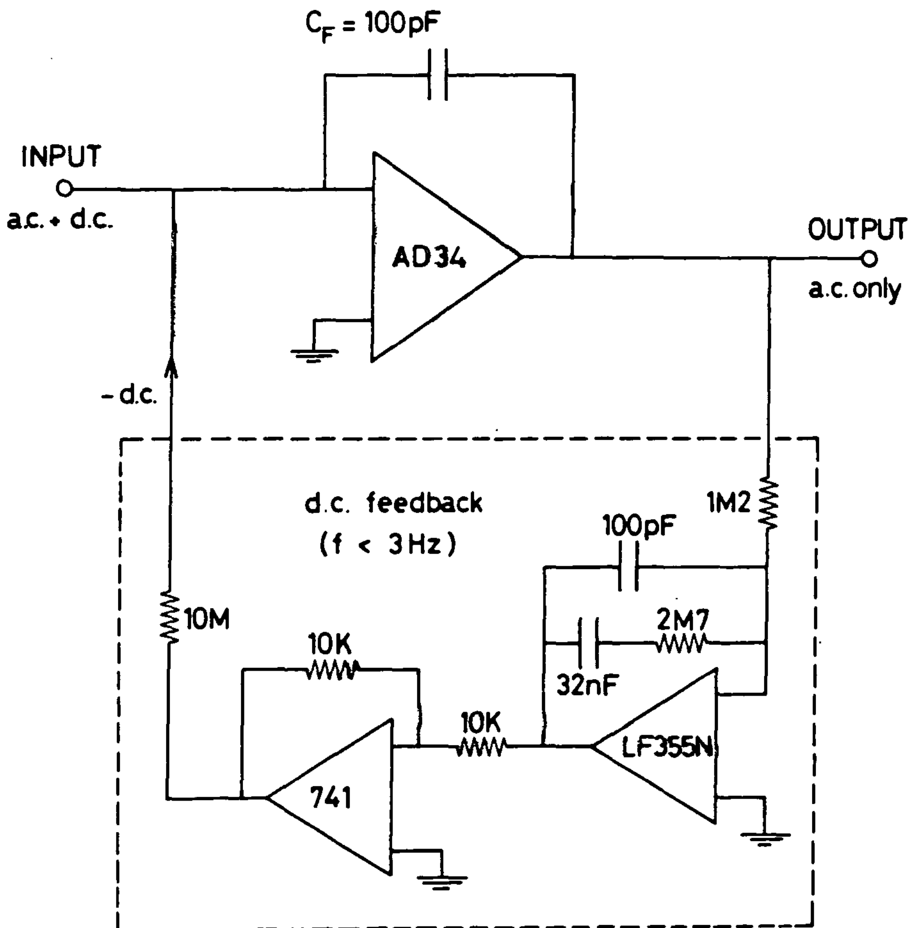

FIGURE 7.3(b): The admittance set-up: sensing circuit for the small signal current incorporating low-frequency/d.c. filter.

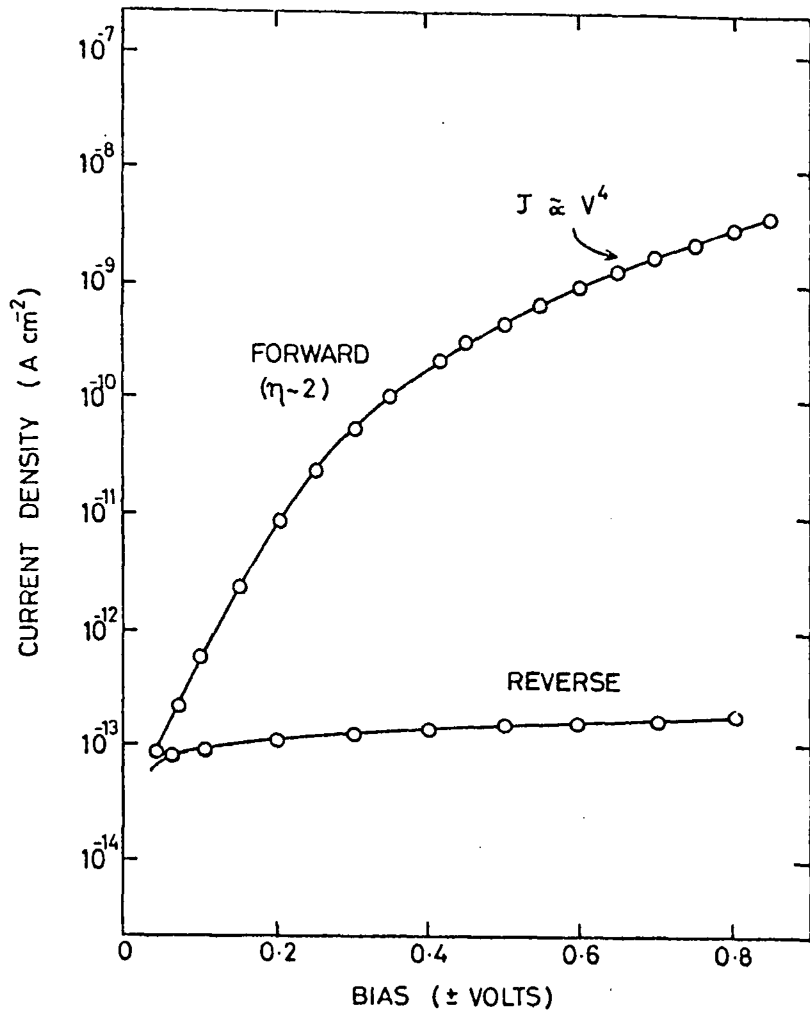

FIGURE 7.4(a): ℓnJ versus V at room temperature for the undoped a-Si/Pd Schottky barrier

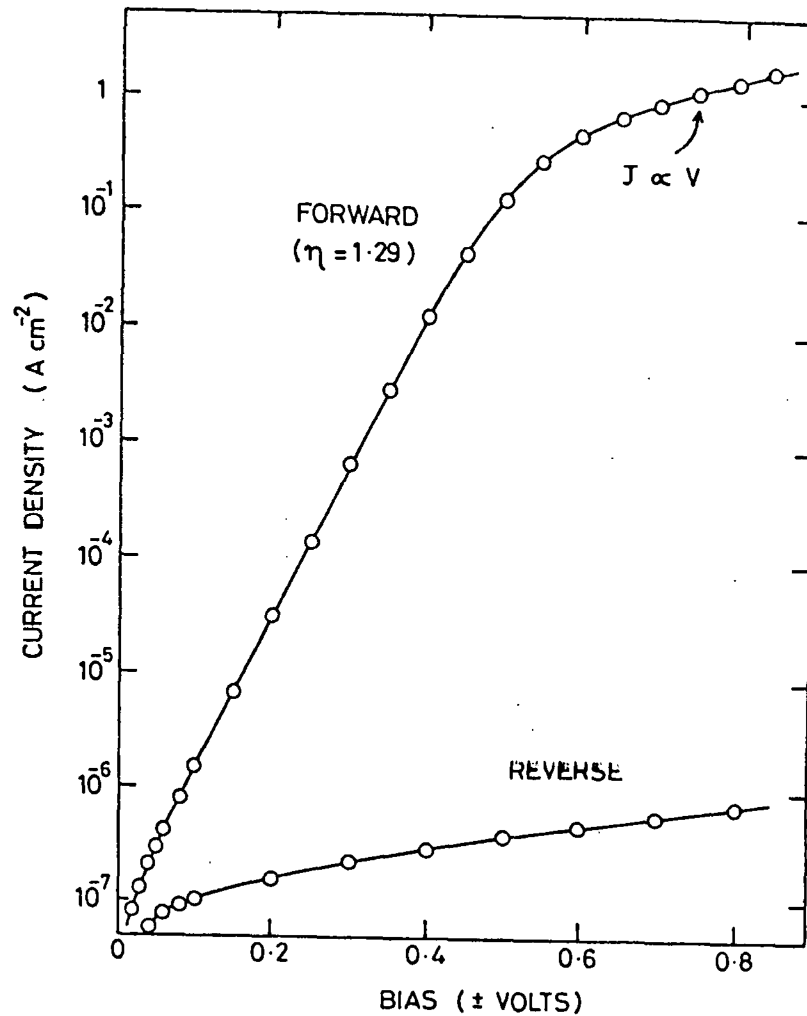

FIGURE 7.4(b): ℓnJ versus V at room temperature for the n-type doped a-Si/Pd Schottky barrier

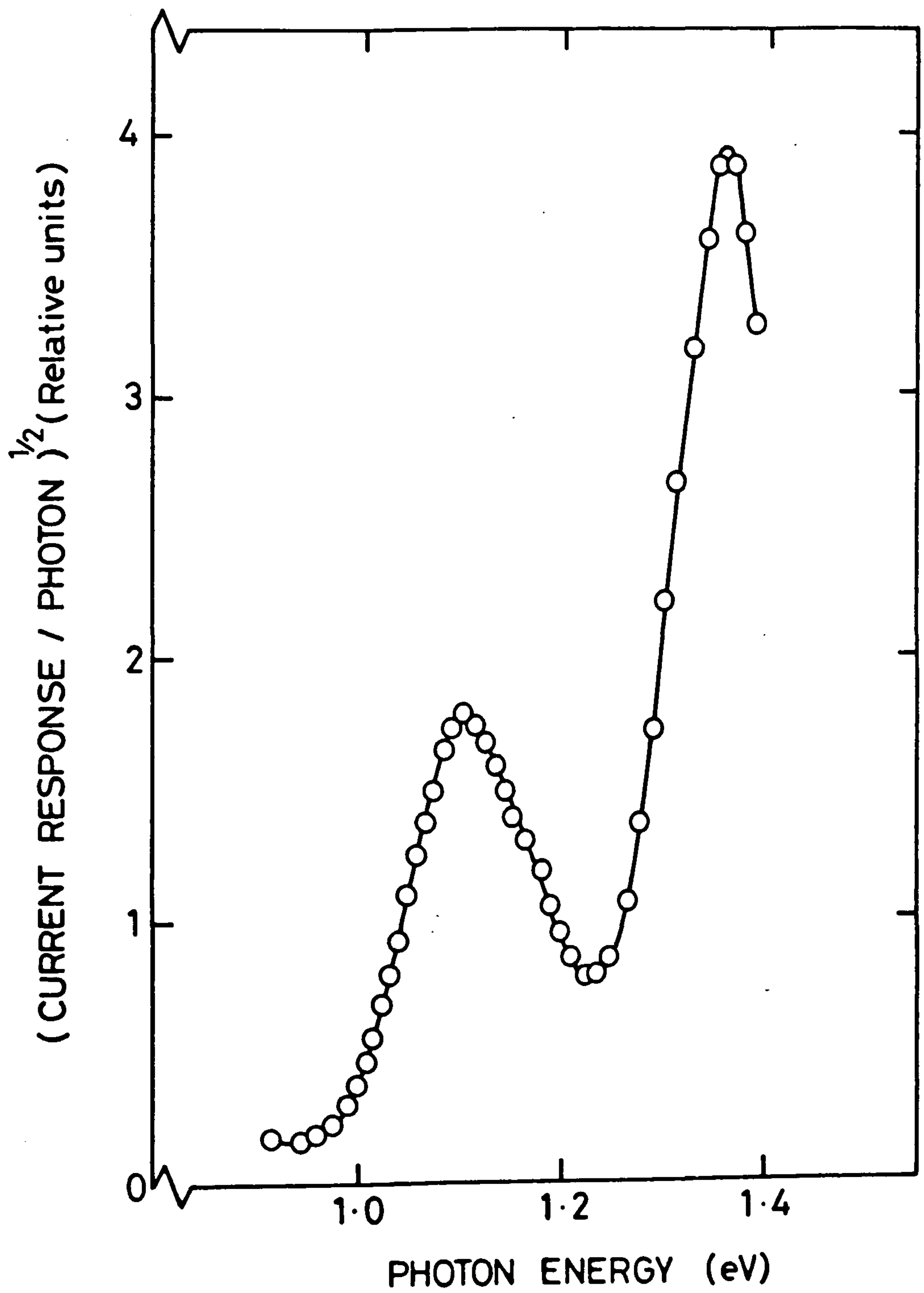

FIGURE 7.5: Fowler plot for the n-type doped a-Si/Pd Schottky barrier.

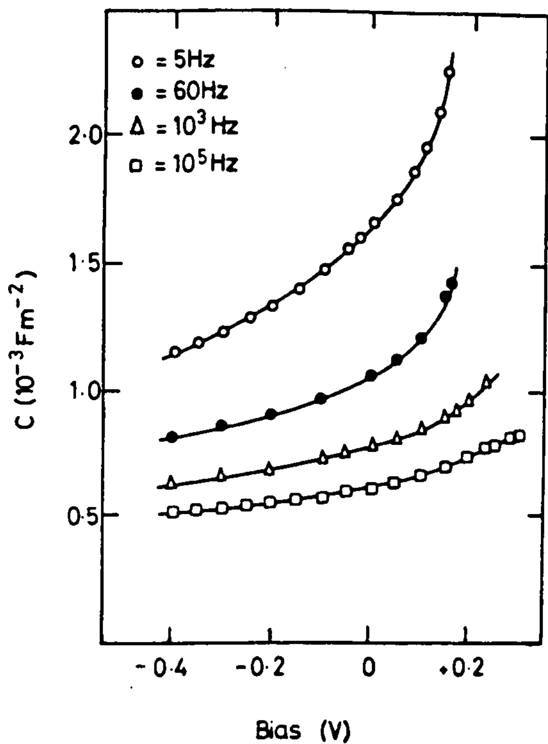

(a) C-V plots

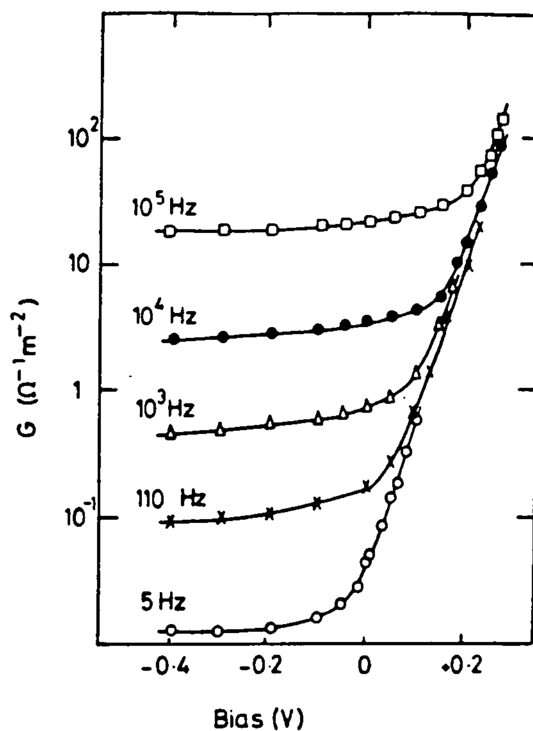

(b) G-V plots

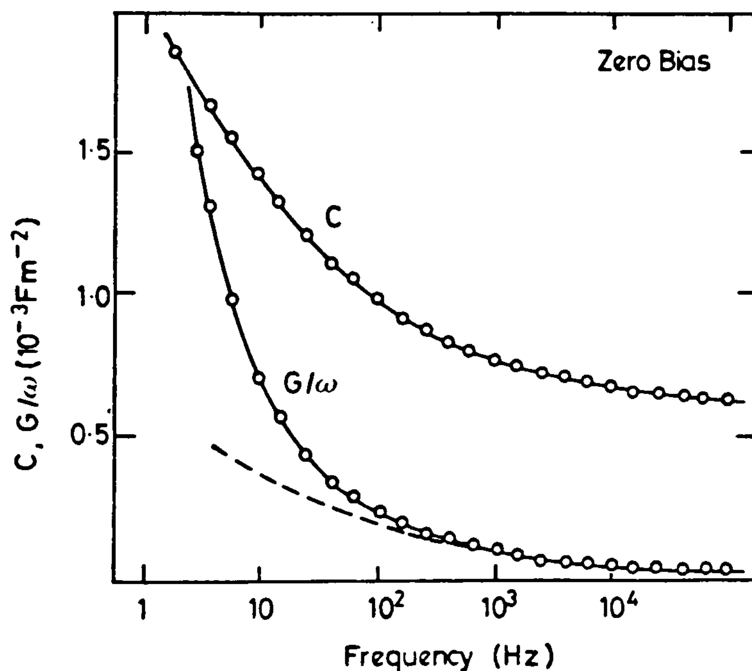

(c) C,G/ω -frequency plots. The dashed line corresponds to the conductance after diode leakage conductance has been subtracted.

FIGURE 7.6: Various room temperature admittance measurements made on the n-type doped a-Si/Pd Schottky barrier.

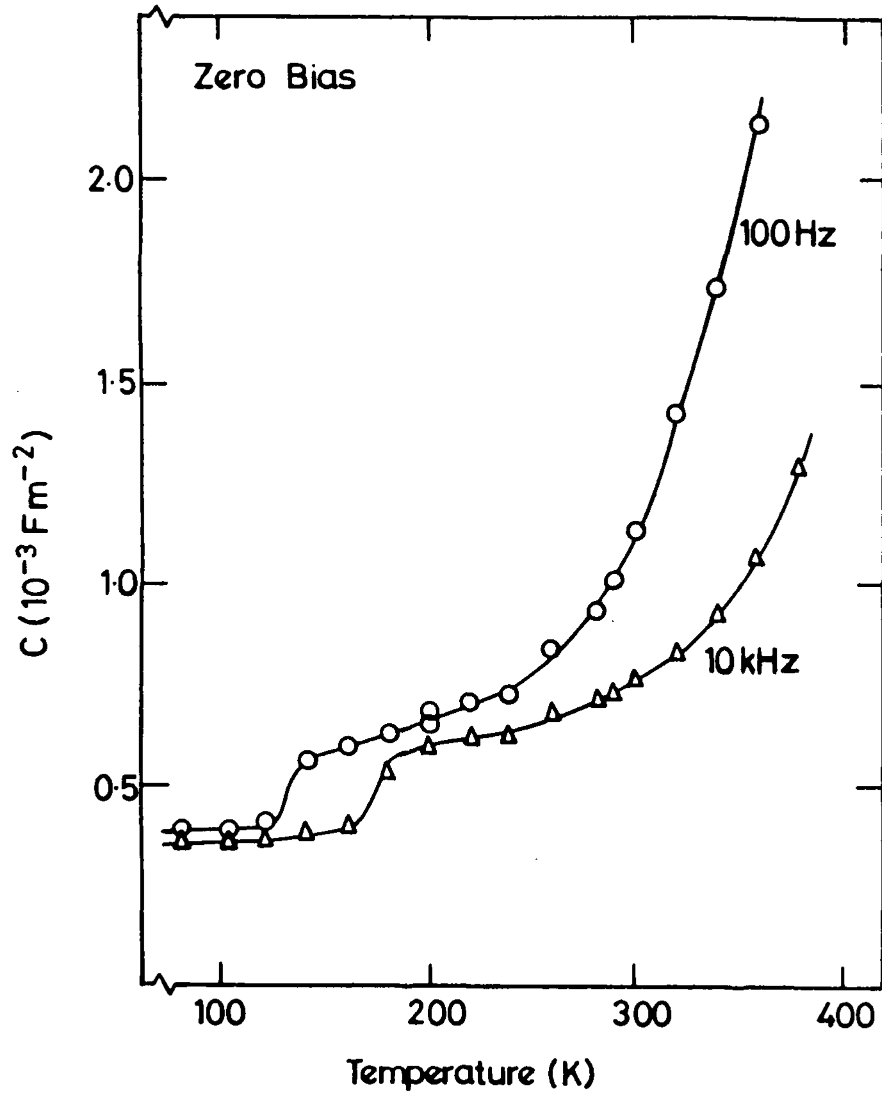

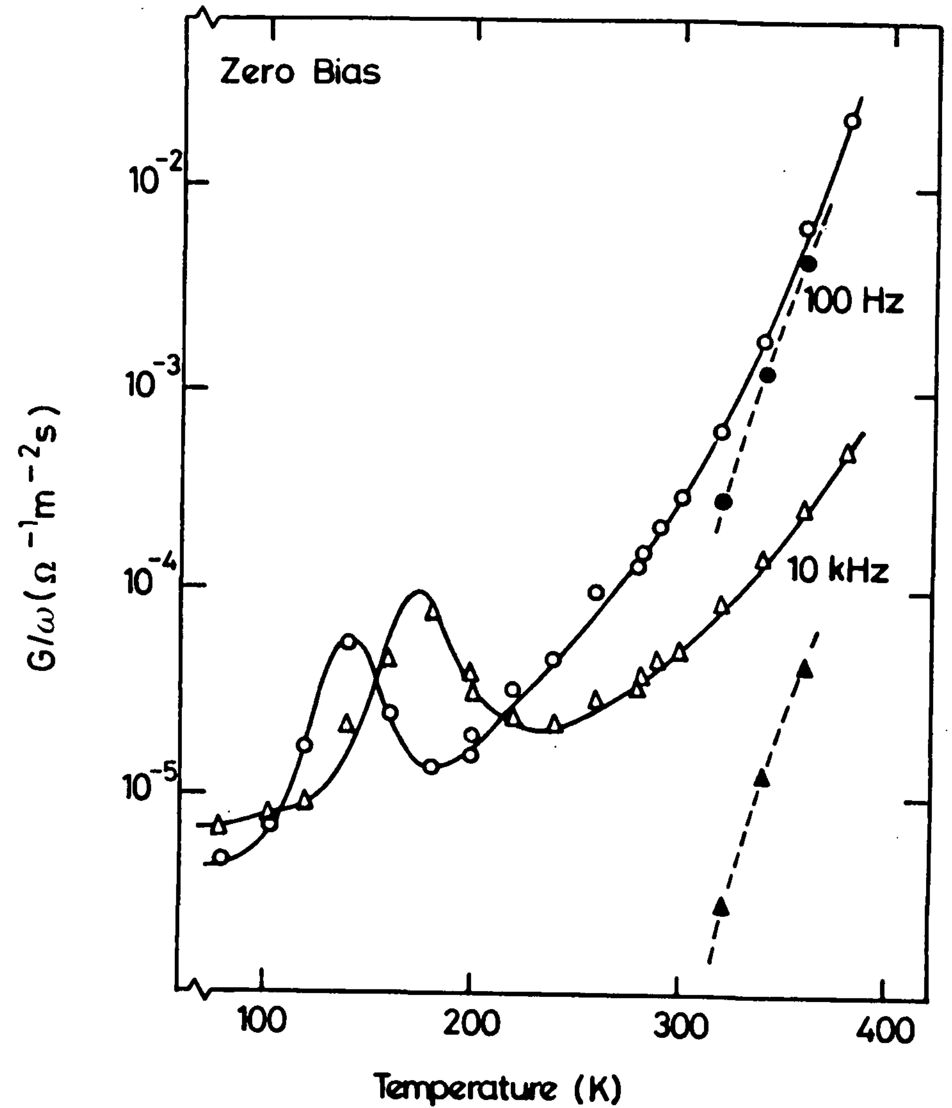

FIGURE 7.7: Variable temperature admittance measurements made on the n-type doped a-Si/Pd Schottky barrier. The dashed lines in the conductance plots are estimates of the conductance due to diode leakage.

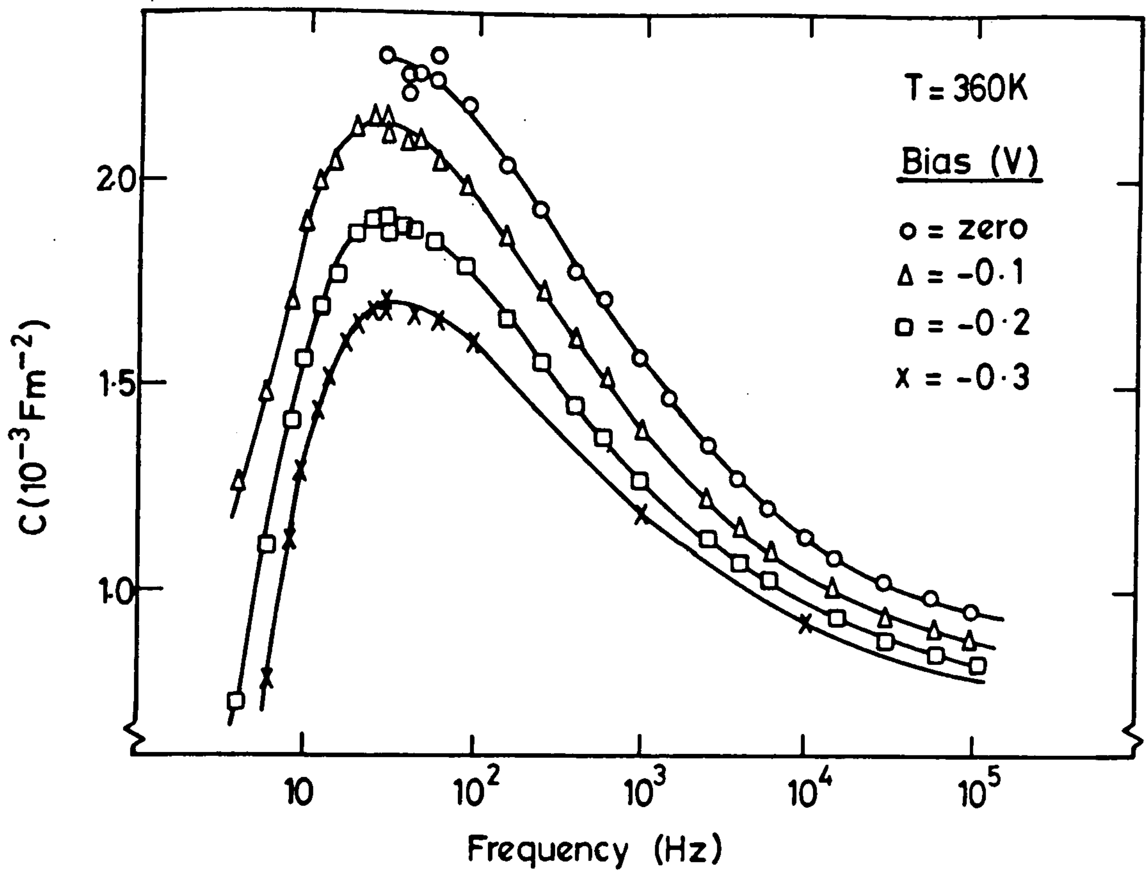

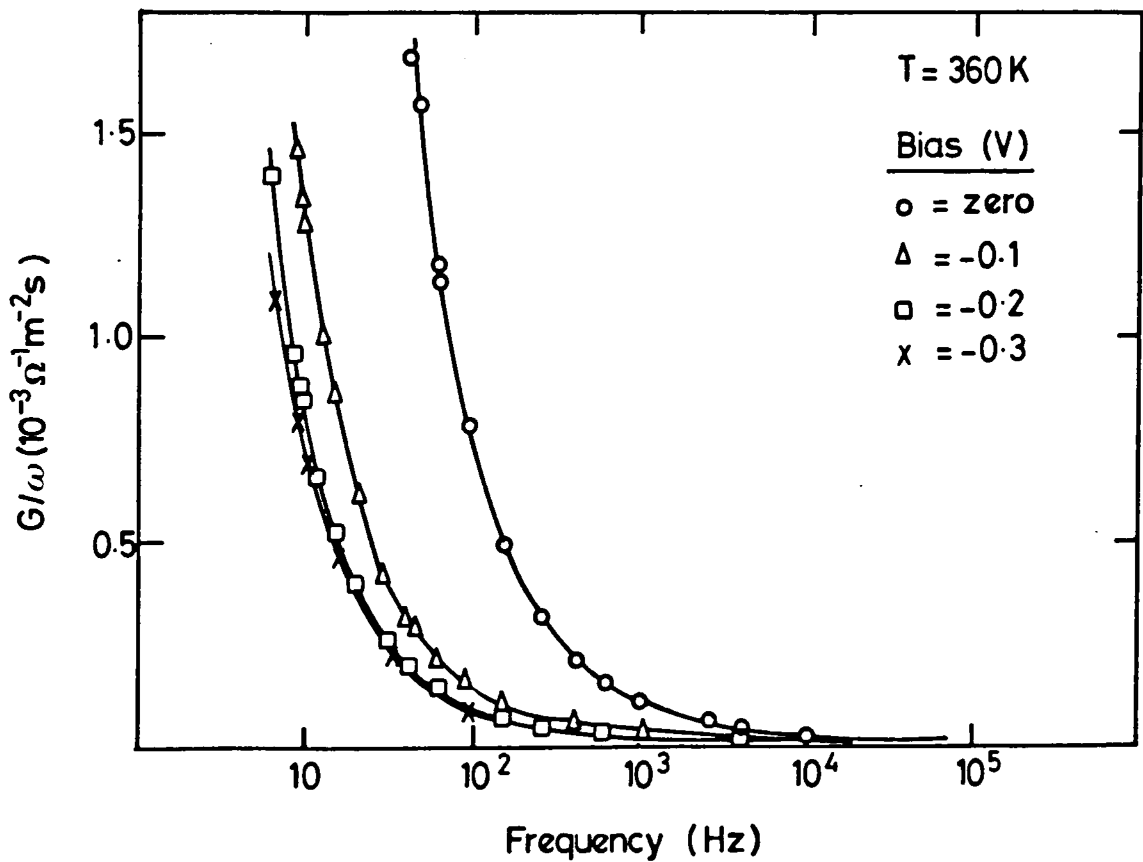

FIGURE 7.8: Admittance measurements made on the n-type doped a-Si/Pd Schottky barrier at an elevated temperature T = 360K.

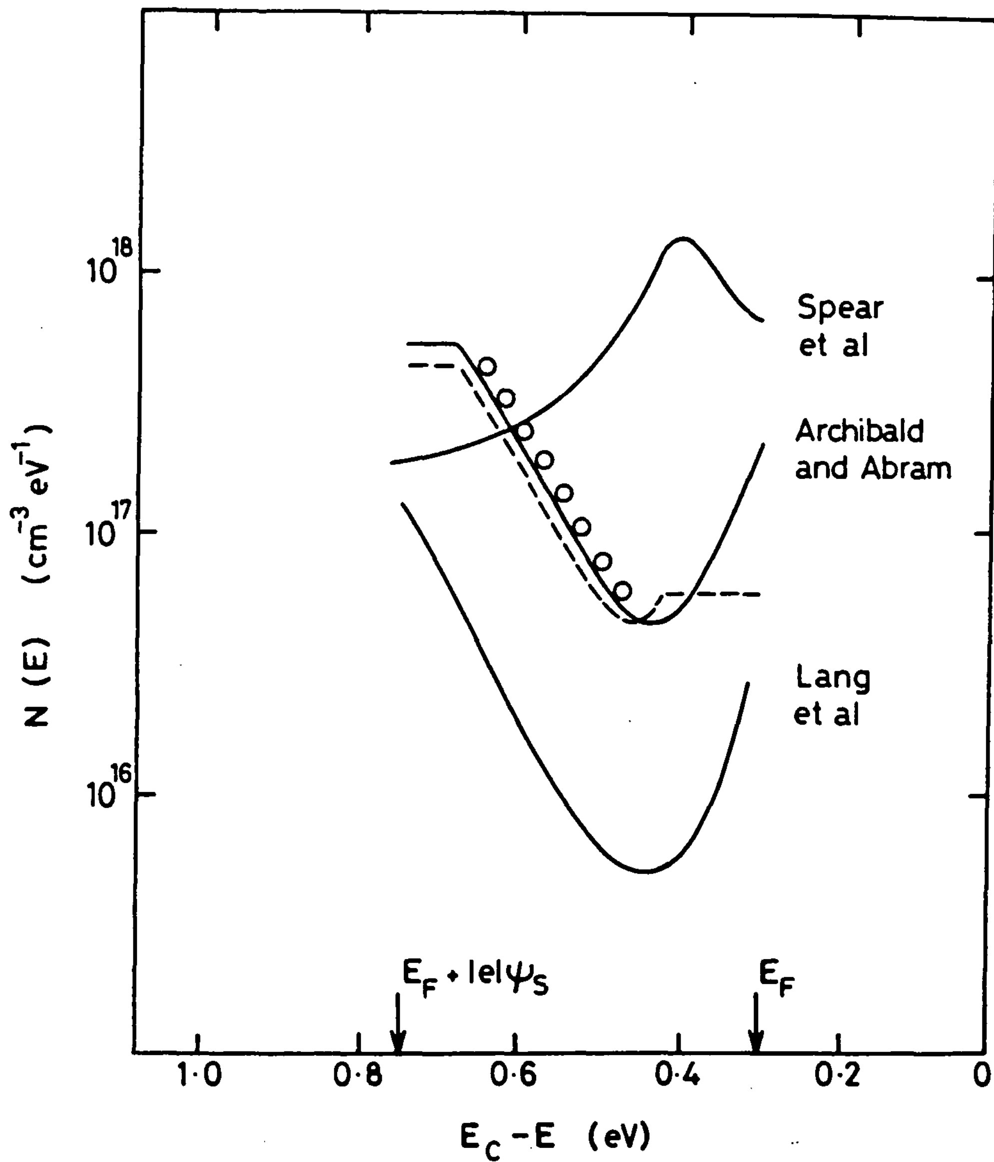

FIGURE 7.9: Various estimates of the gap stage density for a-Si. The estimates marked "Archibald and Abram" use the experimental Schottky barrier admittance results described in the text. The circles correspond to the estimate using method 3. The dashed line of solid line are estimates using method 4. The dashed line is for constant endpoints and the solid line is for the "best guest" endpoint.

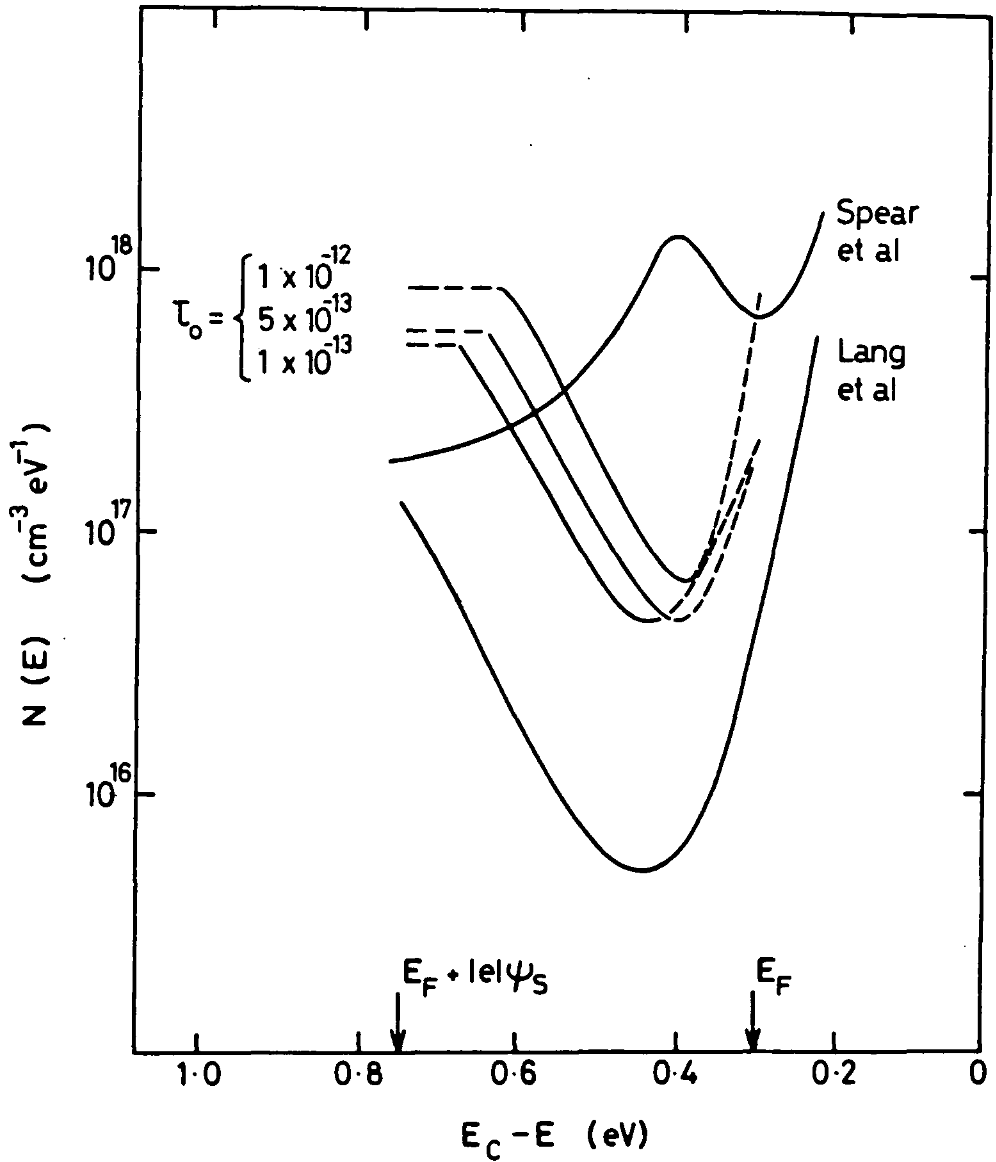

FIGURE 7.10: Several estimates of the gap state density of a-Si using method 4 and various values for τ_o. The dashed lines indicate the chosen endpoint values for N(E). Also shown are the estimates for N(E) as suggested by Spear et al(16) and Lang et al(17).

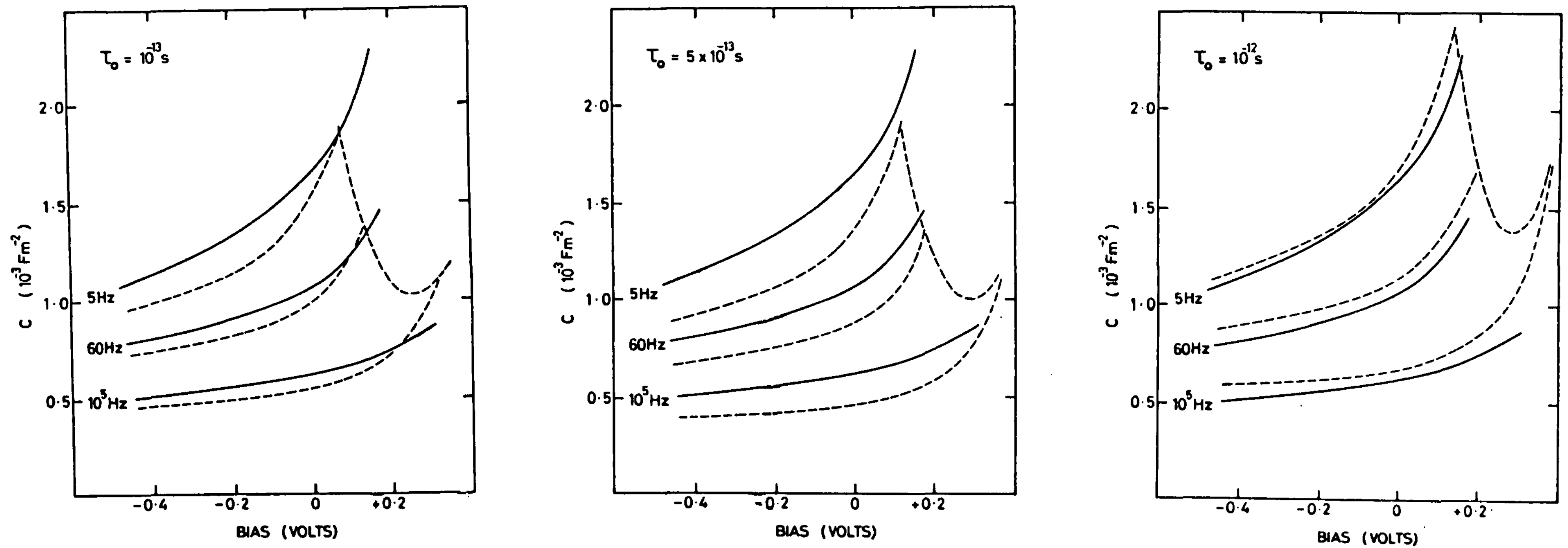

FIGURE 7.11: C-V plots. The experimental plots are drawn in solid lines. The plots drawn in dashed lines were calculated using the gap state densities shown in Fig 7.10 and the theoretical admittance expressions derived in Chapter 5.

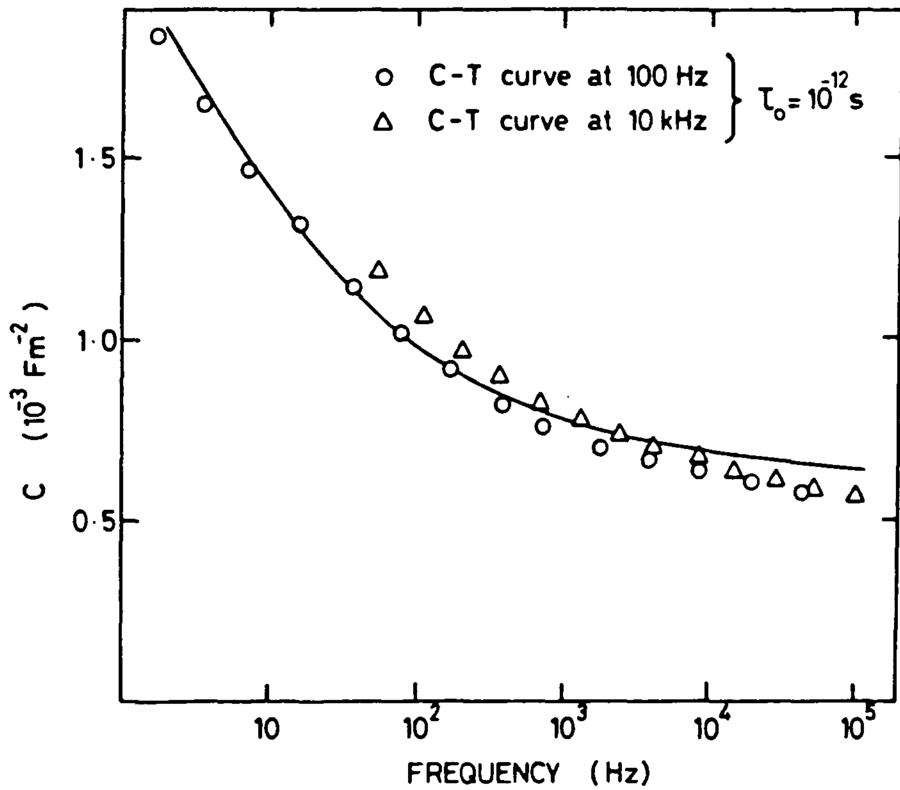

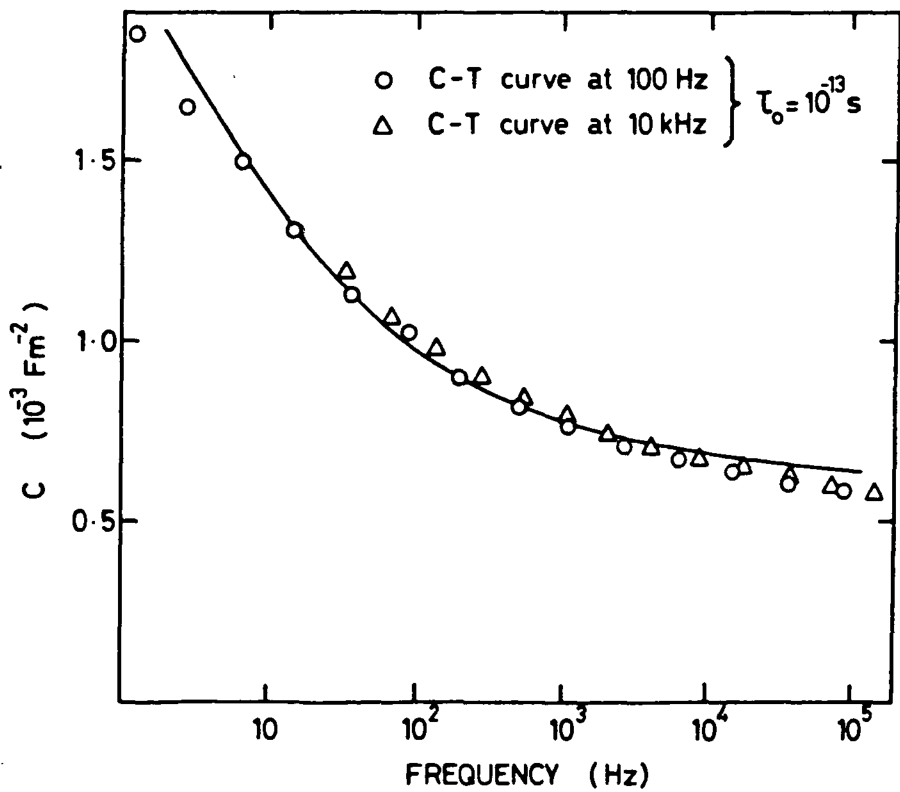

FIGURE 7.12: C-T plots (Fig.7.7) mapped onto the room temperature C-frequency plot using eqn.(7.6) and $\tau_o = 10^{-12}, 10^{-13}$ s.

CHAPTER 8

DISCUSSIONS AND CONCLUSIONS

It was stated at the beginning of this thesis that there is considerable confusion about the microscopic electronic processes pertinent to the behaviour of the admittance of an a-Si Schottky barrier, that the current analyses of admittance measurements lack rigorous justification, and also that the analyses do not extract the maximum amount of information from experimental data. These points have now been examined and a significant contribution has been made towards resolving the problems associated with them.

It has been shown that it is the kinetics of electron capture and emission at gap states which most likely limits the barrier charge response, and using a simple gap state model, described in sub-section 5.3.2, analysis has been developed which leads to a somewhat complicated, but nevertheless analytical expression for admittance (see section 5.4). We can write

$$Y = f(N(E), \tau, \psi_s, \omega, T)$$

where the variables are the gap state density $N(E)$, the gap state lifetime τ, the barrier surface potential ψ_s, the angular frequency of the measuring signal ω, and the sample temperature T.

In Chapter 6, section 6.8, two methods are described for finding $N(E)$ from admittance-frequency plots. One method uses an iterative integration procedure and would require the use of a desk-top computer. The other method, though less reliable, requires no more than a pocket calculator. Indeed this simpler method does not require a detailed knowledge of the admittance calculation.

Experimental measurements were made on an n-type doped (E_C-E_F = 0.3 eV) a-Si Schottky barrier. Extreme care was taken to ensure that spurious experimental artefacts were not introduced into the measurements. A large diode leakage current, large bulk resistance, stray capacitances etc. can have a major effect on the measured values of capacitance and conductance. The experimental measurements turned out to be in excellent agreement with the model calculations. From these measurements a density of states N(E) was found (Fig.7.10) which could be used to generate theoretical admittance plots that closely fit the experimental plots. The deduced N(E) is in approximate agreement with the N(E) deduced by Lang et al from DLTS measurements.

An important aim of the work described in this thesis was to examine the various assumptions and approximations involved in the admittance calculation, and to identify any possible errors or inconsistencies which may be introduced. It has been shown that within the basic model premises the analysis of the admittance is internally consistent both from a physical and a mathematical viewpoint. Moreover the arguments have been developed in such a way that it may be possible to introduce a more sophisticated model of the a-Si Schottky barrier.

It was described in Chapter 3 how there is some controversy over the exact energy distribution of the density of gap states. The two most important techniques for determining N(E), the Field-effect technique and DLTS , give values for N(E) which are not in agreement. It is popularly argued, for example by Dr.LeComber, Dundee University, that the Field effect N(E) is the more reliable and that the "erroneous" DLTS N(E) arises from as yet undetected inconsistencies in the analysis of the DLTS spectra.

The admittance analysis developed here is closely related to the DLTS analysis and in fact Lang and co-workers derive identical admittance results. Importantly however their method of derivation is very mathematical and it is difficult to obtain a clear view of the physics. A better

understanding of the physics is now possible. Furthermore the N(E) deduced from Schottky barrier admittance is in approximate agreement with the DLTS N(E) and so it can be argued that if any inconsistency lies in the analysis of the DLTS data then the same inconsistency is likely to exist in the analysis of the Schottky barrier admittance data. As it is apparent that the admittance analysis has been proven to be internally consistent within the confines of the initial model premises, then if there is an error it must be because of an incorrect model assumption. It is proposed therefore that adjustments might be made to the Schottky barrier model in an attempt to find agreement between the Field effect N(E) and the admittance/DLTS N(E).

Perhaps the most unsatisfactory model assumption is that the gap state capture coefficients are all equal. It may be possible to introduce states with different capture cross-sections, for example, by simultaneously considering several N(E), say $N_1(E)$, $N_2(E)$, $N_3(E)$... with constant cross-sections σ_1, σ_2, σ_3... Such a manipulation may be difficult to incorporate into the existing admittance expressions, but it may be possible to resort to numerical techniques.

The effects of electron transport on the admittance could be examined more thoroughly. It has been argued that the electron transport above the mobility edge does not limit the charge response, except perhaps at measuring frequencies which approach the inverse of the dielectric relaxation time of the bulk a-Si. A more rigorous verification of this result could be achieved by obtaining a complete numerical solution of eqns. (6.50) and (6.51) thus giving the exact functional forms of $\delta E_{Fn}(x,\omega)$ and $\phi(x,\omega)$.

The admittance results could also be used to help investigate the reliability of the Field-effect technique. An important assumption with this technique is that the gap state density at the insulator-semiconductor interface of the FET is the same as the density of gap states in the bulk a-Si. A possible method for investigating this interface state

density is to make admittance measurements on thick insulator MIS a-Si structures fabricated in a similar way to the FET structures. Such measurements on crystalline silicon MIS structures are very common and they can give a detailed knowledge of the interface state density. For a-Si, the Schottky barrier analysis could be used to incorporate the effects of the bulk states into the calculation.

Finally the experimental results presented in this thesis are essentially all from one a-Si sample. Many more Schottky barrier admittance measurements, on a variety of a-Si samples, are required to help substantiate the results. If more ideal devices ($\eta < 1.1$) could be fabricated it would be possible to come to a firmer conclusion about whether Thermionic emission theory or Diffusion theory better describes the diode leakage current. It is also evident that Diffusion theory is itself not entirely satisfactory. Dubious assumptions are made and more general statistical arguments may be needed to properly describe the diffusion-limited case for Schottky barrier current-voltage characteristics.

APPENDIX A

It is required to prove that

$$\frac{1}{\phi_R(x)} \frac{d\phi_R(x)}{dx} = - \frac{C(\psi(x), o)}{\varepsilon\varepsilon_o} , \tag{A1}$$

where

$$C(\psi(x),o) = \left(\frac{|e|\varepsilon\varepsilon_o}{2}\right)^{\frac{1}{2}} \frac{n_B\left(1-e^{-|e|\psi(x)/kT}\right) + \int_{E_F-|e|\psi(x)}^{E_F} N(E)dE}{\left\{ n_B\left(\psi(x) - \frac{kT}{|e|} + \frac{kT}{|e|} e^{-|e|\psi(x)/kT}\right) + \int_o^{\psi(x)} \int_{E_F-|e|\psi}^{E_F} N(E)dEd\psi \right\}^{\frac{1}{2}}} \tag{A2}$$

satisfies the equation,

$$\frac{d^2\phi_R}{dx^2} = \frac{|e|^2}{\varepsilon\varepsilon_o} \left[N(E_F-|e|\psi(x)) + \frac{n_B}{kT} e^{-|e|\psi(x)/kT} \right] , \tag{A3}$$

and the boundary conditions

$$\phi_R(\infty) = o, \quad \left.\frac{d\phi_R}{dx}\right|_{x=\infty} = 0 . \tag{A4}$$

Note that the most general expressions are used which include majority carrier charge and also the small terms in kT. If majority carrier charge need not be considered (sub-section 5.4.5) then the above equations can be simplified by setting the bulk majority carrier density n_B to zero.

First eqn.A1 is rearranged,

$$\frac{d\phi_R}{dx} = - \frac{C}{\varepsilon\varepsilon_o} \phi_R , \qquad (A5)$$

and differentiating gives

$$\frac{d^2\phi_R}{dx^2} = \frac{1}{\varepsilon\varepsilon_o} \left(\frac{C^2}{\varepsilon\varepsilon_o} - \frac{dC}{dx} \right) , \qquad (A6)$$

where $C = C(\psi(x), o)$. Then it is noted that

$$\frac{dC}{dx} = \frac{dC}{d\psi} \frac{d\psi}{dx} = \frac{C^2}{\varepsilon\varepsilon_o} - |e|^2 \left((N(E_F - |e|\psi) + n_B e^{-|e|\psi/kT} \right) . \qquad (A7)$$

Eqn.(6.33) has been used for $d\psi/dx$. By substituting eqn.A7 into eqn.A6 it follows directly that the relation A1 does satisfy differential equation A3.

Also, the relation must lead to a ϕ_R which satisfies the boundary conditions at $x = \infty$. At large x where $\psi(x) << kT/|e|$, the expansion $\exp(-y) \simeq 1-y$, $y << 1$ can be used in eqn.A2. This leads to the following

approximation for relation A1.

$$\frac{1}{\phi_R}\ \frac{d\phi_R}{dx} = -\left(\frac{|e|^2}{\varepsilon\varepsilon_o N(E_F)}\right)^{\frac{1}{2}}\left(\frac{n_B}{kT} + N(E_F)\right) = -K,\ \ \psi(x) << kT/|e|\ , \qquad (A8)$$

where K is a positive constant independent of x. Hence for large x

$$\frac{d\phi_R}{\phi_R} = -\ Kdx \qquad (A9)$$

and integrating from some finite value of x where $\psi(x) << kT/|e|$ to $x = \infty$ gives

$$\phi_R(\infty) = \phi_R(x)e^{K(-\infty + x)} = 0\ , \qquad (A10)$$

and

$$\left.\frac{d\phi_R}{dx}\right|_{x=\infty} = -K\ \phi_R(\infty) = 0\ . \qquad (A11)$$

Therefore the relation is correct.

APPENDIX B

The object of this appendix is to find an estimate for the majority carrier response time in an idealised a-Si Schottky barrier with a constant gap state density ($N(E) = N$) and where the electrons occupying gap states always remain in equilibrium with the conduction band electrons.

The estimate is made using current continuity, which leads to the equation

$$\frac{d^2 \delta E_{Fn}}{dx^2} + \frac{|e|}{kT} \frac{\psi(x)}{L_o} \frac{d\delta E_{Fn}}{dx} = i \frac{\omega}{\omega_D} \cdot \frac{1}{L_o^2} e^{|e|\psi(x)/kT} (\delta E_{Fn} - |e|\phi) \quad \text{(B1)}$$

and the a.c. part of Poisson's equation which we choose to write thus

$$\frac{d^2}{dx^2} (|e|\phi) = - \frac{1}{L_o^2} (\delta E_{Fn} - |e|\phi) . \quad \text{(B2)}$$

The notation and derivation of these equations follow from section 6.5, and in particular $L_o = (\varepsilon\varepsilon_o/|e|^2 N)^{\frac{1}{2}}$ and $\omega_D = |e|\mu n_B/\varepsilon\varepsilon_o$. It proves useful to combine eqns. (B1) and (B2) as follows ,

$$\frac{d^2}{dx^2} (\delta E_{Fn} - |e|\phi) + \frac{|e|}{kT} \frac{\psi(x)}{L_o} \frac{d}{dx} (\delta E_{Fn} - |e|\phi) - \frac{1}{L_o^2} (\delta E_{Fn} - |e|\phi)$$

$$- i \frac{\omega}{\omega_D} \cdot \frac{1}{L_o^2} e^{|e|\psi(x)/kT} (\delta E_{Fn} - |e|\phi) = - \frac{|e|}{kT} \frac{\psi(x)}{L_o} \frac{d}{dx} (|e|\phi) \quad \text{(B3)}$$

and we look at the solution for $F = \delta E_{Fn} - |e|\phi$. F is a measure of the charge response. If $F = -|e|\phi$ then there is complete response, and if $F = 0$ then there is no response.

For a constant gap state density $\psi(x) = \psi_s e^{-x/L_o}$, and as an estimate for the time-varying part of the barrier profile we choose the total response (zero frequency) value, $\phi(x) = \phi_s e^{-x/L_o}$. These results are substituted into eqn.(B3) and for clarity the equation is written in terms of the dimensionless parameters

$$y = \frac{x}{L_o} \quad , \quad \beta = \frac{|e|\psi_s}{kT} \quad , \tag{B4}$$

Then,

$$\frac{d^2F}{dy^2} + \beta e^{-y} \frac{dF}{dy} - F - i\frac{\omega}{\omega_D} e^{\beta e^{-y}} F = \beta|e|\phi_s e^{-2y} . \tag{B5}$$

Consider signal frequencies where $\omega << \omega_D$. Then we argue that as $y \rightarrow \infty$ (i.e. $x \rightarrow \infty$), eqn.(B5) reduces approximately to

$$\frac{d^2F}{dy^2} - F \simeq 0 \, , \qquad y \rightarrow \infty, \tag{B6}$$

with solution

$$F = A\, e^{-y} \quad , \qquad y \rightarrow \infty, \tag{B7}$$

where A is a constant. For $y \rightarrow o$ (i.e. near the metal-semiconductor interface) the last term on the left-hand side will probably dominate and hence

$$-i\frac{\omega}{\omega_D} e^{\beta e^{-y}} F \simeq \beta|e|\phi_s e^{-2y} \, , \qquad y \rightarrow o \, , \tag{B8}$$

with solution

$$F = i \frac{\omega_D}{\omega} \beta|e|\phi_s e^{-2y} e^{-\beta e^{-y}} , \quad y \rightarrow o. \tag{B9}$$

These solutions depend on the estimate for $\phi(x)$, but it will become clear that the only important requirement is that ϕ is a real function.

It is instructive to compare the above charge response with the case when capture and emission processes limit the response. For the capture/emission limiting case the equivalent response function to $F(x,\omega)$ is

$$H(x,\omega) = - \frac{|e|\phi(x,\omega)}{1 + i\omega\tau_{gap}(x)} \tag{B10}$$

where $\tau_{gap}(x)$ is the gap state emission/capture lifetime. Eqn.(B10) follows from the arguments discussed in sub-section 5.4.3. The sub-section shows that the time-varying charge response $\rho_\phi(x,\omega)$ can be given by the equation

$$\rho_\phi(x,\omega) = -|e|N(E_F-|e|\psi(x)) \begin{cases} F(x,\omega) & \text{if response transport limited} \\ H(x,\omega) & \text{if response capture/emission limited} \end{cases} \tag{B11}$$

Now from eqn.(6.6) and using eqn(B4), τ_{gap} can be written thus

$$\tau_{gap}(x) = \tau_F e^{\beta e^{-y}} \tag{B12}$$

where τ_F is the lifetime of a gap state situated at the Fermi level in the

neutral semiconductor bulk. If it is assumed that $\phi(x) = \phi_s e^{-x/L_o} = \phi_s e^{-y}$,

$$H = - \frac{|e|\phi_s e^{-y}}{1 + i\omega\tau_F e^{\beta e^{-y}}} , \tag{B13}$$

and the y = o and y = ∞ limits for H are

$$H = -|e|\phi_s e^{-y} \quad , \; y \to \infty \; , \tag{B14}$$

and

$$H = i \frac{1}{\omega\tau_F} |e|\phi_s e^{-y} \, e^{-\beta e^{-y}} \quad , \; y \to o. \tag{B15}$$

Then comparing eqns. (B7) and (B9) for F, with eqns.(B14) and (B15) for H show that F and H share the same behaviour in the limits $y \to o$ and $y \to \infty$. In eqn.(B7) the constant A plays the role of $-|e|\phi_s$ and in eqn.(B9) ω_D plays the role of $1/\tau_F$. We can argue further that F and H are similar at intermediate values of y.

According to the capture/emission model there is a cut-off in the barrier charge response at a position $x = x_c$. This point is defined by the equality $\omega\tau_{gap}(x_c) = 1$ and at this point the real and imaginary parts of H are equal. It was also shown that because $\tau_{gap}(x)$ is an exponential of an exponential of x, the cut-off occurs within a few kT of barrier. This cut-off is schematically shown in Fig.5.4 .

It is more difficult to deduce the charge response when majority carrier transport is the limiting process. Nevertheless it has been shown that the limits are similar to the capture/emission case, i.e. at small x there is virutally no charge response and at large x there is virtually total charge response. We therefore expect a similar cut-off in charge response around

some point denoted x_{cm}. The obvious defining condition for x_{cm} is

$$\mathrm{Re}\left[F(x_{cm},\omega)\right] = \mathrm{Im}\left[F(x_{cm},\omega)\right] . \tag{B16}$$

but unfortunately we have not found an analytic expression for F at these values of x, ω. Instead either of the two limiting values for F (eqns.(B7) and (B9)) are substituted into eqn.(B5) and an estimate for the relation between ω and x_{cm} is got by setting equal the real and imaginary parts of the left-hand side of eqn.(B5). If eqn.(B7) is used then

$$\omega(x_{cm}) = \omega_D \left(\frac{|e|\psi(x_{cm})}{kT}\right) e^{-|e|\psi(x_{cm})/kT} , \tag{B17}$$

and if eqn.(B9) is used

$$\omega(x_{cm}) = \omega_D \left[2\left(\frac{|e|\psi(x_{cm})}{kT}\right)^2 - 7\left(\frac{|e|\psi(x_{cm})}{kT}\right) - 5\right] e^{-|e|\psi(x_{cm})/kT} , \tag{B18}$$

which for a typical value of $|e|\psi(x)/kT \sim 8$ becomes

$$\omega(x_{cm}) \simeq \omega_D \left(\frac{|e|\psi(x_{cm})}{kT}\right)^2 e^{-|e|\psi(x_{cm})/kT} . \tag{B19}$$

The relatively good agreement between eqns.(B17) and (B19) show that they are probably quite accurate estimates for x_{cm}. Also note that the imaginary factor in eqn.(B5) is an exponential of an exponential function of x. Therefore the change over from F being given by eqn.(B7) to F being given by eqn.(B9) is probably quite quick and hence once again the cut-off in charge response will occur within a few kT of barrier. Note further, following similar arguments to the emission/capture case, if $\psi(x_{cm}) \gg kT/|e|$ then ϕ is almost completely real (see section 6.2). Indeed the total response value

for ϕ is a reasonable order of magnitude estimate.

Finally, the object of this appendix was to find the response time of majority carriers in the depletion region of an a-Si Schottky barrier. The obvious value for this quantity, which is better defined in sub-section 6.5.4, is simply the inverse of eqns. (B17) or (B19) and hence we can write

$$\tau_{maj}(x) = \frac{\varepsilon\varepsilon_o}{|e|\mu N_c^*} \left(\frac{kT}{|e|\psi(x)}\right)^r \exp\left\{\left[(E_c - E_F) + |e|\psi(x)\right]/kT\right\} \quad (B20)$$

where $1 < r < 2$. Eqn.(B20) should be compared directly with eqn.(6.70) of sub-section 6.5.3.

REFERENCES : CHAPTER 2 - "Amorphous semiconductors..."

1. "Electronic Processes in Non-Crystalline Materials", by N.F.Mott and E.A.Davis, Clarendon Press (1979).
2. "Amorphous Semiconductors", Ed.M.H.Brodsky, Topics in Applied Physics 36, Springer-Verlag (1979).
3. A.E.Owen, "Electronic and Structural Properties of Amorphous Semiconductors", Eds.P.G.LeComber and J.Mort, Academic Press, (1973), pp.161.
4. J.S.Dugdale, D.Pavuna and P.Rhodes, Phys.Bull.35, 64 (1984).
5. For example, see "Handbook of Thin Film Technology", Eds.L.I.Maissel and R.Glang, McGraw Hill (1970).
6. For example, see G.N.Jackson, Thin Solid Films 5, 209 (1970).
7. For example, see R.C.Chittick, J.H.Alexander and H.F.Sterling, J.Electrochem. Soc. 116, 77 (1969).
8. For example, see N.Apsley and A.D.Yoffe, J.Non-Cryst.Solids 32, 71 (1979).
9. For example, see A.C.Wright and A.J.Leadbetter, Phys. & Chem, of Glasses 17, 122 (1976).
10. For example, see F.W.Lytle, D.E.Sayers and E.A.Stern, Phys.Rev.B 11, 4825 (1975); E.A.Stern,D.E.Sayers and F.W.Lytle, Phys.Rev.B 11, 4836 (1975).
11. For example, see D.Bermejo and M.Cardona, J.Non-Cryst.Solids 32, 405 (1979); D.Bermejo and M.Cardona, J.Non-Cryst.Solids 32, 421 (1979).
12. G.Etherington, A.C.Wright, J.T.Wenzel, J.C.Dove, J.H.Clarke and R.N.Sinclair, J.Non-Cryst.Solids 48, 265 (1982).
13. For example, see B.A.Vaid and K.C.Sharma, Phys.Stat.Sol.(b) 122, 423 (1984).
14. W.H.Zachariasen, J.Am.Chem.Soc. 54, 3841 (1932).

15. D.E.Polk, J.Non-Cryst.Solids 5, 365 (1971).

16. P. Steinhardt, R.Alben and D.Weaire, J.Non-Cryst.Solids 15, 199 (1974).

17. G.A.N. Connell and R.J.Temkin, Phys.Rev.B 9, 5323 (1974).

18. M.F.Daniel, A.J.Leadbetter, A.C.Wright and R.N.Sinclair, J.Non-Cryst.Solids 32, 271 (1979).

19. D.Turnbull and D.E.Polk, J.Non-Cryst.Solids 8-10, 19 (1972).

20. J.C.Phillips, J.Non-Cryst.Solids 43, 37 (1981).

21. J.C.Phillips, J.Non-Cryst.Solids 35 & 36, 1157 (1980).

22. R.A.Street and N.F.Mott, Phys.Rev. Lett. 35, 1293 (1975).

23. S.R.Elliot, Phil.Mag.B 38, 325 (1978)

24. D.Adler, J.Non-Cryst.Solids 35 & 36, 819 (1980).

25. J. Robertson, Phys.& Chem.of Glasses 23, 1 (1982).

26. H. Michiel, J.M.Marshall and G.J.Adriaenssens, Phil.Mag.B 48, 187 (1983).

27. P.W.Anderson, Phys.Rev. 109, 1492 (1958).

28. N.F.Mott, Phil.Mag. 13, 989 (1966).

29. M.H.Cohen, H.Fritzsche and S.R.Ovshinsky, Phys.Rev.Lett.22, 1065 (1969).

30. N.F.Mott, Phil.Mag.19, 835 (1969).

31. For example, see N.K.Hindley, J.Non-Cryst.Solids 5, 17 (1970).

REFERENCES : CHAPTER 3 - "Hydrogenated amorphous silicon"

1. H.F.Sterling and R.C.G.Swan, Sol.St.Electron. 8, 653 (1965).

2. R.C.Chittick, J.H.Alexander and H.F.Sterling, J.Electrochem.Soc. 116, 77 (1969).

3. M.Taniguchi, M.Hirose and Y.Osaka, J.Crystal Growth 45, 126 (1978).

4. D.L.Miller, H.Lutz, H.Weismann, E.Rock, A.Gosh, S.Ramamoorthy and M.Strongin, J.Appl.Phys. 49, 6192 (1978).

5. G.P. Caesar, S.F.Grimshaw and K.Okumura, Sol.St.Comm. 38,89 (1981).

6. W.Paul, A.J.Lewis, G.A.N.Connell and T.D.Moustakas, Sol.St.Comm. 20, 969 (1976).

7. For example, see W.E.Spear, Adv.in Phys. 26, 811 (1977).

8. J.C.Knights and G.Lucovsky, CRC Crit.Rev.in Sol.St. & Mat.Sci.9, 211 (1980).

9. W.E.Spear and P.G. LeComber, J.Non-Cryst.Solids 8-10, 727 (1972).

10. A.Madan, P.G. LeComber and W.E.Spear, J.Non-Cryst.Solids 20,239 (1976).

11. G.W.Neudeck and A.K.Malhotra, J.Appl.Phys. 46, 2662 (1975).

12. J.E.Mahan and R.E.Bube, J.Non-Cryst.Solids 24, 29 (1977).

13. T. Nakashita, M.Hirose and Y. Osaka, Jap.J.Appl.Phys. 18, 405 (1979).

14. N.B. Goodman, H.Fritzsche and H.Osaki, J.Non-Cryst.Solids 35 & 36, 599 (1980).

15. N.B. Goodman and H.Fritzsche, Phil.Mag. B 42, 149 (1980).

16. M.J.Powell, Phil.Mag.B 43, 93 (1981).

17. R.L.Weisfield and D.A.Anderson, Phil.Mag.B 44, 83 (1981).

18. J.D.Cohen, D.V.Lang, J.C.Bean and J.P.Harbison, J.Non-Cryst.Solids 35 & 36, 581 (1980).

19. J.D.Cohen, D.V.Lang, J.P.Harbison and J.C.Bean, Solar Cells 2 331, (1980).

20. J.D.Cohen, D.V.Lang and J.P.Harbison, Phys.Rev.Lett. 45, 197 (1980).

21. J.D.Cohen and D.V.Lang, Phys.Rev.B 25, 5321 (1982).

22. D.V.Lang, J.D.Cohen and J.P.Harbison, Phys.Rev.B, 5285 (1982).

23. C.H.Hyun, M.S. Schur and A.Madan, J.Non-Cryst.Solids 46, 221 (1981).

24. W. den Boer, J.de Physique (C4) 42, 451 (1981).

25. K.D.MacKenzie, P.G.LeComber and W.E.Spear, Phil.Mag.B 46, 377(1982).

26. S. Furukawa, T.Kagawa and N.Matsumoto, Sol.St.Comm.44,927 (1982).

27. E. Bhattacharya, S.Guha, K.V.Krishna and D.R.Bapat, J.Appl.Phys. 53, 6285 (1982).

28. D.V.Lang, J.Appl.Phys. 45, 3023 (1974).

29. R.A.Street and K.D.Biegelsen, Solid State Comm. 33, 1159 (1980).

30. B.C.Cavanett, S.P.Depinna, I.G.Austin and T.M.Searle, Phil.Mag.B 48, 169 (1983).

31. R.A.Street, Adv.in Phys. 30, 593 (1981).

32. R.J.Loveland, W.E.Spear and A.Al-Sharbaty, J.Non-Cryst.Solids 13 55 (1973/74).

33. W.E.Spear, R.J.Loveland and A.Al-Sharbaty, J.Non-Cryst.Solids 15, 410 (1974).

34. J.Robertson, J.Phys. C 17, L349 (1984).

35. P.G. LeComber and W.E.Spear, Phys.Rev.Lett. 25, 509 (1970).

36. A.R.Moore, Appl.Phys. Lett. 31, 762 (1977).

37. T. Tiedje, B.Abeles, D.L.Morel, T.D.Moustakas and C.R.Wronski, Appl.Phys. Lett. 36, 695 (1980).

38. W.E.Spear and P.G.LeComber, Phil.Mag.33, 935 (1976).

39. D.L. Staebler and C.R.Wronski, J.Appl.Phys. 51, 3262 (1980).

40. P.G.LeComber, D.I.Jones and W.E.Spear, Phil.Mag B 35, 1173 (1977).

41. D.Adler, M.Silver, A.Madan and W.Czubatyi, J.Appl.Phys. 51,6429(1980).

42. R.A.Street, Phil.Mag.B 49, L15 (1984).

43. S.Yamazaki, A.Mase, K.Urata, K.Shibita, H.Shinohara,S.Nagayama, M. Abe, T.Hamatani and K.Suzuki, Electron.Dev.Lett.5,315 (1984).

44. For example, see I.Shimizu, T.Komatsu, K.Saito and E.Inoue, J.Non-Cryst.Solids 35 & 36, 773 (1980).

45. For example, see A.J.Snell, K.D.McKenzie, W.E.Spear and P.G.LeComber, Appl.Phys. 24, 357 (1981).

46. A.E.Owen, P.G. LeComber, G.Sarrabayrouse and W.E.Spear, IEE.Proc. 129, 51 (1982).

47. M. Janai and F.Moser, J.Appl.Phys. 53, 1385 (1982).

REFERENCES : CHAPTER 4 - "Basic physics of....."

1. For example, see M.Schluter, Thin Solid Films 93, 3 (1982).
2. For example, see G.Persky, Sol.St.Electron.15, 1345 (1972).
3. R.Jones, Ph.D.thesis, University of Durham (in preparation).
4. "Metal-Semiconductor Contacts", by E.H.Rhoderick, Clarendon Press (1978).
5. E.H.Rhoderick, IEE Proc.129, 1 (1982).
6. "Electronic Semiconductors", by E.Spenke (translation), McGraw-Hill (1958).
7. "Metal-Semiconductor Rectifiers", by H.K.Henisch,Clarendon Press (1957).
8. "Modern Theory of Solids", by F.Seitz, 5th impression, McGraw-Hill (1940).
9. N.F.Mott, Proc.Cambridge Phil.Soc. 34, 568 (1938).
10. "Metal Rectifiers", by H.K.Henisch, Clarendon Press (1949).
11. J.Bardeen, Phys.Rev.71, 717 (1947).
12. W.E.Spicer, I.Lindau, P.Skeath and C.Y.Su, J.Vac.Sci Technol.17, 1019 (1980).
13. For example, see "Thermodynamics, Kinetic Theory and Statistical Thermodynamics", by F.W.Sears and G.L.Salinger, Addison-Wesley 3rd Ed.(1975), pp.254.
14. C.R.Crowell, W.G.Spitzer, L.E.Howarth and E.E.La Bate, Phys.Rev.127 2006 (1962).
15. For example, see "Semiconductors", by R.A.Smith, Cambridge Univ.Press, 2nd Ed.(1978), pp.171.
16. For example, see E.H.Rhoderick, J.Phys.D. 5, 1920 (1972).
17. A.Deneuville and M.Brodsky, J.Appl.Phys. 50, 1414 (1979).
18. D.Jousse, P.Viktorovitch, L.Vieux-Rochaz and A.Chevenas-Paule, J.Non-Cryst.Solids 35 & 36 , 767, (1980).
19. Y.Mishima, M.Hirose and Y.Osaka, Jpn.J.Appl.Phys. 20, 593 (1981)

20. H.C.Card and E.H.Rhoderick, J.Phys.D. 4, 1589 (1971).

21. H.C.Card and E.H.Rhoderick, J.Phys.D. 4, 1602 (1971).

22. J. McGill, J.I.B.Wilson and S.Kimmond, J.Appl.Phys. 50, 548 (1979).

23. For example, see A.Waxman, J.Shewchun and G.Warfield, Sol.St.Electron 10, 1187 (1967).

24. I. Balberg and D.E.Carlson, Phys.Rev.Lett. 43, 58 (1979).

25. I.Balberg, Phys.Rev.B 22, 3853 (1980).

26. I.Balberg, J.Non-Cryst.Solids 35 & 36, 605 (1980).

27. I.Balberg, J.Electron.Mat. 9, 979 (1980).

28. F.A.Padovani and R.A.Stratton, Sol.St.Electron.9, 695 (1966).

29. A.Y.C. Yu and E.H.Snow, J.Appl.Phys. 39, 3008 (1968).

30. For example, see A.M.Goodman, Surface Science 1, 54, (1964).

31. For example, see "Current Injection in Solids", by M.A.Lampert and P.Mark, Academic press (1970).

32. S.Ashok, A.Lester and S.J.Fonash, IEEE Electron.Dev.Lett. EDL-1, 200 (1980).

33. R.Lahri, M.K.Han and W.A.Anderson, J.Appl.Phys. 54, 928 (1983).

34. R.H. Fowler, Phys.Rev. 38, 45 (1931).

35. B.M.Arora, K.Srivistava and S.Guha, J.Appl.Phys. 53, 1820 (1982).

36. C.R. Wronski, B.Abeles, G.D.Cody and T.Tiedje, Appl.Phys.Lett. 37, 96 (1980).

37. A.M.Cowley, J.Appl.Phys. 37, 3024 (1966).

38. S.J.Fonash, J.Appl.Phys. 54, 1966 (1983).

REFERENCES : CHAPTER 5 - "A Theory of the Admittance...."

1. G.I.Roberts and C.R.Crowell, J.Appl.Phys. 41, 1767 (1970).

2. J. Maserjian, J.Vac.Sci.Technol. 6, 843 (1969).

3. D.L.Losee, J.Appl.Phys. 46, 2204 (1975).

4. "Thermally Stimulated Relaxation in Solids", Ed.P.Braunlich, Springer-Verlag (1979).

5. P.Viktorovitch and D.Jousse, J.Non-Cryst.Solids 35 & 36, 569 (1980).

6. P. Viktorovitch and G.Moddel, J.Appl.Phys. 51, 4847 (1980).

7. P. Viktorovitch, J.Appl.Phys. 52, 1392 (1981).

8. D.V.Lang, J.D.Cohen and J.P.Harbison, Phys.Rev.B 25, 5285 (1982).

9. W.E.Spear, P.G. LeComber and A.J.Snell, Phil.Mag.B 38, 303 (1978).

10. A.J.Snell, K.D.Mackenzie, P.G.LeComber and W.E.Spear, Phil.Mag.B 40 1 (1979).

11. J.Beichler, W.Fuhs, H.Mell, H.M.Welsch, J.Non-Cryst.Solids 35 & 36, 587 (1980).

12. T. Tiedje, C.R.Wronski and J.M.Cebulka, J.Non-Cryst.Solids 35 & 36 743 (1980).

13. T. Tiedje, C.R.Wronski, B.Abeles and J.M.Cebulka, Solar Cells 2, 301 (1980).

14. J. Singh and M.H.Cohen, J.Appl.Phys. 51, 413 (1980).

15. R. Lahri, M.K.Han and W.A.Anderson, J.Appl.Phys. 54, 928 (1983).

16. H.L.Fernandez-Canque, M.C.Abdulrida and J.Allison, Thin Solid Films 110, 241 (1983).

17. I.G.Gibb and A.R.Long, Phil.Mag. B 49, 565 (1984).

18. J.P.Lloyd, Ph.D.Thesis, University of Durham (1984).

19. R.A.Abram and P.J.Doherty, Phil.Mag.B 45, 167 (1982).

20. J.D.Cohen and D.V.Lang, Phys.Rev. B 25, 5321 (1982).

21. "MOS Physics and Technology" by E.H.Nicollian and J.R.Brews, J.Wiley & Sons (1982).

22. I.W.Archibald and R.A.Abram, Phil.Mag. B 48, 111 (1983).

23. W. Shockley and W.T.Read, Phys.Rev. B 87, 835 (1952).

24. "Semiconductor Statistics" by J.S.Blakemore, Pergamon Press (1962).

25. "Metal-Semiconductor Contacts", by E.H.Rhoderick, Clarendon Press (1978).

26. K.Lehovec, Appl.Phys. Lett. 8, 48 (1966).

27. "Polar Molecules" by P.Debye, Dover New York (1929).

28. A.K.Jonscher, Nature 267, 673 (1977).

REFERENCES : CHAPTER 6 - "Comments, and Extensions...."

1. P.Viktorovitch and G.Moddel, J.Appl.Phys.51, 4847 (1980).
2. "The theory of the properties of metals and alloys" by N.F.Mott and H.Jones, Clarendon Press (1936).
3. M.J.Powell, Phil.Mag.B 43, 93 (1981).
4. R.L.Weisfield and D.A.Anderson, Phil.Mag.B 44, 83 (1981).
5. D.V.Lang, J.D.Cohen and J.P.Harbison, Phys.Rev.B 25, 5285 (1982).
6. "MOS Physics and Technology" by E.H.Nicollian and J.R.Brews, J.Wiley and Sons (1982).
7. W.Shockley, Bell System Tech. J.28, 435 (1949).
8. I.W.Archibald and R.A.Abram, Phil.Mag.B 48, 111 (1983).
9. T.Tiedje, C.R.Wronski and J.M.Cebulka, J.Non-Cryst.Solids 35 & 36, 743 (1980).
10. "Rectifying Semiconductor Contacts", by H.K.Henisch, Clarendon Press(1957).
11. I.G.Gibb and A.R.Long, Phil.Mag.B 49, 565 (1984).
12. J.Bardeen, Bell System Tech.J.28, 428 (1949).
13. A.J.Snell, K.D.Mackenzie, P.G. Le Comber and W.E.Spear, Phil.Mag.B 40 1 (1979).
14. C.T.Sah, R.N.Noyce and W.Shockley, Proc.IRE 45, 1228 (1957).
15. N.B.Goodman and H.Fritzsche, Phil.Mag.B 42, 149 (1980).
16. W.Spear, P.G.Le Comber and A.J.Snell, Phil.Mag.B 38, 303 (1978).
17. G.Döhler and M.Hirose, Proc.7th. Int.Conf.on Amorphous and Liquid Semiconductors, Edinburgh (1977), p.372.
18. M.Hirose, T.Suzuki and G.H.Döhler, Jap.J.Appl.Phys.18, Suppl.18-1, 109 (1979).
19. M.Hirose, T.Suzuki and G.H.Döhler, Appl.Phys.Lett. 34, 234 (1979).
20. T.Suzuki, Y.Osaka and M.Hirose, Jap.J.Appl.Phys., L159 (1982).
21. P.J.Doherty and R.A.Abram, Phil.Mag.B 45, 167 (1982).

REFERENCES - CHAPTER 7 - "Experimental measurements..."

1. M. J. Powell, Philips Research Lab, Redhill, private communication.
2. J.I.B.Wilson, Heriot-Watt University, Edinburgh, private communication.
3. Trademark, Millipore Corporation.
4. W. Kern, RCA Rev.39, 278 (1978).
5. For example, see J.P.Lloyd, Ph.D. thesis, University of Durham (1984).
6. For example, see D.L.Staebler and C.R. Wronski, J.Appl.Phys. 51, 3262 (1980).
7. For example, see A.L.Fahrenbruch and R.H.Bube, J.Appl.Phys. 45, 1264 (1974).
8. N.Evans, Ph.D.Thesis, University of Durham (in preparation).
9. M. R. Boudry, J.Phys. E.11, 237 (1978).
10. H.C.G. Ligtenberg, M.Sc. thesis, Groningen State University, Netherlands (1979).
11. M.J.Thompson, N.M.Johnson, R.J.Nemanich and C.C.Tsai, Appl.Phys. Lett. 39, 274 (1981).
12. For example, see J.Batey, Ph.D. thesis, University of Durham (1983).
13. R. S.Crandall, Proc. 14th. IEEE Photovoltaic Specialists Conf., San Diego, California (1980), pp.1221.
14. J. McGill, J.I.B.Wilson and S. Kimmond, J.Appl.Phys.50, 548 (1979).
15. W.E.Spear, Adv.in Phys. 26, 811 (1977).
16. W.E.Spear, P.G. LeComber and A.J.Snell, Phil.Mag B 38, 303 (1978).
17. D.V.Lang, J.D.Cohen and J.P.Harbison, Phys.Rev.B 25, 5285 (1982).
18. I.G. Gibb and A.R.Long, Phil.Mag.B 49, 565 (1984).
19. P. Viktorovitch, J.Appl.Phys. 52, 1392 (1981).